Modelling Human Genetic Disorders in Mice

Anna Marta Migdalska

This dissertation is submitted for the degree of

Doctor of Philosophy

of the

The Wellcome Trust Sanger Institute

Hughes Hall, University of Cambridge

Najukochańszym

Rodzicom

ACKNOWLEDGEMENTS

It has been a pleasure to carry out my PhD project at the Wellcome Trust Sanger Institute for the four past years, and I would like to thank all the people who helped me during this time.

First and foremost, I would like to express my deep gratitude to my supervisor, David Adams, for giving me the opportunity to pursue exciting research projects in his laboratory. I am very grateful for his enormous support and excellent guidance. It was a privilege to work with such an inspirational and enthusiastic mentor.

I would like to thank all current and former members of the Adams laboratory for providing me with help and advice in various aspects of my work. I am particularly grateful to Louise for introducing me to many molecular techniques and for reading my thesis, and to Theo for giving me considerable support with tissue culture and for always ensuring a ready supply of reagents. I would like to thank Rebecca for teaching me qRT-PCR. Also thank you to Cathy, Chi and Radek for always being ready to give advice and for the many instructive discussions we have had.

In addition, I would like to thank members of the Wellcome Trust Sanger Institute Research Support Facility for taking excellent day-to-day care of my mice and for all the technical support they have provided me with.

I would like to express my great appreciation to all member of the Wellcome Trust Mouse Genetics Project for performing some of the phenotypic tests that I applied in my research.

I am very grateful to many other people from the Wellcome Trust Sanger Institute who helped me with my work: Yvette Hooks and Kay Clarke for teaching me histopathological techniques, Peter Ellis and Robert Andrews for their expertise in conducting microarray analysis, and Gabriela Gurria and Darren Logan for their help with behavioural studies.

I would like to thank my thesis committee members, Derek Stemple, Matthew Hurles and Charles Shaw-Smith, for their comments and suggestions throughout my PhD.

I would also like to thank Inês Barroso and Anton Enright for giving me the possibility of doing rotations in their laboratories during the first year of my PhD, and Kathryn Fawcett and Cei Abreu for helping me during these rotations.

I am also very grateful to Mark Arends from the Department of Pathology of the University of Cambridge for his invaluable help with histopathological analysis, and Lionel Willatt from the Department of Medical Genetics at Addenbrooke's Hospital for teaching me FISH analysis.

Thanks to David for proof-reading and helping with the formatting of my thesis, and for many useful discussions and support.

Finally, a massive thank you to my wonderful parents for their endless support in whatever I chose to do, for always being there for me, and for their unconditional love.

DECLARATIONS

This thesis is my own work and contains nothing which is the outcome of work done in collaboration except where specifically indicated in the text.

This thesis does not exceed the word limit of 60,000 as set by the Degree Committee for the Faculty of Biology.

September 2011

ABSTRACT

Rearrangements of the human genome including deletions, duplications, inversions and translocations play a major role in the pathogenesis of many human diseases. In order to facilitate the discovery of dosage-sensitive genomic regions and genes, and to investigate the contribution of genomic rearrangements to the development of different human disorders, many mouse models carrying genomic rearrangements of syntenic regions of the mouse genome have been generated.

During my PhD I have been involved in the generation and phenotypic analysis of two monosomic mouse models carrying deletions syntenic with 21q11.2–q21.1 and 5q35.2–q35.3 in humans.

The first of these models was generated to investigate the contribution of the genes mapped within the *Lipi–Usp25* interval to the development of both various types of cancer and clinical features diagnosed in patients with Monosomy 21 (a disorder associated with intellectual disability, craniofacial, skeletal and/or cardiac abnormalities, and respiratory complications). Monosomic mice displayed impaired memory retention, which models the intellectual disability observed in patients with Monosomy 21. Moreover, when fed on a high-fat diet, monosomic mice exhibited a significant increase in fat mass/fat percentage estimate, severe fatty changes in their livers, and thickened subcutaneous fat. Thus genes within the *Lipi–Usp25* interval are involved in memory retention and the regulation of fat deposition.

The second of these models has been developed to investigate the contribution of the genes mapped within the *4732471D19Rik–B4galt7* interval to the development of clinical features diagnosed in patients with Sotos syndrome (an overgrowth disorder associated with advanced bone age, intellectual disability, hypotonia, facial, cardiovascular and/or urinary/renal abnormalities). Monosomic mice showed dilation of the pelvicalyceal system in the kidneys, which mimics the renal abnormality observed in patients with Sotos syndrome. Thus haploinsufficiency of a gene (or genes) within the *4732471D19Rik–B4galt7* interval successfully models the renal abnormality observed in patients with Sotos syndrome.

CONTENTS

ABBREVIATIONS

°C	degrees Celsius
μCi	microcurie
μF	microfarad
μg	microgram
μl	microlitre
μM	micromolar
AB2.2	129S7/SvEvBrdHprt^{b-m2}
ABR	auditory brainstem response
aCGH	array comparative genomic hybridization
AS	Angelman syndrome
BAC	bacterial artificial chromosome
BMC	bone mineral content
BMD	bone mineral density
BME	β-mercaptoethanol
BMI	body mass index
bp	basepair
cDNA	complementary DNA
CGH	comparative genomic hybridization
cm	centimeter
dB	decibel
ddH_20	double-distilled H_20
DECIPHER	Database of Chromosomal Imbalance and Phenotype in Humans using Ensembl Resources
DEXA	dual-energy X-ray absorptiometry
DGS	DiGeorge syndrome
DMEM	Dulbecco's Modified Eagle Medium
DMSO	dimethyl sulfoxide
dNTP	deoxyribonucleotide triphosphate
DSB	double-strand break
dsDNA	double-stranded DNA

E14Tg2a	129P2/OlaHsd
EDTA	ethylenediaminetetraacetic acid
EFT	Ewing family tumours
ELISA	enzyme-linked immunosorbent assay
EDMD	Emery-Dreifuss muscular dystrophy
ES	embryonic stem
FBS	foetal bovine serum
FISH	fluorescence in situ hybridization
FPLD	familial partial lipodystrophy of the Dunnigan
g	gram
gDNA	genomic DNA
GPS	glutamine/penicillin/streptomycin
HAT	hypoxanthine-aminopterin-thymidine
HFD	high-fat diet
HGPS	Hutchinson-Gilford progeria syndrome
HMT	histone-methyltransferase
HSA	human chromosome
HSW	high stringency wash
HT	hypoxanthine-thymidine
H&E	haematoxylin and eosin
Ig	immunoglobulin
IMS	industrial methylated spirit
ipGTT	intra-peritoneal glucose tolerance test
kb	kilobase
kHz	kilohertz
LB	lysogeny broth
LCR	low-copy repeat
LDL	low-density lipoprotein
LIF	leukaemia inhibiting factor
LOD	logarithm of odds
LOH	loss of heterozygosity
loxP	locus of crossover P1
LPS	lipopolysaccharide

LRP	lipoprotein receptor-related protein
LSW	low stringency wash
Mb	megabase
mbar	milibar
mg	miligram
MICER	Mutagenic Insertion and Chromosome Engineering Resource
ml	mililitre
mm	millimeter
mM	milimolar
MTT	3-(4,5-Dimethylthiazol-2-yl)-2,5-diphenyltetrazolium bromide
NAHR	non-allelic homologous recombination
NCBI	National Center for Biotechnology Information
NEFAC	non-esterified free fatty acids
NFD	normal-fat diet
ng	nanogram
NHEJ	non-homologous end joining
NID	nuclear receptor interaction domain
nm	nanometer
NR	nuclear receptor
NSCLC	non-small cell lung carcinoma
OD	optical density
OMIM	Online Mendelian Inheritance in Man
OS	osteosarcoma
OSCC	oral squamous cell carcinomas
PBS	phosphate buffered saline
PCR	polymerase chain reaction
PCR-SSCP	polymerase chain reaction-single strand conformation polymorphism
PEV	position-effect-variegation
pH	potential of hydrogen
PHD	zinc-finger plant homeodomain
PWS	Prader-Willi syndrome
PWWP	proline-tryptophan-tryptophan-proline

qRT-PCR	real-time quantitative PCR
RA	retinoic acid
rpm	revolutions per minute
s	seconds
SAC	SET-associated cysteine-rich
SCC	squamous cell carcinomas
SCLC	small cell lung carcinoma
SDS	sodium dodecyl sulfate
SET	Su(var)3-9, Enhancer-of-Zeste, Trithorax
SMS	Smith-Magenis syndrome
SMCR	SMS critical region
snoRNA	small nucleoar RNA
SNP	single nucleotide polymorphism
SoS	Sotos syndrome
SSC	saline-sodium citrate
SSLP	simple sequence length polymorphism
STS	sequence-tagged site
TAE	Tris-acetate-EDTA
TBST	tris buffered saline with Tween 20
TC	tissue culture
Tris	tris(hydroxymethyl)aminomethane
TRAIL	tumour necrosis factor related apoptosis-inducing ligand
TSG	tumour suppressor gene
U	unit
UV	ultraviolet
V	volt
VCFS	velocardiofacial syndrome
WAT	white adipose tissue
WBS	Williams syndrome

LIST OF FIGURES

CHAPTER 1 – GENERAL INTRODUCTION

CHAPTER 2 – MATERIALS AND METHODS

CHAPTER 3 – MODELLING A DELETION OF THE HUMAN REGION 21q11.2–q21.1 IN MICE

CHAPTER 4 – MODELLING A DELETION OF THE HUMAN REGION 5q35.2–q35.3 IN MICE

LIST OF TABLES

CHAPTER 4 – MODELLING A DELETION OF THE HUMAN REGION 5q35.2–q35.3 IN MICE

CHAPTER 1

GENERAL INTRODUCTION

1.1 USING THE MOUSE AS A GENETIC TOOL

Mice have frequently been used to model both normal human development and human diseases. This is because they share many similarities with humans, both in terms of physiology and anatomy. Other features that make mice a great model organism include a small body size (which allows them to be housed at high density and makes them easy to handle), a short gestation time and prolificacy in breeding (allowing the generation of a study cohort within a short period of time). The finding that more than 90% of the human and mouse genomes can be divided into regions of conserved synteny, and that about 99% of mouse genes have homologues in the human genome (Waterston 2002) is further evidence that the mouse represents a good model to study human development.

The isolation of pluripotent mouse embryonic stem (ES) cells (Evans 1981), successful regeneration of germ line and somatic tissues from cultured ES cells reintroduced into the blastocyst (Bradley 1984) and the development of chromosome engineering techniques allowing the generation of defined chromosomal rearrangements (Ramirez-Solis 1995) mark key developments in the ability to use the mouse as a genetic tool.

1.2 CHROMOSOME ENGINEERING IN MOUSE ES CELLS

1.2.1 WAYS OF INDUCING CHROMOSOMAL REARRANGENTS IN MICE

Chromosomal rearrangements in mice can be randomly generated by ionizing radiation or exposure to chemical mutagens, such as ethylene oxide

or chlorambucil (Stubbs 1997) (however, the endpoints of such rearrangements cannot be predetermined) or can be precisely introduced into a defined genomic location using chromosome engineering techniques (Ramirez-Solis 1995).

1.2.2 A BRIEF OVERVIEW OF CHROMOSOME ENGINEERING IN MOUSE ES CELLS

Chromosome engineering utilizes the combination of ES cell gene targeting and the Cre/*loxP* site-specific recombination system to generate a defined chromosomal rearrangement (Ramirez-Solis 1995). Briefly, two *loxP* (locus of crossover P1) recombinase recognition sites are sequentially targeted in two predefined loci in the mouse ES cell genome. Subsequently, the expression of Cre, a recombinase that binds to a 13 basepair (bp) sequence flanking the 8 bp core spacer sequence of *loxP* (Sauer 1988), induces targeted recombination between the two *loxP* sites to generate the chromosomal rearrangement.

1.2.3 A STRATEGY TO GENERATE CHROMOSOMAL REARRANGENTS IN MOUSE ES CELLS

The selection of two endpoints is the first step to generating a chromosomal rearrangement. Both genes of known chromosomal location and simple sequence length polymorphism (SSLP) microsatellite markers have been successfully used as endpoints for generating chromosomal rearrangements (Lindsay 1999; Zheng 2000). The next step involves the insertion of a targeting vector containing a *loxP* site, a positive selection cassette (e.g. neomycin), a coat-colour marker (e.g. tyrosinase minigene) and one of two complementary, but independently non-functional, parts of a hypoxanthine phosphoribosyl transferase (*Hprt*) mini-gene (either 5'*Hprt* or 3'*Hprt*) into the first chosen endpoint (Ramirez-Solis 1995; Zheng 1999) (**Figure 1.1**). The successful insertion of the targeting vector into the first endpoint can be identified by positive selection (only the ES cell clones that express the positive selectable marker gene, e.g. the neomycin resistance gene, will survive the selection in a culture medium supplemented with this drug), and subsequently confirmed by either Southern blot analysis or

polymerase chain reaction (PCR). The single-targeted ES cell clones are subsequently targeted with a second vector containing a *loxP* site, a different positive selection cassette (e.g. puromycin), a different coat-colour marker (e.g. K14-agouti transgene) and the complimentary part of the *Hprt* gene into the second chosen endpoint (**Figure 1.1**). As in the case of the first targeting vector, the successful insertion of the targeting vector into the second endpoint can be identified by positive selection, and subsequently confirmed by either Southern blot analysis or PCR. Finally, the double-targeted ES cell clones are electroporated with a Cre-expression vector, e.g. pOG231 (O'Gorman 1997), in order to induce a recombination between two *loxP* sites. Following the electroporation, the ES cell clones are cultured in a medium supplemented with hypoxanthine, aminopterin and thymidine (HAT) in order to select the positive recombinant ES cell clones in which, as a consequence of Cre-mediated recombination, the two parts of the *Hprt* mini-gene have been brought together, making a functional gene. The successful generation of the chromosomal rearrangement can be confirmed by fluorescence in situ hybridization analysis (FISH). Finally, the ES cell clones carrying the engineered rearrangement are injected into mouse blastocysts to generate chimaeras, from which the progeny carrying the chromosomal rearrangement are derived.

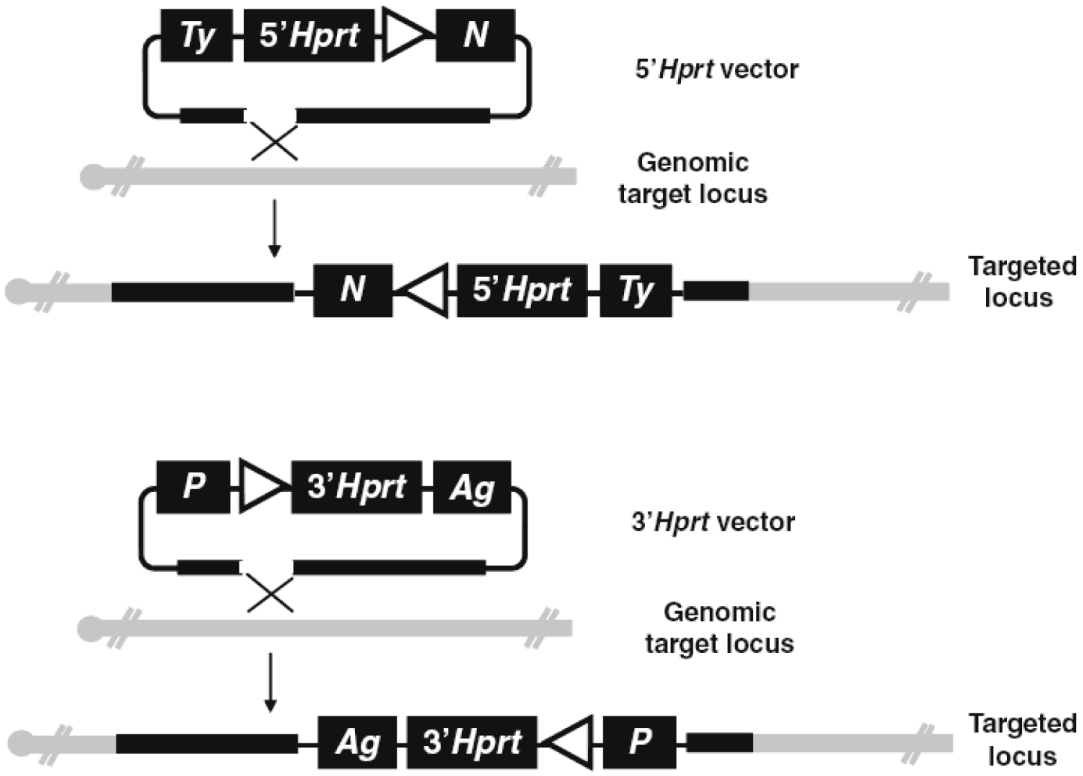

Figure 1.1. Gene targeting in ES cells. Insertional targeting vectors can be used to insert *loxP* sites, positive selectable markers, hypoxanthine phosphoribosyltransferase (*Hprt*) gene fragments and coat-colour markers to predetermined loci in the ES cell genome. The vector (thin black line) is linearized in the region of homology (thick black line) to stimulate targeted insertion into the locus (thick grey line). The 5'*Hprt* vector contains the neomycin selectablemarker (*N*), the 5' end of the *Hprt* minigene, a *loxP* site (white triangle) and the tyrosinase minigene (*Ty*) coat-colour marker. The 3'*Hprt* vector contains the puromycin selectable marker (*P*), the 3' end of the Hprt minigene, a *loxP* site (white triangle) and the agouti (*Ag*) coat-colour marker. Figure taken from van der Weyden *et al*., 2009.

1.2.4 TYPES OF CHROMOSOMAL REARRANGEMENTS GENERATED IN MOUSE ES CELLS

The type of chromosomal rearrangement that is generated in double-targeted ES cells depends on the *loxP* sites orientation, the localization of both *loxP* sites on the same or different chromosomes, and the relative configuration of the two parts of the *Hprt* gene (Ramirez-Solis 1995) (**Figure 1.2, 1.3, 1.4**). *LoxP* sites inserted in the same orientation on the same chromosome result in the generation of a chromosomal deletion, while *loxP* sites inserted in the same orientation on homologous chromosomes result in the generation of chromosomal deletion and duplication (**Figure 1.2**). *LoxP*

sites inserted in the opposite orientation on the same chromosome result in the generation of chromosomal inversion (**Figure 1.3**), whereas *loxP* sites inserted in the same orientation on non-homologous chromosomes result in the generation of chromosomal translocation (**Figure 1.4**).

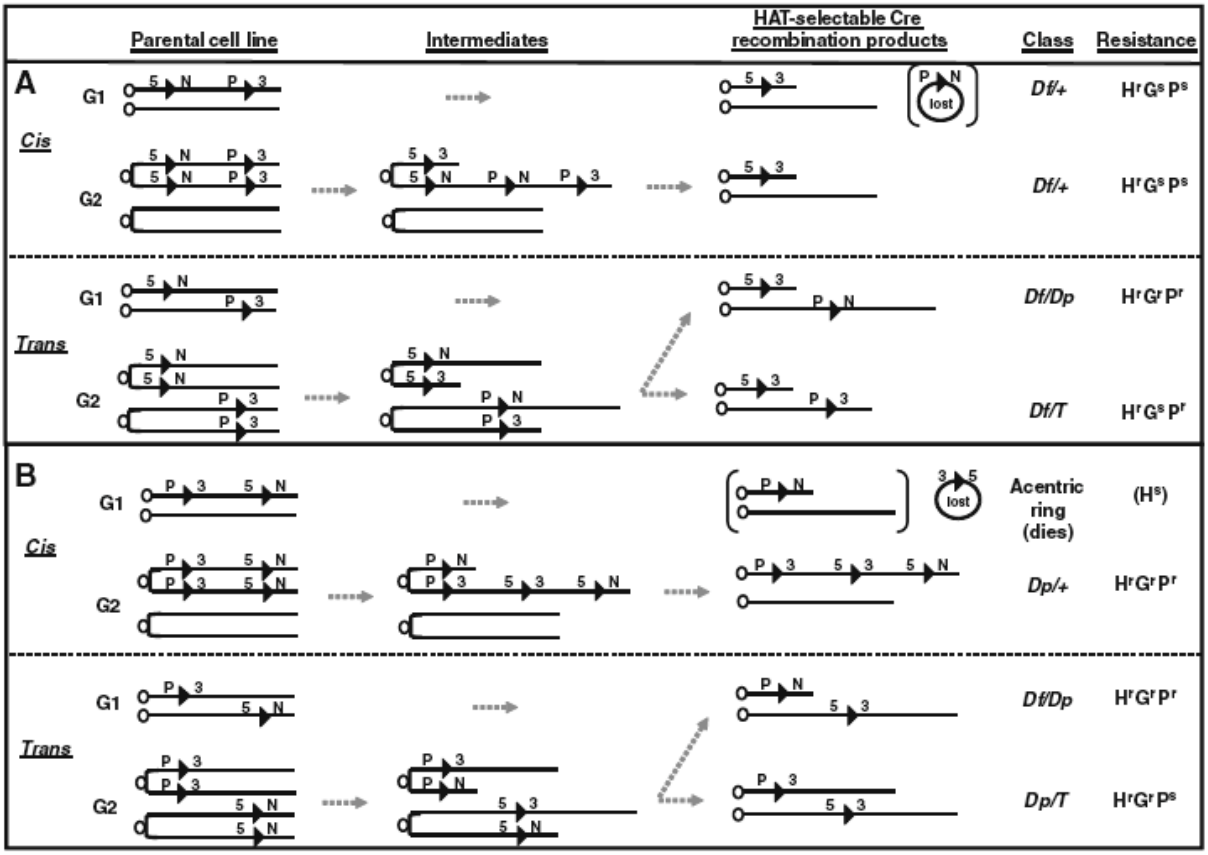

Figure 1.2. Engineering a deletion and/or duplication in embryonic stem cells. When the two *loxP* sites are targeted in the same orientation with respect to the centromere, the half *Hprt* cassettes can lie in two orientations, **(A)** outside the floxed region or **(B)** inside the floxed region. G1 and G2 indicate the different phases of the cell cycle in which recombination occurs. For G2 events, only recombination between *loxP* sites on different chromatids is considered: G2 recombination can also occur between two *loxP* sites on the same chromatid, but these events have the same consequence as the corresponding G1 events and are therefore not shown. The resulting recombination products and hence drug sensitivity (''resistance'') will depend upon whether the *loxP* sites are located in cis (on the same chromosome) or trans (on the two chromosome homologs). Note that using the strategy described in the text, only viable HAT-resistant recombination products are recovered and scored (those products shown in brackets are not HAT selectable). A *loxP* site is indicated by a black triangle, a centromere is indicated by an open circle. Abbreviations: 5, 5'*Hprt* cassette; 3, 3'*Hprt* cassette; *Df*, deficiency (deletion); *Dp*, duplication; G, G418 (neomycin); H, HAT (hypoxanthine, aminopterin and thymidine); N, neomycin selection cassette (conferring resistance to G418); P, puromycin selection cassette (conferring resistance to puromycin); r, resistant; s, sensitive; *T*, targeted. Figure taken from van der Weyden *et al*., 2009.

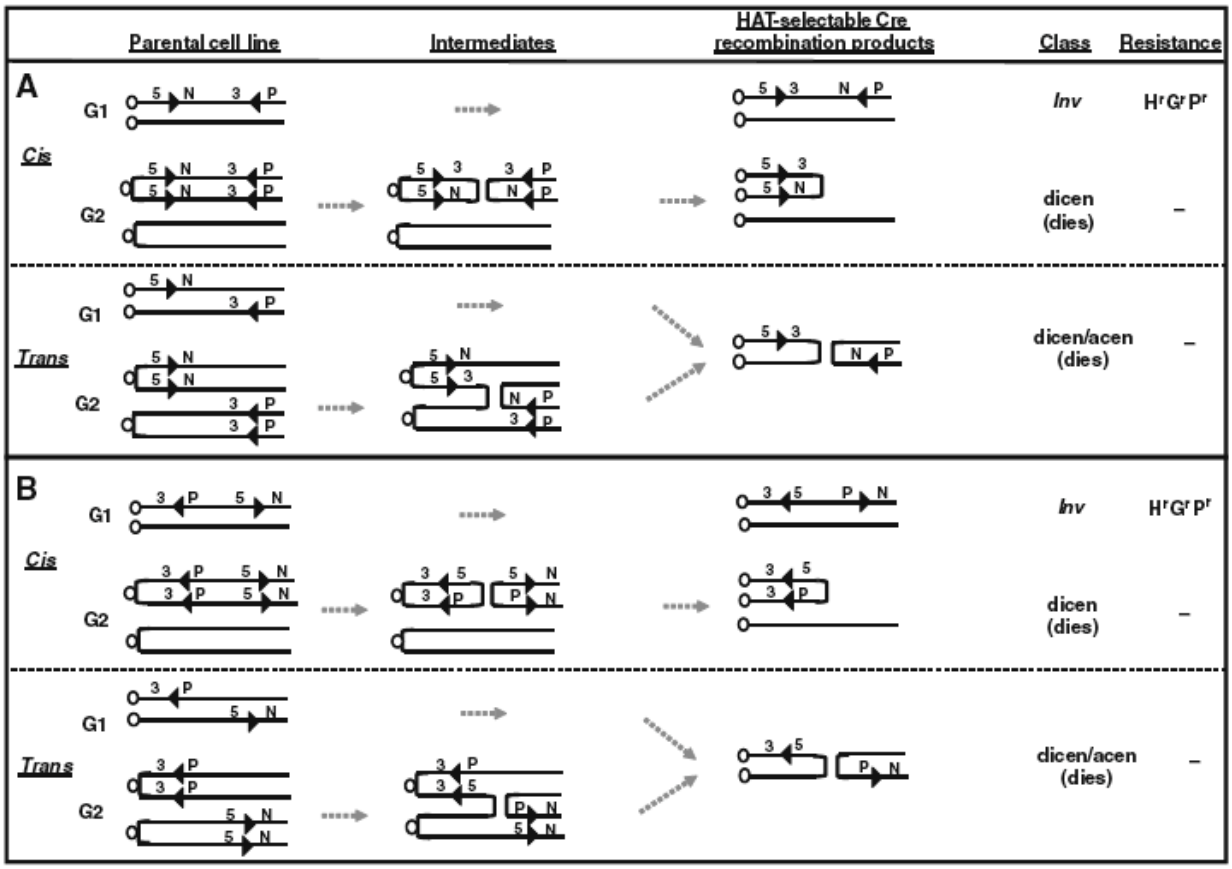

Figure 1.3. Engineering an inversion in embryonic stem cells. When the two *loxP* sites are targeted in the opposite orientation with respect to the centromere, either **(A)** facing towards or **(B)** away from each other, a chromosomal inversion will only occur if the loxP sites are in cis (on the same chromosome). Note that using the strategy described in the text, only viable HAT-resistant recombination products are recovered and scored. Details of the abbreviations and symbols are the same as for **Figure 1.2** (with additional abbreviations: acen, acentric; dicen, dicentric). Figure taken from van der Weyden *et al*., 2009.

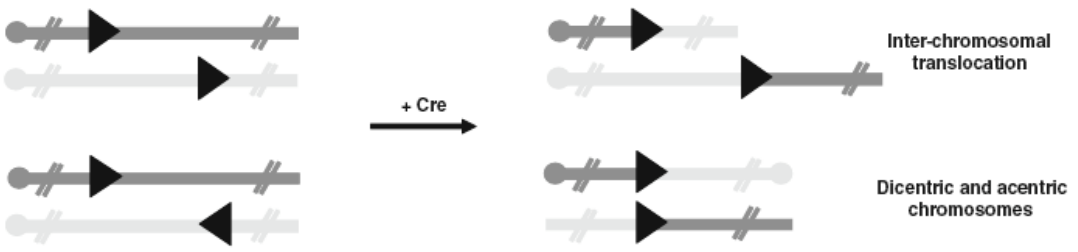

Figure 1.4. Engineering chromosomal translocations. Cre-mediated recombination leads to chromosomal translocation or dicentric and acentric chromosomes, depending on the relative orientations of the *loxP* sites (black triangles) on two non-homologous chromosomes. Figure taken from van der Weyden *et al*., 2009.

1.2.5 TARGETING VECTORS USED TO GENERATE CHROMOSOMAL REARRANGEMENTS IN MOUSE ES CELLS

Two complementary libraries *(*5'*Hprt* and 3'*Hprt*) consisting of insertion targeting vectors have been developed to facilitate the generation of chromosome rearrangements in the mouse ES cells (Zheng 1999). The insertion targeting vectors have been developed by cloning a 129S5/SvEvBrd genomic DNA genomic library into one of two vector backbones, containing either a *loxP* site, a 5' fragment of the *Hprt* gene, a positive selection cassette (neomycin; PGK-neo-bpA) and a coat-colour marker (tyrosinase minigene; *Ty*; resulting in greyish coat on an otherwise albino background) (Yokoyama 1990; Overbeek 1991) or a *loxP* site, a 3' fragment of the *Hprt* gene, a positive selection cassette (puromycin; PGK-puro-bpA) and a coat-colour marker (K14-agouti transgene; *Ag*; resulting in ''butterscotch'' coat in black agouti or non-agouti mice) (Kucera 1996). Each of these insertion targeting vectors requires only linearization within its genomic insert prior to electroporation into the ES cells (Zheng 1999). Moreover, the genomic insert in all of the available insertion targeting vectors is flanked by *Asc*I restriction enzyme sites, which allows inversion of the orientation of the genomic insert relative to the vector backbone or shuttling of the genomic insert between different vector backbones if needed (Zheng 1999).

A great advance in using these two libraries has been achieved by end-sequencing and mapping more than 150,000 clones (insertion targeting vectors) against the genome. All the data is available via the Mutagenic Insertion and Chromosome Engineering Resource (MICER) (htpp://www.sanger.ac.uk/PostGenomics/mousegenomics) (Adams 2004). Moreover, all mapped clones can be found in the Ensembl genome browser (Hubbard 2007) under the DAS source "MICER".

1.3 CHROMOSOMAL REARRANGEMENTS IN HUMANS

1.3.1 TYPES OF CHROMOSOMAL REEARANGEMENTS FOUND IN HUMANS

Unbalanced structural chromosomal abnormalities, ranging from the gain or loss of an entire chromosome to the gain or loss of a small chromosome fragment, are detected in about 3% of all human individuals, while balanced structural chromosomal anomalies, including inversions, translocations and ring chromosomes, are detected in about 0.2% of all human individuals (Shaffer 2009). Altogether, this makes germline and somatic chromosomal abnormalities the most frequent cause of human genetic diseases. The most frequent type of somatic chromosomal abnormalities involves chromosomal translocations, a type of chromosomal rearrangement that is frequently found in human cancers, especially in leukaemias, lymphomas and sarcomas (Rabbitt 1994). On the other hand, the most common type of germline chromosomal abnormalities involves the gain or loss of sex chromosomes, with Triple-X syndrome being an example of the gain of one or more extra copies of the X chromosome in females (Tartaglia 2010) and Klinefelter syndrome being an example of the gain of one or more extra copies of the X chromosome in males (Wikström 2011), whilst Turner syndrome is an example of the loss of one copy of the X chromosome in females (Kesler 2007). The second most frequent type of germline chromosomal abnormalities involves triplication of autosomal chromosomes, with trisomy of chromosome 21 (Down syndrome) (Mégarbané 2009), 18 (Edwards syndrome) (Tucker 2007) and 13 (Patau syndrome) (Iliopoulos 2006) being the most common. However, less frequently occurring autosomal chromosomal deletions seem to have the most severe impact on phenotype, as they reveal both dosage-sensitive genes and recessive mutations, with a deletion of 1.5 – 3 Mb of the 22q11 region causing DiGeorge syndrome (Linday 2001), a deletion of around 5 – 7 Mb of the 15q11–q13 region causing Prader-Willi syndrome and Angleman syndrome (Buiting 2010), or a deletion of 3.7 Mb of the 17p11.2 region causing Smith-Magenis syndrome (Elsea 2008) being just a few examples.

1.3.2 MECHANISMS GENERATING CHROMOSOMAL REARRANGEMETS IN HUMANS

Two distinct mechanisms, namely non-allelic homologous recombination (NAHR) and non-homologous end joining (NHEJ), seem to be relevant for the occurrence of chromosomal rearrangements in humans.

Non-allelic homologous recombination is a form of homologous recombination that is responsible for the generation of the majority of recurrent rearrangements in the human genome (Gu, 2008). Such rearrangemets span the same genomic interval and are found in multiple individuals. NAHR occurs between low copy repeats (LCRs), which are blocks of DNA that show more than 95% sequence identity over at least 1 kb, but are not alleles (Gu, 2008). The alignment of two non-allelic LCRs during mitosis or meiosis followed by the subsequent crossover between them can lead to the generation of genomic rearangements in daughter cells (Gu, 2008). The resulting type of chromosomal rearrangement depends on the localization of both LCRs (whether they are on the same or different chromosomes) and their relative configuration. NAHR between two LCRs located on the same chromosome and in the same orientation leads to the generation of a chromosomal duplication and/or deletion, while NAHR between two LCRs located on the same chromosome but in the opposite orientation leads to invertion of the DNA fragment enclosed between the two LCRs. NAHR between two LCRs located on homologous chromosomes can result in the generation of chromosomal translocation (Gu, 2008). Moreover, exchanges of strands during NAHR tend to cluster in domains termed hotspots that are located within the LCRs. These hotspots are thought to be capable of inducing double-strand breaks (DSBs) (Gu, 2008).

Non-homologous end joining is one of the mechanisms involved in the repair of double-strand breaks in DNA and is also thought to be used in rejoining translocated chromosomes in cancer (Gu, 2008). NHEJ occurs between two DNA sequences that usually show only a very short homology (microhomology) (Gu, 2008). Such microhomologies are frequently present as single-stranded overhangs on both ends of the DSB. NHEJ consists of the detection of DSBs, bringing both ends of the break in close proximity, and modification of the broken DNA overhangs in such a way that they can be

subsequently ligated (Gu, 2008). Interestingly, many of the DSBs that are repaired by NHEJ occur within repetitive elements, including LTRs, long interspersed elements (LINEs) and *Alu* sequences, and in close proximity of particular DNA sequences, such as TTTAAA, that are thought to be capable of causing DSBs (Gu, 2008).

1.4 MODELLING HUMAN CHROMOSOMAL DELETIONS IN MICE

In order to make genotype-phenotype correlations and to get a better insight into the development and pathophysiology of human diseases that are caused by chromosomal deletions, as well as to facilitate the discovery of causative genes that are involved in these pathologies, different mouse models carrying defined chromosomal deletions have been successfully developed (Cattanach 1992; Jiang 1998; Yang 1998; Kimber 1999; Lindsay 1999; Tsai 1999; Puech 2000; Lindsay 2001; Merscher 2001; Walz 2003; Walz 2003; Yan 2004; Bi 2005; Ding 2005; Skryabin 2007; Li 2009).

1.4.1 DiGEORGE SYNDROME MOUSE MODELS

1.4.1.1 DiGEORGE SYNDROME

DiGeorge syndrome (DGS) is named after Dr Angelo DiGeorge who in 1968, described a group of infants with thymic aplasia, congenital hypoparathyroidism, hypocalcaemia, and immune deficiency (DiGeorge 1968). In addition, patients with DGS also show congenital cardiovascular anomalies, craniofacial abnormalities (receding or abnormally small jaw, widely spaced eyes, broad nasal root, midface hypoplasia, cleft palate (overt or submucosal), external ear anomalies), and behavioural defects. However, clinical symptoms in patients diagnosed with DGS show variable expressivity and severity (Linday 2001). DiGeorge syndrome is caused by a microdeletion of the 22q11 region, and together with velocardiofacial syndrome (VCFS) and conotruncal anomaly face syndrome, is classified as the ‘22q11 syndrome’

(Linday 2001). A deletion of a 3 Mb of the 22q11 region encompassing 30 genes is detected in approximately 90% of DGS patients, while a deletion of a 1.5 Mb of the 22q11 region encompassing 24 genes is detected in the remaining individuals (Linday 2001).

1.4.1.2 DiGEORGE SYNDROME (DGS) MOUSE MODELS

So far a few mouse models carrying deletions spanning different fragments of the A3 region of mouse chromosome 16 syntenic to the human 22q11 region have been developed (Kimber 1999; Lindsay 1999; Puech 2000; Lindsay 2001; Merscher 2001) (**Figure 1.5**). Each has been summarized in **Table 1.1** and will be discussed below in more detail.

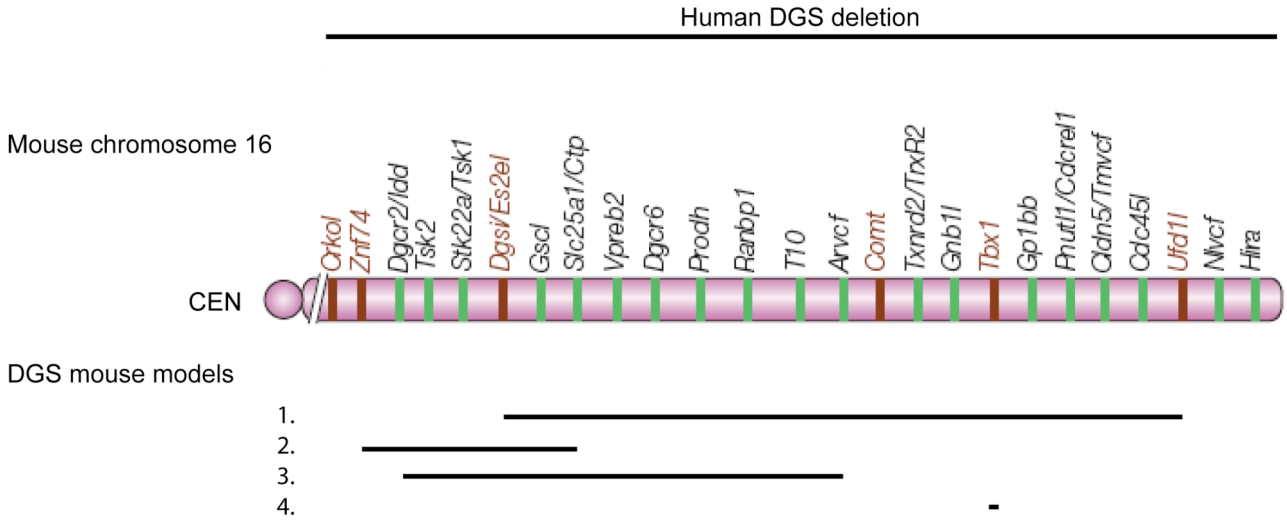

Figure 1.5. DGS mouse models that have been generated to date. Figure modified from Lindsay, 2001.
Legend: 1. Mouse model heterozygous for *Es2–Ufd1l* (*Df1* mouse model) (Lindsay 1999); 2. Mouse model heterozygous for *Znf74l–Ctp* (Kimber 1999); 3. Mouse model heterozygous for *Idd–Arvcf* (Puech 2000); 4. Mouse model heterozygous for*Tbx1* (Lindsay 2001; Merscher 2001).

Table 1.1. Brief summary of DGS mouse models that have been generated to date.

Clinical symptoms observed in humans with DGS	Mouse model heterozygous for *Es2–Ufd1l* (Lindsay 1999)	Mouse model heterozygous for *Znf74l–Ctp* (Kimber 1999)	Mouse model heterozygous for *Idd–Arvcf* (Puech 2000)	Mouse model heterozygous for*Tbx1* (Lindsay 2001; Merscher 2001)
Congenital cardiovascular abnormalities	+	-	-	+
Craniofacial abnormalities	-	-	-	Not reported
Thymic aplasia	-	-	-	Not reported
Behavioural problems	Not reported	+	Not reported	Not reported
Congenital hypoparathyroidism	-	-	-	Not reported
Hypocalcaemia	-	-	Not reported	Not reported
Immune deficiency	-	-	Not reported	Not reported

The first mouse model of DGS (*Df1*) carried a deletion of a 1.2 Mb of mouse chromosome 16, encompassing 22 genes, from *Es2* to *Ufd1l*, and was generated using chromosome engineering (Lindsay 1999) (**Figure 1.5**). Eighteen of these genes were homologous to genes deleted in patients carrying a 1.5 Mb deletion of the 22q11 region. Monosomic *Df1* mice (mice carrying a heterozygous deletion of the *Es2–Ufd1l* region) showed cardiovascular abnormalities, including an interrupted aortic arch type B, a ventricular septal defect and an aberrant right subclavian, similar to those diagnosed in human patients with DiGeorge syndrome. In order to test if haploinsufficiency of a gene (or genes) within the deleted region had a causative impact on the development of heart defects, a monosomic *Df1* deletion was genetically complemented with a reciprocal *Dp1* duplication in mice to restore a normal level of gene expression. The resulting mice were devoid of cardiovascular abnormalities, confirming that a gene (or genes) located within the *Df1* region is important in heart development.

The second mouse model of DGS carried a deletion of around 150 kb of mouse chromosome 16, encompassing 7 genes, from *Znf74l* to *Ctp*, and was generated using conventional replacement gene targeting techniques

(Kimber 1999) (**Figure 1.5**). Monosomic mice (mice carrying a heterozygous deletion of the *Znf74l–Ctp* region) did not display any cardiovascular abnormalities or other phenotypic anomalies observed in human patients with DiGeorge syndrome, but showed an increased prepulse inhibition of the startle response resembling reduced sensomotor gating observed in human patients with schizophrenia. Interestingly, 3 out of 7 genes deleted in these monosomic mice were shared with the monosomic *Df1* mice. This allowed exclusion of these 3 genes, namely *Idd*, *Tsk1* and *Tsk2*, as potential candidate genes for heart development as monosomic mice for the *Znf74l–Ctp* region did not show any cardiovascular defects observed in the monosomic *Df1* mice (Lindsay 1999).

The third mouse model of DGS carried a 550 kb deletion of mouse chromosome 16, encompassing 16 genes from *Idd* to *Arvcf*, and was generated using chromosome engineering (Puech 2000) (**Figure 1.5**). Monosomic mice (mice carrying a heterozygous deletion of the *Idd–Arvcf* region) did not show any cardiovascular defects or other phenotypic abnormalities diagnosed in human patients with DiGeorge syndrome. Interestingly, 13 out of 16 genes deleted in these monosomic mice were shared with the monosomic *Df1* mice. This allowed excluding these 13 genes (including e.g. *Idd*, *Tsk1* and *Tsk2* genes; see above (Kimber 1999)) as potential candidate genes for heart development, as monosomic mice for the *Idd–Arvcf* region did not display any cardiovascular defects, indicating that a candidate gene (or genes) responsible for the cardiovascular abnormalities must lie in the remaining 9 genes deleted in the monosomic *Df1* mice (Lindsay 1999).

Furthermore, the candidate gene approach led to the exclusion of two other genes, namely *Comt* and *Ufd1l*, as mice with mutations in these genes did not show any cardiovascular abnormalities (Puech 2000), while clinical data obtained from human patients identified with mutations in the *GP1Bb* gene allowed the exclusion of the *Gp1bb* gene as a candidate gene for heart development, as individuals with the mutation in the *GP1Bb* gene did not develop any cardiac defects (Puech 2000).

To identify which of the remaining 6 genes were responsible for the development of cardiovascular abnormalities present in human patients with DiGeorge syndrome, a series of genomic DNA fragments-rescue experiments was carried out (Lindsay 2001; Merscher 2001). This led to the identification of a critical region encompassing 4 genes (*Gnb1l, Tbx1, Gp1bb* and *Pnutl1*) that was sufficient to correct the cardiovascular abnormalities (Lindsay 2001; Merscher 2001). Finally, the T-box 1 (*Tbx1*) gene was selected for 'knocking out' because of its high expression in the pharyngeal arches and thus potentially important function in development of the heart (Lindsay 2001; Merscher 2001) (**Figure 1.5**). Indeed, mice carrying a heterozygous null mutation in the *Tbx1* gene displayed cardiovascular abnormalities identical to those observed in the monosomic *Df1* mice (Lindsay 1999), thus providing convincing evidence that haploinsufficiency of the *Tbx1* gene is responsible for cardiovascular defects observed in patients with DiGeorge syndrome (Lindsay 2001; Merscher 2001).

1.4.2 PRADER-WILLI SYNDROME AND ANGELMAN SYNDROME MOUSE MODELS

1.4.2.1 PRADER-WILLI SYNDROME AND ANGELMAN SYNDROME

Prader-Willi syndrome (PWS) is named after Professors Andrea Prader and Heinrich Willi who in 1956, described a group of children with short stature, growth retardation, obesity, small hands, and intellectual disability (Prader 1956). In addition, patients with PWS also show feeding difficulties and a failure to thrive during infancy, hypotonia, facial abnormalities (narrow bifrontal diameter, almond-shaped eyes, triangular mouth), hypogonadism and behavioural problems. The most common cause of PWS is a microdeletion within the paternal copy of the 15q11–q13 region (detected in about 70% of PWS cases), followed by a maternal uniparental disomy, imprinting defects (the paternal chromosome carries a maternal imprint) or chromosome translocations involving the paternal copy of the 15q11–q13 region (Buiting 2010). None of the genes mapped within the 15q11–q13

region have been found to be mutated in individuals with PWS, suggesting that PWS might be a continuous syndrome, in which loss of two or more paternally expressed genes act together to cause the PWS phenotype (Buiting 2010). Indeed, both microdeletions of the paternal 15q11–q13 region encompassing the *SNRPN* gene and microdeletions encompassing the paternally expressed *SNORD116* (*MBII-85*/*Pwcr1*) snoRNAs (small nucleolar RNAs, which are processed from the paternally expressed *SNURF–SNRPN* sense/*UBE3A* antisense transcript) have been detected in some individuals with PWS, suggesting that the deficiency of either the *SNRPN* gene or the *SNORD116* snoRNAs is responsible for the development of clinical features observed in patients with PWS (Buiting 2010). However, identification of balanced translocations that did not affect the expression of the *SNURF–SNRPN* gene, but separated the *SNORD116* snoRNAs from its promoter in patients with PWS allowed the exclusion of the *SNURF–SNRPN* as a candidate gene, providing further evidence that the deletion of the *SNORD116* snoRNAs was responsible for the development of the PWS phenotype in affected individuals (Buiting 2010).

Angelman syndrome (AS) is named after Dr Harry Angelman who in 1965, described a group of children with facial abnormalities, protruding tongues, and excessive laughter. Patients with AS also display microcephaly, profound intellectual disability, absence of speech, seizures, ataxic gait, and sleeping disorders. The most common cause of AS is a microdeletion within the maternal copy of the 15q11–q13 region (detected in about 70% of AS cases), followed by mutations in a maternal copy of the *UBE3A* gene, a paternal uniparental disomy, imprinting defects (the maternal chromosome carries a paternal imprint) or chromosome translocations involving the maternal copy of 15q11–q13 region (Buiting 2010). The loss of function of the maternally expressed *UBE3A* gene is now commonly accepted to be responsible for the development of clinical manifestations observed in patients with AS (Buiting 2010).

1.4.2.2 PRADER-WILLI SYNDROME (PWS) MOUSE MODELS

To date, a few mouse models for PWS have been developed. These models carried either a maternal duplication of the central fragment of the C region of mouse chromosome 7 syntenic to the human 15q11–q13 region or a paternal deletion spanning the C region of mouse chromosome 7 syntenic to the human 15q11–q13 region (Cattanach 1992; Yang 1998; Tsai 1999; Ding 2005; Skryabin 2007) (**Figure 1.6**). Each has been summarized in **Table 1.2** and will be discussed below in more detail.

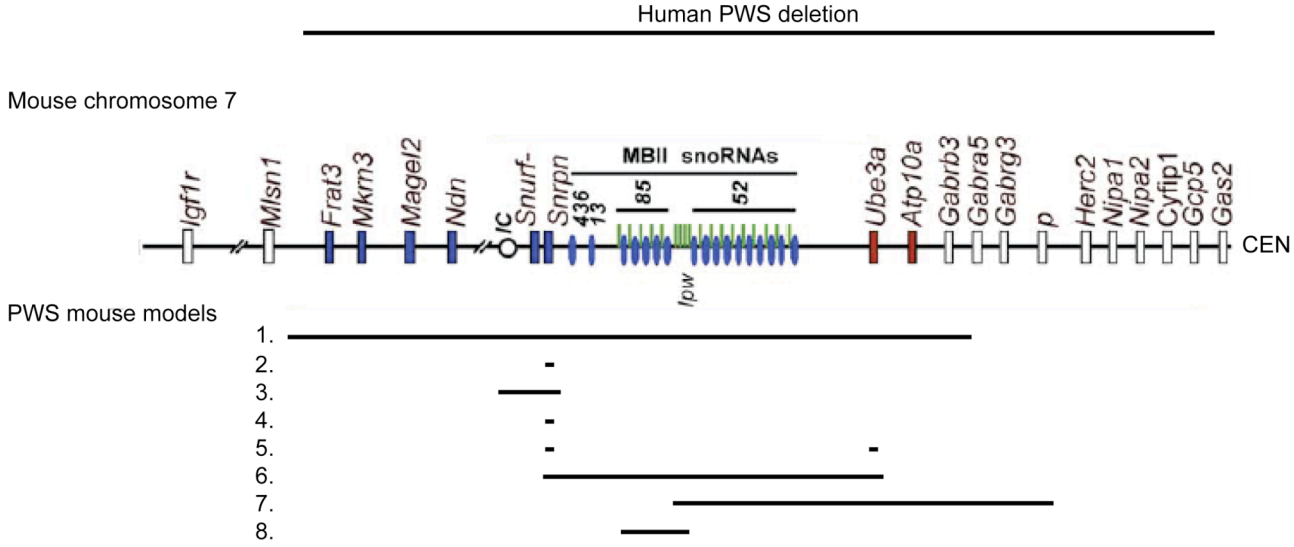

Figure 1.6. PWS mouse models that have been generated to date. Paternally, maternally, and biparentally expressed genes are labelled blue, red, and white, respectively. Figure modified from Skryabin *et al*., 2007.
Legend: 1. Mouse model carrying a maternal uniparental disomy of the central fragment of the C region of mouse chromosome 7 (Cattanach 1992); 2. Mouse model carrying a small intragenic deletion in the paternal copy of the *Snrpn* gene (Yang 1998); 3. Mouse model carrying a deletion of the paternal region of mouse chromosome 7 spanning the *Snrpn* gene and the distal portion of the putative mouse imprinting centre (IC) (Yang 1998); 4. Mouse model carrying a deletion of the exon 2 in the paternal copy of the *Snrpn* gene (Tsai 1999); 5. Mouse model targeted both for a deletion of the exon 2 in the paternal copy of the *Snrpn* gene and a deletion of the paternal copy of the *Ube3a* gene (Tsai 1999); 6. Mouse model carrying a deletion of the paternal region of mouse chromosome 7 from *Snrpn* to *Ube3a* inclusively (Tsai 1999); 7. Mouse model carrying a deletion of the paternal region of mouse chromosome 7 from the pink-eyed dilution (p) locus to undefined breakpoint between the *Snrpn* and *Ube3a* genes (Ding 2005); 8. Mouse model carrying a deletion spanning the paternal region of mouse chromosome 7 encompassing the *SNORD116* (*MBII-85*/*Pwcr1*) snoRNAs and exons A to C of the *Ipw* locus (Skryabin 2007).

Table 1.2. Brief summary of PWS mouse models that have been generated to date.

Clinical symptoms observed in humans with PWS	(1) First PWS mouse model (Cattanach 1992)	(2) Second PWS mouse model (Yang 1998)	(3) Third PWS mouse model (Yang 1998)	(4) Fourth PWS mouse model (Tsai 1999)
Intellectual disability	Not reported	Not reported	Not reported	Not reported
Behavioural problems	Not reported	Not reported	Not reported	Not reported
Feeding difficulties/ failure to thrive during infancy	+	-	+	-
Growth retardation/ short stature	+	-	+	-
Hypotonia	-	-	+	-
Hypogonadism	Not reported	-	-	-
Facial abnormalities	-	-	-	-
Obesity	Not reported	-	Not reported	-
Additional features not observed in humans with PWS			Unable to support themselves on their hind legs	

Legend: (1) First PWS mouse model carried a maternal uniparental disomy of the central fragment of the C region of mouse chromosome 7. (2) Second PWS mouse model carried a small intragenic deletion in the paternal copy of the *Snrpn* gene. (3) Third PWS mouse model carried a deletion of the paternal region of mouse chromosome 7 spanning the *Snrpn* gene and the distal portion of the putative mouse imprinting centre (IC). (4) Fourth PWS mouse model carried a deletion of the exon 2 in the paternal copy of the *Snrpn* gene.

Table 1.2 continued. Brief summary of PWS mouse models that have been generated to date.

Clinical symptoms observed in humans with PWS	(5) Fifth PWS mouse model (Tsai 1999)	(6) Sixth PWS mouse model (Tsai 1999)	(7) Seventh PWS mouse model (Ding 2005)	(8) Eight PWS mouse model (Skryabin 2007)
Intellectual disability	Not reported	Not reported	Not reported	Not reported
Behavioural problems	Not reported	Not reported	Not reported	Not reported
Feeding difficulties/ failure to thrive during infancy	-	+	-	+
Growth retardation/ short stature	-	+	-	+
Hypotonia	-	+	-	-
Hypogonadism	-	-	Not reported	-
Facial abnormalities	-	-	-	-
Obesity	-	-	-	-
Additional features not observed in humans with PWS		Decreased movements; impaired righting ability		

Legend: (5) Fifth PWS mouse model was targeted both for a deletion of the exon 2 in the paternal copy of the *Snrpn* gene and a deletion of the paternal copy of the *Ube3a* gene. (6) Sixth PWS mouse model carried a deletion of the paternal region of mouse chromosome 7 from *Snrpn* to *Ube3a* inclusively. (7) Seventh PWS mouse model carried a deletion of the paternal region of mouse chromosome 7 from the pink-eyed dilution (p) locus to undefined breakpoint between the *Snrpn* and *Ube3a* genes. (8) Eight PWS mouse model carried a deletion spanning the paternal region of mouse chromosome 7 encompassing the *SNORD116* (*MBII-85*/*Pwcr1*) snoRNAs and exons A to C of the *Ipw* locus.

The first mouse model of PWS carried a maternal uniparental disomy of the central fragment of the C region of mouse chromosome 7, and was generated by intercrossing heterozygous mice carrying reciprocal translocations (Cattanach 1992) (**Figure 1.6**). Mice with disomy died in early infancy, presumably due to suckling problems, which phenocopies the feeding difficulties observed in infants with PWS. However, considering that a large number of genes are located within the region of the maternal uniparental disomy, it was not possible to assign an observed phenotype to any particular gene.

The second mouse model of PWS carried a small intragenic deletion in the paternal copy of the *Snrpn* gene, and was generated using homologous

recombination (Yang 1998) (**Figure 1.6**). Mice with the heterozygous *Snrpn* deletion were viable and did not display any phenotypic abnormalities, suggesting that the deletion of the *Snrpn* gene is not sufficient to cause the PWS phenotype.

The third mouse model carried a deletion of the paternal region of mouse chromosome 7 spanning the *Snrpn* gene and the distal portion of the putative mouse imprinting centre (IC), and was generated using homologous recombination (Yang 1998) (**Figure 1.6**). The genomic sequence of the putative mouse IC was also encompassed into the engineered deletion because the human IC appears to control genomic imprinting of six paternally expressed transcripts that have been mapped to the human PWS/AS region (*SNRPN, ZNF217, NDN, IPW, PAR1, PAR5*), and deletions of the distal part of the IC have been reported in individuals with PWS (Yang 1998). Indeed, this deletion affected the imprinting of the region, as mice with this deletion lacked the transcription of the genes normally solely expressed from the paternal 15q11–q13 region, including *Zfp127*, *Ndn* and *Ipw*. At birth, monosomic mice (mice carrying a heterozygous deletion of the *Snrpn* gene and distal IC fragment) were underweight, slightly hypotonic and unable to support themselves on their hind legs, but otherwise normal. However, all of these monosomic mice died in early infancy (the majority died within first 72 hours) due to feeding difficulties and a failure to thrive that resembled observations from infants with PWS. As none of the monosomic mice survived till weaning, it was not possible to assess whether these mice would develop other symptoms observed in PWS patients, including hypogonadism or obesity later in their life.

The fourth mouse model of PWS carried a deletion of the exon 2 in either the paternal copy of the *Snrpn* gene, and was generated using chromosome engineering (Tsai 1999) (**Figure 1.6**). Importantly, this deletion did not affect the imprinting of the region. Mice with the deletion (heterozygous and homozygous) were viable and did not display any phenotypic abnormalities, suggesting that the deletion of the exon 2 of the *Snrpn* gene is not sufficient to cause the PWS phenotype.

The fifth mouse model of PWS was targeted both for a deletion of the exon 2 in the paternal copy of the *Snrpn* gene and a deletion of the paternal

copy of the *Ube3a* gene, and was generated using chromosome engineering (Tsai 1999) (**Figure 1.6**). Mice double-targeted for the *Snrpn* and *Ube3a* genes on the paternal chromosome were viable and did not display any phenotypic abnormalities, thus suggesting that a paternal deletion of the *Ube3a* gene is not important in the development of PWS manifestations.

The sixth mouse model of PWS carried a deletion of the paternal region of mouse chromosome 7 from *Snrpn* to *Ube3a* inclusively, and was generated using chromosome engineering (Tsai 1999) (**Figure 1.6**). Importantly, this deletion did not affect the imprinting of the genes located outside the deleted region. Monosomic pups (pups carrying a heterozygous deletion of the paternal *Snrpn–Ube3a* region) were underweight, showed hypotonia, decreased movements and inadequate feeding. The lethality during infancy and early adulthood was highly increased (80% of mice died before weaning), presumably due to failure to thrive. The monosomic mice that survived beyond weaning were fertile and did not develop obesity. Although the deficiency of a paternally expressed gene (or genes) in the *Snrpn–Ube3a* region is responsible for recapitulation of some PWS symptoms, the lack of other PWS manifestations, including hypogonadism and obesity, suggests the existence of significant developmental differences between mice and humans, as human PWS patients carrying a deletion within the *SNRPN–UBE3A* region displayed both hypogonadism and obesity (Buiting 2010).

The seventh mouse model of PWS (P^{30PUb}) carried a deletion of the paternal region of mouse chromosome 7 from the pink-eyed dilution (p) locus to an undefined breakpoint between the *Snrpn* and *Ube3a* genes, and was generated by ^{239}Pu citrate radiation (Ding 2005) (**Figure 1.6**). Monosomic P^{30PUb} mice were viable and did not display any phenotypic abnormalities. Further defining of the distal P^{30PUb} deletion breakpoints showed that the entire *SNORD115* (*MBII-52*) snoRNAs and *Ipw* locus, but not the *SNORD116* (*MBII-85*/*Pwcr1*) snoRNAs, were encompassed in the deletion region, suggesting that a gene (or genes) associated with the manifestation of the PWS phenotype is mapped between the *Snrpn* and *SNORD115* (*MBII-52*) snoRNAs, thus providing further evidence (in addition to currently available data for human patients with PWS; see above (Buiting 2010)) that the

deficiency of the *SNORD116* snoRNAs is responsible for the development of PWS symptoms.

The eighth mouse model of PWS (*PWScr*) carried a deletion spanning the paternal region of mouse chromosome 7 encompassing the *SNORD116* (*MBII-85*/*Pwcr1*) snoRNAs and exons A to C of the *Ipw* locus, and was generated using chromosome engineering (Skryabin 2007) (**Figure 1.6**). Monosomic *PWScr* pups (pups carrying a heterozygous deletion of the *SNORD116* and proximal part of the *Ipw* locus) were smaller than controls. They displayed postnatal growth retardation from a week of age due to poor feeding, but in contrary to the monosomic mice for the paternal *Snrpn–Ube3a* region (Tsai 1999), they showed only 15% postnatal lethality, thus suggesting that although the deficiency of *SNORD116* (*MBII-85*/*Pwcr1*) snoRNAs seems to be responsible for feeding difficulties, a gene (or genes) located between the *Snrpn* and *SNORD116* (*MBII-85*/*Pwcr1*) snoRNAs is causative for highly increased neonatal lethality in the monosomic mice for the paternal *Snrpn–Ube3a* region. Monosomic *PWScr* mice were fertile and did not develop obesity up to a year of age, but continued to be underweight compared to controls. This was in agreement with phenotypic observation in the monosomic mice for the paternal *Snrpn–Ube3a* region, which were also fertile and non-obese (Tsai 1999), and provided further evidence of the existence of significant developmental differences between mice and humans, as human PWS patients carrying a deletion within the *SNRPN–UBE3A* region, including deletions of only *SNORD116* (*MBII-85*/*PWCR1*) snoRNAs, displayed both hypogonadism and obesity (Buiting 2010).

1.4.2.3 ANGELMAN SYNDROME (AS) MOUSE MODELS

To date, a few mouse models for AS have been developed. These models carried either a paternal duplication of the central fragment of the C region of mouse chromosome 7 syntenic to the human 15q11–q13 region or a maternal deletion spanning the C region of mouse chromosome 7 syntenic to the human 15q11–q13 region (Cattanach 1992; Jiang 1998; Tsai 1999; Ding 2005) (**Figure 1.7**). Each has been summarized in **Table 1.3** and will be discussed below in more detail.

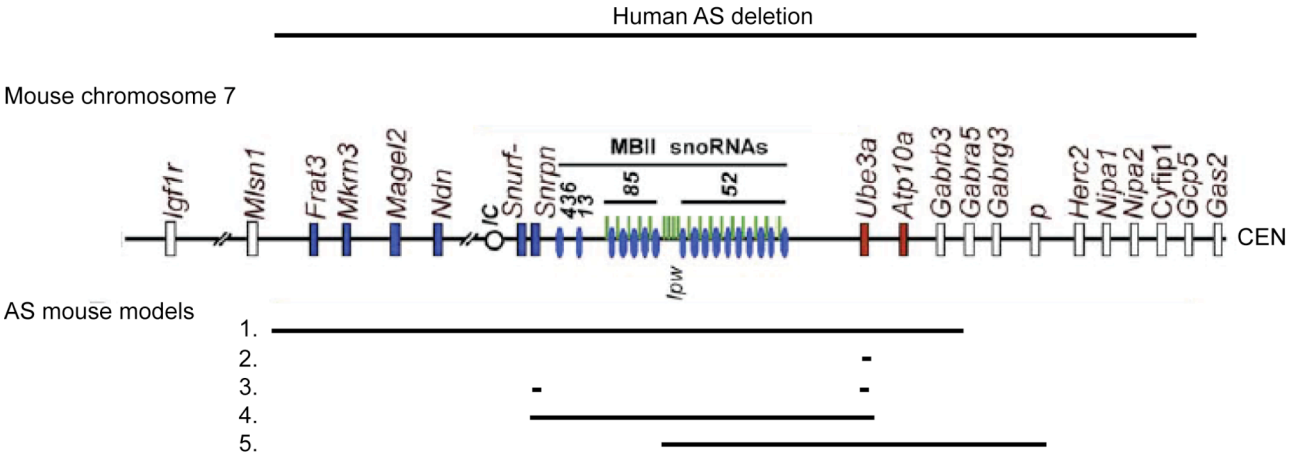

Figure 1.7. AS mouse models that have been generated to date. Paternally, maternally, and biparentally expressed genes are labelled blue, red, and white, respectively. Figure modified from Skryabin *et al*., 2007.
Legend: 1. Mouse model carrying one paternal and two maternal copies of the central fragment of the C region of mouse chromosome 7 (Cattanach 1992); 2. Mouse model carrying a null mutation in the maternal copy of the *Ube3a* gene (Jiang 1998); 3. Mouse model targeted both for a deletion of the exon 2 in the maternal copy of the *Snrpn* gene and a deletion of the maternal copy of the *Ube3a* gene (Tsai 1999); 4. Mouse model carrying a deletion of the maternal region of mouse chromosome 7 from *Snrpn* to *Ube3a*, inclusively (Tsai 1999); 5. Mouse model carrying a deletion of the maternal region of mouse chromosome 7 from the pink-eyed dilution (p) locus to undefined breakpoint between *Snrpn* and *Ube3a* genes (Ding 2005).

Table 1.3. Brief summary of AS mouse models that have been generated to date.

Clinical symptoms observed in humans with AS	(1) First AS mouse model (Cattanach 1992)	(2) Second AS mouse model (Jiang 1998)	(3) Third AS mouse model (Tsai 1999)	(4) Fourth AS mouse model (Tsai 1999)	(5) Fifth AS mouse model (Ding 2005)
Intellectual disability	Not reported	+	Not reported	Not reported	Not reported
Behavioural problems	Not reported	Not reported	Not reported	Not reported	Not reported
Facial abnormalities	Not reported	-	Not reported	Not reported	Not reported
Seizures	Not reported	+	Not reported	Not reported	Not reported
Sleeping disorder	Not reported	Not reported	Not reported	Not reported	Not reported
Ataxic gait	Not reported	-	Not reported	Not reported	Not reported
Microcephaly	Not reported	-	Not reported	Not reported	Not reported
Additional features not observed in humans with AS	Shorter tail length; growth retardation; failure to thrive	Motor impairment; reduction in skeletal size and overall body and brain weight			High-fat diet-induced obesity

Legend: (1) First AS mouse model carried one paternal and two maternal copies of the central fragment of the C region of mouse chromosome 7. (2) Second AS mouse model carried a null mutation in the maternal copy of the *Ube3a* gene. (3) Third AS mouse model was targeted both for a deletion of the exon 2 in the maternal copy of the *Snrpn* gene and a deletion of the maternal copy of the *Ube3a* gene. (4) Fourth AS mouse model carried a deletion of the maternal region of mouse chromosome 7 from *Snrpn* to *Ube3a*, inclusively. (5) Fifth AS mouse model carried a deletion of the maternal region of mouse chromosome 7 from the pink-eyed dilution (p) locus to undefined breakpoint between *Snrpn* and *Ube3a* genes.

The first mouse model of AS carried one paternal and two maternal copies of the central fragment of the C region of mouse chromosome 7, and was generated by intercrossing heterozygous mice carrying reciprocal translocations (Cattanach 1992) (**Figure 1.7**). These mice were smaller and showed reduced viability compared to controls. However, as the cause of their failure to thrive was not determined, it was not possible to speculate if these model recapitulated any aspects of AS.

The second mouse model of AS carried a null mutation in the maternal copy of the *Ube3a* gene, and was generated using chromosome engineering (Jiang 1998) (**Figure 1.7**). Mice with the *Ube3a* mutation displayed many symptoms observed in human patients with AS, including inducible seizures,

context-dependent learning dysfunction, behavioural defects, motor impairment, and reduction in skeletal size and brain weight.

The third mouse model of AS was targeted both for a deletion of the exon 2 in the maternal copy of the *Snrpn* gene and a deletion of the maternal copy of the *Ube3a* gene, and was generated using chromosome engineering (Tsai 1999) (**Figure 1.7**). Mice double-targeted for the *Snrpn* and *Ube3a* genes on the maternal chromosome were viable and were predicted to develop phenotypic abnormalities similar to those observed in mice carrying a null mutation in the *Ube3a* gene (Jiang 1998), though this was not assessed.

The fourth mouse model of AS carried a deletion of the maternal region of mouse chromosome 7 from *Snrpn* to *Ube3a* inclusively, and was generated using chromosome engineering (Tsai 1999) (**Figure 1.7**). Importantly, this deletion did not affect the imprinting of the genes located outside the deleted region. Monosomic mice (mice with carrying a heterozygous deletion of the maternal *Snrpn–Ube3a* region) were viable and did not show increased lethality. They were predicted to develop phenotypic abnormalities potentially resembling those observed in mice carrying a null mutation in the *Ube3a* gene (Jiang 1998), though this was not assessed.

The fifth mouse model of AS (P^{30PUb}) carried a deletion of the maternal region of mouse chromosome 7 from the pink-eyed dilution (p) locus to an undefined breakpoint between *Snrpn* and *Ube3a* genes, and was generated by ^{239}Pu citrate radiation (Ding 2005) (**Figure 1.7**). Monosomic P^{30PUb} mice were viable but developed obesity when fed on a high-fat diet due to the deletion of the *Atp10c* gene (a high-fat diet-induced obesity has been previously associated with the lack of the *Atp10c* expression), and were predicted to develop phenotypic abnormalities similar to those observed in mice carrying a null mutation in the *Ube3a* gene (Jiang 1998), as further defining of the distal P^{30PUb} deletion breakpoints showed that the *Ube3a* gene was encompassed in the deletion region, though this was not assessed.

1.4.3 SMITH-MAGENIS SYNDROME MOUSE MODELS

1.4.3.1 SMITH-MAGENIS SYNDROME

Smith-Magenis syndrome (SMS) is named after Drs Ann C. M. Smith and R. Ellen Magenis who in 1986, first described a group of children with brachycephaly, midface hypoplasia, prognathism, hoarse voice, speech delay with or without hearing loss, intellectual disability, growth impairment, and behavioural difficulties (Smith 1986). In addition to this, patients with SMS are also diagnosed with skeletal, eye, heart and kidney abnormalities, sleep disturbance, seizures, teenager and adult obesity, reduced pain and temperature perception, hypotonia, and chronic ear infections. The most common cause of SMS is an interstitial microdeletion of the 17p11.2 region, encompassing the retinoic acid-induced 1 (*RAI1*) gene (detected in about 90% of SMS cases), followed by mutations in the *RAI1* gene (detected in remaining 10% of SMS cases) (Elsea 2008). Approximately a 3.7 Mb deletion of the 17p11.2 region mediated through non-allelic homologous recombination between flanking low-copy repeats is detected in approximately 70% of SMS deletion patients. The remaining deletion SMS patients carry deletions spanning smaller or larger fragments of the 17p11.2 region derived from either alternative low-copy repeats or non-homologous recombination (Elsea 2008). Analysis of SMS patients carrying deletions spanning smaller fragments of the 17p11.2 region led to an identification of the SMS critical region (SMCR). Further analysis of the genes mapped within the SMCR in SMS individuals in whom the deletion of the 17p11.2 region was not detected resulted in identification of mutations within exon 3 of the *RAI1* gene, suggesting that haploinsufficiency of the *RAI1* gene is responsible for the development of the most typical clinical manifestations observed in SMS patients. However, other genes located within the SMCR are believed to modify the variability and degree of severity of SMS symptoms (Elsea 2008). Interestingly, patients carrying the reciprocal duplication of the 17p11.2 region have also been identified. However, the patients with 17p11.2 duplication display less severe symptoms than patients with SMS deletion, as there are observed only with

mild to borderline intellectual disability, and some behavioural abnormalities (Walz 2003).

1.4.3.2 SMITH-MAGENIS SYNDROME (SMS) MOUSE MODELS

So far a few mouse models carrying deletions spanning different fragments of the region of mouse chromosome 11 syntenic to the human 17p11.2 region have been developed (Walz 2003; Walz 2003; Yan 2004; Bi 2005) (**Figure 1.8**). Each has been summarized in **Table 1.4** and will be discussed below in more detail.

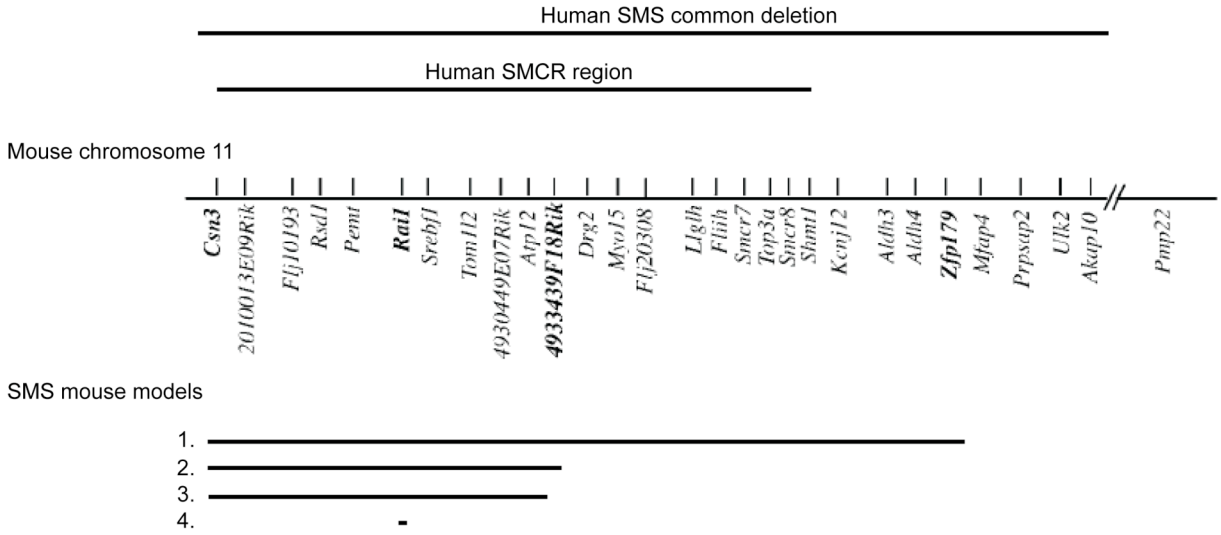

Figure 1.8. SMS mouse models that have been generated to date. Figure modified from Yan *et al*., 2004.
Legend: 1. *Df(11)17* mouse model (mouse model heterozygous for *Csn3–Zfp*) (Walz 2003; Walz 2003); 2. *Df(11)17-1* mouse model (Yan 2004); 3. *Df(11)17-2* mouse model (Yan 2004); 4. *Df(11)17-3* mouse model (Yan 2004); 5. Mouse model heterozygous for *Rai1* (Bi 2005).

Table 1.4. Brief summary of SMS mouse models that have been generated to date.

Clinical symptoms observed in humans with SMS	*Df(11)17* mouse model (Walz 2003; Walz 2003)	*Df(11)17-1* mouse model (Yan 2004)	*Df(11)17-2* mouse model (Yan 2004)	*Df(11)17-3* mouse model (Yan 2004)	Mouse model heterozygous for *Rai1* (Bi 2005)
Intellectual disability	-	Not reported	Not reported	Not reported	Not reported
Behavioural problems	+	Not reported	Not reported	Not reported	Not reported
Craniofacial abnormalities	+	+	+	+	+
Multiple organ abnormalities	-	-	-	-	Not reported
Seizures	+	-	-	-	Not reported
Hypotonia	Not reported	Not reported	Not reported	Not reported	Not reported
Sleeping disturbance	+	-	-	-	Not reported
Growth impairment	+	Not reported	Not reported	Not reported	+
Chronic ear infections	Not reported	Not reported	Not reported	Not reported	Not reported
Reduced pain and temperature perception	Not reported	Not reported	Not reported	Not reported	Not reported
Obesity	+	+	+	+	+
Additional features not observed in humans with SMS	Male-specific reduced fertility				

The first mouse model (*Df(11)17*) of SMS carried a 2 Mb deletion of mouse chromosome 11, from *Csn3* to *Zfp79* that was syntenic to the genomic interval most commonly deleted in SMS patients, and was generated using chromosome engineering (Walz 2003; Walz 2003) (**Figure 1.8**). Monosomic *Df(11)17* mice (mice carrying a heterozygous deletion of the *Csn3–Zfp79* region) recapitulated some of clinical features observed in SMS patients, including craniofacial abnormalities, growth impairment (up to 1 month of age), seizures, obesity (from 4 months of age), and abnormal circadian rhythm. Moreover, the monosomic *Df(11)17* males were also hypoactive and showed reduced fertility.

The subsequent three monosomic mouse models of SMS (*Df(11)17-1*, *Df(11)17-2* and *Df(11)17-3*) carried different sub-deletions of the genomic interval most commonly deleted in SMS patients (all of which included the *Rai1* gene), and were generated using retrovirual-mediated chromosome

engineering (Yan 2004) (**Figure 1.8**). All three monosomic mouse models displayed craniofacial abnormalities (however, the severity of craniofacial defects was much less pronounced than in the monosomic *Df(11)17* mice (Walz 2003)), and obesity, but did not show seizures or abnormal circadian rhythm. This confirms the existence of the SMCR which contains a gene (or genes), most likely the *Rai1* gene, that are sufficient to cause some of the SMS manifestations (Elsea 2008). However, other genes located within the genomic interval most commonly deleted in SMS patients are likely to both modify the degree of severity of craniofacial abnormalities and obesity and be responsible for the manifestation of other SMS symptoms.

In order to discriminate a role of the *Rai1* gene in the development of SMS phenotypes, including craniofacial abnormalities and obesity, a mouse model carrying a null mutation in the *Rai1* gene was generated using a candidate gene approach (Bi 2005) (**Figure 1.8**). Mice with the heterozygous *Rai1* mutation ($Rai^{+/-}$ mice) showed growth impairment between 4 to 7 weeks of age, were obese from 20 (males) or 23 (females) weeks of age, and showed craniofacial abnormalities similar to those observed both in humans and mice, confirming that a haploinsufficiency of the *Rai1* gene is sufficient to recapitulate some of the SMS phenotypes (Elsea 2008). However, the severity of craniofacial defects in the $Rai^{+/-}$ mice was similar to the monosomic *Df(11)17-1*, *Df(11)17-2* and *Df(11)17-3* mice (Yan 2004), but reduced in comparison to the monosomic *Df(11)17* mice (Walz 2003), further suggesting the influence of other genes located within the genomic interval most commonly deleted in SMS patients on the expressivity of craniofacial abnormalities and the variability of the other SMS manifestations.

In parallel with the generation of the monosomic *Df(11)17* mouse model, a mouse model (*Dp(11)17*) carrying a reciprocal 2 Mb duplication of mouse chromosome 11, from *Csn3* to *Zfp79*, that was syntenic to the genomic interval most commonly deleted in SMS patients was generated using chromosome engineering (Walz 2003). *Dp(11)17/+* mice (mice carrying a duplication of the *Csn3–Zfp79* region) were underweight, but did not display SMS features observed in the monosomic *Df(11)17* mice (Walz 2003), including craniofacial abnormalities, seizures or reduced male fertility. However, the *Dp(11)17/+* males were hyperactive, and showed learning

impairment in the contextual fear conditioning test (Walz 2003). Moreover, analysis of mice carrying both the deletion and reciprocal duplication (*Df(11)17/Dp(11)17*) revealed no apparent phenotypic abnormalities, suggesting that most of SMS abnormalities observed in the *Df(11)17/+* and *Dp(11)17/+* mice result from gene dosage imbalances (Walz 2003).

1.4.4 WILLIAMS SYNDROME MOUSE MODELS

1.4.4.1 WILLIAMS SYNDROME

Williams syndrome (known also as Williams-Beuren syndrome, WBS) is named after Dr J. C. P. Williams who in 1961, described a group of children with supravalvular aortic stenosis, craniofacial abnormalities (short cranial base, flat nasal bridge, periorbital fullness, malar flattening, short up-turned nose with anteverted nostrils, a long flat filtrum, full cheeks, prominent lips, wide mouth, small chin), and intellectual disability (Williams 1961). WBS patients also show weakness of connective tissues, short stature, reduced brain volume, motor impairment, and behavioural difficulties. The most common cause of the WBS is a 1.5 Mb microdeletion of the 7q11.23 region that is mediated through non-allelic homologous recombination between flanking low-copy repeats (Li 2009). This deletion encompasses 25 genes that are predominantly expressed in the brain. The phenotype-genotype correlation has so far been established for only one of these genes, namely the elastin (*ELN*) gene, whose deletion or disruption leads to supravalvular aortic stenosis, and thus is sufficient to cause a cardiac symptom observed in WBS patients (Li 2009).

1.4.4.2 WILLIAMS SYNDROME (WBS) MOUSE MODELS

So far several knock-out mouse models for different genes located within the genomic interval most commonly deleted in WBS patients have been developed (Li 2009). However, most of those mouse models, except for heterozygous *Cyln2* and heterozygous *Gtf2ird1* mouse models, either showed no phenotypical abnormalities or were not analysed (Hoogenraad 2002;

Young 2008; Li 2009) (**Figure 1.9**). Moreover, a few mouse models carrying deletions spanning different fragments of the G2 region of mouse chromosome 5 syntenic to the human 7q11.23 region have been developed (Li 2009) (**Figure 1.9**). Each has been summarized in **Table 1.5** and will be discussed below in more detail.

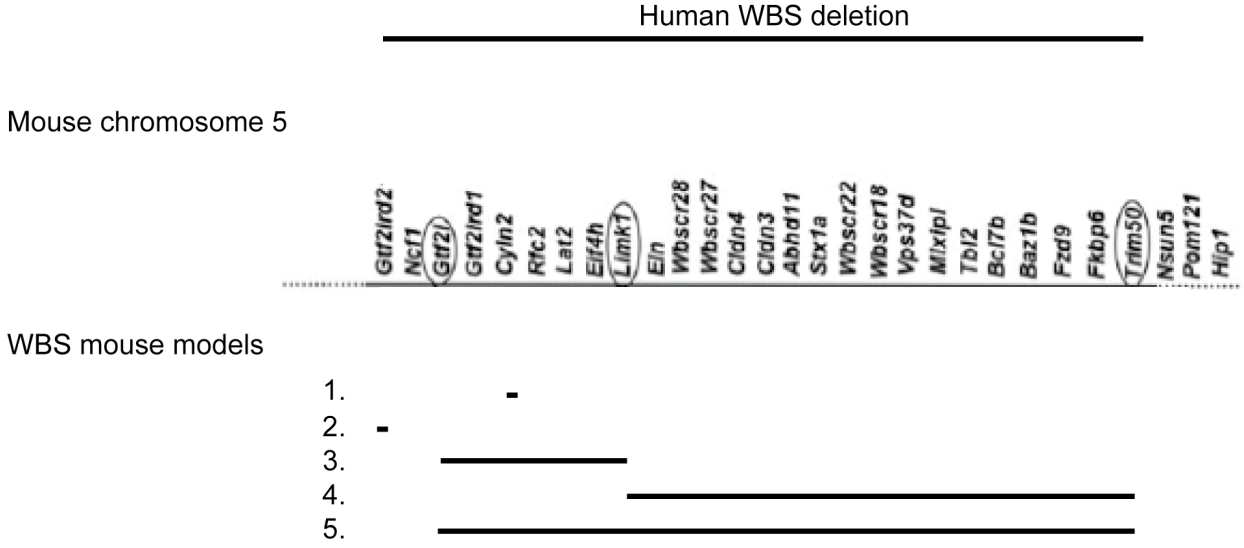

Figure 1.9. WBS mouse models that have been generated to date. Figure modified from Li *et al*., 2009.
Legend: 1. Mouse model heterozygous for *Cyln2* (Hoogenraad 2002); 2. Mouse model heterozygous for *Gtf2ird1* (Young 2008); 3. PD mouse model (mouse model heterozygous for *Gtf2i–Limk1*) (Li 2009); 4. DD mouse model (mouse model heterozygous for *Limk1–Fkbp6*) (Li 2009); 5. PD/DD mouse model mouse model heterozygous for *Gtf2i– Fkbp6*) (Li 2009).

Table 1.5. Brief summary of WBS mouse models that have been generated to date.

Clinical symptoms observed in humans with WBS	Mouse model heterozygous for *Cyln2* (Hoogenraad 2002)	Mouse model heterozygous for *Gtf2ird1* (Young 2008)	PD mouse model (Li 2009)	DD mouse model (Li 2009)	PD/DD mouse model (Li 2009)
Cardiovascular abnormalities	Not reported	Not reported	-	-*	-*
Craniofacial abnormalities	-	-	-	+	+
Intellectual disability	+	-	-	+	+
Behavioural problems	+	+	+	-	+
Motor impairment	+	Not reported	+	+	+
Weakness of connective tissues	Not reported	Not reported	-	+	+
Short stature	+	+	+	+	+
Reduced brain volume	-	-	+ (females)	+	+

* Although, monosomic DD and D/P mice did not show any cardiovascular abnormalities upon histopathological examination, significantly decreased anterior abdominal aortic wall motion was observed in both monosomic DD and D/P mice.

Mice carrying a heterozygous deletion of the *Cyln2* gene showed growth and motor deficiency, learning and behavioural impairment, brain anomalies, reduced synaptic plasticity, and hippocampal dysfunction (Hoogenraad 2002) (**Figure 1.9**), while mice with partial deletion of the *Gtf2ird1* gene displayed mild growth impairment and behavioural abnormalities (Young 2008) (**Figure 1.9**).

Two mouse models carrying a complimentary proximal (PD) and distal (DD) monosomic deletion syntenic to the genomic interval most commonly deleted in WBS patients have been generated using chromosome engineering (Li 2009) (**Figure 1.9**). The proximal deletion encompassed the region from *Gtf2i* to *Limk1* inclusively (monosomic PD mice), while the distal deletion spanned the region from *Limk1* to *Fkbp6* inclusively (monosomic DD mice). Also, the double heterozygous mice carrying both the proximal and distal deletion (monosomic D/P mice) (**Figure 1.9**), and thus carrying the deletion syntenic to the entire genomic interval most commonly deleted in WBS patients, were derived (Li 2009). Monosomic PD, DD and D/P mice showed

reduced body weight and impairment in motor skills and coordination. However, monosomic D/P mice displayed more severe growth retardation and more severe abnormalities in motor skills and coordination, suggesting that genes mapped to both PD and DD genomic intervals might be involved in the manifestation of these phenotypes. Monosomic PD and D/P, but not DD mice, showed increased social interest, indicating that genes in the PD region are likely to contribute to the development of increased sociability observed in WBS individuals. Monosomic DD and D/P, but not PD mice, had shorter skulls, showed reduced overall brain weight and learning impairment suggesting that genes in the DD region are likely to be responsible for the development of craniofacial abnormalities, reduced brain weight and intellectual disability observed in WBS patients. Interestingly, the existing genotype-phenotype correlation, suggesting that the deficiency or disruption of the *ELN* gene leads to supravalvular aortic stenosis in humans, has been challenged by monosomic DD and D/P mouse models, and thus by mice carrying deletions encompassing the *Eln* gene, as monosomic DD and D/P mice did not show any cardiovascular abnormalities upon histopathological examination. On the other hand, as significantly decreased anterior abdominal aortic wall motion was observed in both monosomic DD and D/P mice, the contribution of the *Eln* gene to the development of supravalvular aortic stenosis cannot be excluded. Altogether, these three mouse models recapitulated several phenotypes observed in WBS individuals, and helped to narrow down the genomic region, where dosage-sensitive genes responsible for different aspects of WBS can be further searched.

Mouse models have both advantages and disadvantages. On the one hand, the currently existing mouse models carrying defined chromosomal deletions have greatly improved our understanding of the molecular and cellular basis of some human deletion syndromes. They have also helped to identify causal genes responsible for the development of at least some of the clinical manifestations that are observed in patients. For example, a sequential development of mouse models for DiGeorge syndrome led to the identification of the *Tbx1* gene as responsible for cardiovascular abnormalities diagnosed in DGS individuals. Other mouse models helped to narrow down the genomic

intervals within which causative genes contributing to the development of clinical phenotypes identified in humans occur. For example, phenotypic analysis of the PD and DD mouse models of Williams syndrome identified a correlation between increased sociability observed in WBS individuals and the deletion of genes within the PD interval, and established a link between craniofacial abnormalities, reduced brain weight and intellectual disability observed in WBS patients with the deletion of genes mapped within the DD interval.

However, on the other hand, we need to be aware of the limitations that we might encounter when using mice as a model organism. In many instances mouse models recapitulated only a subset of clinical manifestation observed in patients with genomic disorders. For example, hypogonadism and obesity, two cardinal clinical manifestations observed in patients with Prader-Willi syndrome, have never been identified in any of the PWS mouse models, despite the fact that at least eight mouse models of Prader-Willi syndrome, each carrying a different chromosomal rearrangement, have been generated. The inability to recapitulate some of the clinical phenotypes identified in patients with deletion syndromes clearly suggests the existence of significant developmental differences between mice and humans, and thus places certain limitations on the use of mice as a model organism (at least in some cases). Also, we need to be aware that certain phenotypic features that are observed in humans with genomic disorders might be impossible to model or reliably identify in mice. For example, facial abnormalities, such as almond-shaped eyes and triangular mouth observed in PWS patients or full cheeks, prominent lips and wide mouth observed in DGS individuals cannot be reliably modelled in mice due to significant differences in facial appearance between mice and humans.

In some instances several mouse models of the same syndrome have been generated. For example, in PWS syndrome at least eight mouse models were generated. This is for two reasons. Firstly, by initially deleting a large region and then progressively generating models with smaller and smaller deletions, it is possible to narrow down the region within which the causative gene might be found. Secondly, although mouse models may carry the same deletion, they might have a different genetic background, and this could in

some circumstances lead to different manifestations of the clinical phenotypes observed in humans.

Despite the success of mouse models, there are still many questions that remain to be answered. For example, although the relevant gene has been identified in PWS syndrome, the mouse model does not recapitulate many of the clinical manifestations of the human phenotype. Perhaps it would be interesting to model this deletion in another organism, perhaps one closer to humans, which might better capture the observed human phenotype.

To sum up, there are still many human deletion syndromes, such as Sotos syndrome and Monosomy 21 syndrome, which remain to be modelled in mice. The generation of these will hopefully lead to genotype-phenotype correlations and to an increased insight into the development and pathophysiology of these disease phenotypes.

CHAPTER 2

MATERIALS AND METHODS

2.1 MATERIALS

2.1.1 REAGENTS

• PBS (phosphate buffered saline; PAA, cat. #: H15-002)

• BME (β-mercaptoethanol; Sigma-Aldrich, cat. #: M7522)

• Hypoxanthine-aminopterin-thymidine (HAT) supplement (Invitrogen, cat. #: 21060-01)

• Hypoxanthine-thymidine (HT) supplement (Invitrogen, cat. #: 41065-012)

• Trypsin (+ glucose)

0.1 g of ethylenediaminetetraacetic acid (EDTA) (Sigma-Aldrich, cat. #: E5134) and 0.5 g of D-glucose (Sigma-Aldrich, cat. #: G7528) were added to 500 ml of PBS (Invitrogen, cat. #: 14190094). The mixture was sterilised through a 0.2 µm syringe filter. Subsequently 5 ml of chicken serum (Invitrogen, cat. #: 16110082) and 10 ml of 2.5% trypsin were added to the mixture (Invitrogen, cat. #: 15090046) and aliquots were stored at -20ºC.

• GPS (glutamine/penicillin/streptomycin)

58.4 g of glutamine (Amresco, cat. #: 0374-500G), 10 g of streptomycin (Sigma-Aldrich, cat. #: S9137-100G) and 6 g of penicillin (Sigma-Aldrich,

cat. #: P3032-100MU) were added to 2 l of Milli-Q H_2O. The mixture was sterilised through a 0.2 µm syringe filter and aliquots were stored at -20ºC.

• G418 (125 mg/ml)

10 ml of PBS was added to 5 g of geneticin (Invitrogen, cat. #: 11811031). The mixture was diluted to a final volume of 30.8 ml, sterilised through a 0.2 µm syringe filter and aliquots were stored at -20ºC.

• 0.1% gelatin

25 ml of 2% gelatin solution (Sigma-Aldrich, cat. #: G1393) was added to 500 ml of PBS (1x; without magnesium chloride; without calcium chloride – Invitrogen cat #: 14190094).

• M15 medium (was used for no more then 3 weeks due to glutamine & BME lose potency)

90 ml of foetal bovine serum (FBS) (PAA, cat. #: A15-101), 6 ml of GPS and 6 ml of BME (100x stock) were added to 500 ml of high glucose Dulbecco's Modified Eagle Medium (DMEM) (PAA, cat. #: E15-011). If feeder cells were not used, leukaemia inhibiting factor (LIF) was added to M15 medium.

If selection was required:

- for G418:

  0.56 ml of stock G418 (125 mg/ml) was added to obtain a final concentration of 125 µg/ml,

  0.672 ml of stock G418 (125 mg/ml) was added to obtain a final concentration of 150 µg/ml,

  0.784 ml of stock G418 (125 mg/ml) was added to obtain a final concentration of 175 µg/ml,

  0.896 ml stock G418 (125 mg/ml) was added to obtain a final concentration of 200 µg/ml.

- for puromycin

  100 mg of puromycin (Sigma-Aldrich, cat. #: P8833) was added to 33.3 ml of PBS to obtain a final concentration of 3 mg/ml.

All components of M15 medium, except high glucose DMEM and FBS, were sterilised through a 0.2 µm syringe filter. High glucose DMEM was stored at +4°C, while all the components of M15 medium were stored at -20°C.

• M7 feeder culture medium

45 ml of FBS (aliquots were stored in -20°C) and 6 ml of GPS were added to 500 ml of knockout DMEM.

• Freeze medium (was always made fresh before use)

10% FBS and 10% dimethyl sulfoxide (DMSO; Sigma-Aldrich cat #: D2650-100ML) were added to 80% knockout DMEM and the mixture was sterilised through a 0.2 µm syringe filter.

• Hepes/M15 medium

1 ml of 1 M hepes buffer (Invitrogen, cat #: 15630049) was added to 49 ml of M15 medium.

2.2 METHODS

2.2.1 CELL CULTURE

2.2.1.1 CULTURE CONDITIONS OF ES CELL LINES

The feeder-free ES cell line, E14Tg2a (129P2/OlaHsd), was cultured as previously described (Smith 1991). The feeder-dependent ES cell line, AB2.2 (129S7/SvEvBrdHprt$^{b\text{-}m2}$), was cultured as previously described (Ramirez-Solis 1995), on the puromycin-resistant feeder cell line, MEF P-SNL 76/7-4. Both ES cell lines were cultured in M15 medium and maintained at 37°C with 5% CO_2, with the medium changed daily unless stated otherwise.

2.2.1.2 TRANSFECTION OF TARGETING VECTORS INTO ES CELLS BY ELECTROPORATION

Approximately 100 µg of a targeting vector's DNA was linearized with the appropriate restriction enzyme overnight. Next morning, the targeting vector's DNA was purified by ethanol precipitation. 2.5 times the volume of 100% ethanol was added to the tube containing the mixture of the vector and restriction enzyme, vortexed, and left on ice for 5 minutes. Then, the tube was centrifuged at 12,000 rpm for 1 minute and the ethanol was discarded. The pellet was washed twice with 70% ethanol and subsequently air-dried at room temperature. The air-dried targeting vector's DNA was re-suspended in 0.1 ml of PBS to a final concentration of 1 mg/ml. 15 µg of DNA was used for electroporation, unless stated otherwise. ES cell electroporation was performed as described previously (Ramirez-Solis 1993). 80% confluent ES cells were fed 2 – 3 hours before electroporation. Then, the medium was aspirated and the plate/flask washed twice with PBS. Next, 1x trypsin was added to the plate/flask according to **Table 2.1**, and the plate/flask was incubated at 37°C for 4 minutes. After incubation the M15 medium was added to the plate/flask according to **Table 2.1** to neutralize the trypsin. The cells were next centrifuged at 1,200 rpm for 3 minutes, the medium was aspirated and the cells re-suspended in PBS to a final concentration of 1 x 10^7 cells/ml. 1 x 10^7 ES cells were mixed with 15 µg of the targeting vector's DNA and immediately transferred into a 0.4 cm gap cuvette (Biorad, cat #: 165-2081). The electroporation was carried out using a Biorad "Gene Pulser" (Biorad, cat #: 165-2660) at 230 V, 500 µF (AB2.2 cells) or at 800 V, 25 µF (E14Tg2a cells). After electroporation, the cuvette was left for at least 5 minutes in the tissue culture (TC) hood before the ES cells were plated onto either 10 cm feeder plate (AB2.2 ES cells) or pre-gelatinised 10 cm non-feeder plate (E14Tg2a ES cells; gelatin was added to the flask/plates and left for at least 5 minutes before being aspirated; see **Table 2.1** for the appropriate gelatin quantity). Drug selection (G418 or puromycin depending on the targeting vector) was usually initiated 24 hours post-electroporation and, unless stated otherwise, continued for 10 days to allow the formation of single ES cell colonies. When drug selection was finished, the plate was used to pick single ES cell colonies.

2.2.1.3 PICKING ES CELL COLONIES

The medium was aspirated from the 10 cm plate and, after rinsing with PBS, 10 ml of PBS was added to the plate to cover the cells. Individual colonies were picked using a Pipetman® and added into a well of a 48-well round bottom plate, which was filled with 100 μl of trypsin. Then the plate was incubated in a TC incubator at 37°C for 4 minutes before adding 500 μl of fresh M15 medium to each well. Next, vigorous pipetting separated the ES colonies into single cells, and the ES cell suspension was then transferred to a replicate 48-well plate and incubated at 37°C with 5% CO_2.

2.2.1.4 PASSAGING ES CELLS

ES cells were ready for passaging when they reached approximately 80% confluence. At this time, the medium was aspirated and the flask/plate washed with PBS. 1x trypsin was added (according to **Table 2.1**) and the flask/plate incubated at 37°C for 4 minutes. M15 medium was then added to the flask/plate (according to **Table 2.1**) and the ES cell colonies were dispersed into single cells by pipetting the culture up and down. The ES cell culture suspension was then split into a 1:4 ratio and distributed between 2 feeder or 2 pre-gelatinised non-feeder flasks/plates for AB2.2 ES cells or 4 pre-gelatinised non-feeder flasks/plates for E14Tg2a ES cells (gelatin was added to the flask/plates and left for at least 5 minutes before being aspirated; see **Table 2.1** for the appropriate gelatin quantity). Two pre-gelatinised non-feeder flasks/plates were then used for extraction of genomic DNA (gDNA) from ES cells of both lines for subsequent analysis with Southern blotting (see sections), whilst the other 2 plates were used for expansion of both lines of ES cells. The flasks/plates were incubated in a TC incubator at 37°C with 5% CO_2.

Table 2.1. Volumes.

Flask/Plates	Gelatin	1x trypsin	Re-suspension medium final volume	Culture medium
T25 flask	5 ml	1 ml	10 ml	10 ml
T75 flask	10 ml	3 ml	15 ml	40 ml
T150 flask	15 ml	5 ml	25 ml	60 ml
10 cm plate	10 ml	3 ml	15 ml	40 ml
48-well plate	250 μl	100 μl	500 μl	500 μl

2.2.1.5 FREEZING ES CELLS

ES cells were ready for freezing when they reached about 80% confluence. ES cells were fed 3 hours before freezing, after which time the medium was aspirated, and the flask/plate washed once with PBS before trypsin was added (according to **Table 2.1**). The flask/plate was then incubated at 37°C for 4 minutes, before M15 medium was added (according to **Table 2.1**) to re-suspend the ES cells. The ES cell colonies were separated into single cells by gently pipetting the culture up and down, and the ES suspension then transferred into a sterile tube and centrifuged at 400 rpm for 5 minutes. Next, the supernatant was aspirated and ES cells were re-suspended in an appropriate volume of the freeze medium (according to **Table 2.1**) and immediately transferred into cryo-vials (Fisher Scientific, cat #: 375353) with a maximum of 1 ml per vial. The cryo-vials were then quickly transferred to an -80°C freezer and after 24 hours transferred to a liquid nitrogen tank for long-term storage.

2.2.1.6 THAWING ES CELLS

ES cells were removed from freezer/liquid nitrogen and thawed quickly (by rolling between the hands). The thawed ES cell suspension was transferred to a sterile tube containing less than 10 ml of warm medium, which was then centrifuged at 300 rpm for 5 minutes. The supernatant was aspirated and ES cells re-suspended in 10 ml of warm ES medium and plated onto T25 feeder flasks (AB2.2 ES cells) or to T25 pre-gelatinised non-feeder

flasks (E14Tg2a ES cells). The flask was incubated at 37°C with 5% CO_2. The ES cells were re-fed daily with fresh M15 medium and, once 80% confluency was reached, cells were passaged, frozen or used for other experiments.

2.2.1.7 ELECTROPORATION OF THE ES CELLS WITH THE pOG231 CRE-EXPRESSION VECTOR

20 µg of the pOG231 Cre-expression vector (O'Gorman 1997) was electroporated into 3.0 x 10^6 double-targeted AB2.2 ES cells using Biorad Gene Pulsar 2 at 230 V, 500 µF. The recombinants were first selected in HAT medium (M15 medium supplemented with 12 ml of 50x HAT) for 7 days and then recovered in HT medium (M15 medium supplemented with 12 ml of 50x HT) for 2 days. 48 clones were picked and expanded on a 48-well feeder plate. The plate was replicated, and sib-selection performed to determine the drug resistance of the clones. The correct recombinants should be G418−sensitive, puromycin−sensitive and HAT−resistant. The clones with this combination of drug resistance/sensitivity were expanded and confirmed by Southern blot analysis (as described in section 2.2.3.5).

2.2.1.8 PREPARING ES CELLS FOR MICROINJECTION

When ES cells reached approximately 80% confluence they were ready for micro-injections. The day prior to microinjection, the cells were passaged (as described above) to remove any poor quality, differentiated cells. On the day of microinjection, the medium was aspirated, the plate/flask washed once with PBS, and trypsin added (according to **Table 2.1**). The plate/flask was incubated at 37°C for 4 minutes before M15 medium was added (according to **Table 2.1**) to re-suspend the ES cells. The ES suspension was then transferred into a sterile tube and centrifuged at 400 rpm for 5 minutes. Next, the supernatant was aspirated and ES cells were re-suspended in 500 µl of Hepes/M15 medium. The suspension was mixed thoroughly to separate ES cells, transferred to a cryo-vial and immediately placed on ice to prevent the ES cells from adhering to each other.

2.2.2 GENERATION OF DELETION MICE

2.2.2.1 GENERATION OF THE *Df$^{Lipi\text{-}Usp25}$*/+ ES CELL LINE

The 5'*Hprt* MICER targeting vector MHPN69h23 (Adams 2004) and the 3'*Hprt* targeting vector (Pusp-3HPAg; constructed by recombineering to capture a 6963 bp fragment telomeric to *Usp25* from 129Sv BAC clone: bMQ134j07 (Adams 2005)) were used to generate a chromosomal deletion of a 1.6 Mb of mouse chromosome 16 syntenic to the human region 21q11.2–q21.1. Approximately 15 µg of MHPN69h23 plasmid was linearized with *Nhe*I and electroporated into E14Tg2a ES cells. Stable integrants were selected in M15 medium containing G418 (175 µg/ml) and positive clones (that had undergone homologous recombination with the target locus) were identified by Southern blotting using a probe amplified with the primers 5'-AGG CAA AAA CCA AGA CCT CA-3' and 5'-ATG GTG GCA ATG TTC TCA CA-3' on *Stu*I digested genomic ES cell DNA. The expected lengths of Southern restriction fragments were 15 and 17 kb for wildtype and targeted alleles respectively. Then approximately 15 µg of Pusp-3HPAg plasmid was linearized with *Swa*I and electroporated into MHPN69h23-targeted E14Tg2a ES cells and selected in M15 medium containing puromycin (3 µg/ml). Southern blotting was performed to identify positive recombinants using a probe amplified with the primers 5'-GTG CCC ACA TGG TTT TCT TT-3' and 5'-CAA CTC TCG CCT CAC ACA AA-3' on *Bam*HI digested genomic ES cell DNA. The expected lengths of Southern restriction fragments were 12 and 22.6 kb for wildtype and targeted alleles respectively. The double-targeted E14Tg2a ES cell clones were electroporated with the pOG231 Cre-expression vector (O'Gorman 1997) and selected in HAT medium (Ramirez-Solis 1995; Liu 1998). Subsequently, the HAT-resistant ES cell clones were selected with G418 and puromycin to identify the clones sensitive to both drugs, and so ES cell clones with both targeting vectors were inserted in *cis*. Finally, the presence of the desired deletion between *Lipi* and *Usp25*, generated by *cis*-recombination, was confirmed by both FISH (see section 2.2.2.3 below for details) and PCR using the primers

5’-AAG GGT GTT TAT TCC CCA TGG ACT AAT TAT G-3’ and 5’-CCT TCA TCA CAT CTC GAG CAA GAC GTT CAG-3’. The expected size of the PCR product was 1869 bp for the deletion allele. The deletion allele was designated $Df^{Lipi\text{-}Usp25}$ and ES cell clones carrying $Df^{Lipi\text{-}Usp25}$/+ were injected into albino C57BL/6J$^{c/c}$ blastocysts for germline transmission as described previously (Ramirez-Solis 1995).

2.2.2.2 GENERATION OF THE CONDITIONAL $Df^{4732471D19Rik\text{-}B4galt7}$/+ ES CELL LINE

The 5’*Hprt* MICER targeting vector MHPN55m07 (Adams 2004) and the 3’*Hprt* MICER targeting vector MHPP265c24 (Adams 2004) were used to generate a chromosomal deletion of a 1.1 Mb of mouse chromosome 13 syntenic to the human region 5q35.2–q35.3. Approximately 15 µg of MHPN55m07 plasmid was linearized with *Kpn*I and electroporated into AB2.2 ES cells. Stable integrants were selected in M15 medium containing G418 (175 µg/ml). Southern blotting was performed to identify positive recombinants using a probe amplified with the primers 5’-GTC TGT TGT TAA AAG CTA AAA CCT TAG A-3’ and 5’-TGA GCT ACA GTT TGG TTC TGG TGG ATA AAC-3’ on *Bst*EII-digested genomic ES cell DNA. The expected lengths of Southern restriction fragments were 8.5 and 24.5 kb for wildtype and targeted alleles respectively. Then approximately 15 µg of MHPP265c24 was linearized with *Nco*I and electroporated into MHPN69h23-targeted AB2.2 ES cells, which were subsequently selected in M15-containing puromycin (3 µg/ml). Southern blotting was performed to identify positive recombinants using a probe amplified using primers 5’-CAG TAA TAT AGT AGA AGC ATG GTC CAT-3’ and 5’-ATG ATA CTG AAC ACA GAC AAC AGA GGC TGC T-3’ on *Spe*I-digested genomic ES cell DNA. The expected lengths of Southern restriction fragments were 21 and 13 kb for wildtype and targeted alleles respectively. The double-targeted AB2.2 ES cell clones were electroporated with the pOG231 Cre-expression vector (O’Gorman 1997) and selected in HAT medium (Ramirez-Solis 1995; Liu 1998). Subsequently, the HAT-resistant ES cell clones were selected with G418 and puromycin to

identify the clones sensitive to both drugs, and so ES cell clones with both targeting vectors were inserted in *cis*. Finally, the presence of the desired deletion between *4732471D19Rik* and *B4galt7*, generated by *cis*-recombination, was confirmed by both FISH (see section 2.2.2.3 below for details) and PCR using the primers 5'-AAG GGT GTT TAT TCC CCA TGG ACT AAT TAT G-3' and 5'-CCT TCA TCA CAT CTC GAG CAA GAC GTT CAG-3'. The expected size of the PCR product was 1869 bp for the deletion allele. The deletion allele was designated $Df^{4732471D19Rik\text{-}B4galt7}$, and ES cell clones carrying the conditional deletion (i.e. not the actual cells that were electroporated with Cre) were injected into albino C57BL/6J$^{c/c}$ blastocysts to generate germline chimeras carrying the conditional deletion as described previously (Ramirez-Solis 1995). Subsequently, mice with the conditional deletion were bred with CAG-Cre mice to generate the $Df^{4732471D19Rik\text{-}B4galt7}$/+ mice.

2.2.2.3 FLUORESCENT IN SITU HYBRIDIZATION (FISH)

Chromosome spreads from ES cells were performed as described previously (Robertson 1987). Bacterial artificial chromosome (BAC) clones were used as probes for FISH (Baldini 1994). To detect ES cell clones carrying $Df^{Lipi\text{-}Usp25}$/+, BAC clone RP24-200E18 (located inside the deletion) and BAC clone RP23-246B23 (located outside the deletion) were used, while to detect ES cell clones carrying $Df^{4732471D19Rik\text{-}B4galt7}$/+, BAC clone RP23-99C7 (located inside the deletion) and BAC clone RP24-204D5 (located outside the deletion) were used. BAC clone RP24-200E18 and BAC clone RP24-204D5 were labelled with biotin and detected with three layers of antibodies: 1) Texas red avidin DCS (Vector Laboratories, cat. #: A-2016), 2) biotinylated anti-avidin D made in goat (Vector Laboratories, cat. #: BA-0300) and 3) Texas red avidin D (Vector Laboratories, cat. #: A-2006). In contrast, BAC clone RP23-246B23 and BAC clone RP23-99C7 were labelled with digoxigenin and detected with FITC conjugated mouse anti-dig monoclonal antibody and further amplified with rabbit or rabbit anti-mouse IgG (4 µg/ml Texas red avidin DCS; Vector Laboratories, cat. #: A-2016, 4 µg/ml biotinylated anti-avidin D; Vector Laboratories, cat. #: BA-0300 plus 1 µg/ml mouse anti-digoxigenin; LifeSpan BioSciences, cat. #: LS-C64857) or

1:500 – 1000 dilution of mouse anti-digoxin (Sigma-Aldrich, cat. #: D8156), 4 µg/ml Texas Red Avidin DCS (Vector Laboratories, cat. #: A-2016) plus 10 µg/ml goat anti-mouse IgG (whole molecule) – FITC antibody (Sigma-Aldrich, cat. #: F0257) or 7.5 µg/ml rabbit anti-mouse IgG (whole molecule) – FITC antibody (Sigma-Aldrich, cat. #: F7506)).

2.2.2.4 USE OF ANIMALS

Mice were treated in accordance with local ethical committee guidelines and the UK Animals (Scientific Procedures) Act 1986, and all procedures were carried out in accordance with Home Office guidelines (United Kingdom).

2.2.3 DNA METHODS

2.2.3.1 PURIFICATION OF BAC DNA

Glycerol stocks of BAC clones were inoculated in 1 – 2 ml of lysogeny broth (LB) with kanamycin (30 µg/µl) and left in a shaking incubator at 37°C overnight. The next day, 1 ml of the overnight culture was inoculated in 50 – 100 ml of LB with kanamycin (30 µg/µl) and left in a shaking incubator at 37°C overnight. The BAC DNA was extracted using Plasmid Plus Maxi Kit (Qiagen, cat. #: 12963) according to the manufacture's instructions. The overnight culture was centrifuged at 16,000 rpm for 5 minutes and the pellet was then re-suspended in 8 ml of Buffer P1. Next, 8 ml of Buffer P2 was added to the mixture, gently mixed by inverting until the lysate appeared viscous, and incubated at room temperature for 3 minutes. The QIAfilter Cartridge was placed into a new tube, and 8 ml of Buffer S3 was added to the lysate and mixed by inverting 4 – 6 times. The lysate was then transferred to the QIAfilter Cartridge and incubated at room temperature for 10 minutes. During incubation, QIAGEN Plasmid Plus spin columns were placed into the QIAvac 24 Plus and Tube Extenders were inserted into each column. Next, the plunger was gently inserted into the QIAfilter Cartridge and the cell lysate

was filtered into the tube. 5 ml Buffer BB was added to the cleared lysate and mixed by inverting 4 – 6 times. The lysate was transferred to a QIAGEN Plasmid Plus spin column on the QIAvac 24 Plus. Approximately a 300 mbar vacuum was applied until the liquid had been drawn through all columns. The DNA was washed, 0.7 ml Buffer ETR was added and a vacuum was applied until the liquid had been drawn through all the columns. 0.7 ml Buffer PE was added and a vacuum was applied until the liquid had been drawn through all columns. The column was centrifuged at 10,000 rpm for 1 minute in a tabletop microcentrifuge to completely remove residual wash buffer. The QIAGEN Plasmid Plus spin column was placed into a clean 2 ml tube. The DNA was eluted by adding 400 µl Buffer EB or H_2O to the centre of the QIAGEN Plasmid Plus spin column followed by centrifuging for 1 minute.

2.2.3.2 EXTRACTION OF GENOMIC DNA FROM ES CELLS

ES cells were incubated in 150 µl of lysis buffer [50 mM tris(hydroxymethyl)aminomethane (Tris) (pH 7.4), 50 mM EDTA (pH 8), 0.5% Sodium Dodecyl Sulfate (SDS), and 1 mg/ml proteinase K (added fresh)] at 55°C – 65°C overnight in a humidified chamber. The next morning the ES cell suspension was centrifuged at 4,000 rpm for 3 minutes. Then the supernatant was added to a fresh tube containing 250 µl of 100% ethanol and mixed by inversion to precipitate until gDNA was seen. To pellet gDNA, samples were centrifuged at 13,000 rpm for 1 minute. Then the supernatant was discarded, 1 ml of 70% ethanol was added to the gDNA pellet, mixed by inverting the tube several times, and centrifuged at 13,000 rpm for 1 minute. Finally, the supernatant was discarded, and the gDNA pellet was air-dried before being resuspended in an appropriate volume of 10 mM Tris-HCl (pH 7.4).

2.2.3.3 EXTRACTION OF GENOMIC DNA FROM EAR OR TAIL BIOPSIES

Ear or tail biopsies were incubated in 150 µl (ear) or 500 µl (tail) of lysis buffer [50 mM Tris (pH 7.4), 50 mM EDTA (pH 8), 0.5% SDS, and 1 mg/ml proteinase K (added fresh)] at 55°C – 65°C overnight. The next morning samples were centrifuged at 13,000 rpm for 3 minutes to pellet down

fur and undigested tissue. Then the supernatant was added to a fresh tube containing 250 µl (ear) or 900 µl (tail) of 100% ethanol and mixed by inversion to precipitate the gDNA. To pellet the gDNA, samples were centrifuged at 13,000 rpm for 1 minute. Then the supernatant was discarded, 1 ml of 70% ethanol was added to the gDNA pellet, mixed by inverting the tube several times, and centrifuged at 13,000 rpm for 1 minute. Finally, the supernatant was discarded, and the gDNA pellet was air-dried before being resuspended in an appropriate volume of 10 mM Tris-HCl (pH 7.4).

2.2.3.4 POLYMERASE CHAIN REACTION (PCR)

2.2.3.4.1 DESIGN AND SYNTHESIS OF PRIMERS FOR PCR

Oligonucleotides were designed using the Primer3 design package hosted by the Whitehead Institute for Biomedical Research at http://frodo.wi.mit.edu/primer3/. Primers were ordered from Sigma-Aldrich. Primers were diluted with H_2O to a stock concentration of 100 µM. Working dilutions were then made to a concentration of 10 µM (see **Table 2.2** for primer sequences).

Table 2.2. PCR primer sequences.

Name	5' to 3'	Length (bp)
Del_*Hprt*_F	AAGGGTGTTTATTCCCCATGGACTAATTATG	1869
Del_*Hprt*_R	CCTTCATCACATCTCGAGCAAGACGTTCAG	
Del_vector_F	ACACCAGAACCCTAGCATGG	659
Del_vector_R	GCCTACATACCTCGCTCTGC	
Del_F	CTAGTACAGTCGGTAAGAACAAAATAGTGTCTATCAATAGTGGACTGG	898
Del_R	GGTGTTTATTCCCCATGGACTAATTATGGACAGG	
Mosaic_F	CTGTACACATTTCTTCTCAAGCACTGGCTATGCATGTATAC	356
Mosaic_R	CACCGCTGAATATGCATAAGGCAGGCAAGATGGCGCGTCC	
Cre_F	GTCGATGCAACGAGTGATGAG	881
Cre_R	ATCTCCGGTATTGAAACTCCAGC	
*DfLipi-Usp25*_wt_F	CCTGTGGCCAATTCAAAAGT	526
*DfLipi-Usp25*_wt_R	TTCAGCTGGCCTTTTTCACT	
*DfRik-B4galt7*_wt_F	CTTCCTGCCTCAACCTCTTG	698
*DfRik-B4galt7*_wt_R	TTGAAGCTCACAGTGCCTTG	
Bloom_F1	TCATTTTGGCAGTCCACCTC	300
Bloom_R1	GTCGCTCTAATCCTTTCCATTC	
Bloom_F2	CTCACCAGATAGCAAGCAG	2700
Bloom_R3	TTAAGACCAGGGCTAGACAG	
MICEpuro	CTAGTACAGTCGGTAAGAACAAAATAGTGTCTATCAATAGTGGACTGG	330
MICERcmn	CTGTACACATTTCTTCTCAAGCACTGGCTATGCATGTATAC	
MICERneo	CACCGCTGAATATGCATAAGGCAGGCAAGATGGCGCGTCC	356
MICERcmn	CTGTACACATTTCTTCTCAAGCACTGGCTATGCATGTATAC	
MHPN55m07_F	GTCTGTTGTTAAAAGCTAAAACCTTAGA	506
MHPN55m07_R	TGAGCTACAGTTTGGTTCTGGTGGATAAAC	
MHPP265c24_F	CAGTAATATAGTAGAAGCATGGTCCAT	450
MHPP265c24_R	ATGATACTGAACACAGACAACAGAGGCTGCT	
MHPN69h23_F	AGGCAAAAACCAAGACCTCA	455
MHPN69h23_R	ATGGTGGCAATGTTCTCACA	
3'fragment_F	GTGCCCACATGGTTTTCTTT	429
3'fragment_R	CAACTCTCGCCTCACACAAA	

2.2.3.4.2 GENERAL PCR PROTOCOLS

Two different PCR systems were used to carry out PCR reactions. The first system, ABgene Thermo-Start™ *Taq* DNA Polymerase (Thermo Scientific, cat. #: AB0908/A), was used for the majority of PCR reactions. The second system, *TaKaRa LA Taq*™ (Takara Biotechnology, cat. #: RR002A),

was used for reactions where a larger fragment was to be amplified.

The reaction mixture for the PCR reactions carried out using ABgene Thermo-Start™ *Taq* DNA Polymerase was prepared by combining 2.5 µl 10x ABgene Thermo-Start PCR Buffer, 1.5 µl $MgCl_2$ (25 mM), 0.5 µl dNTP mixture (20 mM), 0.125 µl ABgene Thermo-Start *Taq* DNA Polymerase (5 U/µl), 0.5 µl of each forward and reverse primer (10 µM), 5 – 100 ng DNA template, and an appropriate volume of double-distilled H_2O (ddH_2O) to bring the reaction to a final volume of 25 µl. The cycling conditions were: 95°C for 15 minutes (initial denaturation), 30 – 40 cycles of denaturation (95°C for 30 seconds) then annealing (55 – 65°C for 30 – 60 seconds) then extension (72°C for 30 – 90 seconds), followed by 72°C for 5 – 10 minutes (final extension). The annealing temperature depended on the primer pair used, while the extension time was 1 minute for every 1 kb of target fragment.

The reaction mixture for the PCR reactions carried out using *TaKaRa LA Taq*™ were prepared by combining 2.1 µl 10x TaKaRa LA™ Buffer II (Mg^{2+} free), 2.1 µl $MgCl_2$ (25 mM), 3.36 µl dNTP mixture (2.5 mM of each dNTP), 0.17 µl *TaKaRa LA Taq*™ DNA Polymerase (5 U/µl), 0.08 µl each of forward and reverse primer (10 µM), 5 – 100 ng DNA template, and appropriate volume of ddH_2O to bring a reaction to a final volume of 20 µl. The cycling conditions were: 94°C for 5 minutes (initial denaturation), 35 cycles of denaturation (94°C for 15 seconds) then annealing (56°C for 30 seconds) then extension (68°C for 2:30 minutes), followed by 68°C for 7 minutes (final extension).

The products of PCR reactions were mixed with 5x loading dye (0.25% bromophenol blue, 0.25% xylene cyanol FF in 30% glycerol (made up in ddH_2O)), and loaded onto ethidium bromide-containing 1 – 2% agarose gels (UltraPure™ Agarose (Invitrogen, cat. #: 16500-500) dissolved in 1x Tris-acetate-EDTA (TAE) buffer (40 mM Tris acetate, 1 mM EDTA)). The PCR bands were then visualised by placing the gel on a UV transilluminator.

2.2.3.5 SOUTHERN BLOTTING

2.2.3.5.1 Digestion of the DNA samples

5 – 10 µg of genomic DNA (in a total volume of no more than 40 µl) was digested overnight with 2 µl of an appropriate restriction enzyme, 5 µl 10x restriction buffer and sufficient ddH_2O to make a 50 µl final reaction volume. The digestion temperature depended on the requirements of the individual enzyme.

2.2.3.5.2 Electrophoresis and transfer of the DNA

The digested fragments, as well as one lane of molecular weight marker DNA (*Lambda DNA/HindIII markers*; Promega, cat. #: G1711), were separated by electrophoresis on an ethidium bromide-containing 0.8% agarose gel run at 60 – 80 V (depending on the width, length and thickness of the gel). Upon completion of electrophoresis, a fluorescent ruler was placed alongside the gel on the UV transilluminator, and the ruler and gel were photographed (to allow estimation of the size of the bands if the markers did not show up on the blot after hybridization). Next, the gel was washed twice for 10 minutes in depurination buffer (40 ml of concentrated HCl in 2 l of Mili-Q H_2O) and then once for 15 minutes in neutralization buffer (0.4 M NaOH, 1 M NaCl). The transfer of DNA samples from the gel to the membrane was achieved by capillary action. A strip of 3 MM Whatman paper was placed in the gel-running apparatus (the strip was slightly wider in width than the gel across the gel-running apparatus, allowing the ends of the paper to reach over the edge of the platform into a reservoir containing the neutralization buffer). Next, the gel was inverted (turned face-down) and placed on top of the Whatman paper on the gel box. On top of the gel was placed a sheet of positively charged nylon membrane (Amersham Hybond-XL; GE Healthcare Life Sciences, cat. #: RPN203S) that had been soaked in Mili-Q H_2O followed by neutralization buffer. Two pieces of Whatman paper (pre-soaked in Mili-Q H_2O) were placed on top of the membrane. Finally, a 10 – 15 cm layer of absorbent paper towel was placed on top of the Whatman paper. Following the overnight transfer, the transfer apparatus was disassembled and the membrane washed in wash buffer

(0.5 M Tris HCl, 1 M NaCl in Mili-Q H_2O) for 15 minutes. Then the membrane was placed inbetween some filter paper and baked at 80°C for 2 hours.

2.2.3.5.3 Hybridization, preparation of the probe and washing the blot

The membrane was pre-hybridized for 2 hours in Amersham Rapid-hyb™ Buffer (GE Healthcare Life Sciences, cat. #: RPN1636) at 65ºC in a rotating hybridization oven (about 10 – 15 ml of buffer was used per blot depending on its size). The probe was labelled using the Prime-It® II Random Primer Labeling Kit (Agilent Technologies, cat. #: 300385), according to the manufacturer's instructions. Briefly, 50 ng of probe was added to a Mili-Q H_2O to make 25 µl, and then 10 µl of Random 9-mer primers were added. The mixture was heated at 100ºC for 5 minutes and then placed on ice for 1 minute. Next, 10 µl of buffer, 1 µl of Klenow polymerase and 5 µl of αP^{32}–dCTP (=50 µCi) was added to the mixture, which was subsequently incubated at 37ºC for at least 15 minutes. Then, the probe was cleaned up through the Illustra ProbeQuant™ G-50 Micro column (GE Healthcare Life Sciences, cat. #: 28-9034-08). To do this, the bottom of the column was snapped off and the column placed in an eppendorf tube before being centrifuged at 4,000 rpm for 2 minutes. The column was then put in a new eppendorf tube and the probe was added to the gel resin that had pelleted in the column. After re-centrifugation, the column was discarded and the purified probe (i.e. the eluant) was heated at 100ºC for 5 minutes. The tube was then placed on ice for 1 minute, before being added to the pre-hybridized membrane. After 5 hours of hybridization at 65ºC, the blot was washed in the rotating tube with a low stringency wash (LSW; 2x SSC, 0.1% SDS) for 15 minutes, followed by a high stringency wash (HSW; 0.5x SSC, 0.1% SDS) for another 15 minutes. Then the blot was removed from the tube, wrapped in cling film, placed into a hybridization film cassette, where it was exposed to an X-ray film (Fisher Scientific, cat. #: P10M000274A) overnight at -80ºC. The film was then developed the next morning using the Compact X4 film processor (Xograph), according to the manufacturer's instructions.

2.2.4 RNA METHODS

2.2.4.1 TOTAL RNA EXTRACTION FROM TISSUES

Total RNA was isolated from mouse tissues using TRIzol (Invitrogen, cat. #: 15596-018) according to the manufacturer's instructions. Snap frozen tissues were transferred into RNase-free eppendorf tubes, where they were then homogenized in 1 ml of TRIzol (Invitrogen, cat. #: 15596-018). The homogenate was then centrifuged at 12,000 rpm at 4°C for 10 minutes and the supernatant transferred to a fresh RNase-free eppendorf tube and 200 µl of chloroform. The tube was vigorously shaken for 15 seconds, incubated at room temperature for 2 minutes and centrifuged at 12,000 rpm at 4°C for 10 minutes. The aqueous phase was removed and transferred to a fresh RNase-free eppendorf tube, and the RNA precipitated by adding 500 µl of isopropyl alcohol. The sample was incubated at room temperature for 10 minutes and then centrifuged at 12,000 rpm at 4°C for 10 minutes. The RNA pellet was washed once with 1 ml of 75% ethanol and centrifuged at 7,500 rpm at 4°C for 5 minutes. The air-dried RNA was re-suspended in an appropriate volume of RNase-free H_2O.

2.2.4.2 DNase TREATMENT OF RNA

RNA was DNase treated using TURBO^{TM} DNase kit (Ambion, cat. #: AM2238) according to the manufacturer's instructions. 12 µg of total RNA in a volume of 21.5 µl of RNase-free H_2O was mixed with 2.5 µl of 10x TURBO DNase buffer and 1 µl of TURBO DNase. The mixture was incubated at 37°C for 30 minutes, flicked and then incubated at 37°C for an additional 30 minutes. 6 µl of inactivation reagent was added and the mixture was vortexed before being incubated at room temperature for 5 minutes (while incubating, the content of the tube was flicked a few times). The tube was centrifuged at 12,000 rpm for 90 seconds. The supernatant was carefully transferred into a new tube and 50 µl of 100% ethanol was added. After inverting the tube several times, it was placed in a freezer for 10 minutes, before being centrifuged at 13,000 rpm at 4°C for 10 minutes. The pellet was air-dried for 5 minutes and then resuspended in 15 µl of RNase-free H_2O.

2.2.4.3 EXPRESSION ARRAY ANALYSIS

DNase-treated RNA was amplified using the Illumina® TotalPrep™-96 RNA Amplification Kit (Applied Biosystems, Carlsbad, CA) according to the manufacturer's instructions. Expression profiling of the RNA was performed using a MouseWG-6 v2.0 expression beadchip kit (Illumina, Essex UK), according to the manufacturer's instructions. Microarray data was imported in the R programming language for processing. We used the lumi package [http://www.bioconductor.org/] to perform quality control on array data (samples were removed if there were concerns over their quality). These data were then quantile-normalised (Yang 2001) as implemented in the lumi package [http://www.bioconductor.org/packages/ 2.0/bioc/html/lumi.html] and limma package (Smyth 2004). Data were p-value adjusted to yield a sorted list of differentially expression genes (Benjamini 2001).

2.2.4.4 FIRST STRAND COMPLEMENTARY DNA (cDNA) SYNTHESIS

1 µg of total RNA was made up to 21 µl with RNase-free H_2O in an RNase-free eppendorf tube. Next, 20 µl of the mixture was added to Sprint^{TM} RT Complete Product tube (Clontech, cat. #: 639525), mixed by pipetting, and incubated at 42°C for 1 hour. The tube was then incubated at 70°C for 10 minutes, to terminate the reaction.

2.2.4.5 REAL-TIME QUANTITATIVE PCR (qRT-PCR)

The quantitative PCR reactions were performed with SYBR® Green PCR Master Mix (Applied Biosystems, cat. #: 4309155) on the ABI 7900HT sequence detection system, according to the manufacturer's instructions. 12.5 µl of SYBR® Green PCR Master Mix was mixed with 1 µl of forward primer, 1 µl of reverse primer (see **Table 2.3** for qRT-PCR primers sequences), 8.5 µl of ddH_2O and 2 µl of cDNA. The cycle conditions were: 50°C for 2 minutes, 95°C for 10 minutes, 40 cycles of 95°C for 15 seconds and then 60°C for 1 minute, followed by 95°C for 15 seconds. The final quantitation was determined relative to the average CT of the house-keeping genes *Eif1a*, *Hprt1* and *Gapdh* (Livak 2001). Data were statistically analysed using the two-tailed Student's *t*-test.

Table 2.3. qRT-PCR primer sequences.

Gene	Forward: 5' to 3'	Reverse: 5' to 3'
Eif1a	AAAAACAGGCGCAGAGGTAAA	TCCTCACACCGTCAAAGCAC
Hprt1	TCAGTCAACGGGGGACATAAA	GGGGCTGTACTGCTTAACCAG
Gapdh	AGGTCGGTGTGAACGGATTTG	TGTAGACCATGTAGTTGAGGTCA
Tmem45a	TGGGCTTTTGGTGGACTATGA	CCAGCTATACCAGTGAGAGACA
Plnxd1	TCGCTGCCAATCCCTAATAAGA	TGACCTGGTTTGGAACTGTTG
Elovl1	TCCAAAGCTACCCTCTGATGG	AGGGAGAGTATCACCAGTGAGA
Man2b2	AAAGCATGAGAGCCTATGCAG	GCCTCCGAGAACAAACTCCA
Atp5g3	TCTGCATCAGTGTTATCTCGGC	CACCAGAACCAGCAACTCCTA
Mrap	ACATAGACCTCATTCCTGTGGA	TGTGTTCCGACTTACGCTTGT
Rbm38	TGCTCCCCGAGTGTGTTTC	GTACTTTCTGAGCGATGCGTC
Tnxb	TCCGTGTAGACTCAGCAAAGG	CCCCACGATAAGAGACAGCG
Gtf2ird1	TTCGTCCTCTAACCCAGAGTC	ACAGAATTAGGGTGAAGTTCGGA
Thbs3	ATGGAGAAGCCGGAACTTTGG	AGTGAGTAAAGCTGTCCGAATCT
Lrpap1	CACAACCTCAACGTCATCCTG	AGCACATTGTACTCCTGGATCTT
Trpc4ap	ACATGGCTCGACAATGCGTT	TGCTTAGAGAAGGGAACACAGT
Samsn1	CCAAGTCCCTATGACACCGAC	CCTGGATAGTCTGGTGGTTCT
Lmna	ACCCCGCTGAGTACAACCT	TTCGAGTGACTGTGACACTGG
Bmp1	TTGTACGCGAGAACATACAGC	CTGAGTCGGGTCCTTTGGC

2.2.5 HISTOLOGY AND IMMUNOHISTOCHEMISTRY

2.2.5.1 COLLECTION AND EMBEDDING OF TISSUES/EMBRYOS

Mouse tissues and embryos (at E10.5, E11.5, E12.5 and E14.5) for histopathological analysis were collected into 10% neutral buffered formalin, embedded in paraffin and 5 μm sections placed on glass slides. The only exception was for bones, which were decalcified in 10% EDTA for 7 days prior to embedding in paraffin.

2.2.5.2 HEMATOXYLIN AND EOSIN (H&E) STAINING

The sections were first de-waxed using xylene washes (1x for 3 minutes and 1x for 2 minutes), subsequently re-hydrated in a decreasing series of industrial methylated spirit (IMS) (Leica, cat. #: 03655EG) dilutions

(2x in 100% IMS for 1 minute and 1x in 70% IMS for 1 minute) and rinsed in ddH_2O for 1 minute before staining with hematoxylin and eosin. The staining protocol was as follows: Harris's Hematoxylin solution (Raymond A Lamb, cat. #: 10874) for 3 minutes, tap H_2O for 1 minute, 1% acid alcohol for 20 seconds, ddH_2O for 30 seconds, tap H_2O for 3 minutes, 1% eosin (Raymond A Lamb, cat. #: 10814) for 3 minutes, and H_2O for 10 seconds. Then, the slides were dehydrated in an increasing series of IMS dilutions (1x in 70% IMS for 2 minutes, 2x in 100% IMS for 1 minute), cleared using xylene washes (2x for 90 seconds), and finally covered using the Thermo Scientific Shandon Synthetic Mountant (Fisher HealthCare, cat #: 6769007).

2.2.5.3 VON KOSSA STAINING

The sections were first de-waxed using xylene washes (1x for 3 minutes and 1x for 2 minutes), subsequently re-hydrated in a decreasing series of industrial methylated spirit (IMS) (Leica, cat. #: 03655EG) dilutions (2x in 100% IMS for 1 minute and 1x in 70% IMS for 1 minute) and rinsed in ddH_2O for 1 minute before staining with the von Kossa kit (Diagnostic BioSystems, cat. #: KT028) according to the manufacturer's instructions. Briefly, the slides were incubated in 5% silver nitrate solution for 24 hours in complete darkness, rinsed in ddH_2O, stained with 5% sodium thiosulfate solution for 3 minutes, rinsed in running tap H_2O, and nuclear fast red stained for 5 minutes. Then, the slides were dehydrated in an increasing series of IMS dilutions (1x in 70% IMS for 2 minutes, 2x in 100% IMS for 1 minute), cleared using xylene washes (2x for 90 seconds), and finally cover-slipped using the Thermo Scientific Shandon Synthetic Mountant (Fisher HealthCare, cat #: 6769007).

2.2.5.4 IMMUNOHISTOCHEMISTRY

The sections were first de-waxed using xylene washes (1x for 5 minutes and 1x for 4 minutes), subsequently rehydrated in a decreasing series of industrial methylated spirit (IMS) (Leica, cat. #: 03655EG) dilutions (1x in 100% IMS for 3 minutes, 1x in 100% IMS for 1 minute and 1x in 70% IMS for 1 minute), rinsed in ddH_2O for 1 minute, and finally moved to tap H_2O. Then, the sections were boiled in a pre-heated 10 mM citric acid buffer

(1.92 g of citric acid anhydrous (Sigma-Aldrich, cat. #: 251275) in 1 l ddH_2O, pH6 with NaOH (Sigma-Aldrich, cat. #: 221465)) in a microwave set up at 750 W for 10 – 15 minutes. The slides were gradually cooled in running tap H_2O for 10 minutes. Next, the sections were put in a 3% hydrogen peroxide (Sigma-Aldrich, cat. #: H1009-500ML) solution for about 20 minutes. The slides were put into Tris Buffered Saline with Tween 20 (TBST) solution (50 ml of 1 M Tris (pH 7.4), 30 ml of 5 M NaCl (Analar, cat. #: 10241), 500 μl of Tween 20 (Sigma-Aldrich, cat. #: 7949) diluted in 1 l ddH_2O) for 5 minutes. Wax barriers were drawn around the tissue sections on each slide using a pap pen (Vector laboratories, cat. #: H-4000). Approximately 100 μl of Blocking solution (15 μl of goat serum (VECTASTAIN®EliteABC Kit (Rabbit IgG); Vector Laboratories, cat. #: PK6101) in 1 ml of TSBT) was then applied to each section, which was then incubated in a humidified chamber at room temperature for 30 minutes. Then the blocking solution was tipped away, and each section incubated with approximately 100 μl mixture of the primary antibody in TBST (cleaved caspase-3 (Asp175) Antibody (Cell Signaling, cat #: 9661S) was used at 1:50 dilution in TBST) in a humidified chamber at room temperature for 1 hour. Following the incubation with the primary antibody, the sections were washed in TBST for 5 minutes and incubated with approximately 100 μl mixture of the secondary antibody in TBST (5 μl of secondary antibody (VECTASTAIN®EliteABC Kit (Rabbit IgG); Vector Laboratories, cat. #: PK6101) diluted in 1 ml of TBST) and incubated in the humidified chamber at room temperature for 30 minutes. The sections were then washed with TSBT for 5 minutes and incubated with approximately 100 μl of a mixture consisting of 10 μl of vector A (VECTASTAIN®EliteABC Kit (Rabbit IgG); Vector Laboratories, cat. #: PK6101) and 10 μl of vector B (VECTASTAIN®EliteABC Kit (Rabbit IgG); Vector Laboratories, cat. #: PK61010) diluted in 1 ml of TBST in a humidified chamber at room temperature for 45 minutes. Next, the sections were washed with TSBT for 15 minutes. To develop a colour, each section was incubated with approximately 100 μl mixture consisting of 5 ml of ddH_2O, 2 drops of Buffer Stock Solution (Vector Laboratories, cat #: SK-4100), 4 drops of DAB Stock Solution (Vector Laboratories, cat #: SK-4100) and 2 drops of Hydrogen

Peroxide Solution (Vector Laboratories, cat #: SK-4100). The sections were then washed with TSBT for 5 minutes, stained with hematoxylin solution for 2 minutes and placed in tap H_2O. Then, the slides were dehydrated in a decreasing series of IMS dilutions (1x in 100% IMS for 2 minutes, 1x in 100% IMS for 2 minutes and 1x in 70% IMS for 1 minute), cleared using xylene washes (2x for 90 seconds), and finally cover-slipped using the Thermo Scientific Shandon Synthetic Mountant (Fisher HealthCare, cat #: 6769007).

2.2.5.5 FISH ANALYSIS ON TISSUE SECTIONS MOUNTED ON GLASS SLIDES

The slides were first de-waxed using xylene washes (3x for 5 minutes), subsequently re-hydrated in 100% industrial methylated spirit (IMS) (Leica, cat. #: 03655EG) (2x for 5 minutes), and air-dried. Next, the sections were subjected to pre-treatment for digestion, which consisted of incubation in 0.2 M HCl (100 ml of 1 M HCl to 400 ml of ddH_2O) for 26 minutes, washing in ddH_2O for 3 minutes, incubation in 10 mM citric acid (0.768 g of citric acid to 400 ml of ddH_2O; pH 6.0 using 10% sodium hydroxide) at 82°C for 3 hours, and washing in ddH_2O for 3 minutes. Subsequently, the slides were blot dried and subjected to proteinase K digestion. Namely, 500 μl of 0.5 μg/ml proteinase K solution was added to the pre-heated proteinase K buffer solution (50 ml of 2x saline-sodium citrate (SSC); pH 7.0) at 39°C and subsequently the mixture was applied to the slides. The slides were digested for 22 minutes, washed in ddH_2O for 3 minutes, dehydrated through 70%, 90% and 100% IMS each for 1 minute, and air-dried. Next, 6 – 10 μl of FISH probe was added per slide and then the slide was cover-slipped and sealed with rubber cement (Elmer's, cat. #: 231). Slides were put in the Slide Moat™ (Boekel Scientific, cat. #: 240000) and double-stranded DNA (dsDNA) was denaturated at 75°C for 5 minutes and then hybridized at 37°C overnight (14 –20 hours). The next day, the rubber cement was removed and the slides were placed into 2x SSC to remove coverslips. Then, the slides were blot-dried, washed in post hybridization buffer (100 ml of 20x SSC, 847 ml ddH_20 and 3 ml of Tergitol-type nonyl phenoxypolyethoxylethanol-40

(NP-40); pH 7.0) at 72°C for 4 minutes, rinsed in ddH_2O for 1 minute, and dried at 45°C using the Slide Moat™. Finally, 10 μl of 4',6-diamidino-2-phenylindole (DAPI) nuclear counterstain was added to the slide and then the slide was cover-slipped and sealed with nail varnish (Miss Sporty, cat. #: 105901). The slides were stored at 4°C and scored within 7 days.

2.2.6 PHENOTYPIC PROCEDURES

14 heterozygous (monosomic) *Df*$^{Lipi\text{-}Usp25}$ mice and 14 controls (wildtype littermates) fed on a high-fat diet (HFD) from 4 weeks of age were subjected to a robust phenotypic screening program in order to thoroughly determine whether clinical features diagnosed in patients with Monosomy 21 syndrome could be observed in monosomic *Df*$^{Lipi\text{-}Usp25}$ mice. See **Table 2.4** for a brief summary of the phenotypic tests. Members of the Wellcome Trust Sanger Institute Mouse Genetics Project performed these tests, while I generated the mouse cohort, genotyped all mice prior to testing and was present in an observational capacity when all the tests were conducted. Also, I statistically analysed all the results that were generated from the tests and interpreted the data.

Table 2.4. Short summary of the phenotypic tests performed on 14 monosomic *Df*$^{Lipi\text{-}Usp25}$ mice and 14 wildtype littermates fed on a high-fat diet.

Time	Name of the test	Purpose of the test
Weekly; from 4-week old	Weighting mice	To monitor the body weight
4-week old	Hair dysmorphology	To check for the coat formation and development
6-week old	Hair follicle cycling	To investigate the hair follicle cycling
9-week old	Open field	To measure the locomotion, habituation and fear/anxiety responses to a novel environment
9-week old	SHIRPA	To assess for the presence of gross motor and neurological abnormalities
9-week old	Grip strength	To assess the neuromascular function and muscular strength of the fore and all paws
10-week old	Dysmorphology	To check for the presence of any gross dysmorphological abnormalities
10-week old	Hot plate	To assess for the thermal pain perception
12-week old	Indirect calorimetry	To investigate mouse metabolism, circadian pattern and behaviour (mouse activity and to some extent its exploratory behaviour)
13-week old	Glucose tolerance	To obtain fasted, basal blood glucose concentrations To investigate glucose tolerance and clearance
14-week old	Auditory brainstem response	To assess the hearing sensitivity across a broad range of frequencies
14-week old	Dual energy X-ray absorptiometry (DEXA)	To obtain the body composition and bone mineral data
14-week old	X-ray imaging	To obtain high-resolution X-ray images of the mouse skeleton
15-week old	Core temperature stress	To obtain the basal body temperature To assess the stress-induced hyperthermia
15-week old	Eye morphology screen	To detect gross morphological abnormalities in the eye morphology
16-week old	Heart weights	To assess the weight of the mouse's heart
16-week old	Haematology panel	To analyse the variable whole blood parameters
16-week old	Plasma chemistry panel	To analyse the variable clinical chemistry parameters

Note: DEXA was also performed on 8- or 25-week old mice fed on a high-fat diet, and on 8-, 25-week old or on 1-year old mice fed on a normal-fat diet. X-ray was also performed on 1-year old mice fed on a normal-fat diet.

2.2.6.1 ANAESTHESIA WITH KETAMINE/XYLAZINE AND ANTISEDAN

When the mouse needed to be placed under general anaesthesia, it was weighed and 100 μl ketamine/xylazine and antisedan (Sigma-Aldrich) was injected intraperitoneally per 10 g of body weight. After administering anaesthesia, the mouse was put into a clean cage placed on top of a heat mat, and anaesthesia confirmed by checking for a righting reflex. After the test procedure was finished, but at least 15 minutes after anaesthesia was administered, antisedan was administered to reverse the anaesthetic state. The mouse was returned to the cage and placed on its side to help in breathing. The cage was placed within the Techniplast heated IVC recovery rack and mice in the cage were checked every 30 minutes. Mice were usually fully recovered within 1 – 2 hours after the injection of antisedan.

2.2.6.2 DIET TYPES

2.2.6.2.1 Normal-fat diet

Unless otherwise indicated, mice were fed on a standard laboratory chow (a normal-fat diet; NFD) (Autoclavable Mouse Breeder Diet 5021, a version of Mouse Diet 9F 5020; Lab Diet, cat. #: 5021) containing not less than 9% crude fat, 20% crude protein and 63% carbohydrate.

2.2.6.2.2 High-fat diet

A small fraction of mice were fed on a high-fat diet (HFD) (Western RD; Special Diets Services, cat. #: 829100) containing 21.4% crude fat, 17.5% crude protein and 50% carbohydrate from 4 weeks of age.

2.2.6.3 WEIGHING MICE

Mice were weighed weekly from 4 weeks of age to obtain and monitor their body weight over 12 subsequent weeks. Each mouse was placed in a container on the scales. The scale then counted down from 5 seconds and produced an average weight read-out on the display. The container was cleaned with 70% ethanol after weighing all mice from the same cage.

2.2.6.4 HAIR DYSMORPHOLOGY

This analysis was performed to check for coat formation and development in 4-week old mice. First, the back of the mouse was examined for the presence of guard hair. Next, the dorsal and ventral coat was checked for the presence of abnormalities, such as long, short, rough, sparse, coarse, fine hair and/or visible skin. Subsequently, the area behind the mouse's ears was examined for the presence or absence of hair. The tail was checked for the presence or absence of hair along its length, as well as the tip. Finally, the whiskers were checked for the presence of abnormalities, such as short, long, curly, disorientated, and/or absent hairs.

2.2.6.5 HAIR FOLLICLE CYCLING

This test was performed to investigate hair follicle cycling. This test is dependent on the mouse age and therefore all mice were tested when they were 43 days old. This time point was chosen on the basis of previous internal data, which suggested that at 43 days of age, a mouse is the most likely to leave the anagen phase and enter the catagen phase, a phase which can be recognised by a skin colour change from black to grey-pink. On the day of the test, a fingernail-sized mid-dorsum patch was shaved in order to allow examination of the skin colour, and thus allow discrimination of the hair follicle cycling stage. The results were recorded as follows: "yes" if the skin was black, "no" if the skin was dark grey, grey or pink, and "non-synchronous" if the skin showed non-uniform colouration. The test was not performed if the mouse was albino or any other coat colour where the skin is non-pigmented (such a mouse was scored as an albino). In the case of agouti mice, any colour other than black was recorded as "no".

2.2.6.6 OPEN FIELD

This test was performed to measure locomotion, habituation and fear/anxiety responses to a novel environment. The test was conducted during the light period of the light-dark cycle. At least 5 minutes before the test, the light levels in the room were adjusted to 5 lux. All mice were individually tested for 10 minutes using the ActiMot2 surrounding an open field apparatus (TSE Systems) (**Figure 2.1**). At the beginning of the test, each

mouse was individually transferred to the arena, half way along the Y axis from a height of 5 cm with its tail parallel to the wall, and left undisturbed for the duration of the test. The anxiety and exploratory behaviour were recorded by camcorder for later analysis. Analysis was performed using ActiMot software for Windows (TSE Systems). The following parameters of the mice behaviour were recorded: total distance travelled (arena, periphery and centre), total resting time (arena, periphery and centre), total time (periphery and centre), average speed (arena, periphery and centre), total rears, latency to enter centre, number entries to centre, percentage distance moved in centre, and percentage time spent in centre. Average speed was calculated by dividing the total distance by the total time spent moving. The open field apparatus was cleaned with 70% ethanol after testing each mouse.

Figure 2.1. Photo of an ActiMot2 surrounding an open field apparatus. Photo taken from http://www.tse-systems.com/products/behavior/anxiety/open-field.htm.

2.2.6.7 SmithKline Beecham Pharmaceuticals; Harwell, MRC Mouse Genome Centre and Mammalian Genetics Unit; Imperial College School of Medicine at St Mary's; Royal London Hospital, St Bartholomew's and the Royal London School of Medicine; Phenotype Assessment (SHIRPA)

This procedure was applied to assess for the presence of gross motor and neurological abnormalities. Mice were transferred to the test area 15 minutes before testing. After acclimatization, each mouse was first observed in the viewing jar (**Figure 2.2**) for 1 minute, and the following behaviours were recorded: body position (if the mouse was inactive, active or markedly active); palpebral closure; the presence or absence of lacrimation, tremor, defecation and urination. Subsequently, the mouse was transferred from the viewing jar to the centre of the arena (**Figure 2.3**) from approximately 30 cm above the arena floor and its behaviour was recorded for 30 seconds after it landed on the arena floor. The following parameters were scored: transfer arousal (the reaction to the new environment was recorded, namely if the mouse started to move instantly, froze briefly or froze for a period longer than a few seconds), gait (including ataxia), tail elevation (if during forward movement the tail was dragged, elevated or horizontally extended), pelvic elevation during forward movement, convulsions, head bobbing/circuling, locomotor activity (the number of squares that the mouse entered with all four feet during the total time spent in the arena), and touch escape (the mouse was approached from its front and subsequently the reaction of the mouse to touching the back of its neck was recorded). Also, whilst in the arena, the mouse was checked for its startle response after administering the sound stimulus from the click box (the stimulus was applied for the first time when the mouse stopped moving in the arena). Next, the mouse was lifted from the arena by the tail and suspended briefly to check for positional passivity (in other words to check if the mouse struggled when being held by the tail), trunk curl (to see if the mouse curled forward from its head towards its abdomen), and limb grasping. Finally, the mouse was placed on the metal grid on the top of the arena and checked for pinna touch reflex (the proximal part of the inner canthus was touched lightly with the tip of a fine cotton probe and the mouse's ear was observed for retraction), corneal touch reflex (the cornea was touched lightly with the tip of a fine cotton probe and the mouse's eye was

observed for the eye-blink response) and contact righting reflex (the mouse was placed in the 30 mm Perspex tube and the tube was slowly rotated by 180° to check whether or not the mouse attempted a righting reflex). During the whole SHIRPA test, the mouse was observed for evidence of biting and vocalization. All the equipment used was cleaned with 70% ethanol after testing each mouse.

Figure 2.2. Photo of a SHIRPA viewing jar. Photo taken from http://phenome.jax.org/db/q?rtn=projects/docstatic&doc=Lake2/Lake2_Protocol.

Figure 2.3. Photo of a SHIRPA arena. Photo taken from http://phenome.jax.org/db/q?rtn=projects/docstatic&doc=Lake2/Lake2_Protocol.

2.2.6.8 GRIP STRENGTH

A grip strength test was performed to assess the neuromuscular function and muscular strength of the fore and hind paws, and was recorded using a grip strength meter (BIO-GT3; Bioseb) (**Figure 2.4**)**.** The mouse was lowered towards the apparatus grid, being held only by its tail, until it gripped the grid with its fore paws only. When the tension of the grip was felt, the mouse was pulled back slowly by the tail (the mouse torso was kept horizontal to the grid) until the grip was released. Three trials of fore paws were performed immediately one after the other. Next, the mouse was lowered towards the apparatus grid, being held only by its tail, until it gripped the grid with both its fore and hind paws. When the tension of the grip was felt, the mouse was pulled back slowly by the tail (the mouse torso was kept parallel to the grid) until the grip was released. Three trials of all paws were performed immediately one after the other. At the end, an average value of both fore and fore/hind paw grip strength was calculated. The grip strength meter was cleaned with 70% ethanol after testing each mouse.

Figure 2.4. Photo of a grip strength meter. Photo taken from http://www.bioseb.com/bioseb/anglais/default/item_id=48_cat_id=2_Test%20d/item.php?mode=photo&id=62.

2.2.6.9 DYSMORPHOLOGY

Whole body morphology was examined to check for the presence of any abnormalities. First, the mouse was placed on the cage grid and checked for any obvious dysmorphologies in the physical appearance; irregularities in the shape of the body, head, tail, ears, and/or eyes; and irregularities in the coat colour, skin pigmentation, hair distribution and development. Next, the mouse was scruffed and observed for the presence or absence of whiskers; irregularities in the genitals; malformations of the ventral and lateral sides of head and body; shape, number and colour of the incisors; number and shape of digits; number, size and colour of paw pads; paw size and limb size; and irregularities in skin pigmentation on limbs.

2.2.6.10 HOT PLATE

This procedure was performed to assess for thermal pain perception. Each mouse was placed on a plate (TSE Systems) that had been heated to 52°C (**Figure 2.5**). The latency to the first response and the type of response were recorded. Mice that did not respond after 30 seconds were removed from the plate. The plate was cleaned with 70% ethanol after testing each mouse.

Figure 2.5. Photo of a hot plate meter. Photo taken from http://www.tse-systems.com/products/other-products/analgesia/hot-plate.htm.

2.2.6.11 INDIRECT CALORIMETRY

This experiment was performed to investigate the metabolism, circadian pattern and behaviour (mouse activity and to some extend its exploratory behaviour). Each mouse was weighed and then placed into a separate calorimetry cage (TSE Systems) with a handful of woodchips from its original cage (**Figure 2.6**). The reference cage was set up alongside cages

containing mice and the gas values were recorded from the reference cage an hour after the start of the experiment. The whole experiment lasted approximately 21 hours and consisted of a 5-hour light phase acclimatization period, followed by a 12-hour dark phase, and at least a 3-hour light phase. The following parameters were measured: cumulative food intake, activity (recorded as beam breaks), volume of oxygen consumed and volume of carbon dioxide produced. The respiratory exchange ratio and energy expenditure were derived from the above data. The water intake was assessed as the difference in water bottle weight before and after the experiment. When the experiment was finished, the mouse was returned to its original cage.

Figure 2.6. Photo of a calorimetry cage. Photo taken from http://www.tse-systems.com/download/TSE_Metabolism_LabMaster_PhenoMaster_20081014.pdf.

2.2.6.12 INTRA-PERITONEAL GLUCOSE TOLERANCE TEST (ipGTT)

This procedure was applied to obtain the fasted, basal blood glucose concentrations as well as to investigate glucose tolerance and clearance. Before the ipGTT, mice were fasted overnight for no more than 16 hours. The next day, each mouse was weighed and then a sample of blood was collected (representing 'fasting blood') before a bolus of 20% glucose was administrated by intra-peritoneal injection. Subsequently, blood samples were taken 15, 30, 60 and 120 minutes after the glucose administration. All blood samples were tested for their glucose concentration using Accu-Check® Aviva blood glucose meter (Roche) and Accu-Check® Aviva strips (Roche) modified such that there was no interference with maltose. Blood samples were taken from the tail. The tip of the tail was cut using a blade. The blood was brought to the tip of the tail by running two fingers laterally up the mouse's tail from the base of the tail. The dripping blood was applied to the yellow tip of an Accu-Check® Aviva strip (the other end of the strip was inserted into the Accu-Check® Aviva blood glucose meter), and the blood glucose concentration (in mmol/l) was read from the meter's screen.

2.2.6.13 AUDITORY BRAINSTEM RESPONSE (ABR)

This procedure was performed to assess the hearing sensitivity across a broad range of frequencies. Each mouse was first tested with a click box to check for the presence of the Preyer Reflex, then anaesthetized with ketamine/xylazine by intraperitoneal injection (as described in section 2.2.6.1) and placed on a heating blanket in a sound chamber. After anaesthesia was confirmed, sub-dermal needle electrodes were inserted (active electrode on vertex, reference electrode overlying left bulla, and ground electrode overlying right bulla). The mouse was placed lying in a prone position with paws forward, facing the loudspeaker at a distance of 20 cm and an initial click-evoked ABR (256 clicks @ 70 dB Sound Pressure Level (SPL)) was recorded from the mouse's scalp to ensure a good ABR was present. Then, ABRs were recorded at the following frequencies and levels: 6 kHz (20 – 85 dB), 12 kHz (0 – 70 dB), 18 kHz (0 – 70 dB), 24 kHz (10 – 70 dB) and 30 kHz (20 – 85 dB), presented in 5 dB intervals. At the end, a final

click-evoked ABR (e.g. 256 clicks at 70 dB SPL) was recorded. Subsequently, the electrodes were carefully removed and anaesthesia was reversed using antisedan (as described in section 2.2.6.1), and the mouse was returned to its original cage.

2.2.6.14 DUAL ENERGY X-RAY ABSORPTIOMETRY (DEXA)

This procedure was applied to obtain comprehensive body composition and bone mineral data. The mouse was either anaesthetised (ketamine/xylazine) (as described in section 2.2.6.1) or euthanized by asphyxiation with rising levels of carbon dioxide. Then, the body weight and length were measured, and X-ray images were collected using a Lunar PIXImus II Bone Densitometer (GE Medical Systems) (**Figure 2.7**). To do this, the mouse was placed ventrally onto the white sticky DEXA tray (**Figure 2.7**). The head of the mouse was placed to the left with its snout in the holding slot. The paws were placed away from the body with pads down. The tail was curled to the left around the body so it was entirely within the scanning zone but such that it did not obstruct any other body parts. The mouse was then subjected to the DEXA scan. When all X-ray images were taken, the anaesthesia was reversed using antisedan (if applicable) (as described in section 2.2.6.1). The PIXImus software package generated the image of the entire mouse and provided bone mineral and body composition data. The PIXImus software package also automatically analysed the resulting images, excluding the skull, to calculate total tissue mass, body fat mass, lean mass, fat percentage estimate, bone area, bone mineral density (BMD), and bone mineral content (BMC). Quality control measurements using a ‘phantom’ mouse were performed before each imaging session.

Figure 2.7. Photo of a Lunar PIXImus II Bone Densitometer. Photo taken from http://phenome.jax.org/db/q?rtn=projects/docstatic&doc=Donahue1/Donahue1_Protocol.

2.2.6.15 X-RAY IMAGING

This procedure was conducted to obtain high-resolution X-ray images of the mouse skeleton. X-ray scans were taken using a Faxitron system MX20 (Faxitron X-ray Coorporation). The mouse was either anaesthetised (ketamine/xylazine) (as described in section 2.2.6.1) or euthanized by asphyxiation with rising levels of carbon dioxide, and then five X-ray images acquired, specifically whole body (dorso-ventral and lateral), head (dorso-ventral and lateral) and left forepaw (dorso-ventral). In order to take the dorso-ventral X-ray image of the whole body, the mouse was arranged ventrally in the image zone with its head pointing towards the upper left corner of the zone and its rear towards the lower right corner with the red crosshair on its back. The paws were placed away from the body with the pads down. The tail was curled to the left around the body so it did not cover any other

body parts but fitted completely into the X-ray zone. In order to take the lateral X-ray image of the whole body, the mouse was placed on its side in the image zone with its head pointing towards the upper left corner of the zone and its rear towards the lower right corner with the red crosshair on its rump. The right hind paw was pulled out horizontally and taped perpendicular to the surface. The left hind paw was pulled out and taped to the surface to make it look as natural as possible. The tail was curled behind the mouse's body and along its spine so it did not cover any other body parts but fitted completely into the X-ray zone. In order to take the dorso-ventral X-ray image of the head, the mouse was arranged ventrally in the image zone with its head in the centre. The head was placed in such a way that the red crosshair was on the top of its head just above the ears. In order to take the lateral X-ray image of the head, the mouse was placed on its side onto the image zone with its head in the centre. The head was placed in such a way that the vertical red crosshair was between its eye and ear, and the horizontal crosshair was along its mouth or snout. In order to take the dorso-ventral X-ray image of the left fore paw, the mouse was arranged ventrally in the image zone with its left forelimb in the lower left quadrant of the zone and with the fore paw being in the upper left quadrant. The mouse was placed in such a way that the red crosshair was just below the ear of the mouse. When all X-ray images were taken, the anaesthesia was reversed using antisedan (if applicable) (as described in section 2.2.6.1). The following parameters/abnormalities were recorded: skull shape; morphology of zygomatic bone, maxilla, mandible, teeth, scapula, clavicle, humerus, radius, ulna, femur, tibia, fibula, pelvis and joints; number, shape and fusion of ribs; shape of ribcage and spine; presence or absence of scoliosis, kyphosis or lordosis; number of cervical, thoracic, lumbar, caudal and pelvic vertebrae; transitional vertebrae; shape and fusion of vertebrae; processes on vertebrae and spinous; transverse processes; fusion of processes; number of digits; digital integrity; and presence or absence of polysyndactylism, brachydactylism or syndactylism.

2.2.6.16 CORE TEMPERATURE STRESS

This procedure was performed to determine the basal body temperature and to assess stress-induced hyperthermia. The basal core body

temperature was measured rectally using a TH-5 thermometer with a RET-3 probe (Viking Medical). Mice were transferred to the test area 1 hour before testing, and after acclimatization they were placed on the wire grid of the clean cage. The hind-end of the mouse was raised (the mouse was held by the base of its tail), letting the mouse grip the grid with only its fore paw. Next, using the middle finger, pressure was applied onto the lumbar spinal region of the mouse to arch its back, and the probe was gently introduced into the mouse rectum. After the measurement was taken, the mouse was placed in a clean cage and left there for 15 – 30 minutes. Thereafter, a second reading was taken before the mouse was returned to its original cage.

2.2.6.17 EYE MORPHOLOGY SCREEN

This procedure was performed to detect gross morphological abnormalities in the eye. Both eyes were assessed for the presence of any morphological changes using a slit lamp (Zeiss SL130) and ophthalmoscope (Heine Omega 500). Images on the slit lamp were collected using a LEICA DFC420. Images of the fundus were collected using a topical endoscope (BERCI Tele-Otoscope with HOPKINS straight forward 0°, diameter 3 mm, Halogen cold light fountain light source) and camera (Nikon D40x with Nikon AF 85 mm F1.8D AF Nikkor lens). During the examination, the mouse was first observed for general abnormalities in eye general morphology and size, eye bulging and eyelid closure. Next, both eyes were examined when undilated using the slit lamp. The following parameters/abnormalities were recorded: presence of blood in or around the eye; discharge in or around the eye; corneal morphology, opacity, vascularisation and mineralization; lens stalk; pupil shape, position, dilation and light response (to test this response, the light was dimmed for a few seconds and then brought to its original level); and iris position and pigmentation. Subsequently, both eyes were examined when dilated (induced with 1% tropicamide and/or neosynephrine) using the slit lamp. The following parameters were recorded: lens morphology and opacity (non suture or snowflake), corneal irregularities, and synechia. Finally, both eyes were examined in a dilated state using an ophthalmoscope. The following parameters/abnormalities were recorded: retina morphology,

structure and pigmentation; blood vessel morphology pattern, number and structure; optic disc morphology; Bergmeister's papilla morphology; and whether a cataract was visible.

2.2.6.18 RETRO-ORBITAL BLEED

This procedure was applied to obtain high-quality blood samples from the retro-orbital sinus via a capillary tube. Each mouse was anaesthetized with ketamine/xylazine by intraperitoneal injection (as described in section 2.2.6.1). After anaesthesia was confirmed, the capillary tube was inserted into the space between the globe and the lower eyelid at an approximately 45° angle. Next, the capillary was directed gently in a ventrolateral direction while rotating the capillary tube, and the flowing blood was collected into the capillary tube. From each mouse, two collection tubes were filled with dripping blood. 50 μl of blood was collected into an EDTA-coated tube (Kabe Labortechnik) for subsequent haematological analysis (this tube was kept on ice), while 1 ml of blood was collected into a lithium heparin-coated tube (Kabe Labortechnik) for subsequent clinical chemistry analysis (this tube was kept at room temperature). After the blood was collected, the mouse was culled by cervical dislocation.

2.2.6.19 HEART WEIGHTS

This procedure was performed to assess the weight of the mouse's heart. Each mouse was terminally anaesthetized with ketamine/xylazine by intraperitoneal injection (as described in section 2.2.6.1). After anaesthesia was confirmed, its heart was dissected out and weighed before being placed in a 10% neutral buffered formalin for subsequent histopathological analysis.

2.2.6.20 HAEMATOLOGY PANEL

This procedure was performed to analyse the following whole blood parameters: white and red blood cell count; mean corpuscular volume; haemoglobin; erythrocyte indices (hematocrit, mean corpuscular haemoglobin, mean corpuscular haemoglobin concentration, and red blood cell distribution width); platelet count; and mean platelet volume. The

non-fasted mouse was terminally anaesthetised with ketamine/xylazine and 50 μl of blood was collected into the EDTA-coated tube (Kabe Labortechnik) by retro-orbital bleeding. All blood samples were automatically analysed using a haematology analyser (scil Vet animal blood counter, Horiba Medical, cat. #: RS 232).

2.2.6.21 PLASMA CHEMISTRY PANEL

This procedure was performed to analyse the following parameters from the blood plasma: sodium, potassium, chloride, glucose, triglycerides, cholesterol, high density lipoprotein, low density lipoprotein, non-esterified free fatty acids (NEFAC), glycerol, amylase, alanine aminotransferase, alkaline phosphatase, creatine kinase, aspartate aminotransferase, total bilirubin, total protein, albumin, creatinine, urea, calcium, magnesium, iron, phosphatase, lactate dehydrogenase, and uric acid. The non-fasted mouse was terminally anaesthatised with ketamine/xylazine and 1 ml of blood was collected into a lithium heparin-coated tube (Kabe Labortechnik) by retro-orbital bleeding. All plasma samples were automatically analysed in an Olympus AU400 chemistry immunoanalyser (Alternative Biomedical Solutions).

2.2.6.22 BEHAVIOURAL TESTS

These tests used male monosomic *Df*$^{Lipi\text{-}Usp25}$ mice and male wildtype littermate controls fed on a normal-fat diet who were 3- to 7-month old and were group-housed from weaning. All mice were prehandled for 1 – 2 minutes every day for four days prior to testing for habituation.

2.2.6.22.1 ELEVATED PLUS MAZE

This test was performed to assess anxiety responses to a novel environment. The elevated plus maze was made of Plexiglas and homogeneously illuminated with tests performed under dim light. The apparatus consisted of a central square and four 30 cm long and 5 cm wide black arms, of which two were closed by 15 cm high walls and two were open (**Figure 2.8**). The maze was elevated 40 cm off the floor (**Figure 2.8**). The

test was conducted during the light period of the light-dark cycle. At least 5 minutes before the test, the light levels in the room were adjusted to medium. Each mouse was placed in the centre square in such way that it faced both towards the open arm and away from the experimenter, and left to explore the maze for a single 5-minute session with the experimenter out of view. Each mouse was tested once. When the test was finished, the mouse was put back into its original cage, and the maze was cleaned with 70% ethanol before testing another mouse. All test sessions were recorded and subsequently analysed with the Noldus Ethovision 3 video tracking software (Tracksys Ltd., UK). The tracking system recorded time spent in each arm and number of entries into each arm, with an animal being considered inside a zone whenever its centre point lay within.

Figure 2.8. Photo of an elevated plus maze. Photo taken from http://www.med-associates.com/mazes/elevated-maze.htm).

2.2.6.22.2 SOCIAL RECOGNITION TEST

This test was performed to assess 24-hour social memory retention. The test was performed under red light, using 3 different 2-month old male stimulus mice (C57BL/6NTac/USA (mouse A), 129P2/OlaHsd (mouse B) and C57BL/6NTac/USA (mouse C)) sedated with ketamine/xylazine (i.p. 1 g/0.1 g per kg of body weight). Test mice were first habituated for 10 minutes to a test arena identical to their home cage. On day 1, for the habituation-dishabituation test, a stimulus mouse A was placed into the test arena for 1 minute. The same stimulus mouse A was subsequently presented four times at 10 minutes intervals. In the fifth trial, a stimulus mouse B was presented for 1 minute. On day 2, for the discrimination test, the animals were simultaneously presented with stimulus mouse A (familiar animal that was encountered on trials 1 – 4 on day 1) and mouse C (new unfamiliar animal) for 2 minutes. All trials were recorded with an overhead camera and the videos were subsequently scored blind of genotype using a handheld stopwatch. The amount of time the test animal spent investigating, by direct oronasal contact or close approach (about 1 cm), sniffing towards the stimulus mice A and C, was recorded. If the test animal spent longer investigating a novel stimulus animal (mouse C) than the familiar one (mouse A), this was taken as evidence for social recognition. The discrimination ratio was taken as the amount of time spent investigating the familiar stimulus animal (mouse A) divided by the sum of time spent investigating both stimulus mice A and C. These data are presented as a mean and a standard error in the mean, and were analysed using GraphPad Prism software (GraphPad Software Inc.). Statistical analysis for the habituation-dishabituation test data was performed using a two-way ANOVA with repeated measures for trial and genotype as factor and a Tukey-HSD *post hoc* test. Discrimination data was analysed using the two-tailed Student's *t*-test based on the discrimination ratio.

2.2.6.23 INFECTIONS OF MICE WITH BACTERIA

2.2.6.23.1 *CITROBACTER RODENTIUM* INFECTION – AN OVERVIEW

An equal number of female wildtype and mutant mice were infected with

Citrobacter rodentium lux when they were 6 weeks of age (see section 2.2.6.23.1.2 below for details). Mice were monitored and weighed daily for 28 days post-infection. Faecal samples from each mouse were collected on day 1 post-infection, and then every 2 – 3 days until day 27 post-infection (see section 2.2.6.23.3.2 below for details). The amount of bacteria in faecal samples was enumerated by serial dilution and plating onto agar plates (see section 2.2.6.23.4 below for details). On day 14 post-infection, half of the mice (of each genotype) were culled by cervical dislocation, and spleens, livers, caecal patches, caecums and at least 6 cm of distal colon, and caecal contents were extracted for bacterial counts (see section 2.2.6.23.3.2 below for details). The amount of bacteria in collected tissues/ceacal contents was enumerated by serial dilution and plating onto agar plates (see section 2.2.6.23.4 below for details). The 6 cm of distal colon was weighed, checked for signs of gross hyperplasia, and a 5 mm section from the most distal colon was removed and placed into 10% neutral buffered formalin for subsequent histopathological analysis. All these analyses were repeated on the remaining mice at day 28 post-infection.

2.2.6.23.1.1 PREPARING INOCULUM TO INFECT MICE WITH *C. RODENTIUM*

One cryo-vial of *Citrobacter rodentium* lux was put into a conical flask containing 100 ml of LB with kanamycin (50 mg/ml) and naladixic acid (50 mg/ml). The flask was incubated in a shaking incubator at 37°C overnight. The next morning, 20 ml of the overnight culture was added to a 50 ml Falcon tube and centrifuged at 40,000 rpm for 10 minutes. Next, the supernatant was removed and the pellet resuspended in 10 ml of PBS. This was called the 'inoculum'.

2.2.6.23.1.2 INFECTING MICE WITH *C. RODENTIUM*

1.5 ml of the inoculum was drawn up into a syringe with the gavage needle. Once the air bubbles had floated to the top, the volume of the syringe was adjusted so there was 1 ml of inoculum. Prior to the infection, a mouse was anaesthetized using 100% isoflurane gas, IsoFlo (Abbott, cat. #: 05260-05). Next, the gavage needle was gently slid down the

oesophagus and into the stomach of the anaesthetized mouse that was being held in the scruffed position. The plunger was slowly depressed and 0.2 ml of the inoculum injected into the stomach. The gavage needle was then gently withdrawn and the mouse put back into its original cage and closely observed util it recovered.

2.2.6.23.2 *SALMONELLA* TYMPHIMURIUM INFECTION – AN OVERVIEW

An equal number of male control and mutant mice were infected with *Salmonella* Typhimurium TET C when they were 6 weeks of age (see section 2.2.6.23.2.2 below for details). Mice were monitored and weighed daily for 28 days post-infection. On day 14 post-infection, half of the mice (of both genotypes) were culled by cervical dislocation and the spleens, livers and caecal contents were extracted for bacterial enumeration (see section 2.2.6.23.3.2 below for details). The amount of bacteria was enumerated by serial dilution and plating onto agar plates (see section 2.2.6.23.4 below for details). Additionally, 1/4 of the spleen and one lobe of the liver were dissected from each mouse, and placed into 10% neutral buffered formalin for subsequent histopathological analysis. On day 28 post-infection, the remaining mice were terminally anaesthatised with ketamine/xylazine, bled via cardiac puncture to obtain blood serum for testing for anti TET C specific antibodies by enzyme-linked immunosorbent assay (ELISA) (IgG, IgG1 and IgG2a) (see section 2.2.6.23.6 below for details), and then analysed in the same way as the day 14 post-infection mice.

2.2.6.23.2.1 PREPARING INOCULUM TO INFECT MICE WITH *S.* TYPHIMURIUM

100 μl of *Salmonella* Typhimurium M525 TET C was added to a universal tube containing 10 ml of PBS and then gently vortexed. Next, 100 μl of its content were added into another universal tube containing 10 ml of PBS and gently vortexed. This was called the ‘inoculum’.

2.2.6.23.2.2 INFECTING MICE WITH *S.* TYPHIMURIUM

Prior to infection with *Salmonella* Typhimurium, the mouse was put into a

heat chamber box (Harvard Apparatus UK, cat. #: IC016000) set at 37ºC for 20 to 30 minutes. 1.5 ml of the inoculum was drawn up into a syringe and, once the air bubbles had floated to the top, the volume of the syringe was adjusted so there was 1 ml of inoculum. Then the mouse was removed from the heat chamber box and placed in a restraining tube. The needle was gently inserted into a tail vein and the plunger slowly depressed util 0.2 ml of the inoculum had been injected into the vein. Finally, the needle was gently withdrawn and the mouse returned to its original cage.

2.2.6.23.3 PROCESSING OF BLOOD FOR SERUM AND TISSUES, CAECAL CONTENTS AND FAECAL SAMPLES FOR BACTERIAL COUNTS FROM MICE INFECTED WITH *C. RODENTIUM* OR *S.* TYMPHIMURIUM

2.2.6.23.3.1 BLOOD

Blood tubs were centrifuged at 13,000 rpm for 5 minutes. The top layer of serum was transferred into a fresh eppendorf tube and stored at -20°C.

2.2.6.23.3.2 TISSUES/FAECAL CONTENTS

Tissues/caecal contents were collected into plastic bags, which were then weighed. The contents were then thoroughly broken up by hitting them with the lid part of a falcon tube and 5 ml of ddH_2O added into each bag. The bag was left at room temperature for 10 minutes before being placed in the Stomacher machine (Seward) set at the highest speed for 2 minutes. The resulting liquid content was used to prepare the serial dilutions for bacterial enumeration.

2.2.6.23.3.3 FAECAL SAMPLES

Faecal samples were collected into eppendorf tubes, which were then weighed. Next, 100 μl of PBS was added for every 0.01 g of faecal sample and the whole content was vortexed for about 5 minutes until the faecal sample was fully homogenized. Then the eppendorf tube was centrifuged at 13,000 rpm for 1 minute and the liquid content used to prepare the serial dilutions for bacterial enumeration.

2.2.6.23.4 BACTERIA ENUMERATION IN TISSUES, CAECAL CONTENTS AND FAECAL SAMPLES

To count the amount of bacteria in collected tissues, caecal contents or faecal samples, a serial dilution of each sample was prepared, which was then plated onto agar plates. Specifically, five 10-fold dilutions were prepared in a 96-well plate for each sample (1:1, 1:10, 1:100, 1:1000, 1:10000, 1:100000 dilutions of the sample). To do this, 200 μl of sample (liquid content) either from the bag (tissues or caecal contents) or eppendorf tube (feacal samples) was placed into well 1A of a 96-well plate (this represents the neat (N) concentration). Next, the contents of well 1A was pipetted up and down a few times and 50 μl was transferred into well 3A well containing 450 μl of ddH_2O (for tissues or caecal contents) or 450 μl of PBS (for feacal samples) to obtain a 1:10 dilution. This process was repeated in the same way in order to transfer 50 μl of the content from well 3A to 5A, 5A to 7A, 7A to 9A, and 9A to 11A to obtain 1:100, 1:1000, 1:10000, 1:100000 dilutions respectively. The tips were changed after each transfer. Next, 20 μl of dilution from wells 1A, 3A, 5A, 7A, 9A, and 11A was pipetted up and down a few times and plated on an LB agar plate containing kanamycin (50 mg/ml) and naladixic acid (50 mg/ml). Once dry, the plates were inverted and put in an incubator at 37°C overnight.

2.2.6.23.5 COUNTING THE BACTERIAL COLONIES FROM TISSUES, CAECAL CONTENTS AND FAECAL SAMPLES

LB agar plates were removed from the incubator after being left overnight at 37°C. Plates were placed against a light surface such that the lids were facing downwards. The colonies were counted by hand with a marker pen that was used for marking each individual colony.

2.2.6.23.6 DETERMINATION OF IMMUNOGLOBULIN TITRE FROM BLOOD SERUM

Each well of the Nunc MaxiSorp™ flat-bottom 96 well plate (eBioscience, cat. #: 44-2404-21) was coated with 50 μl of 2 mg/ml TET C protein (antigen) solution in coating buffer (0.1 M Na_2HPO_4; pH 9). Three

plates were prepared at the same time. Plates were then sealed and incubated at 4°C overnight. The next day, the coating solution was flicked out of the plates and 150 μl of blocking buffer (3% Bovine Serum Albumin (BSA) in 1x PBS, kept on ice) was added to each well. Plates were then sealed and incubated at room temperature for 1 hour. After incubation, the blocking buffer was flicked out of all plates and the plates were rinsed with wash buffer (0.05% Tween-20 in 1x PBS). Next, 112.5 μl of antibody buffer (1% BSA in 1x PBS, kept on ice) was added to the top row of wells and 100 μl of the buffer was added to the remaining wells. In a fresh eppendorf tube, 6 μl of serum (containing the primary antibody) from 4 control and 4 mutant mice was added to 54 μl of antibody buffer. Then 12.5 μl of the diluted serum was added to the top row of wells of each plate. The order of serums was as follows: mutant M1, M2, M3 and M4, 2 blank wells, wildtype W1, W2, W3 and W4, and 2 blank wells. Next, the serums were serially diluted down each plate. The serums in the top row of wells were mixed by pipetting a few times, then 25 μl was transferred to the second row. This process was repeated all the way down the plate (i.e. all 8 rows) and tips were changed after each transfer. Then the plates were sealed and incubated at 37°C for 1 hour. After incubation, the diluted serum was flicked out of the plates, which were then washed three times with wash buffer for 5 minutes. Then 100 μl of the HRP-conjugated secondary antibody (either Ig, IgG1 or IgG2a) was added to the plate (secondary antibodies were diluted 1:1000 in antibody buffer). The plates were sealed and incubated at 37°C for 1 hour. The secondary antibody was then flicked out of the plates, which were washed three times with the wash buffer for 5 minutes. Then *o*-phenylenediamine tablets (Sigmafast tablet set; Sigma-Aldrich, cat#: P9187) were added to 20 ml of ddH_2O in a 50 ml Falcon tube and kept on ice. The ELISA reaction was developed by adding 50 μl of *o*-phenylenediamine mixture to each well of the plate. Plates were then sealed and incubated at room temperature for 15 minutes. After the wells in the top row had turned brown, the reactions were terminated by the addition of 20 μl of stop solution (12.5% sulphuric acid) to each well. The absorbance of the plate was read using the benchmark plate reader at an optical density (OD) of 490 nm.

2.2.7 TUMOUR WATCH STUDY

Blm$^{m3/m3}$ homozygous knockout mice (Luo 2000) were provided by Professor Allan Bradley (The Wellcome Trust Sanger Institute, Hinxton, Cambridge, UK). The *Blm*$^{m3/m3}$ mice were crossed with the *Df*$^{Lipi\text{-}Usp25}$*/+ mice* to generate a cohort of mice for tumour watch study. From all obtained mice, only mice with the following genotypes were used in the study: 1) *Df*$^{Lipi\text{-}Usp25}$*/+, Blm*$^{m3/m3}$, 2) *Df*$^{Lipi\text{-}Usp25}$*/+, Blm*$^{+/+}$, 3) *+/+, Blm*$^{m3/m3}$. Mice on tumour watch were observed twice a day for signs of illness/morbidity, at which time a full necropsy was performed and all tissues macroscpically examined before being placed in 10% neutral buffered formalin for histopathological analysis.

CHAPTER 3

MODELLING A DELETION OF THE HUMAN REGION 21q11.2–q21.1 IN MICE

3.1 GENERAL OVERVIEW

Haploinsufficiency of human chromosome 21 results in a rare condition known as Monosomy 21. Complete Monosomy 21 typically results in prenatal death, and thus most cases described are partial or mosaic. Patients with Monosomy 21 display a variety of clinical features, including intellectual disability, craniofacial, skeletal and/or cardiac abnormalities, and respiratory complications. In addition, partial deletions of the long arm of human chromosome 21 have also been observed in several types of solid tumours. To search for dosage-sensitive genes involved in these human pathologies, we used chromosome engineering to generate a monosomic mouse model carrying a deletion of the *Lipi* to *Usp25* interval, syntenic with 21q11.2–q21.1 in humans. Haploinsufficiency for the six genes in this interval resulted in no gross morphological defects. Behavioural analysis including open field and measures of anxiety and social interaction were normal in monosomic mice. They did, however, display impaired memory retention compared to control animals, which models the intellectual disability observed in patients with Monosomy 21. Moreover, when fed a high-fat diet (HFD), monosomic mice exhibited a significant increase in fat mass/fat percentage estimate compared with controls, severe fatty changes in their livers, and thickened subcutaneous fat. Thus genes within the *Lipi–Usp25* interval are involved in memory retention and the regulation of fat deposition.

3.2 INTRODUCTION

3.2.1 OVERVIEW OF HUMAN CHROMOSOME 21

Chromosome 21 is the smallest human autosome (Hattori 2000). This acrocentric chromosome spans almost 47 Mb of DNA and corresponds to about 1 – 1.5% of the genome (Hattori 2000). According to the current Ensembl annotation (Human GRChr37), chromosome 21 and contains 232 known protein-coding genes, 7 novel protein-coding genes and 141 pseudogenes. The genomic regions of human chromosome 21 show synteny to mouse genomic regions located on chromosomes 16, 17 and 10 (Hattori 2000). Analysis of the DNA sequence of human chromosome 21 revealed that 81% of known human genes overlapped with mice genes by at least one exon (Frazer 2001).

3.2.2 BRIEF DESCRIPTION OF GENES MAPPED TO THE HUMAN REGION 21q11.2–q21.1

The human region 21q11.2–q21.1 spans 1.7 Mb and contains only eight genes (*LIPI*, *RBM11*, *ABCC13*, *HSPA13*, *SAMSN1*, *AF1651138.1*, *NRIP1*, and *USP25*). Six of these genes, namely *LIPI*, *RBM11*, *HSPA13*, *SAMSN1*, *NRIP1* and *USP25*, are conserved between human and mouse.

The lipase, member 1 (*LIPI*) gene consists of 10 exons and is expressed only in the testis (Wen 2003). The *LIPI* gene encodes a 460 amino acid phospholipase that hydrolyzes phosphatidic acid to produce lysophosphatidic acid (Hiramatsu 2003). Exon sequencing of *LIPI* identified a single nucleotide polymorphism (SNP) (C55Y) in two patients with hypertriglyceridemia, suggesting that this missense mutation might be a causal factor for hypertriglyceridemia. Also, at least one other SNP was found to be associated with variation in plasma cholesterol in unrelated populations (Wen 2003).

The RNA binding motif protein 11 like (*RBM11*) gene consists of 5 exons and is expressed only in the testis (Brun 2003). The full-length isoform of RBM11 (RBM11a) has an RNA recognition motif (a putative RNA-binding domain) that is known to bind single-stranded RNAs (Brun

2003). Two truncated isoforms of RBM11 (RBM11b and RBM11c) are devoid of an RNA recognition motif, and thus are unable to bind single-stranded RNAs (Brun 2003).

The ATP-binding cassette, sub-family C (CFTR/MRP), member 13 (*ABCC13*) pseudogene consists of 14 exons and is expressed in a variety of tissues, including brain, placenta, lung, liver, pancreas, ovary, bone marrow, and in the digestive system, from ileum to rectum, with especially high expression detected in the colon (Yabuuchi 2002). *ABCC13* encodes a 325 amino acid protein that consists of four transmembrane domains homologous to ABCC1 (MRP1), ABCC2 (MRP2), ABCC3 (MRP3) and ABCC6 (MRP6) proteins, but is devoid of Walker A, Walker B, and signature C motifs, and thus results in production of a non-functional ABC protein (Yabuuchi 2002). *ABCC13* belongs to the superfamily of genes encoding ATP-binding cassette (ABC) transporters that are involved in the transport of different molecules across membranes and modulation of ion channels. More specifically, *ABCC13* is a member of the multidrug resistance-associated protein (MRP, ABCC) subfamily of genes that play a role in multidrug resistance (Yabuuchi 2002).

The heat shock protein 70kDa family, member 13 (*HSPA13*) gene (previously known as *STCH*) consists of 5 exons and is constitutively expressed in a variety of tissues, including heart, brain, placenta, lung, liver, skeletal muscle, kidney and pancreas (Otterson 1994). *HSPA13* encodes a 471 amino acid protein that associates with microsome membranes and contains an ATPase domain that shows activity independent of peptide stimulation. HSPA13 belongs to the heat shock protein 70 family, of which members are involved in processing and transport of cytosolic and secretory proteins and disposal of denaturated or misfolded proteins (Otterson 1994). However, in contrast to the other members of the family, HSPA13 is not inducible by heat shock (Otterson 1994).

The SAM domain, SH3 domain and nuclear localization signals 1 (*SAMSN1*) gene (previously known as *HACS1*) consists of 8 exons and is highly expressed in immune tissues and haematopoietic cells, and shows low level expression in many other tissues, including heart, brain, placenta and lung (Claudio 2001). *SAMSN1* encodes a 441 amino acid protein that consists

of an SH3 motif and a SAM domain that are found in adaptor proteins that are involved in signalling pathways, and thus seems to be involved in cytoplasmic signal transduction in cells (Claudio 2001). *SAMSN1* may potentially play a role in the development of haematopoietic tumours, as it is mapped to the 21q11.2 region that is frequently disrupted by translocation events (Mitelman 1997).

The nuclear receptor interacting protein 1 (*NRIP1*) gene consists of 3 exons and is expressed in a variety of tissues, including breast, bone, lung, cervix, ovary, placenta, liver and fibroblast (Cavailles 1995). *NRIP1* encodes a 1158 amino acid protein that contains an amphipathic α-helix that is found in proteins that are involved in ligand-dependent transcription stimulation by nuclear receptors (Cavailles 1995). In fact, NRIP1 modulates the transcriptional activity of the oestrogen receptor by interacting with the hormone-dependent activation domain AF2 of this receptor (Cavailles 1995).

The ubiquitin-specific processing protease 25 (*USP25*) gene consists of 25 exons (Valero 1999). USP25 encodes 3 protein isoforms that are generated by alternative splicing (Bosch-Comas 2006). The USP25a isoform is expressed in a variety of tissues, including brain, heart, kidney, liver, lung, prostate, testis, spleen, thymus, and skeletal muscle (Bosch-Comas 2006). The USP25b isoform is expressed in all the aforementioned tissues except skeletal muscle, however, its level of expression is much lower than that of USP25a (Bosch-Comas 2006). In contrast, the USP25m isoform has a very restricted expression pattern, and can only be detected in heart and skeletal muscle (Bosch-Comas 2006). USP25 belongs to the ubiquitin-specific processing protease (UBP) subfamily of deubiquitinating enzymes that rescue proteins from degradation by the 26S proteasome (Valero 1999). Moreover, the USP25m isoform seems to regulate muscle differentiation and functioning, because it interacts with sarcomeric proteins (Bosch-Comas 2006).

3.2.3 MONOSOMY 21 SYNDROME

The triplication of chromosome 21 (or a subset of genes mapped to the long arm of this chromosome) is responsible for Down syndrome. In contrast, haploinsufficiency of genes on human chromosome 21 results in Monosomy

21. Only partial or mosaic monosomies of chromosome 21 have been diagnosed in living individuals, and thus it is believed that complete monosomy of chromosome 21 results in prenatal death (Joosten 1996; Mori 2004). Clinical phenotypes observed in patients with partial monosomies of chromosome 21 are very heterogeneous. Some patients show only mild to moderate intellectual disability, and have no other apparent dysmorphic or congenital malformations (Wakui 2002; Tinkel-Vernon 2003), while others are diagnosed with a variety of severe clinical symptoms, such as intellectual disability, microcephaly, epilepsy, craniofacial, skeletal, cardiac and/or renal abnormalities, and respiratory difficulties (Chettouh 1995; Riegel 2005; Lyle 2008; Katzaki 2010; Lindstrand 2010; Roberson 2010).

To date, four comprehensive studies have been performed using array comparative genomic hybridization (aCGH) and high-density single nucleotide polymorphism (SNP) genotyping to define the breakpoint regions present in patients with Monosomy 21 and to correlate these breakpoints with phenotype (Lyle 2008; Katzaki 2010; Roberson 2010; Lindstrand 2010).

Array comparative genome hybridization performed by Lyle *et al* identified eight new partial monosomies of chromosome 21 and refined the mapping of three previously described ones (Lyle 2008). All the partial Monosomy 21 cases had unique breakpoints and varied in size, ranging from 1.48 to 18.2 Mb. The identified partial monosomies were subsequently grouped into three broad regions of human chromosome 21 on the basis of observed monosomy phenotype in patients. Deletions within/of the "centromeric" region, from the centromere to around 31.2 Mb, were associated with a severe phenotype, including profound intellectual disability and a variety of craniofacial malformations. No cases with a deletion spanning the entire "medial" region, from 31.2 to 36 Mb, were identified. Only one patient with a partial aneuploidy of the medial region was reported, and this patient had a severe phenotype. The apparent absence of patients carrying a deletion spanning the entire medial region might suggest that haploinsufficiency for genes in this interval results in prenatal death. Deletions within/of the "telomeric" region, from around 36 – 37.5 Mb to the telomere, were associated with a milder phenotype, including mild to moderate intellectual disability, and either the complete absence of craniofacial

malformations or the presence of only minor craniofacial abnormalities (Lyle 2008).

Array comparative genome hybridization performed by Katzaki *et al* identified three new patients with partial monosomies of chromosome 21, spanning the 21q22.11–q22.12 region (Katzaki 2010). All three new cases were diagnosed with severe developmental retardation, dysmorphic malformations, behavioural problems, and thrombocytopenia. Subsequently, they compared clinical symptoms observed in these three new cases with clinical features previously reported in six other patients with the overlapping 21q22.11–q22.12 deletions. They concluded that two potential clinical phenotypes related to the 21q22 microdeletions (including the *RUNX1* gene) could be defined, namely syndromic thrombocytopenia with developmental and growth retardation and thrombocytopenia with/without mild dysmorphic abnormalities (Katzaki 2010).

High-density single nucleotide polymorphism genotyping performed by Robertson *et al* identified ten new partial monosomies of chromosome 21 (Roberson 2010). These cases were divided into two cohorts. Cohort A consisted of three patients that had relatively mild phenotypes characterized by intellectual disability (mild to moderate) and the presence of only a few dysmorphic abnormalities. Cohort B consisted of seven patients that had more severe phenotypes characterized by intellectual disability (moderate to severe, if the severity was assessed), and the presence of multiple congenital anomalies, including craniofacial, cardiac and skeletal defects. They also collected and included information about twelve additional cases of partial Monosomy 21 obtained from the Database of Chromosomal Imbalance and Phenotype in Humans using Ensembl Resources (DECIPHER) (Firth 2009) and commented on three cases described previously by Lindstrand *et al* (Lindstrand 2010; Roberson 2010). The data obtained from all these cases were classified and interpreted according to their locations within the “centromeric”, “medial” or “telomeric” regions of human chromosome 21 described previously by Lyle *et al* (Lyle 2008; Roberson 2010).

Four new cases, two DECIPHER cases and two Lindstrand *et al* cases of partial Monosomy 21 were mapped to/within the “centromeric” region of

chromosome 21 (Roberson 2010). In contrast to Lyle *et al*, they observed that not all of their cases with deletions of/within the “centromeric” region had a severe phenotype. For example, one of their patients with a deletion spanning the entire “centromeric” region was diagnosed with only mild dysmorphia and an absence of any intellectual, cardiac or renal defects (Roberson 2010). It is worth noticing that one of the cases described by Lindstrand *et al* had a large deletion within the “centromeric” region of chromosome 21 spanning approximately 14 Mb but also did not show a severe clinical phenotype, and was diagnosed with normal to late speech development, normal to mildly delayed social, emotional and cognitive development and some abnormalities in gross and fine motor functions (Lindstrand 2010). Robertson *et al* hypothesised that, perhaps, deletions or translocations of chromosomes other than 21 might contribute to the variety of observed phenotypes in patients with deletions of/within the “centromeric” region.

Four new cases, three DECIPHER cases and two Lindstrand *et al* cases of partial Monosomy 21 were mapped to/within the “medial” region of chromosome 21 (Roberson 2010). In addition to two DECIPHER cases that had deletions that spanned almost the entire “medial” region of chromosome 21, two new cases and two Lindstrand *et al* cases had deletions that substantially overlapped with the “medial” region of chromosome 21. The presence of cases that had such large deletions of the “medial” region is in contrary to the finding of Lyle *et al*, who identified only one patient with a small partial deletion of the “medial” region of chromosome 21, and questions the Lyle *et al* hypothesis that deletions of the “medial” region are not compatible with life.

Six new cases and eight DECIPHER cases of partial Monosomy 21 were mapped to/within the “telomeric” region of chromosome 21 (Roberson 2010). In agreement with Lyle *et al,* deletions of/within the “telomeric” region were the most prevalent, and patients with such deletions were diagnosed with a less severe range of clinical features (Roberson 2010).

Lindstrand *et al* suggested that deletions spanning the *ITSN1* gene might form a critical region of intellectual disability, and deletions spanning the *KCNE1*, *RCAN1*, *CLIC6* and *RUNX1* genes might form a critical region of severe cardiac abnormalities (Lindstrand 2010). Nevertheless, some of

Robertson *et al* new cases, DECIPHER cases and Lyle *et al* cases that were diagnosed with intellectual disability and/or severe cardiac malformations, had deletions that did not span any of the above genes, which stresses the importance of searching for additional genes that are responsible for the clinical phenotypes observed in Monosomy 21 patients (Roberson 2010).

3.2.4 MOUSE MODELS OF MONOSOMY 21 SYNDROME

In parallel with human genetics approaches, monosomic mouse models have been generated to facilitate the identification of dosage-sensitive genes involved in the clinical features observed in patients with Monosomy 21 (Olson 2004; Besson 2007; Olson 2007; Yu 2010). Synteny exists between human chromosome 21 (HSA21) and mouse chromosomes 16 (MMU16), 17 (MMU17) and 10 (MMU10). Specifically, about 23.2 Mb of human chromosome 21, from 21q11.2 to 21q22.3, is homologous to C3.1–C4 on MMU16, 1.1 Mb of 21q22.3 is homologous to the B1 band on MMU17 and 2.3 Mb of the 21q22.3 region is syntenic to C1 on MMU10.

A mouse model carrying a heterozygous deletion of MMU16, syntenic to the human region 21q22.12–q22.3 displayed a significant reduction in both overall brain and hippocampus volume and in body size, but had a notably larger cerebellum, and a higher density of both Purkinje cells and granule cells (Olson 2007). Nevertheless, these changes did not show any correlation with abnormal functioning of the hippocampus measured in the Morris water maze assay or by electrophysiology (Olson 2007), suggesting that this region of mouse chromosome 16 might be excluded from further searches for a causative gene (or genes) for partial Monosomy 21-associated intellectual disability.

A mouse model carrying a heterozygous deletion of MMU10, syntenic to the distal part of human region 21q22.3 located between the *PRMT2* and *COL6A1* genes, showed no gross morphological or behavioural anomalies. However, it exhibited an increased inflammatory reaction after intranasal lipopolysaccharide (LPS) administration, an impaired airway response, and an enhanced secretion of pro-inflammatory cytokines (Besson 2007). These

results suggested that some genes in the deleted region might be responsible for the regulation of lung function and inflammation (Besson 2007).

In contrast, a mouse model carrying a heterozygous deletion of MMU10, syntenic to the human region located between the *PRMT2* and *PDXK* genes, showed both impairment in spatial learning and memory when assessed in the Morris water maze tasks, and in context-associated learning when examined by the contextual fear conditioning test (Yu 2010). Interestingly, 13 out of 41 syntenic genes located on mouse chromosome 10, namely the genes located between the *Prmt2* and *Col6a1* genes, could be excluded as candidate genes for partial Monosomy 21-associated intellectual disability, as heterozygous deletion of these genes did not result in learning impairment in mice (Besson 2007).

A mouse model carrying the deletion of the region of mouse chromosome 17 syntenic to the human region located between the *ABCG1* and *RRP1B* genes displayed impairment in context-associated learning when examined by the contextual fear conditioning test (Yu 2010), suggesting that a causative gene (or genes) for partial Monosomy 21-associated intellectual disability might be among the 19 syntenic genes located on mouse chromosome 17.

3.2.5 INCREASED FREQUENCY OF TUMOUR FORMATION IN PATIENTS WITH DELETIONS OF THE PROXIMAL END OF THE LONG ARM OF CHROMOSOME 21

Apart from the association of partial deletions of human chromosome 21 with Monosomy 21, partial loss of the proximal end of the long arm of chromosome 21 has been observed in several types of solid tumours, including cancers of the ovary, stomach, breast, oral cavity and bone (Cliby 1993; Ohgaki 1998; Yamamoto 2003; Aoki 2005; Chen 2005; dos Santos Aguiar 2007).

In a search for candidate tumour suppressor genes (TSGs), Cliby *et al* analysed 37 epithelial ovarian tumours for loss of heterozygosity (LOH) using 70 polymorphic markers that were distributed along all human autosomal chromosome arms, except for the short arms of acrocentric chromosomes.

They reported a frequency of LOH greater than 35% for several chromosome arms, including the long arm of human chromosome 21 (21q) (Cliby 1993).

Ohgaki *et al* studied 142 breast tumours for LOH using 11 polymorphic microsatellite markers distributed along the long arm of chromosome 21. They found LOH for single or multiple markers in 31% of analysed tumours. The highest LOH was identified for the 21q21 region, suggesting the presence of at least one candidate TSG within this region (Ohgaki 1998).

Dos Santos Aguiar *et al* studied 41 paediatric osteosarcomas (OSs) by comparative genomic hybridization (CGH). They observed a broad range of both gains and losses of different chromosomal arms. Interestingly, they found chromosome 21 abnormalities in 70% of analysed tumours, with losses being much more prevalent than gains. Of the losses, the deletion of the 21q11.2–q21 region was the most frequently detected, suggesting the possible existence of candidate TSGs in this region that might be involved in the development of OSs (dos Santos Aguiar 2007).

Yamamoto *et al* analysed 40 primary oral squamous cell carcinomas (SCCs) for LOH using 30 polymorphic microsatellite markers distributed along the long arms of chromosomes 2, 3 and 21. They reported a frequency of LOH greater than 20% for several markers mapping to all three studied chromosome arms, including increased LOH for markers mapping to the chromosome region 21q11.1 (52.4% frequency of LOH), 21q21 (21.6% frequency of LOH) and 21q22.1 (22.2% frequency of LOH). Their finding suggests that the existence of candidate TSGs in the 21q11.1–q22.1 region are likely to play a role in the development of SCCs (Yamamoto 2003).

Following up on Yamamoto *et al* results, Chen *et al* analysed 43 additional primary oral squamous cell carcinomas (OSCCs) for LOH using 12 polymorphic microsatellite markers distributed along the 21q11.1–q21.1 region. The highest LOH (60%) was observed in two separate areas of the 21q11.1–q21.1 region, suggesting the existence of at least two candidate TSGs in the 21q11.1–q21.1 region that might account for the development of OSCC (Chen 2005).

Sakata *et al* studied 45 differentiated stomach adenocarcinomas for LOH using 10 polymorphic microsatellite markers distributed along the long

arm of human chromosome 21. They found LOH for single or multiple markers in 44% of analysed adenocarcinomas. They also suggested the existence of at least two candidate TSGs on 21q (one mapping to the 21q21 region and the other to the 21q22.1 region) that might be responsible for the development of differentiated stomach tumours (Sakata 1997).

Aoki *et al* conducted a genome-wide linkage analysis using 392 polymorphic microsatellite markers distributed along the entire genome on a group of 170 Japanese sib-pairs diagnosed with stomach cancer. They found that the 1p32, 2q33–q35, 11p13–p14 and 21q21 chromosomal regions showed evidence for linkage with multipoint logarithm of odds (LOD) scores greater than 1.18, corresponding to $P<0.01$ (Aoki 2005). Subsequently, they selected 66 genes that mapped to the 21p11–q22 region and carried out a case-control study using 126 SNPs (Aoki 2005). They identified five SNPs in the stress 70 protein chaperon family member (*STCH*) gene to be significantly associated with stomach cancer ($P<0.05$).

Yamagata *et al* analysed 20 stomach tumour and 20 stomach non-tumour samples for somatic mutations in the *STCH* gene using direct sequencing (Yamagata 2008). They found a heterozygous deletion spanning a 12 bp of the *STCH* gene in one of the 20 analysed sample pairs. This mutation caused a deletion of four amino acids in the conserved ATP-binding domain, which subsequently resulted in the loss of ATP-binding function of the STCH protein. They also showed that cells containing a mutated version of the STCH protein were not sensitive to tumour necrosis factor related apoptosis-inducing ligand (TRAIL)-induced cell death, so the *STCH* gene seems to be involved in cell proliferation and survival, and thus might be regarded as a candidate gene conferring susceptibility to stomach cancer (Yamagata 2008).

Moreover, loss of heterozygosity at chromosome 21q has been a recurrently observed alternation found in lung cancer (Sato 1994; Kohno 1998; Groet 2000; Yamada 2008).

In a search for tumour suppressor candidate genes, Sato *et al* analysed 41 squamous lung cell carcinomas and 119 lung adenocarcinomas for LOH on all human autosomal chromosome arms using Southern blot analysis. In squamous lung cell carcinomas they reported a significant

frequency of LOH for several chromosome arms, including the long arm of human chromosome 21 (21q) ($P<0.05$), suggesting the possible existence of candidate TSGs in this region that might play a role in the development of squamous lung cell carcinoma.

Groet *at al* analysed 34 informative non-small cell lung carcinomas for LOH using 4 polymorphic microsatellite markers distributed along a 4.5 Mb segment of the 21q11.1–q21.1 region. They found LOH of the entire segment in 13 and partial LOH of the segment in two studied carcinomas. Analysis of the endpoints of two partial LOHs of the 21q11.1–q21.1 region enabled them to exclude the *STCH* and *NRIP1* genes from further candidate TSG analysis, as none of these genes were deleted in any of these tumours. Within the overlapping region for both entire and partial deletions of the 21q11.1–q21.1 region they identified a novel gene, *USP21* (currently known as *USP25*), encoding an ubiquitin-specific protease. Subsequently, they performed direct cycle sequencing of the *USP21* gene in all the 34 tumour samples, but found no mutations in any functional domains of the gene. Thus they concluded that the *USP21* gene is unlikely to be a TSG, and further analysis is required to search for a candidate TSG that might play a role in the development of non-small cell lung carcinoma.

Yamada *et al* analysed 85 lung cancer lines for the presence of a homozygous deletion in the 21q11.1–q21.1 region using 12 sequence-tagged site (STS) markers. They found that one non-small cell lung carcinoma line had a homozygous deletion encompassing the region from *LIPI* to *C21orf34* inclusively. They further analysed the *SAMSN1* and *USP25* genes, as these genes are the only genes mapped within the deletion that showed detectable expression in normal lung cells and frequent down-regulation in lung cancer cell lines, as judged by Northern blot analysis. Polymerase chain reaction-single strand conformation polymorphism (PCR-SSCP) analysis did not find any mutations in the *SAMSN1* gene in any of the analysed lung cancer cell lines and tumours, suggesting that the *SAMSN1* gene is unlikely to be a TSG. Also, transfection of a cancer cell line carrying a homozygous deletion of the 21q21.1 region with expression vectors for either the *SAMSN1* or *USP25* gene did not result in cell growth inhibition measured with an MTT

(3-(4,5-Dimethylthiazol-2-yl)-2,5-diphenyltetrazolium bromide) assay, and thus did not provide any evidence for the tumour suppression function of any of these genes. In addition, they observed frequent downregulation of *let-7c*, *miR-125b-2* and *miR-99a* in human lung cancer cell lines and lung tumours, and so they transfected a cancer cell line carrying a homozygous deletion of the 21q21.1 region with expression vectors for either of these miRNAs, but did not observe cell growth inhibition measured with an MTT assay, and thus did not obtain any evidence for the tumour suppression function of any of these miRNAs in lung carcinoma.

Kohno *et al* analysed 12 small cell lung carcinoma (SCLC) and 20 non-small cell lung carcinoma (NSCLC) lines using Southern and Northern blot analysis to detect mutations in the *ANA* (abundant in neuroepithelium area) gene that is mapped within the 21q11.2–q21.1 region. They identified homozygous deletion of the *ANA* gene in one of the NSCLC lines. Next, they analysed 18 SCLCs and 47 SCLCs for LOH, and detected LOH for 7 SCLCs and 24 SCLCs. Finally, they showed that PCR-SSCP analysis did not find any somatic mutations in the *ANA* gene in any of the 6 SCLC and 23 SCLC lines that were previously identified with LOH, and concluded that the *ANA* gene is unlikely to play a role in the development of lung cancer.

Moreover, the importance of chromosome 21q in cancer pathogenesis was strengthened by the dataset released by the Cancer Genome Project (http://www.sanger.ac.uk/cgi-bin/genetics/CGP/cghviewer/CghHome.cgi). This dataset catalogued the structural genomic variations in almost 800 cancer cell lines and revealed the presence of deletions in 50 cell lines in the chromosomal region 21q11.2–q21.1. These deletions mainly encompassed the *SAMSN1* and *USP25* genes, which have previously been reported as being down-regulated in human lung cancer (Yamada 2008), the *NRIP1* gene that encodes a ligand-dependent co-repressor that limits retinoic acid (RA) mediated tumour cell differentiation of embryonal carcinoma (the pluriopotent stem cells of testicular germ cell tumours) (Heim 2007), and the *LIPI* gene that shows a high expression in Ewing family tumours (EFT) (Foell 2008).

In summary, on the one hand, the decreased incidence of solid tumours in patients with Down syndrome (Hasle 2000) and recurrently observed partial losses of the long arm of chromosome 21 in patients diagnosed with different types of solid tumours, strongly suggest the existence of TSGs or growth control genes on chromosome 21q that still await discovery. On the other hand, the existence of a potential causative link between cancer and Monosomy 21 seems to be questionable. Firstly, none of the clinical data currently available for Monosomy 21 patients carrying "centromeric" deletions reports any cases in which tumours were diagnosed (Wakui 2002; Tinkel-Vernon 2003, Lyle 2008; Roberson 2010; Lindstrand 2010). Secondly, there is no clinical data suggesting that any of the patients carrying a deletion of the proximal end of the long arm of chromosome 21 who were diagnosed with cancer displayed any of the clinical features identified in patients with Monosomy 21 (Cliby 1993; Ohgaki 1998; Yamamoto 2003; Aoki 2005; Chen 2005; dos Santos Aguiar 2007). However, the potentially increased risk of cancer development in individuals with Monosomy 21 cannot be excluded, as the medical history of Monosomy 21 patients is not known beyond the initial clinical evaluation, and so the possible occurrence of tumours in individuals with Monosomy 21, especially later in their lives, might have be missed. Also, it cannot be excluded that some of the patients diagnosed with tumours might actually present some of the phenotypic abnormalities that are characteristic for Monosomy 21 individuals, but that this was not noticed or taken into account at the time of diagnosis. Thus, to be able to answer the question about the existence of a potential causative link between cancer and Monosomy 21, it is necessary to both follow the medical history of Monosomy 21 patients carrying "centromeric" deletions throughout their lives, and to re-examine all patients carrying a deletion of or within the proximal end of chromosome 21 (who at some point developed cancer) for the presence of any clinical manifestations observed in Monosomy 21 patients.

3.2.6 GENERATION OF A NEW MOUSE MODEL OF MONOSOMY 21 SYNDROME

To our knowledge all currently available mouse models for Monosomy 21 provide phenotypic data only on the deletions that are syntenic to human regions located between 21q21.3 and the telomere (Besson 2007; Olson 2007; Yu 2010). Thus the contribution of additional regions/genes to the development of clinical features observed in patients with Monosomy 21 remains unclear. Also, to date no mouse models have been generated to investigate the contribution of genes mapped to the proximal end of human chromosome 21 to the development of different types of cancer. To this end, we used chromosome engineering to generate a new mouse model of Monosomy 21, $Df^{Lipi\text{-}Usp25}$, carrying a deletion syntenic to 21q11.2–q21.1 in human, to assess the contribution of the six genes conserved between human and mouse that are mapped within this 1.6 Mb interval to the development of clinical features diagnosed in patients with Monosomy 21 and different types of cancer.

It should be mentioned that the approach we have taken to investigate the contribution of a deletion of the *Lipi–Usp25* region to the formation of different types of tumour does not exactly recapitulate the situation that occurs in humans. Namely, in humans cancer formation takes place during the individual's life, with a deleterious mutation initially occurring in a single somatic cell that is subsequently clonally expanded. However, our monosomic mice carry a germline deletion of the *Lipi–Usp25* region, and so the mutation is present in all body cells throughout both pre- and postnatal development. This might potentially cause the development of different clinical manifestations or accelerate the progression of cancer development.

3.3 RESULTS

3.3.1 GENERATION OF MONOSOMIC MICE FOR THE 1.6 Mb *Lipi–Usp25* REGION

The *Lipi* and *Usp25* genes are located at the proximal and distal ends of a 1.6 Mb region in the C3.1 band of mouse chromosome 16 (MMU16), which is syntenic to the human region 21q11.2–q21.1 (**Figure 3.1A**). This region on human chromosome 21 (HSA21) contains eight genes (NCBI build h36), whereas the syntenic region in MMU16 contains only 6 genes (NCBI build m37) (**Figure 3.1B**) orthologous to their HSA21 counterparts, as there are no murine orthologs of *ABCC13* and *AF165138.1*. The *Lipi–Usp25* deletion was generated using chromosomal engineering (Zheng 1999) as described in Material and Methods (**Figure 3.2A**). Briefly, E14tg2a ES cells were sequentially electroporated with targeting vectors containing a portion of the *Hprt* selection cassette (5' or 3'*Hprt*), a *loxP* site and a coat colour marker (agouti or tyrosinase). The targeting vector containing the 5'*Hprt* cassette (MICER clone: MHPN69h23) (Adams 2004) was inserted proximal to *Lipi* and the targeting vector containing the 3'*Hprt* cassette (pUSP-3HPAg) was inserted distal to *Usp25* (**Figure 3.2A**). The correct insertion of both targeting vectors was confirmed by Southern blot analysis on *Stu*I- or *Bam*HI-digested gDNA extracted from ES clones selected either in G418 or puromycin using a 5′ and 3′ Southern external probe, respectively (**Figure 3.2A, 3.2B**). Double-targeted clones in which both targeting vectors were inserted on the same chromosome (*cis*) were electroporated with a Cre-expression vector, and subsequently selected in a medium containing hypoxanthine, aminopterin and thymidine (HAT) to isolate ES clones carrying a chromosomal deletion generated via recombination of the *loxP* sites (**Figure 3.2A**). The deletion allele was designated $Df^{Lipi\text{-}Usp25}$ (alternatively named *Ms(Lipi-Usp25)1Dja*, and abbreviated as *Ms1Dja*). The presence of the deletion in *Hprt*-resistant ES clones was confirmed by FISH (**Figure 3.2C**). The positive ES clones were used to generate chimaeras, which transmitted $Df^{Lipi\text{-}Usp25}$ to their progeny.

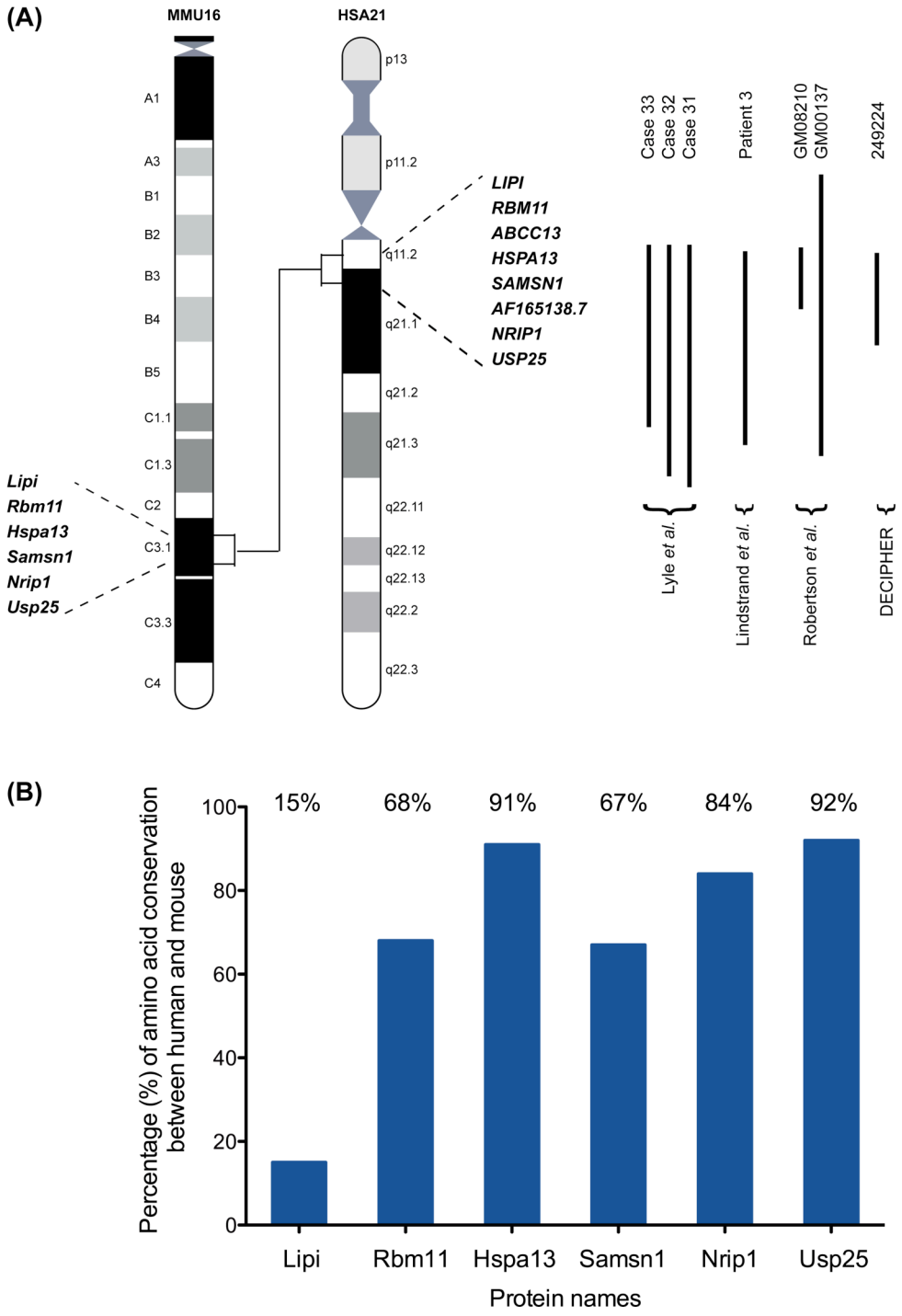

Figure 3.1. (A) Schematic representation of the q11.2–q21.1 interval on HSA21 and the syntenic region in the C3.1 band on MMU16. Genes that mapped to the human 21q11.2–q21.1 region (NCBI build h36) and the C3.1 band on MMU16 (NCBI build m37) are listed. Studies describing partial Monosomy 21 patients with deletions involving the 21q11.2–q21.1 region (as indicated by the length of the black line) are shown. **(B)** The percentage of amino acid conservation for genes within the interval between human and mouse is shown (NCBI build h36). These calculations are based on the longest Ensembl transcript.

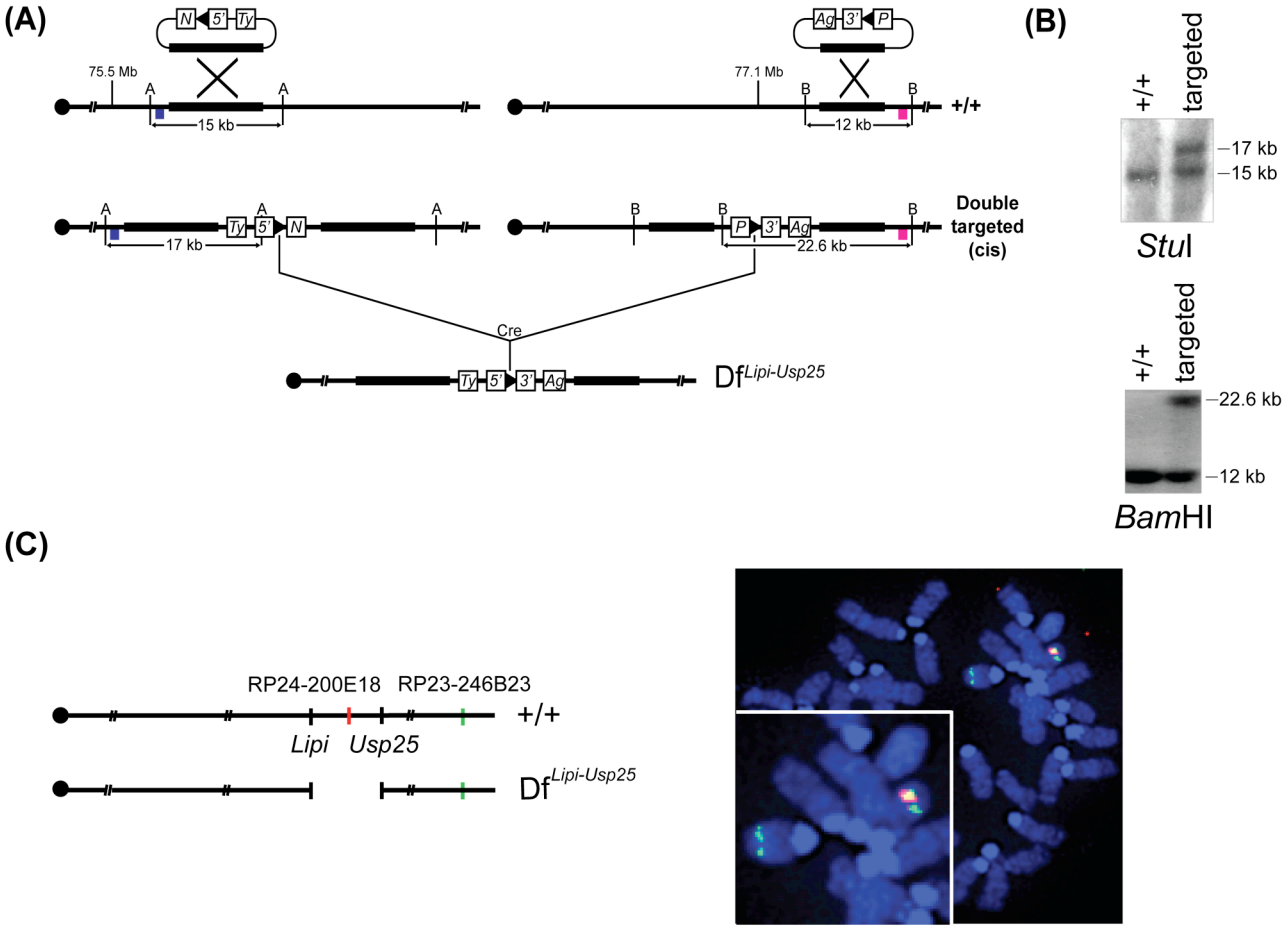

Figure 3.2. Generation of a 1.6 Mb deletion between the *Lipi* and *Usp25* loci using Cre/*loxP*-mediated chromosomal engineering. (A) Strategy to generate the chromosomal rearrangement (NCBI build m37). The targeting vectors containing a *loxP* site (arrowhead), a selectable antibiotic resistance gene (*N* or *P*), a coat colour marker (*Ty* or *Ag*) and part of the *Hprt* gene (5′ or 3′) were integrated successively in the *Lipi* locus and the *Usp25* locus. The coloured boxes (blue and pink) indicate the location of the probes (5' and 3', respectively) used for Southern blotting. A, *Stu*I; B, *Bam*HI; 5', 5'*Hprt*; 3', 3'*Hprt*; *N*, neomycin-resistance gene; *P*, puromycin-resistance gene; *Ty*, tyrosinase minigene, *Ag*, K-14 agouti gene. **(B)** The targeting events were checked by Southern analysis showing an additional *Stu*I fragment of 17 kb compared with the wildtype allele (15 kb) for the *Lipi* locus and an additional *BamH*I fragment of 22.6 kb compared with the wildtype allele (12 kb) for the *Usp25* locus. **(C)** Interphase FISH analysis with BAC probes that map in the region of the deletion (red) and outside (green). Chromosomes from the ES cells double-targeted in *cis* ($Df^{Lipi\text{-}Usp25}$) showed two green and only one red signal due to the deletion of the *Lipi–Usp25* region, while chromosomes from the wildtype ES cells showed two green and two red signals.

3.3.2 HOMOZYGOUS DELETION OF THE *Lipi–Usp25* REGION RESULTS IN EMBRYONIC LETHALITY

Heterozygous (monosomic) $Df^{Lipi\text{-}Usp25}$ mice were viable, fertile and did not show any overt phenotypical abnormalities. To check if wildtype, heterozygous and homozygous offspring were born at normal Mendelian ratios, monosomic $Df^{Lipi\text{-}Usp25}$ mice were intercrossed. Genotyping of 47 progeny did not recover any homozygous (nullisomic) $Df^{Lipi\text{-}Usp25}$ mice (**Figure 3.3A**), showing that the nullisomic deletion resulted in prenatal death. In order to establish the time of death, embryos from monosomic intercrosses were collected at different timepoints during gestation (E14.5, E12.5, E11.5 and E10.5; **Figure 3.3A**). No nullisomic embryos were found at E14.5 (0/32 embryos, P=0.0011) and E11.5 (0/20 embryos, P=0.0098), and only one very necrotic nullisomic embryo was found at E12.5 (1/40 embryos, P=0.0010) (**Figure 3.3A**). Also, there was an increased incidence of embryo resorption between E10.5 and E12.5. Nullisomic embryos were identified at E10.5 at low but still within normal Mendelian ratios (8/52 embryos, P=0.1093), indicating that the majority of embryonic lethality in the nullisomic embryos happened on or before E10.5 (**Figure 3A**). Morphological analysis showed that all nullisomic embryos were markedly smaller than their monosomic and wildtype littermates (**Figure 3.3B**), suggesting developmental retardation. To reveal the reason for embryonic lethality, the nullisomic embryos, as well as their heterozygous and wildtype littermates harvested at E10.5 and E12.5, were analysed histopathologically (**Figure 3.3C, 3.3D**). The hematoxylin and eosin staining showed an increase in the number of apoptotic cells in the neural tube of the nullisomic embryos compared to the monosomic and wildtype littermates (**Figure 3.3C**). To confirm this increased apoptosis, immunostaining was performed using cleaved caspase-3 (Asp175), an apoptotic marker (**Figure 3.3D**). Cleaved caspase-3-positive cells indicated that apoptosis was much more prevalent in the neural tube of the nullisomic embryos compared to the monosomic and wildtype littermates collected at E10.5 (**Figure 3.3D**). In contrast, very few cells labelled by cleaved caspase-3 were present in the neural tube of the nullisomic embryo collected at E12.5 compared to nullisomic embryos harvested at E10.5

(**Figure 3.3D**). Instead, empty areas in the neural tube of the E12.5 nullisomic embryos were observed, suggesting that the apoptotic cells were degraded in the neural tube by E12.5 (**Figure 3.3D**). This indicates that the majority of embryonic lethality in the nullisomic embryos was mostly due to degeneration of the neural tube.

(A)

Litters	Age	+/+	$Df^{Lipi\text{-}Usp25}/+$	$Df^{Lipi\text{-}Usp25}/Df^{Lipi\text{-}Usp25}$	P
8	E10.5	16	28	8	0.1093
3	E11.5	10	10	0	0.0098
7	E12.5	19	20	1	0.0010
5	E14.5	17	15	0	0.0011
7	P21	16	31	0	0.0001

(B)

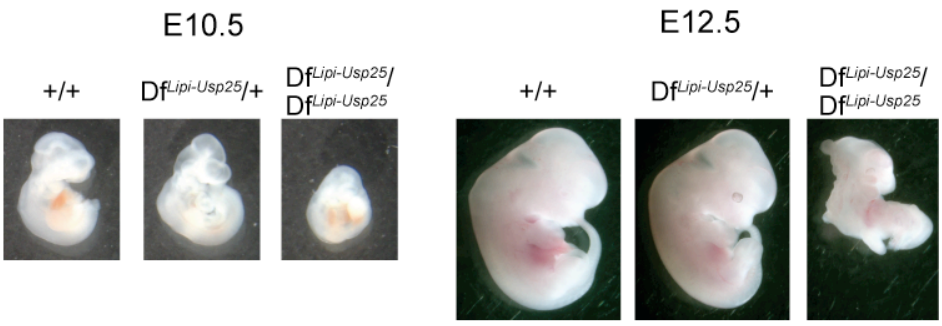

(C)

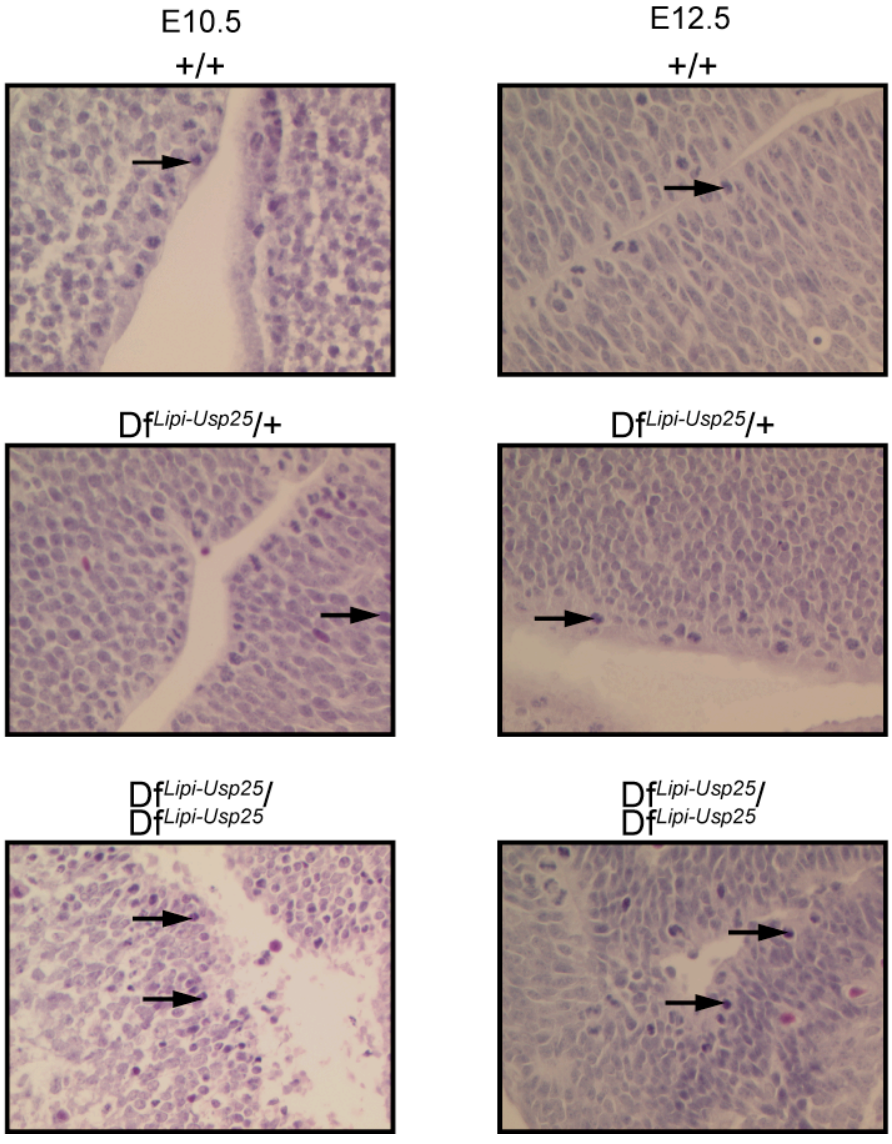

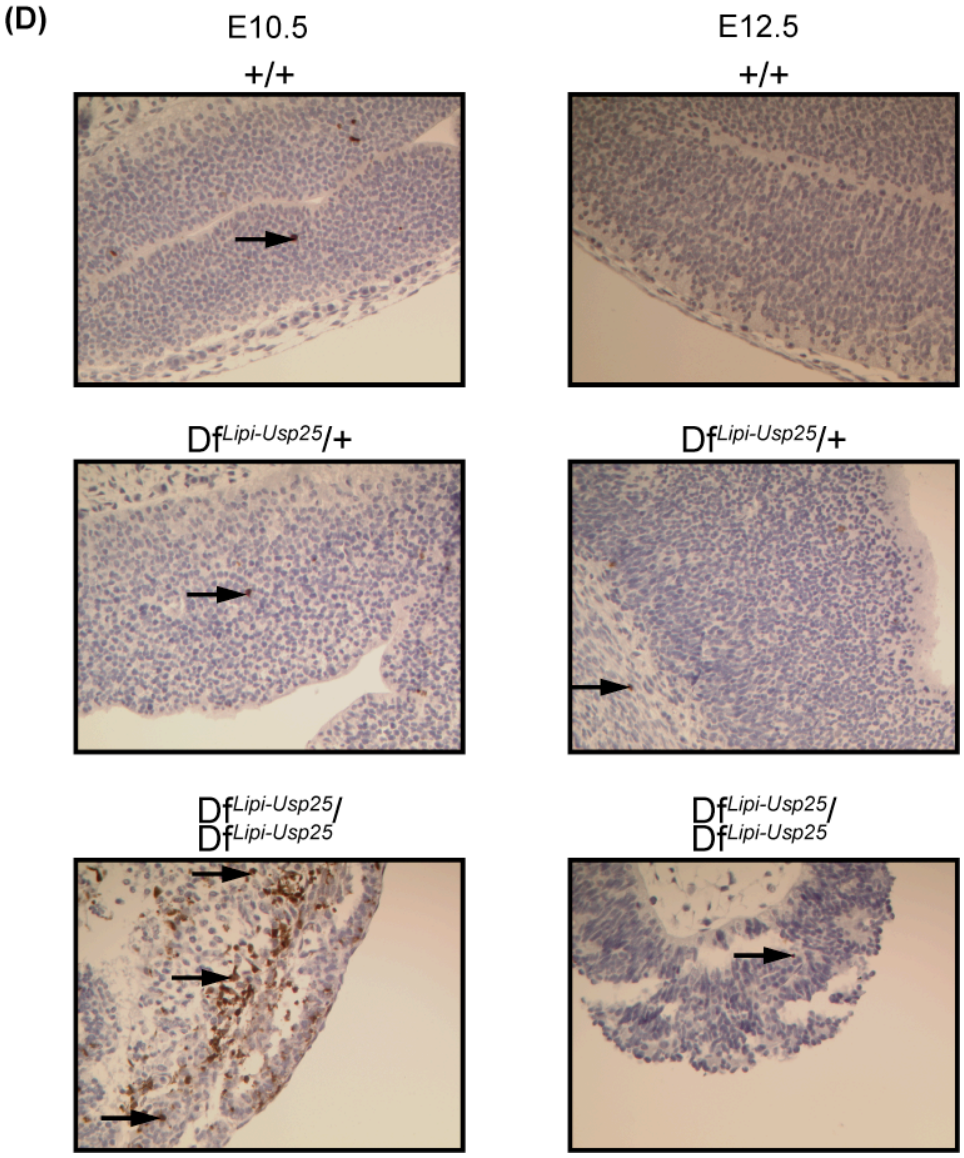

Figure 3.3. Embryonic lethality of mice homozygous for the *Lipi–Usp25* deletion. **(A)** Genotyping of E10.5, E11.5, E12.5 and E14.5 embryos, and P21 (3-week old) mice from monosomic $Df^{Lipi\text{-}Usp25}$ intercrosses. Experimental data was statistically analysed using the Chi-square test. **(B)** Photos of wildtype (+/+), monosomic ($Df^{Lipi\text{-}Usp25}$/+) and nullisomic ($Df^{Lipi\text{-}Usp25}$/ $Df^{Lipi\text{-}Usp25}$) embryos collected at E10.5 and E12.5. Longitudinal measurements are 4 mm, 4 mm and 2.7 mm for the wildtype, monosomic and nullisomic embryos collected at E10.5 respectively. Longitudinal measurements are 9 mm, 9 mm and 4.7 mm for the wildtype, monosomic and nullisomic embryos collected at E12.5 respectively. **(C)** Haematoxylin and eosin-stained sections of neural tubes from wildtype, monosomic and nullisomic embryos collected at E10.5 and E12.5. Dark purple staining indicates apoptotic cells (indicated by arrows). **(D)** Immunohistochemical analysis using a cleaved caspase-3 (Asp175) antibody showed a markedly increased number of apoptotic cells (brown staining; indicated by arrows) in the neural tube of nullisomic embryos collected at E10.5. Note also the empty spaces in the neural tube of nullisomic embryos collected at E12.5 compared to the intact structure of the neural tube of wildtype and monosomic embryos. Images are representative and taken at x200 magnification.

3.3.3 PHENOTYPIC ANALYSIS OF MONOSOMIC MICE

To determine whether clinical features diagnosed in patients with Monosomy 21 syndrome can be observed in the heterozygous (monosomic) *Df*$^{Lipi\text{-}Usp25}$ mice, 14 monosomic mice and 14 wildtype littermates (controls) fed on a high-fat diet (HFD) from the age of 4 weeks were subjected to a series of tests designed to analyse their morphology, behaviour, motor skills, neuromuscular function, pain perception, hearing, metabolism and haematology. Tests were carried out between 4 and 16 weeks of age, depending on the specific test. See **Material and Methods Table 2.4** for a short summary of the phenotypic tests performed; the results for each of the tests can be found at the Wellcome Trust Sanger Institute Mouse Resources Portal under the name Mdel (http://www.sanger.ac.uk/mouseportal/).

3.3.3.1 PHENOTYPIC ANALYSIS OF MONOSOMIC MICE REVEALS THAT LOSS OF ONE COPY OF THE *Lipi–Usp25* REGION DOES NOT AFFECT GENERAL MORPHOLOGY, MOTOR OR NEUROMASCULAR FUNCTION

The monosomic mice were viable, fertile and did not show any overt phenotype upon observation. They showed no gross motor or neurological abnormalities and a similar level of pain perception, muscle strength and hearing compared with the control animals (wildtype littermates) (**Table 3.1**).

The general dysmorphology and eye morphology tests found a difference between the controls and monosomic mice with respect to eye pigmentation (**Table 3.1**). Pigmentation of the eyes was observed in albino monosomic mice and abnormal iris pigmentation observed in albino monosomic males. However, this can be explained by the presence of coat colour markers (agouti and tyrosinase) present in the constructs used for gene-targeting in the ES cells. Thus it was concluded that the monosomic mice did not suffer pigmentation dysmorphology.

Table 3.1. Short summary of the results obtained from phenotypic tests performed on 14 monosomic *Df*$^{Lipi\text{-}Usp25}$ mice and 14 wildtype littermates fed on a high-fat diet.

Time	Name of the test	Result
Weekly; from 4-week old	Weighting mice	No significant changes
4-week old	Hair dysmorphology	No significant changes
6-week old	Hair follicle cycling	No significant changes
9-week old	Open field	No significant changes
9-week old	Modified SHIRPA	No significant changes
9-week old	Grip strength	No significant changes
10-week old	Dysmorphology	Significant changes in both monosomic males and females compared to their wildtype littermates
10-week old	Hot plate	No significant changes
12-week old	Indirect calorimetry	No significant changes
13-week old	Glucose tolerance	No significant changes
14-week old	Auditory brainstem response	No significant changes
14-week old	Dual energy X-ray absorptiometry (DEXA)	Significant changes in both monosomic males and females compared to their wildtype littermates
14-week old	X-ray imaging	No significant changes
15-week old	Core temperature stress	No significant changes
15-week old	Eye morphology screen	Significant changes in both monosomic males and females compared to their wildtype littermates
16-week old	Heart weights	No significant changes
16-week old	Haematology panel	No significant changes
16-week old	Plasma chemistry panel	No significant changes

3.3.3.2 BEHAVIOURAL PHENOTYPING OF MONOSOMIC MICE REVEALS THAT LOSS OF ONE COPY OF THE *Lipi–Usp25* REGION IS ASSSOCIATED WITH A DEFICIT IN MEMORY RETENTION

Even though no differences were observed in the monosomic mice upon open field testing, as no significant changes in locomotion, habituation and fear/anxiety responses to a novel environment between monosomic and control mice were observed (**Table 3.1, Figure 3.4A-D**), we decided to explore further their behaviour and cognition.

12 monosomic mice and 12 wildtype littermate controls fed on a normal-fat diet (NFD) were used in an elevated plus maze test of anxiety and a social recognition paradigm with a long-term social memory component. Both monosomic and wildtype animals showed a preference for the closed arm compared to the open arm of the elevated plus maze, as measured by the amount of time spent in the open arm and the number of entries into the open and closed arm (**Figure 3.5A, 3.5B, 3.5C**; two-way ANOVA: repeated measures for *Trial*, $F_{4,64}$=25.86, P<0.0001, effect for *genotype* $F_{1,64}$=11.26, P=0.943). The social recognition test showed that the monosomic animals were able to recognise two different (sedated) male stimulus animals (mouse A and mouse B) (**Figure 3.6A**; two-way ANOVA: repeated measures for *Trial*, $F_{4,64}$=25.86, P<0.0001, trial 4 versus trial 5, P<0.05, *post hoc* analysis). Both groups of mice had similar initial levels of investigation and spent increasingly lower amounts of time investigating the repeatedly presented stimulus animal (mouse A) (**Figure 3.6A**; two-way ANOVA effect for *genotype* $F_{1,64}$=11.26, P=0.943, interaction *Trial* x g*enotype* $F_{4,64}$=1.762, P=0.1475). Both of these results suggest normal levels of anxiety and social interaction. However, when subjected to a 24-hour social memory retention test, monosomic mice were incapable of distinguishing a familiar stimulus animal (mouse A) from an unfamiliar one (mouse C) (**Figure 3.6B**; ratio of investigation het versus wt, P<0.05 compared with the two-tailed Student's *t*-test). Wildtype animals, in contrast, retained the memory of the familiar stimulus animal (mouse A) and investigated it less frequently.

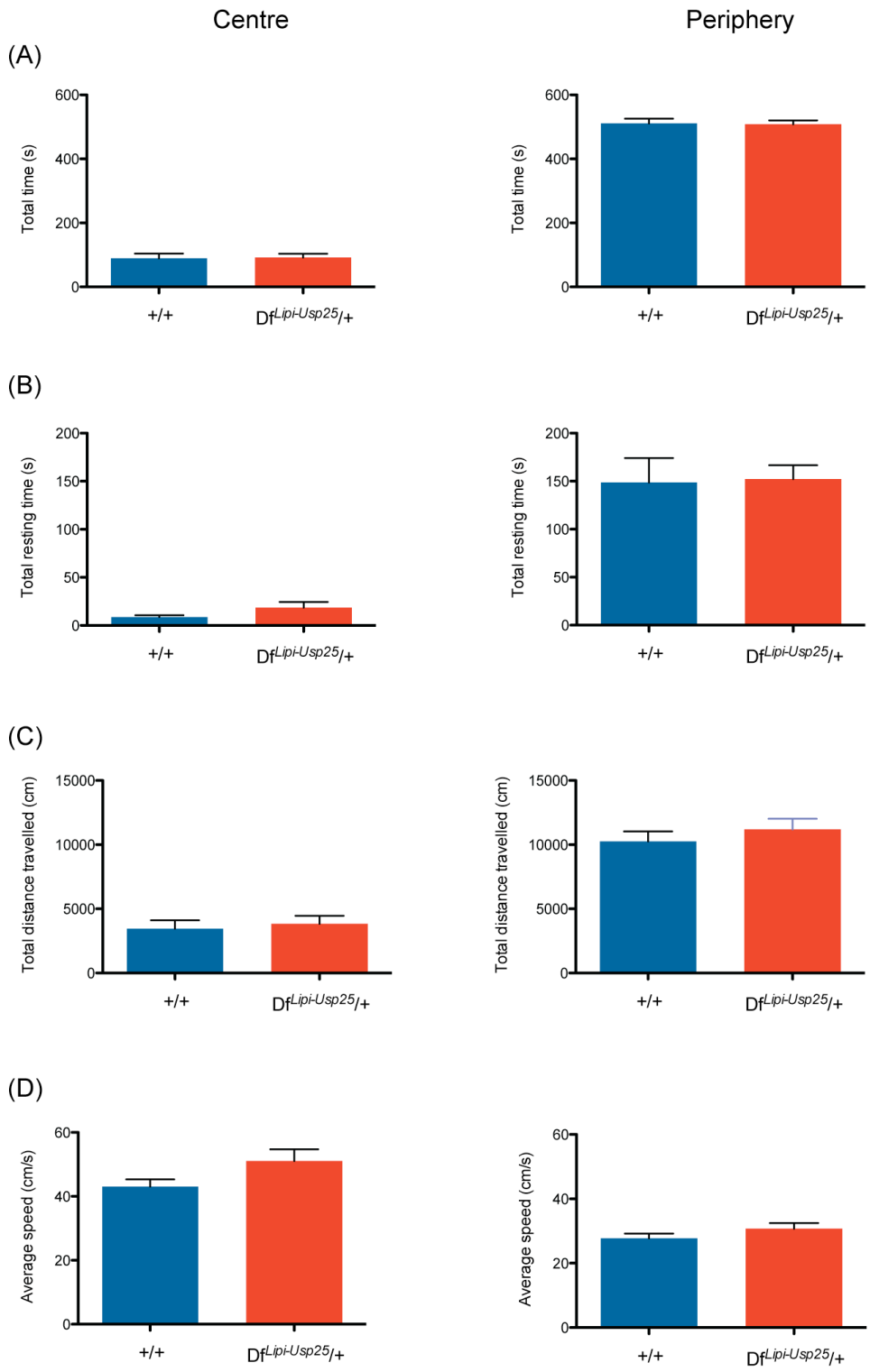

Figure 3.4. Open field results recorded at centre and periphery for 14-week old control (+/+) and monosomic (*Df*$^{Lipi\text{-}Usp25}$/+) littermates. (A) Total time (s, seconds). **(B)** Total resting time (s, seconds). **(C)** Total distance travelled (cm, centimetres). **(D)** Average speed (cm/s, centimetres/seconds). Data was statistically analysed using the two-tailed parametric Welsch's *t*-test. 7 males and 7 females were analysed per genotype.

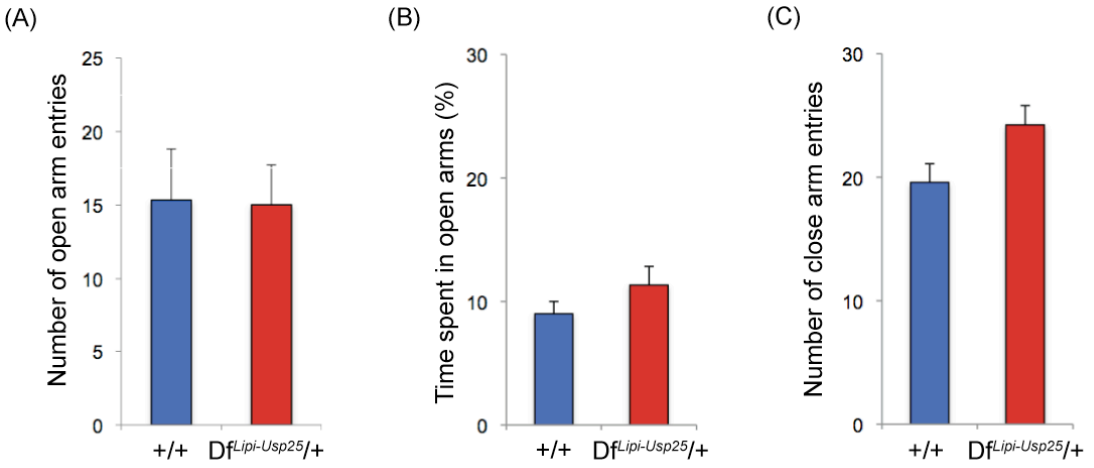

Figure 3.5. Elevated plus maze results recorded at open and close arm for 14-week old control (+/+) and monosomic (*Df*$^{Lipi\text{-}Usp25}$/+) male littermates. (A) Percentage of time spent in the open arms. **(B)** Number of entries into the open arms. **(C)** Number of entries into the closed arms. Both monosomic (*Df*$^{Lipi\text{-}Usp25}$/+) and control (+/+) mice spent similar amount of time in the open arms and had comparable number of entries into the open and closed arms. Data was statistically analysed using the two-tailed Student's *t*-test. 12 males were analysed per genotype.

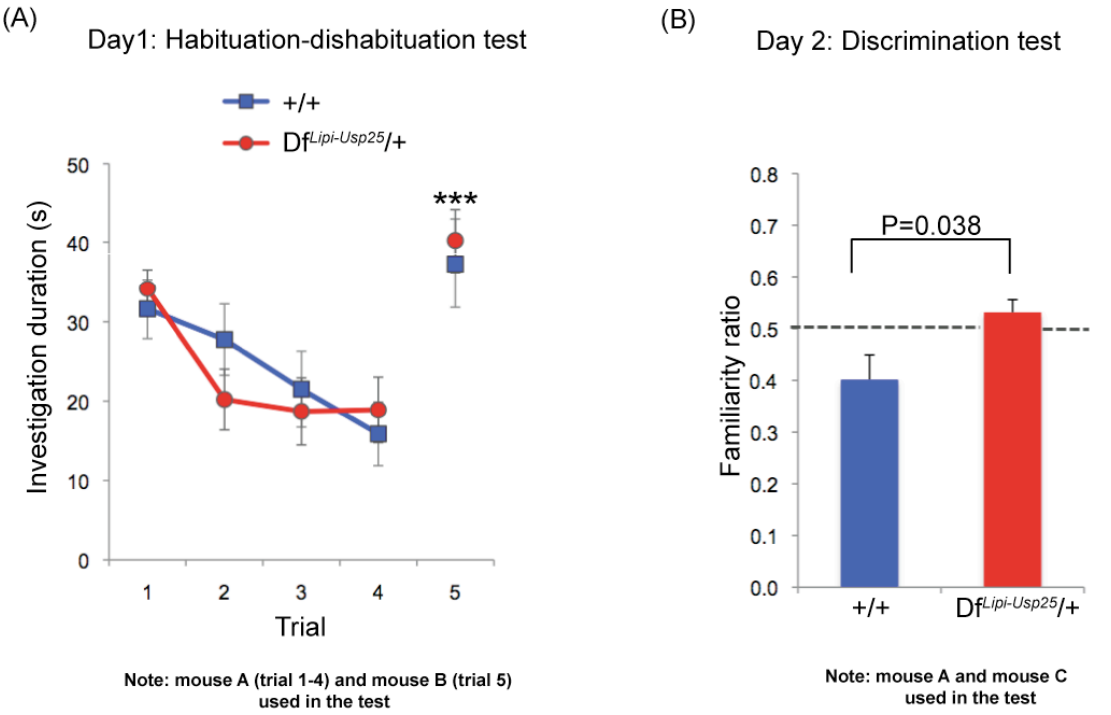

Figure 3.6. Social recognition test. (**A)** Habituation-dishabituation test. Both monosomic (*Df*$^{Lipi\text{-}Usp25}$/+) (n=10) and control (+/+) (n=8) mice recognised two different stimulus animals (mouse A and mouse B), as shown by the decline in the investigation time over trials 1 to 4 when they were repetitively presented the same (familiar) stimulus animal (mouse A) and an increase in the investigation time on trial 5 when they were presented with a novel stimulus animal (mouse B) (trial 4 versus trial 5, *** P<0.0001, *post-hoc* analysis after two-way ANOVA). **(B)** Discrimination test. 24 hours after the habituation-dishabituation test. When given a choice between the familiar stimulus mouse (mouse A, that is the mouse used for trials 1 to 4 on day 1) and a new unfamiliar mouse (mouse C), control mice spent significantly less amount of time investigating the familiar stimulus mouse (mouse A) than the unfamiliar one (mouse C). *Df*$^{Lipi\text{-}Usp25}$/+ did not recognise the familiar from the unfamiliar animal, shown by a familiarity ratio close to 0.5 ("chance", dotted line). Control animals had a significantly smaller familiarity ratio than *Df*$^{Lipi\text{-}Usp25}$/+ mice (two-tailed Student's *t*-test). Five animals (two mutants and three wildtypes) were taken out of the analysis because of their low investigation times (less than 10 seconds on trial 1).

3.3.3.3 ANALYSIS OF THE BODY COMPOSITION OF MONOSOMIC MICE REVEALS THAT LOSS OF ONE COPY OF THE *Lipi–Usp25* REGION RESULTS IN INCREASED FAT DEPOSITION

Analysis of the metabolic related measurements obtained from the dual-energy X-ray absorptiometry (DEXA) scan showed that 14-week old monosomic mice fed on a HFD exhibited a statistically significant increase infat mass and fat percentage estimate (**Table 3.1, Figure 3.7A, 3.7B**).

However, no significant differences in lean mass were observed compared to their wildtype littermates (**Table 3.1, Figure 3.7C**). Interestingly, the average weights of the monosomic mice were not statistically different when compared to the wildtype littermates (**Table 3.1, Figure 3.7D**). However, despite the increased level of fat deposition in monosomic mice, indirect calorimetry did not reveal any significant metabolic differences between the monosomic mice and the controls. In particular, no changes in food intake were observed (**Table 3.1**). Moreover, glucose tolerance tests, as well as the analysis of whole blood and plasma clinical chemistry parameters, including the analysis of the cholesterol, non-esterified free fatty acids, low and high density lipoproteins, triglycerides, and glucose level, did not show any significant differences between the monosomic mice and the wildtype littermates that could explain the observed increase in fat deposition in the monosomic mice (**Table 3.1**).

Finally, as both monosomic mice and the control mice (their wildtype littermates) were on a mixed C57BL/6Jc-/c- – 129P2/OlaHsd genetic background, wildtype C57BL/6Jc-/c- and 129P2/OlaHsd mice fed on a HFD were analysed to evaluate whether these mouse strains were prone to a HFDinduced increase in fat deposition (**Figure 3.8**). Both wildtype C57BL/6Jc/c and 129P2/OlaHsd mice showed much lower fat percentage estimate compared to both monosomic mice and controls (**Figure 3.8**), hence confirming that the HFD-induced increase in fat deposition observed in the monosomic mice was not due to their genetic background.

Thus taken together, we conclude that, whilst monosomy of the *Lipi–Usp25* region does not have a dramatic impact on morphology, motor skills, whole-body metabolism and haematology, it does affect memory retention and the deposition and/or metabolism of fat.

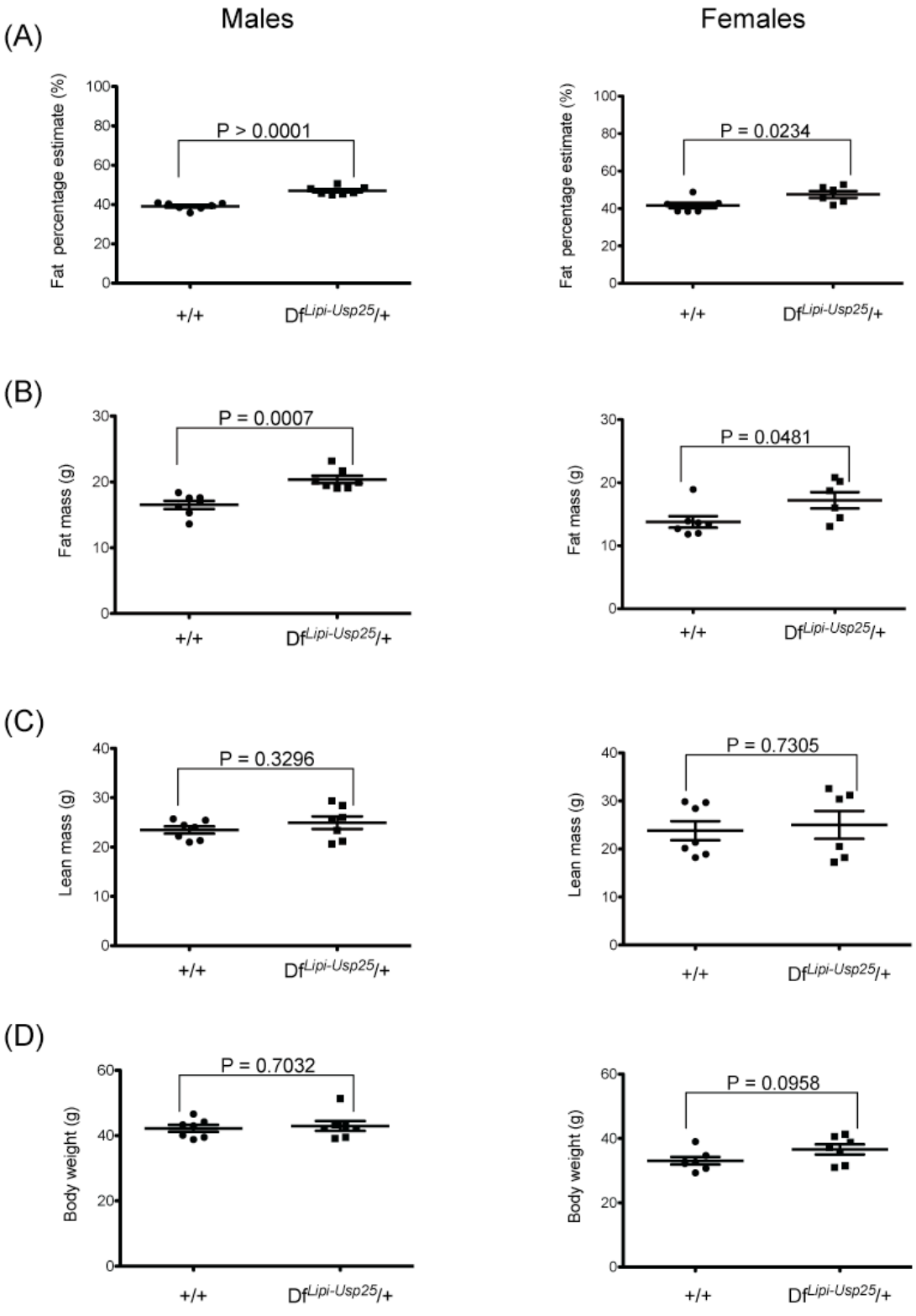

Figure 3.7. DEXA and body weight analysis of 14-week old control (+/+) and monosomic (*Df*$^{Lipi\text{-}Usp25}$/+) littermates fed a high-fat diet. (A) DEXA results showing fat percentage estimate in male and female littermates. **(B)** DEXA results showing fat mass in male and female littermates. **(C)** DEXA results showing lean mass in male and female littermates. **(D)** Body weight results in male and female littermates. Data was statistically analysed using the two-tailed Student's *t*-test. 7 males and 7 females were analysed per genotype.

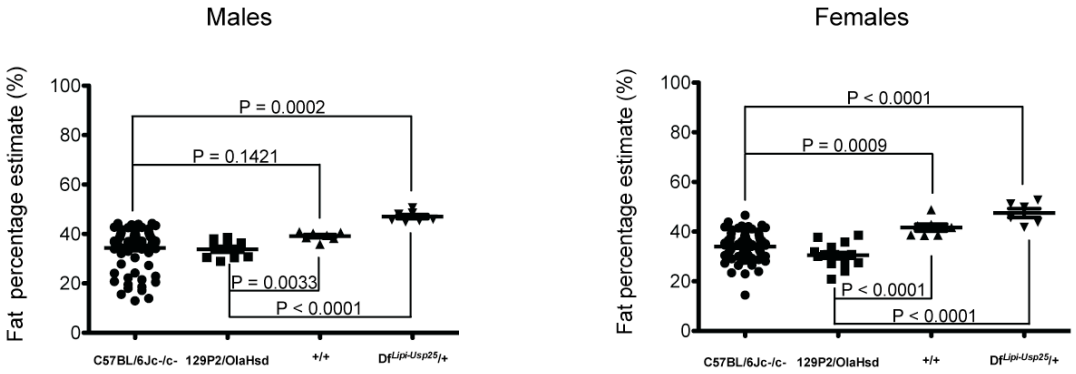

Figure 3.8. Comparison of fat percentage estimate of 14-week old wildtype C57BL/6Jc-/c- and 129P2/OlaHsd mice with control (+/+) and monosomic (*Df*$^{Lipi\text{-}Usp25}$/+) littermates fed on a high-fat diet. Data was obtained from DEXA analysis and statistically analysed using the two-tailed Student's *t*-test.

3.3.4 INCREASED BODY FAT PERCENTAGE IN MONOSOMIC MICE FED ON A HIGH-FAT DIET

Following the preliminary DEXA results, which suggested that the monosomic mice fed on a HFD exhibited a statistically significant increase in fat mass and fat percentage estimate, additional monosomic mice and littermate controls fed on a HFD were analysed by DEXA analysis at additional time points, namely at 8 and 25 weeks. As expected, both monosomic and control mice showed a gradual increase in fat mass and fat percentage estimate with age (**Figure 3.9A, 3.9B, 3.10A, 3.10B**). However, the monosomic mice showed a significantly higher increase in fat mass and fat percentage estimate compared to controls at both 8 and 25 weeks of age (**Figure 3.9A, 3.9B, 3.10A, 3.10B**).

Interestingly, lean mass was significantly decreased in 8-week old monosomic males compared to the controls (**Figure 3.9C**). No significant alterations in lean mass were observed in 8-week old monosomic females and in 25-week old monosomic mice compared to the controls (**Figure 3.9C, 3.10C).**

Next the average weight of the two groups of mice at each time point was compared to see if the increase in fat mass and fat percentage estimate was reflected in the overall body weight gain (**Figure 3.9D, 3.10D**). Average

body weight was significantly increased in 8-week old monosomic females compared to the controls (**Figure 3.9D**). No statistically significant differences in body weights were observed in 8-week old monosomic males compared to the controls (**Figure 3.9D**). However, both 25-week old monosomic males and females exhibited a statistically significant increase in their body weights compared to the controls (**Figure 3.10D, 3.11A, 3.11B**). The body weight gain observed in 25-week old monosomic mice is most likely due to their increased fat deposition as their lean mass was not significantly changed compared to the controls (**Figure 3.10C**).

3.3.5 INCREASED FAT DEPOSITION IN MONOSOMIC MICE IS HIGH-FAT DIET-INDUCED

In order to check if the HFD was the causal factor for the increase in fat deposition, monosomic mice and controls fed on a NFD were subjected to the DEXA analysis at 8 and 25 weeks of age (**Figure 3.9A–D, 3.10A–D**). At 8 week of age, only the monosomic males showed a statistically significant increase in fat mass, while both monosomic males and females exhibited a statistically significant increase in fat percentage estimate compared to the littermate controls (**Figure 3.9A, 3.9B**). However, the increase in fat percentage estimate was much more obvious in monosomic mice fed on a HFD (**Figure 3.9A**). In contrast, 25-week old monosomic mice fed on a NFD did not show a statistically significant increase in fat mass or fat percentage estimate compared to the controls (**Figure 3.10A, 3.10B**).

Interestingly, lean mass was significantly decreased in 8-week old monosomic females compared to their littermate controls (**Figure 3.9C**). No statistically significant alterations in lean mass were observed in 8-week old monosomic females and in both 25-week old monosomic males and females compared to the controls (**Figure 3.9C, 3.10C**).

Next, the average body weights of 8- and 25-week old monosomic mice and controls fed on a NFD were compared (**Figure 3.9D, 3.10D**). No statistically significant differences in the average body weights were observed in either 8-week or 25-week old monosomic mice compared to controls (**Figure 3.9D, 3.10D**).

Finally, the DEXA analysis was also carried out on 1-year old monosomic mice and their wildtype littermates fed on a NFD. No statistically significant increase in fat percentage estimate was observed in the monosomic mice compared to controls (**Figure 3.12A**). However, a significant increase in fat mass was observed in the monosomic females compared to controls (**Figure 3.12B**). Moreover, a significant increase in lean mass and body weight was observed in the monosomic females compared to their littermate controls, while no statistically significant changes were detected between the monosomic males and controls (**Figure 3.12C, 3.12D**).

Thus it seems that the HFD is the causal factor resulting in increased fat mass and fat percentage estimate, and thus in increased fat deposition, in monosomic mice.

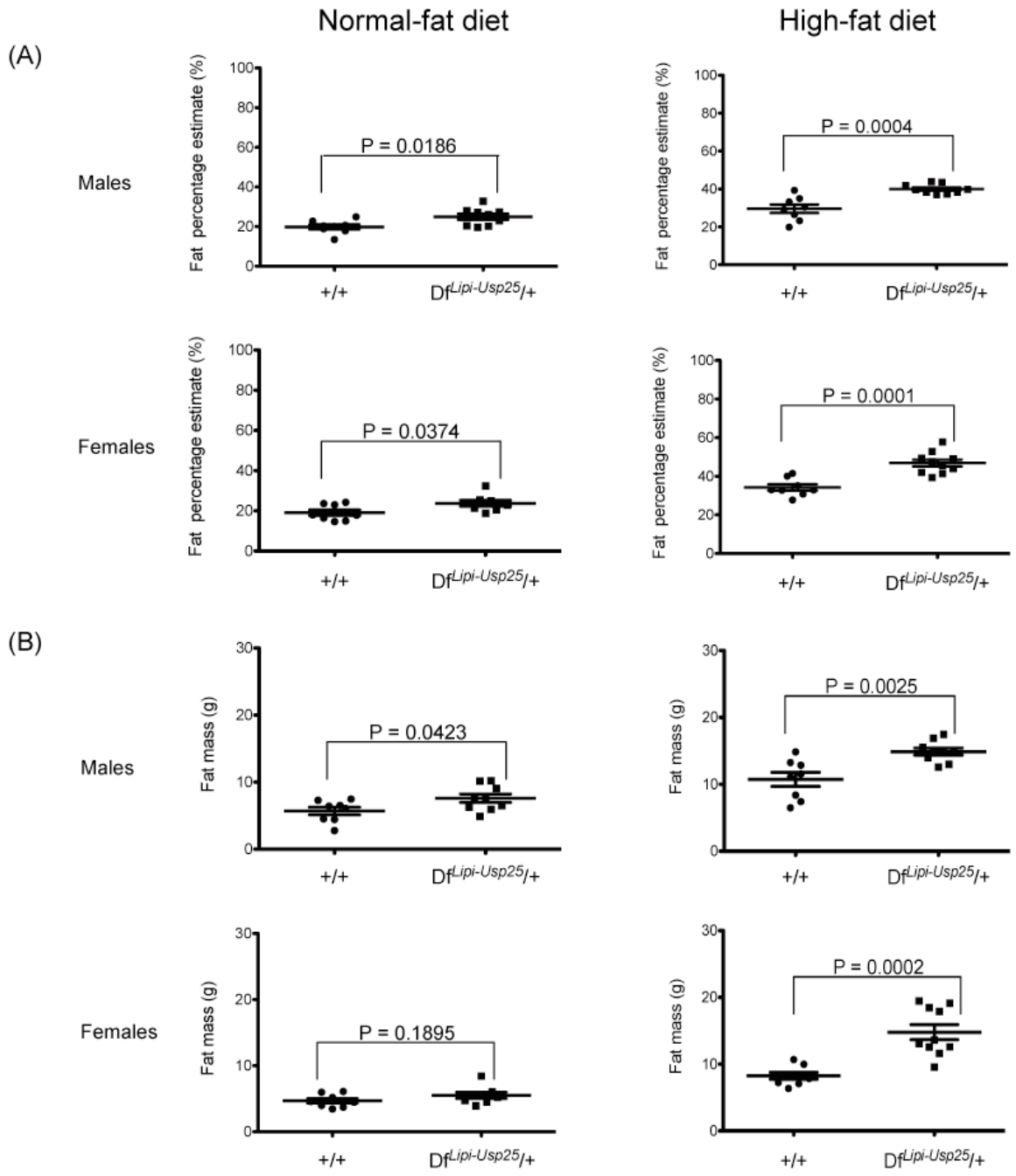
(A)
Normal-fat diet
High-fat diet
Males
Females
Fat percentage estimate (%)
P = 0.0186
P = 0.0004
P = 0.0374
P = 0.0001
+/+
Df Lipi-Usp25 /+
(B)
Fat mass (g)
P = 0.0423
P = 0.0025
P = 0.1895
P = 0.0002

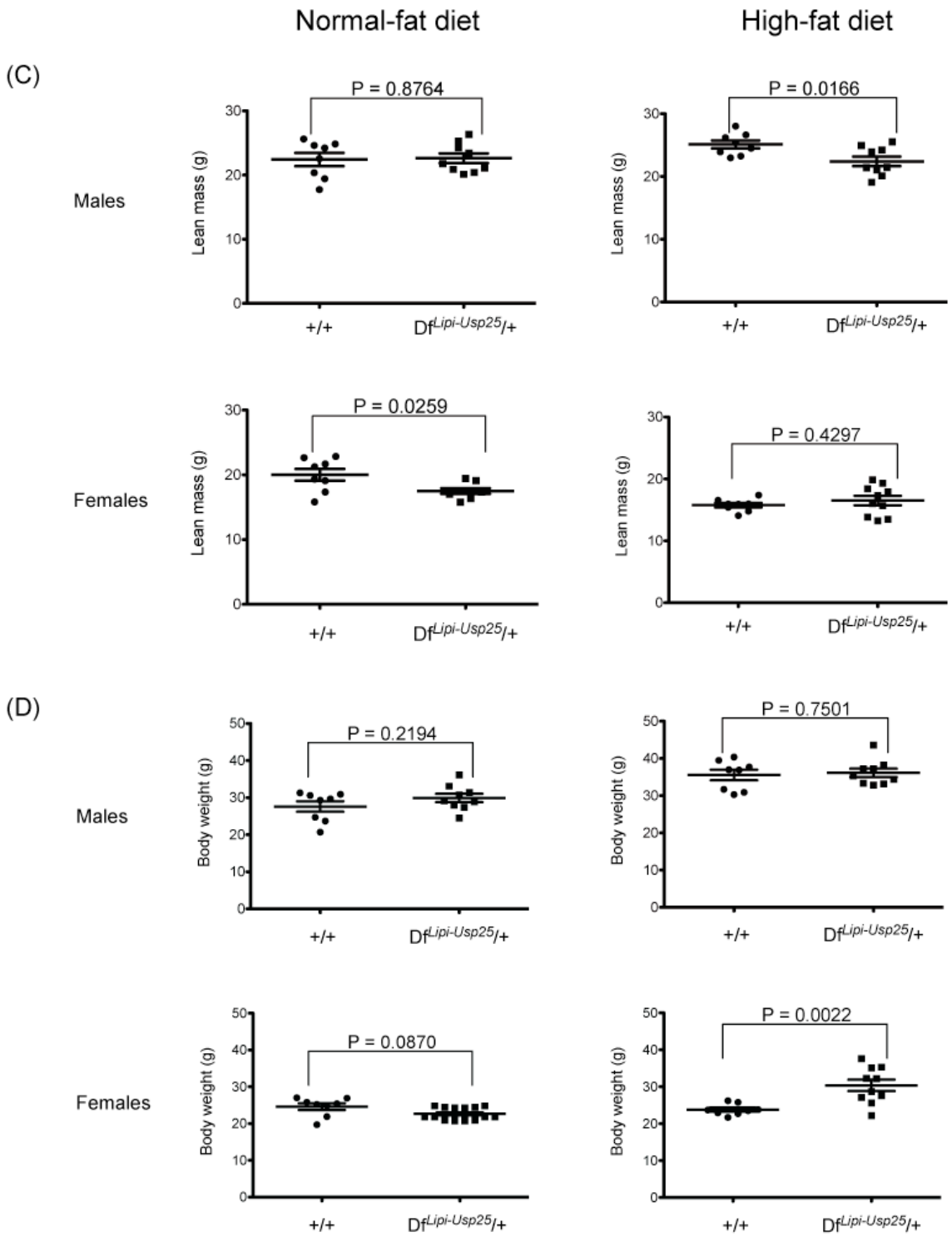

Figure 3.9. DEXA and body weight analysis of 8-week old control (+/+) and monosomic (*Df*$^{Lipi\text{-}Usp25}$/+) littermates fed either on a normal-fat or a high-fat diet. (A) DEXA results showing fat percentage estimate in male and female littermates. **(B)** DEXA results showing fat mass in male and female littermates. **(C)** DEXA results showing lean mass in male and female littermates. **(D)** Body weight results in male and female littermates. Data was statistically analysed using the two-tailed Student's *t*-test. Normal-fat diet: 9 monosomic (*Df*$^{Lipi\text{-}Usp25}$/+) males were compared with 8 control (+/+) males and 8 monosomic (*Df*$^{Lipi\text{-}Usp25}$/+) females were compared with 8 control (+/+) females. High-fat diet: 9 monosomic (*Df*$^{Lipi\text{-}Usp25}$/+) males were compared with 8 control (+/+) males and 10 monosomic (*Df*$^{Lipi\text{-}Usp25}$/+) females were compared with 8 control (+/+) females.

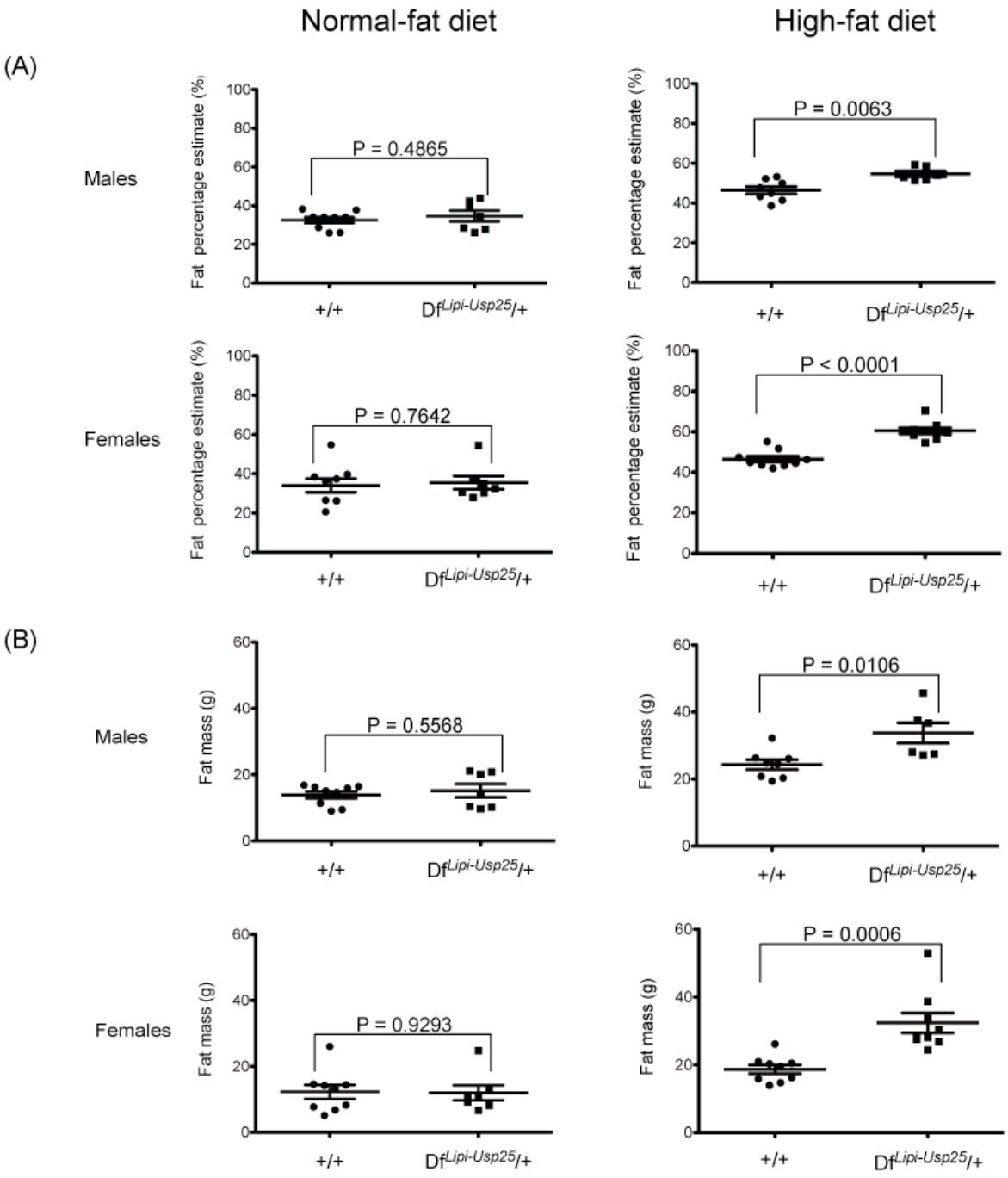
Normal-fat diet
High-fat diet
(A)
Males
Females
Fat percentage estimate (%)
P = 0.4865
P = 0.0063
P = 0.7642
P < 0.0001
(B)
Fat mass (g)
P = 0.5568
P = 0.0106
P = 0.9293
P = 0.0006
+/+
Df Lipi-Usp25 /+

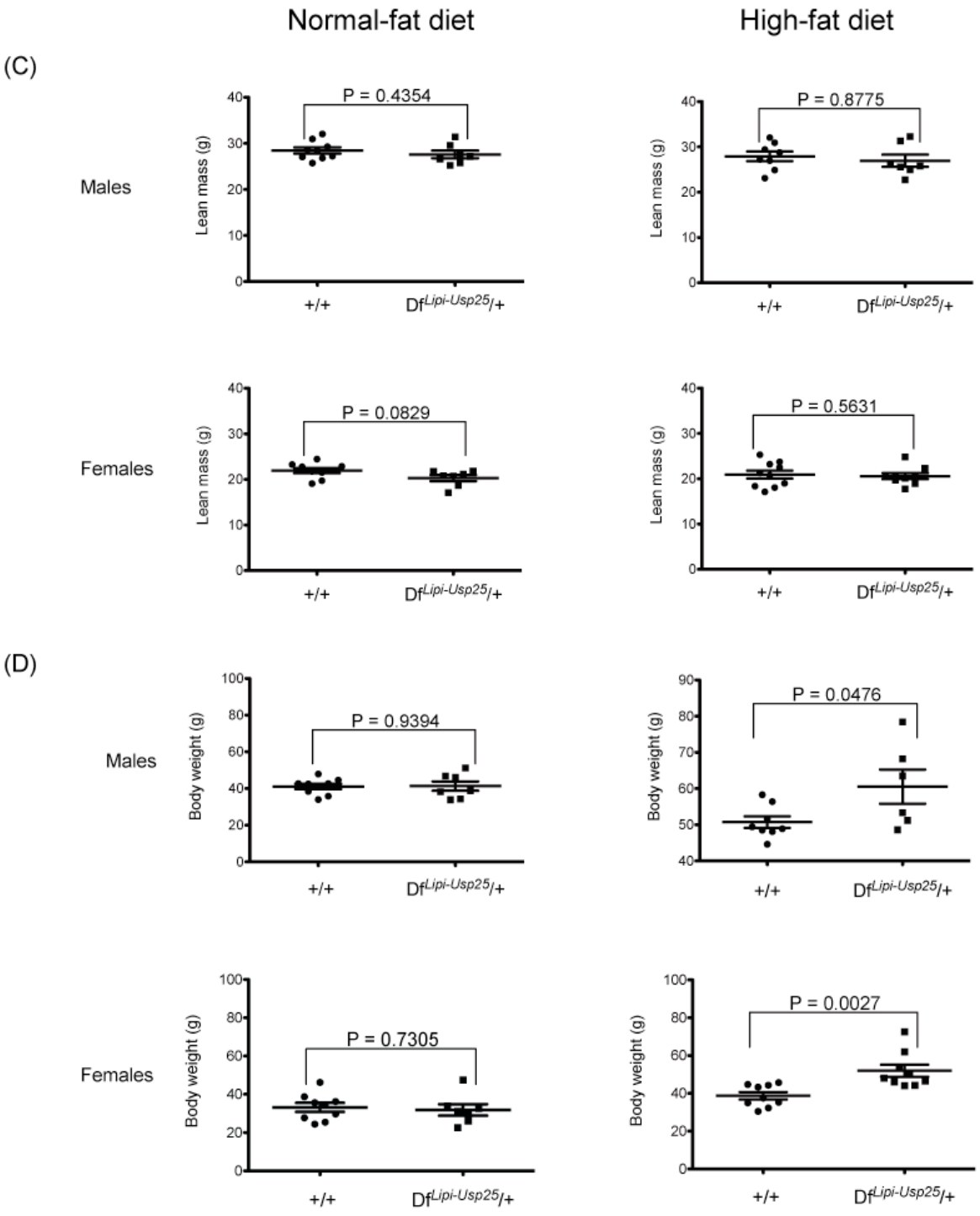

Figure 3.10. DEXA and body weight analysis of 25-week old control (+/+) and monosomic (*Df*$^{Lipi\text{-}Usp25}$/+) littermates fed either on a normal-fat or a high-fat diet. **(A)** DEXA results showing fat percentage estimate in male and female littermates. **(B)** DEXA results showing fat mass in male and female littermates. **(C)** DEXA results showing lean mass in male and female littermates. **(D)** Body weight results in male and female littermates. Data was statistically analysed using the two-tailed Student's *t*-test. Normal-fat diet: 7 monosomic (*Df*$^{Lipi\text{-}Usp25}$/+) males were compared with 9 controls (+/+) males and 7 monosomic (*Df*$^{Lipi\text{-}Usp25}$/+) females were compared with 9 control (+/+) females. High-fat diet: 7 monosomic (*Df*$^{Lipi\text{-}Usp25}$/+) males were compared with 8 controls (+/+) males and 9 monosomic (*Df*$^{Lipi\text{-}Usp25}$/+) females were compared with 10 control (+/+) females.

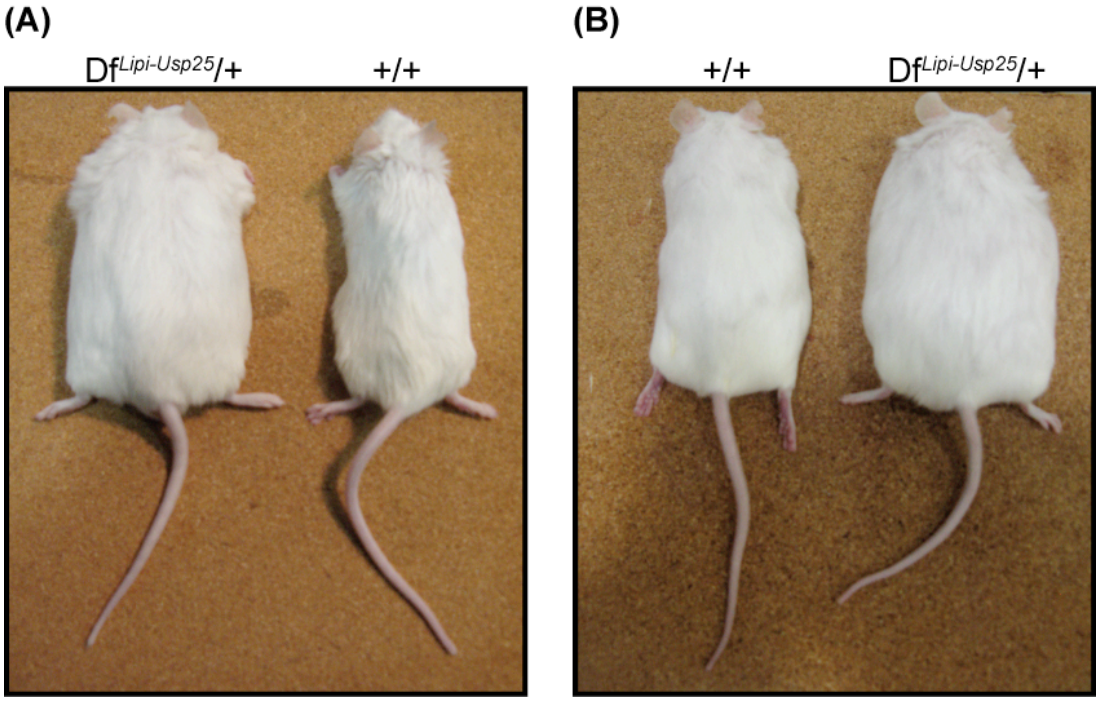

Figure 3.11. Photos of 25-week old control (+/+) and monosomic (*Df*$^{Lipi\text{-}Usp25}$/+) littermates. (A) Photo of 25-week old males fed on a high-fat diet. **(B)** Photo of 25-week old females fed on a high-fat diet.

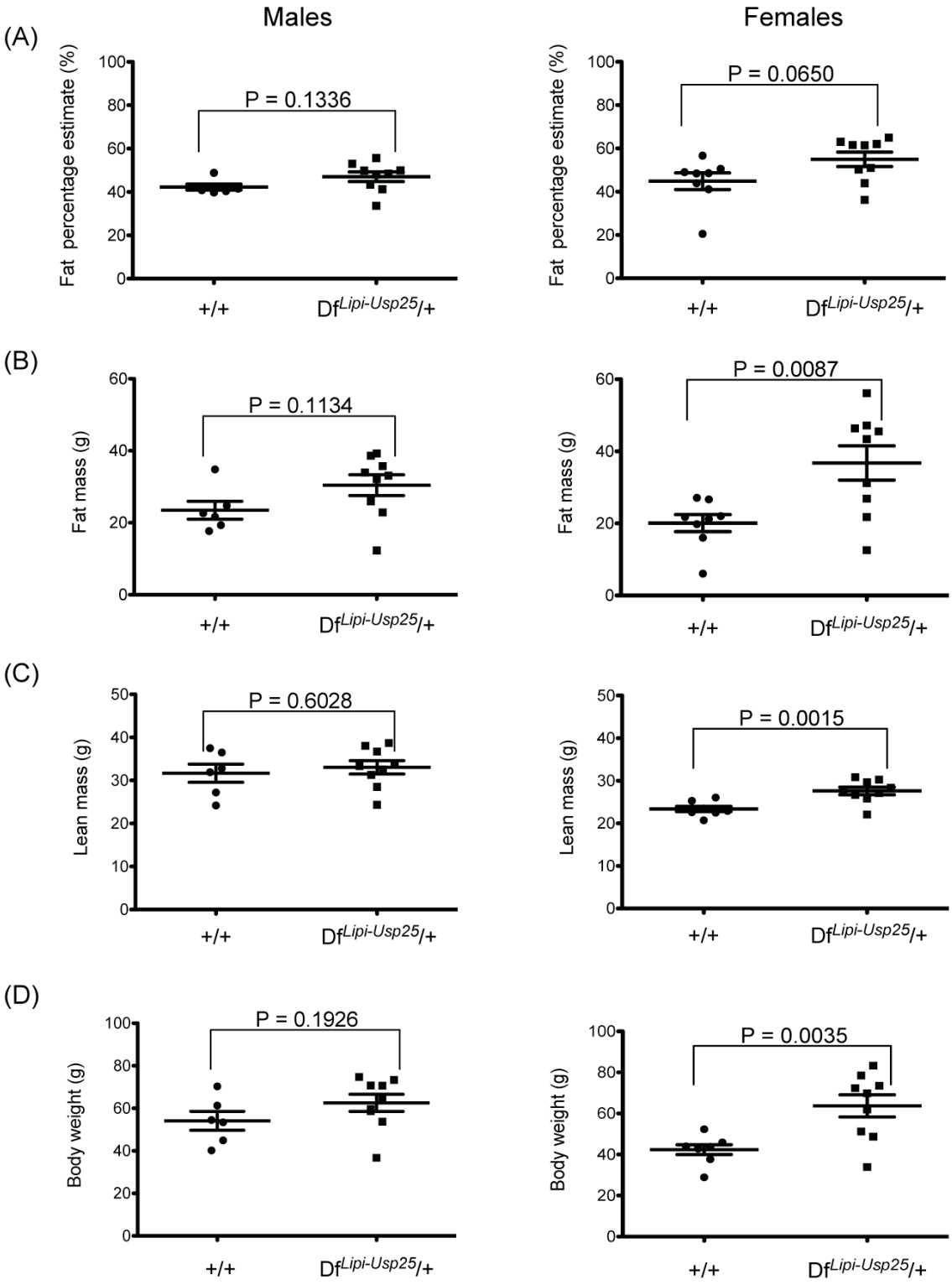

Figure 3.12. DEXA and body weight analysis of 1-year old control (+/+) and monosomic (*Df*$^{Lipi\text{-}Usp25}$/+) littermates fed on a normal-fat diet. (A) DEXA results showing fat percentage estimate in male and female littermates. **(B)** DEXA results showing fat mass in male and female littermates. **(C)** DEXA results showing lean mass in male and female littermates. **(D)** Body weight results in male and female littermates. Data was statistically analysed using the two-tailed Student's *t*-test. 9 monosomic (*Df*$^{Lipi\text{-}Usp25}$/+) males were compared with 6 control (+/+) males and 9 monosomic (*Df*$^{Lipi\text{-}Usp25}$/+) females were compared with 8 control (+/+) females.

3.3.6 INCREASED FATTY CHANGES IN THE LIVERS OF MONOSOMIC MICE FED ON A HIGH-FAT DIET

The histopathological analysis of different tissues stained with haematoxylin and eosin (H&E) of 8- and 25-week old control and monosomic mice fed on a HFD did not reveal any anatomical abnormalities of any organs, except for the presence of hepatic fatty changes in 8- and 25-week old monosomic mice (**Figure 3.13, 3.14A**) and a significantly thicker layer of subcutaneous fat (photos of all adipose sections placed on glass slides were taken under the same magnification, and subsequently the average thickness of subcutaneous adipose layer was calculated after taking three measurements of the fat layer width from each of the sections) and enlarged fat cells in 25-week old monosomic mice (**Figure 3.14B**). Specifically, the livers of 8-week old monosomic mice showed moderate fatty changes compared to mild fatty changes in the controls (**Figure 3.13**). The fatty changes in livers of the monosomic mice, as well as the controls, accelerated with age, and were regarded as severe to very severe in 25-week old monosomic mice compared to mild to moderate in the controls (**Figure 3.14A**).

The histopathological analysis of the livers stained with H&E of 8- and 25-week old monosomic mice fed on a NFD did not demonstrate the presence of any fatty changes compared to the controls (**Figure 3.13, 3.14A**). Interestingly, a broad range of fatty changes (from mild through moderate to severe) were observed in the livers of 1-year old monosomic mice and their control littermates fed on a NFD (**Figure 3.15A**). Moreover, the layer of subcutaneous fat showed differential thickness, from medium to thick, in each individual from both monosomic and control mice at 1 year of age (photos of all adipose sections placed on glass slides were taken under the same magnification, and subsequently the average thickness of subcutaneous adipose layer was calculated after taking three measurements of the fat layer width from each of the sections) (**Figure 3.15B**).

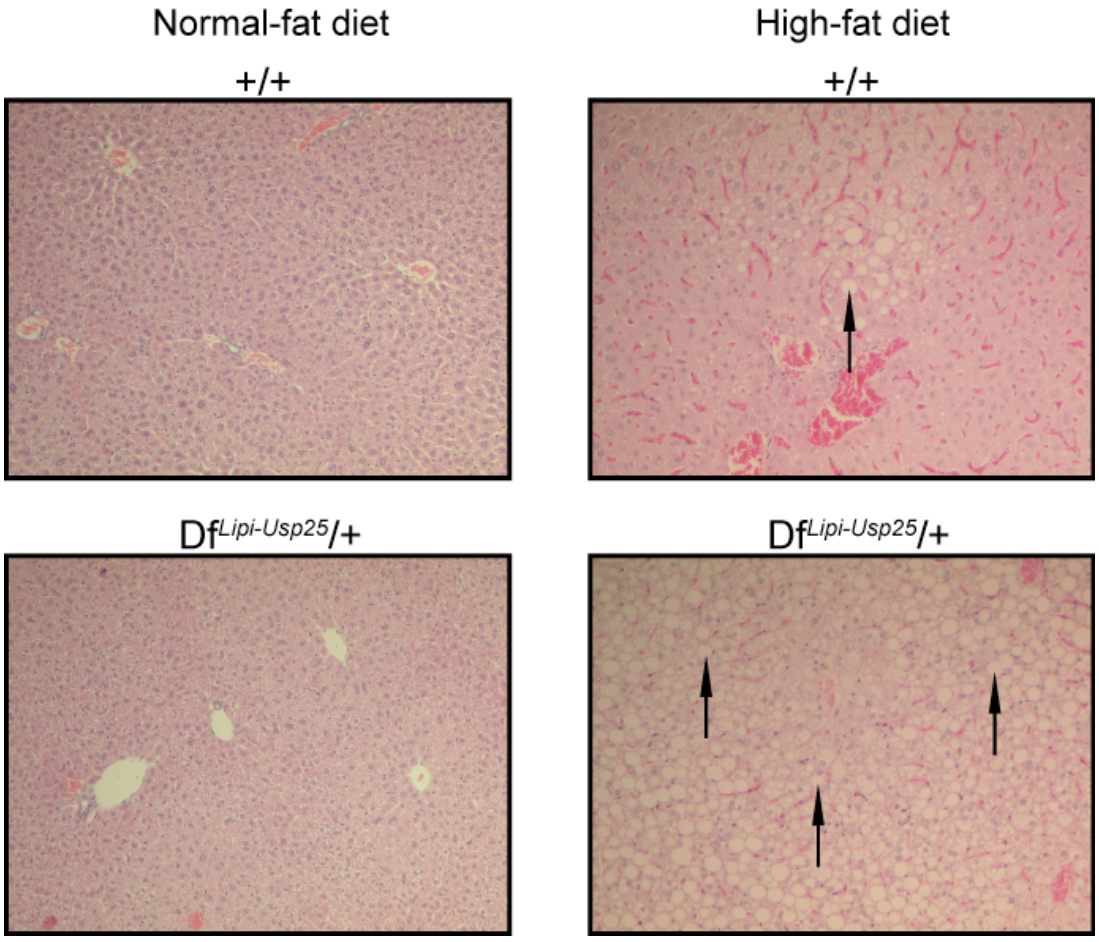

Figure 3.13. Histopathological analysis of livers collected from 8-week old control (+/+) and monosomic (*Df*$^{Lipi\text{-}Usp25}$/+) littermates fed either on a normal-fat or a high-fat diet. Haematoxylin and eosin-stained liver sections from control (+/+) and monosomic (*Df*$^{Lipi\text{-}Usp25}$/+) mice. Livers of control (+/+) and monosomic (*Df*$^{Lipi\text{-}Usp25}$/+) mice fed on a normal-fat diet showed no fatty changes. Livers of control (+/+) mice fed on a high-fat diet showed very mild fatty changes compared to moderate fatty changes in livers of monosomic (*Df*$^{Lipi\text{-}Usp25}$/+) mice. Note increased number of adipose cells (visible as white oval cells; indicated by arrows) in liver sections from monosomic (*Df*$^{Lipi\text{-}Usp25}$/+) compared to control (+/+) littermates. Images are representative and taken at x100 magnification.

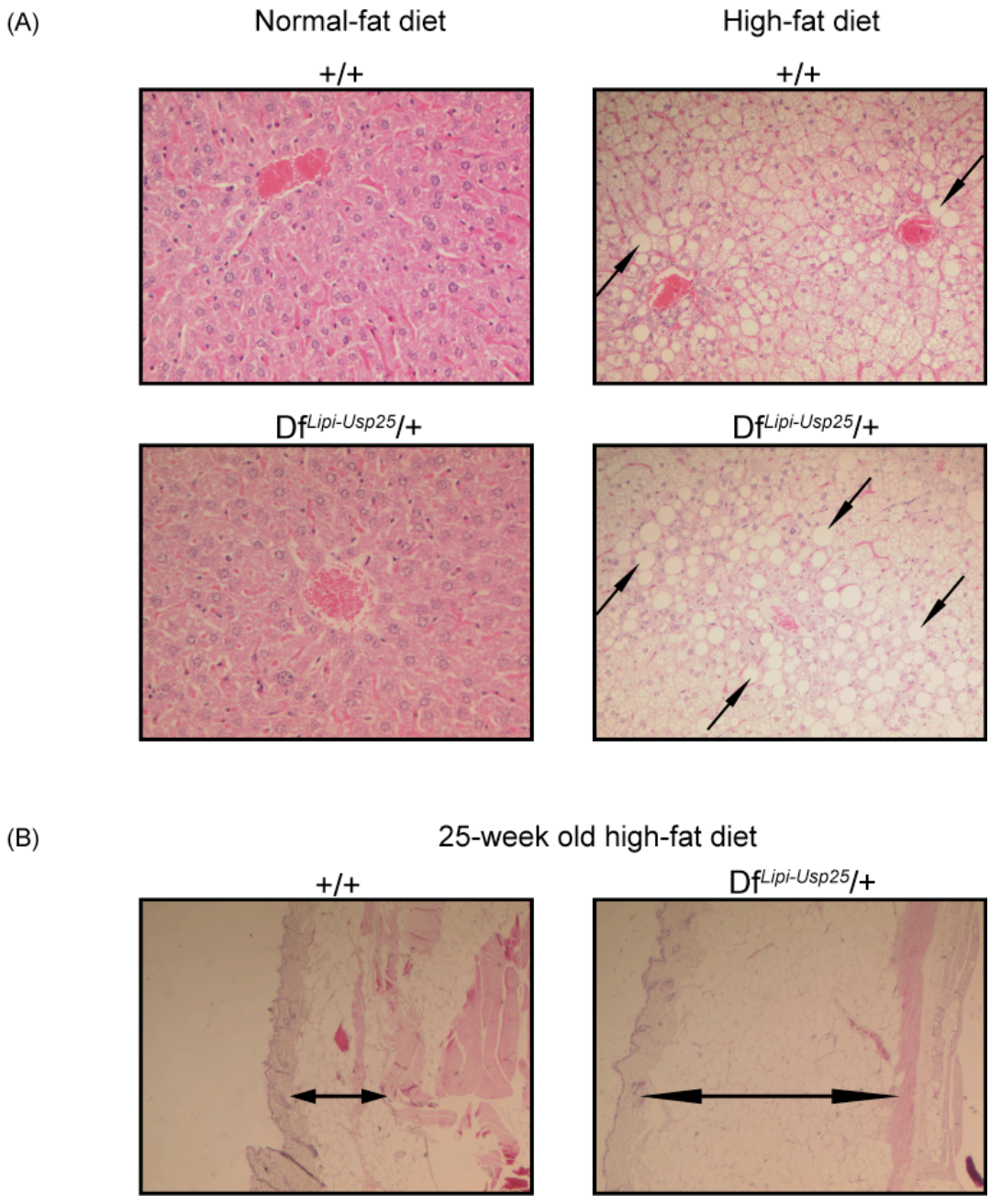

Figure 3.14. Histopathological analysis of livers and skin sections collected from 25-week old control (+/+) and monosomic (*Df*$^{Lipi\text{-}Usp25}$/+) littermates fed either on a normal-fat or a high-fat diet. (A) Haematoxylin and eosin-stained liver sections from control (+/+) and monosomic (*Df*$^{Lipi\text{-}Usp25}$/+) mice. Livers of control (+/+) and monosomic (*Df*$^{Lipi\text{-}Usp25}$/+) mice fed on a normal-fat diet showed no fatty changes. Livers of control (+/+) mice fed on a high-fat diet showed mild to moderate fatty changes compared to severe and very severe fatty changes in livers of monosomic (*Df*$^{Lipi\text{-}Usp25}$/+) mice. Note markedly increased number of adipose cells (visible as white oval cells; indicated by arrows) in liver sections from monosomic (*Df*$^{Lipi\text{-}Usp25}$/+) compared to control (+/+) littermates. Images are representative and taken at x100 magnification. **(B)** Haematoxylin and eosin-stained skin sections from control (+/+) and monosomic (*Df*$^{Lipi\text{-}Usp25}$/+) mice fed on a high-fat diet. Skin sections from monosomic (*Df*$^{Lipi\text{-}Usp25}$/+) mice have a markedly thicker fat layer (indicated by arrows) and fat cells are enlarged when compared to control (+/+) mice. Images are representative and taken at x50 magnification. One skin section was analysed per mouse and three measurements of the fat layer thickness were taken from the section. Skin sections were collected from 16 monosomic (*Df*$^{Lipi\text{-}Usp25}$/+) mice and 18 control (+/+) mice.

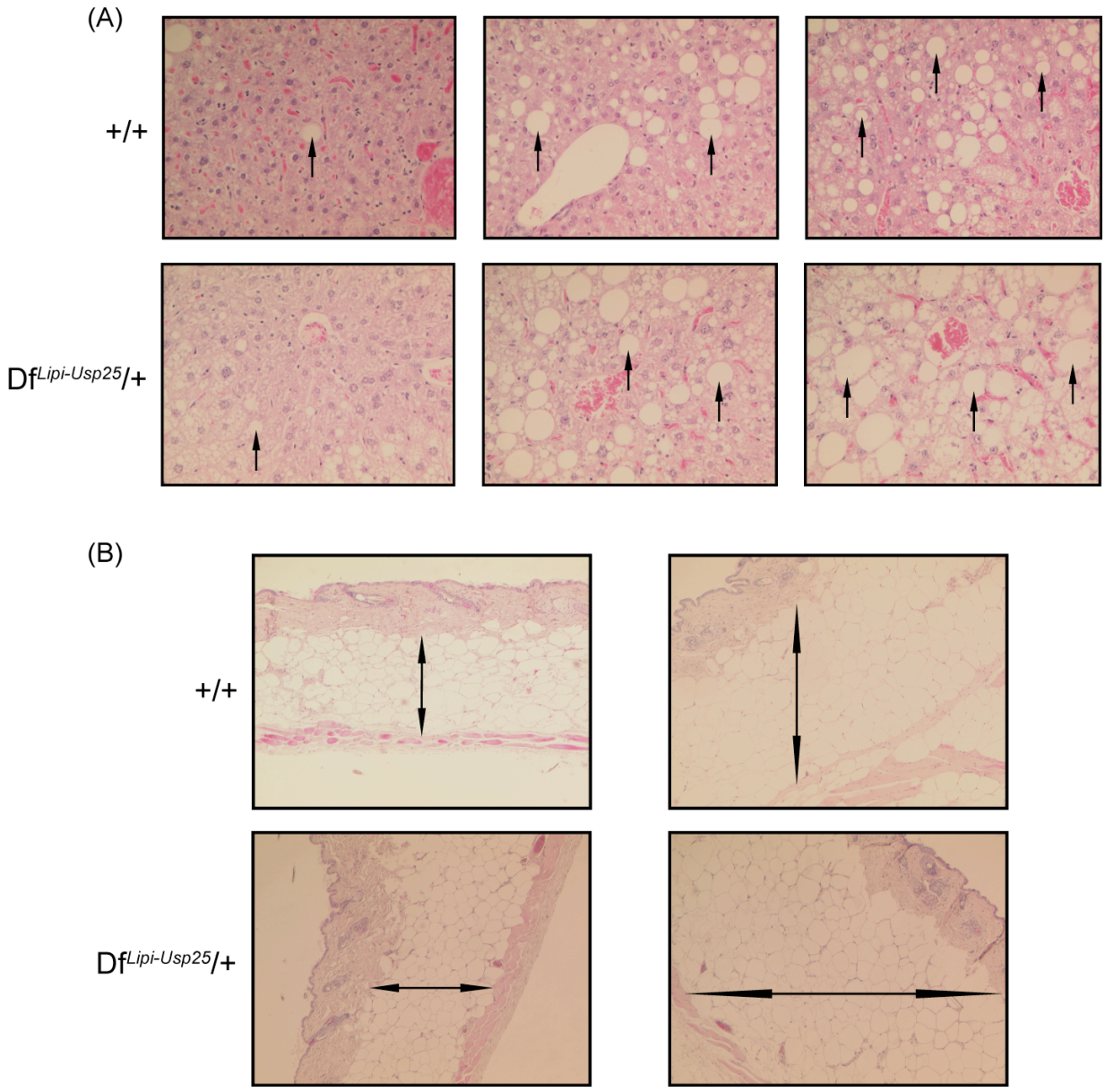

Figure 3.15. Histopathological analysis of livers and skin sections collected from 1-year old control (+/+) and monosomic (*Df*$^{Lipi\text{-}Usp25}$/+) littermates fed on a normal-fat diet. (A) Haematoxylin and eosin-stained liver sections from control (+/+) and monosomic (*Df*$^{Lipi\text{-}Usp25}$/+) mice. Livers of both control (+/+) and monosomic (*Df*$^{Lipi\text{-}Usp25}$/+) mice showed mild through moderate to severe fatty changes (from left to right; visible as white oval cells; indicated by arrows). Images are representative and taken at x200 magnification. **(B)** Haematoxylin and eosin-stained skin sections from control (+/+) and monosomic (*Df*$^{Lipi\text{-}Usp25}$/+) mice. Skin sections from both control (+/+) and monosomic (*Df*$^{Lipi\text{-}Usp25}$/+) mice showed a differential thickness of subcutaneous fat layer (indicated by arrows), from medium (left) to thick (right). Images are representative and taken at x50 magnification. One skin section was analysed per mouse and three measurements of the fat layer thickness were taken from the section. Skin sections were collected from 16 monosomic (*Df*$^{Lipi\text{-}Usp25}$/+) mice and 18 control (+/+) mice.

3.3.7 EXPRESSION ANALYSIS OF SUBCUTANEOUS ADIPOSE TISSUE IN MONOSOMIC MICE FED ON A HIGH-FAT DIET

To look at differentially expressed genes in adipocytes from monosomic and control mice fed on a high-fat diet (n=9 per genotype at 16 weeks of age), expression array analysis was performed. Analysis of the obtained data showed significantly altered expression ('raw' P values lower than 0.0015) of 30 genes (13 up-regulated, 17 down-regulated) (**Table 3.2**). However, given that the 'adjusted' p values for these genes were not significant, we performed quantitative RT-PCR (qRT-PCR) on a subset of these genes to validate our findings. Of the 15 genes analysed by qRT-PCR (selected on the basis of their rank or biological function), 2 were significantly up-regulated (*Tmem45a* and *Rbm38*; P=0.0085 and P=0.0081 respectively), and 4 were significantly down-regulated (*Plxnd1*, *Lrpap1*, *Samsn1* and *Lmna*; P=0.0047, P=0.0021, P=0.0057 and P=0.0002 respectively) (**Figure 3.16**). Moreover, *Samsn1* appears to be the only gene in the *Lipi–Usp25* deletion region to be expressed in adipose tissue and, as expected, this gene showed a significant reduction in its expression level.

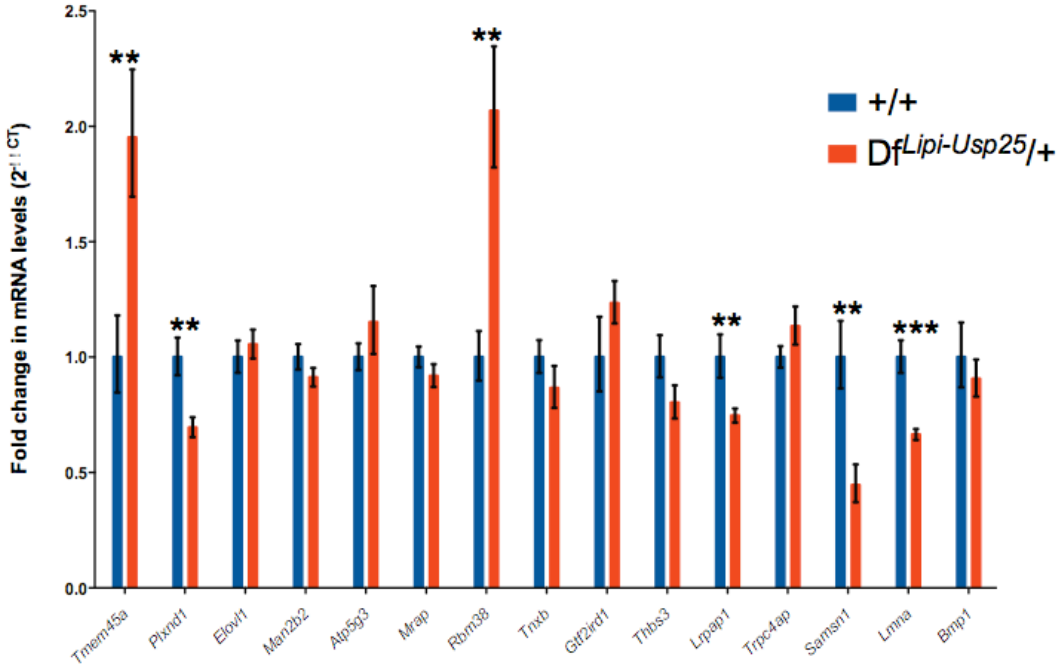

Figure 3.16. Quantitative RT-PCR (qRT-PCR) analysis of adipose tissue. qRT-PCR was performed on abdominal subcutaneous adipose tissue of 16-week old high fat diet-fed monosomic (*Df*$^{Lipi\text{-}Usp25}$/+) and control (+/+) mice (n=9 per genotype at 16 weeks). Asterisks indicate statistical significance; ** P<0.01, *** P<0.005 (two-tailed Student's *t*-test).

Table 3.2. Gene expression analysis of subcutaneous adipose tissue from monosomic (*Df*$^{Lipi\text{-}Usp25}$) and control (+/+) littermates fed on a high-fat diet. Gene expression data were obtained using RNA extracted from the subcutaneous adipose tissue of 16-week old HFD-fed monosomic and control mice (n=9 per genotype). The RNA was analysed on Illumina Mouse WG-6 v2.0 beadchips. Data were analysed and P-value adjusted (as described in the Methods) to yield a sorted list of differentially expressed genes. The differentially expressed genes with a raw P value <0.0015 are listed. Differential expression levels are shown as log fold change (LogFC) in the monosomic samples relative to the controls (a negative value indicates decreased expression). "qRT-PCR" shows whether there was a statistically significant difference in expression of the gene between the monosomic mice and controls (Yes, P<0.005; No, P>0.005; N.T., not tested). Functions/processes were based on gene ontology classifications as listed by Mouse Genome Informatics (http://www.informatics.jax.org/).

Gene	Official name	Ensembl ID (v61)	Log fold change	Average expression	Raw P value	Adjusted P value	qRT-PCR	Function/Processes (GO terms)
Tmem45a	Transmembrane protein 45a	ENSMUSG00000022754	0.245	7.0	0.0001	0.6402	Yes	Unknown
Plxnd1	Plexin D1	ENSMUSG00000030123	-0.393	8.1	0.0001	0.6402	Yes	Semaphorin receptor activity, regulation of branching involved in salivary gland morphogenesis, angiogenesis
Elovl1	Elongation of very long chain fatty acids-like 1	ENSMUSG00000006390	-0.236	9.3	0.0001	0.6402	No	Fatty acid biosynthetic processes
A	Nonagouti	ENSMUSG00000027596	0.169	6.7	0.0001	0.6402	N.T.	Melanocortin receptor binding activity, generation of precursor metabolites/energy
Man2b2	Mannosidase 2, alpha B2	ENSMUSG00000029119	-0.129	7.4	0.0002	0.6402	No	Carbohydrate metabolic processes
Atp5g3	ATP synthase, H+ transporting, mitochondrial F0 complex, subunit C3 (subunit 9)	ENSMUSG00000018770	0.213	12.8	0.0002	0.7142	No	ATP synthesis coupled proton transport
Mrap	Melanocortin 2 receptor accessory protein	ENSMUSG00000039956	-0.579	11.1	0.0004	0.7514	No	Adrenocorticotropin hormone and melanocortin receptor binding activity, brown fat cell differentiation
Rbm38	RNA binding motif protein 38	ENSMUSG00000027510	0.143	6.9	0.0005	0.7514	Yes	3'-UTR-mediated mRNA stabilization, negative regulation of cell proliferation
Zfp703	Zinc finger protein 703	ENSMUSG00000085795	-0.083	6.9	0.0005	0.7514	N.T.	Mammary gland epithelial cell differentiation & proliferation
Tnxb	Tenascin XB	ENSMUSG00000033327	-0.345	8.6	0.0006	0.7514	No	Cell-cell adhesion, extracellular matrix organization, lipid metabolic processes
Gtf2ird1	General transcription factor II I repeat domain-containing 1	ENSMUSG00000023079	0.169	7.6	0.0007	0.7514	No	DNA-dependent regulation of transcription
Ecm1	Extracellular matrix protein 1	ENSMUSG00000028108	-0.400	9.7	0.0007	0.7514	N.T.	Angiogenesis, regulation of bone mineralization
Pdk1	Pyruvate dehydrogenase kinase, isoenzyme 1	ENSMUSG00000006494	0.145	7.3	0.0007	0.7514	N.T.	Carbohydrate metabolic process
Thbs3	Thrombospondin 3	ENSMUSG00000028047	-0.121	7.0	0.0008	0.7514	No	Cell adhesion, growth plate cartilage development & ossification
Hist1h4f	Histone cluster 1, H4f	ENSMUSG00000069274	-0.260	7.3	0.0008	0.7514	N.T.	Unknown

Table 3.2 continued. Gene expression analysis of subcutaneous adipose tissue from monosomic (*Df*$^{Lipi\text{-}Usp25}$) and control (+/+) littermates fed on a high-fat diet.

Gene	Official name	Ensembl ID (v61)	Log fold change	Average expression	Raw P value	Adjusted P value	qRT-PCR	Function/Processes (GO terms)
Chchd10	Coiled-coil-helix-coiled-coil-helix domain containing 10	ENSMUSG00000049422	0.845	10.6	0.0008	0.7514	N.T.	Unknown
Lrpap1	Low density lipoprotein receptor-related protein associated protein 1	ENSMUSG00000029103	-0.337	11.4	0.0009	0.7514	Yes	Low-density lipoprotein particle receptor binding
Trpc4ap	Transient receptor potential cation channel, subfamily C, member 4 associated protein	ENSMUSG00000038324	0.110	7.9	0.0010	0.7514	No	Protein ubiquitination
Slpi	Secretory leukocyte peptidase inhibitor	ENSMUSG00000017002	-0.908	8.8	0.0010	0.7514	N.T.	Peptidase inhibitor activity
Uqcrc2	Ubiquinol cytochrome c reductase core protein 2	ENSMUSG00000030884	0.255	10.7	0.0010	0.7514	N.T.	Metal ion binding, electron transport chain
Samsn1	SAM domain, SH3 domain and nuclear localization signals, 1	ENSMUSG00000022876	-0.268	7.0	0.0010	0.7514	Yes	Unknown
Tsnax	Translin-associated factor X	ENSMUSG00000056820	0.239	9.7	0.0010	0.7514	N.T.	Cell differentiation, spermatogenesis
Diras2	DIRAS family, GTP-binding RAS-like 2	ENSMUSG00000047842	-0.358	7.3	0.0011	0.7514	N.T.	GTP catabolic processes
4930533 K18Rik	-	ENSMUSG00000047692	-0.165	7.7	0.0011	0.7514	N.T.	Unknown
Nmt1	N-myristoyltransferase 1	ENSMUSG00000020936	0.116	10.2	0.0012	0.7514	N.T.	Transferase activity, N-terminal protein myristoylation
Hist1h1c	Histone cluster 1, H1c	ENSMUSG00000036181	0.319	11.5	0.0012	0.7514	N.T.	Nucleosome assembly
Lmna	Lamin A	ENSMUSG00000028063	-0.200	7.4	0.0013	0.7514	Yes	Nucleus organization, sterol regulatory element binding protein import into nucleus, ventricular cardiac muscle cell development
Susd2	Sushi domain containing 2	ENSMUSG00000006342	-0.095	6.9	0.0013	0.7514	N.T.	Immune response, polysaccharide binding
Mtmr14	Myotubularin related protein 14	ENSMUSG00000030269	0.108	7.5	0.0014	0.7514	N.T.	Phosphatase activity
Bmp1	Bone morphogenetic protein 1	ENSMUSG00000022098	-0.374	9.1	0.0014	0.7514	No	Metalloendopeptidase activity, cartilage/bone development

3.3.8 HISTOPATHOLOGICAL ANALYSIS OF BONES OF 10-WEEK OLD MONOSOMIC MICE FED ON A NORMAL-FAT DIET SUGGESTS THAT LOSS OF ONE COPY OF THE *Lipi–Usp25* REGION MIGHT AFFECT BONE OSSIFICATION

In parallel with the phenotypic screening approach, different tissues stained with H&E collected from 10-week old control and monosomic mice fed on a NFD were subjected to detailed histopathological analysis. The examination did not reveal the existence of any anatomical changes of any organs, except tibias. Namely, decreased endochondral ossification in the cartilage of tibias was observed in the monosomic mice compared to controls (**Figure 3.17**).

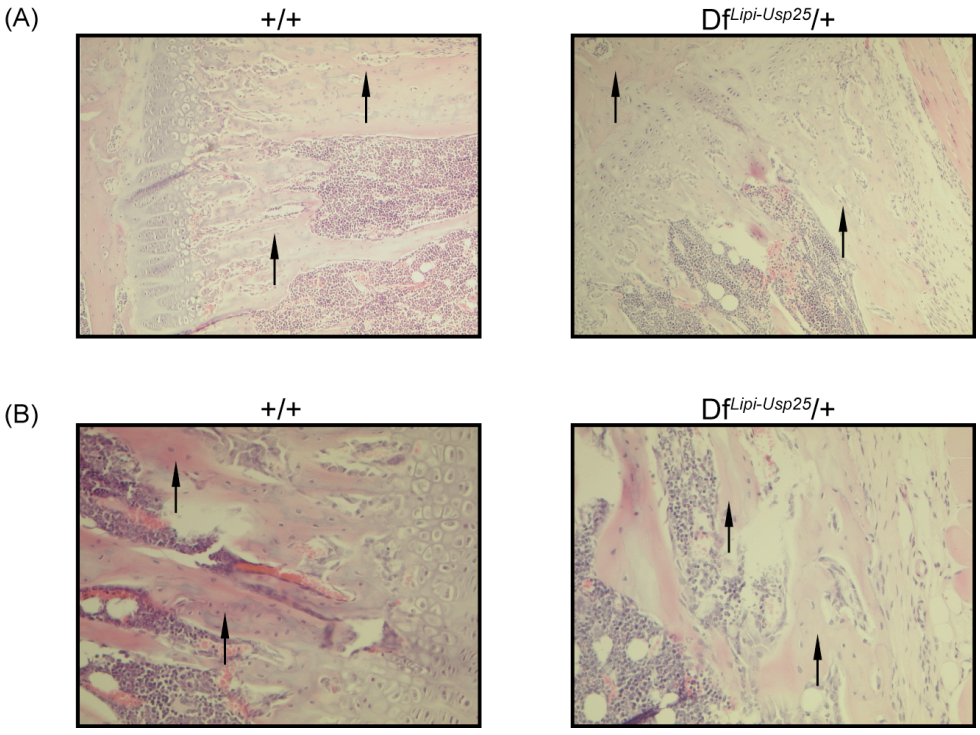

Figure 3.17. Histopathological analysis of bones collected from 10-week old control (+/+) and monosomic (*Df*$^{Lipi\text{-}Usp25}$/+) littermates fed on a normal-fat diet. (A) Haematoxylin and eosin-stained tibias sections from control (+/+) and monosomic (*Df*$^{Lipi\text{-}Usp25}$/+) males. Tibias of monosomic (*Df*$^{Lipi\text{-}Usp25}$/+) males showed lower endochondral ossification (visible as light pink staining of cartilage; indicated by arrow) compared to control (+/+) males (visible as darker pink staining of cartilage; indicated by arrow). Images are representative and taken at x100 magnification. **(B)** Haematoxylin and eosin-stained tibias sections from control (+/+) and monosomic (*Df*$^{Lipi\text{-}Usp25}$/+) females. Tibias of monosomic (*Df*$^{Lipi\text{-}Usp25}$/+) females showed lower endochondral ossification (visible as light pink staining of cartilage; indicated by arrows) compared to control (+/+) females (visible as dark pink staining of cartilage; indicated by arrows). Images are representative and taken at x200 magnification.

3.3.9 FOLLOW-UP ANALYSIS OF BONES OF 8-, 25-WEEK AND 1-YEAR OLD MONOSOMIC MICE REVEALS THAT LOSS OF ONE COPY OF THE *Lipi–Usp25* REGION DOES NOT AFFECT BONE OSSIFICATION

Following the preliminary histopathological results, suggesting that the monosomic mice fed on a NFD exhibit decreased endochondral ossification, bones of additional monosomic mice and littermate controls fed on a NFD were analysed by DEXA (to measure bone mineral density) and histopathologically (to evaluate the level of endochondral ossification of the cartilage) at additional time points, specifically at 8 and 25 weeks and 1 year of age (**Figure 3.18A, 3.18B, 3.19A, 3.19B, 3.21A, 3.21B**). No significant differences in bone mineral density were observed between control and monosomic mice at any of the time points (**Figure 3.18A, 3.19A, 3.21A**). In addition, no histopathological changes in the cartilage and/or in the cortical bone shaft of any analysed bones (tibia, femur, radius, ulna, sternum and ribs) were observed in monosomic mice at 8 and 25 weeks and 1 year of age (**Figure 3.18B, 3.19B, 3.21A**). Bones of 25-week old mice were further analysed with von Kossa staining to compare the level of calcium deposition between monosomic mice and their littermate controls. No differences in the calcium deposition were observed (**Figure 3.20**).

Thus we conclude that monosomy of the *Lipi–Usp25* region does not have an impact on endochondral ossification, bone mineral density or calcium deposition.

3.3.10 INCREASED FAT MASS IN 8- AND 25-WEEK OLD MICE DOES NOT LEAD TO THE INCREASE IN BONE MASS

The existence of the relationship between body fat mass and bone metabolism has been reported by various studies (Zhao 2008; Holecki 2010). However, it still remains unclear whether increased body fat mass has a protective effect on bone tissue, and thus causes increased bone mass, since contradicting results have been provided by these studies (Zhao 2008; Holecki 2010).

To test whether increased fat mass is linked with increased bone mass, we decided to compare the level of bone mineral density and the level of endochondral ossification in the cartilage and/or in the cortical bone shaft of monosomic and control mice fed either on a NFD or a HFD. Bones of 8- and 25-week old control and monosomic mice fed on a HFD showed no significant differences in bone mineral density, except for a decrease in bone mineral density in 8-week old monosomic males compared to controls (**Figure 3.18A, 3.19A**). In addition, no histopathological changes in the cartilage and/or in the cortical bone shaft were observed in monosomic mice at 8 and 25 weeks of age (**Figure 3.18B, 3.19B**). Furthermore, despite significant differences being observed in fat mass in both groups (**Figure 3.22A, 3.23A, 3.24A, 3.25A**), no significant differences in bone mineral density were observed between monosomic mice fed on a NFD or a HFD, or between control mice fed on a NFD or a HFD at any analysed time points (**Figure 3.22B, 3.23B, 3.24B, 3.25B**). Thus we did not observe any beneficial effects of significantly increased fat mass on bone mass in the monosomic mice compared to their littermate controls, or any correlation between significantly increased fat mass and increased bone mass in the monosomic and control mice fed on a HFD compared with those on a NFD. Altogether, our results do not support a hypothesis suggesting a protective effect of increased fat mass on bone tissue.

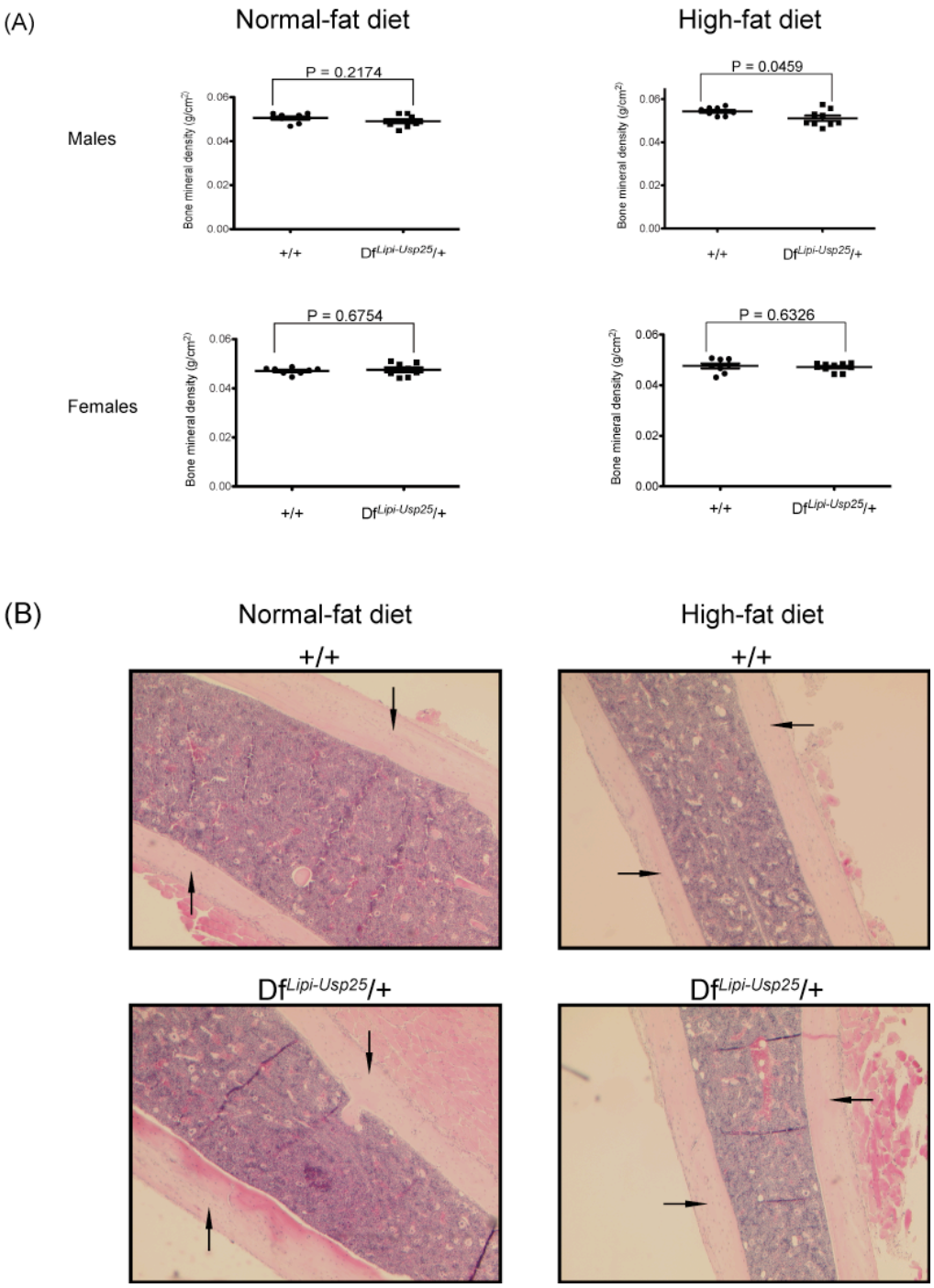

Figure 3.18. DEXA and histopathological analysis of bones collected from 8-week old control (+/+) and monosomic (*Df*$^{Lipi\text{-}Usp25}$/+) littermates fed on a normal-fat or high-fat diet. (A) DEXA results showing bone mineral density in male and female littermates fed on a normal-fat or high-fat diet. Data was statistically analysed using the two-tailed Student's *t*-test. Normal-fat diet: 9 monosomic (*Df*$^{Lipi\text{-}Usp25}$/+) males were compared with 8 control (+/+) males and 8 monosomic (*Df*$^{Lipi\text{-}Usp25}$/+) females were compared with 8 control (+/+) females. High-fat diet: 9 monosomic (*Df*$^{Lipi\text{-}Usp25}$/+) males were compared with 8 control (+/+) males and 10 monosomic (*Df*$^{Lipi\text{-}Usp25}$/+) females were compared with 8 control (+/+) females. **(B)** Haematoxylin and eosin-stained bone sections from control (+/+) and monosomic (*Df*$^{Lipi\text{-}Usp25}$/+) mice fed on a normal-fat or high-fat diet. No changes in the cortical bone ossification levels (visible as pink staining of the cortical bone shaft; indicated by arrows) were observed between the monosomic (*Df*$^{Lipi\text{-}Usp25}$/+) and control (+/+) mice. Images are representative and taken at x50 magnification.

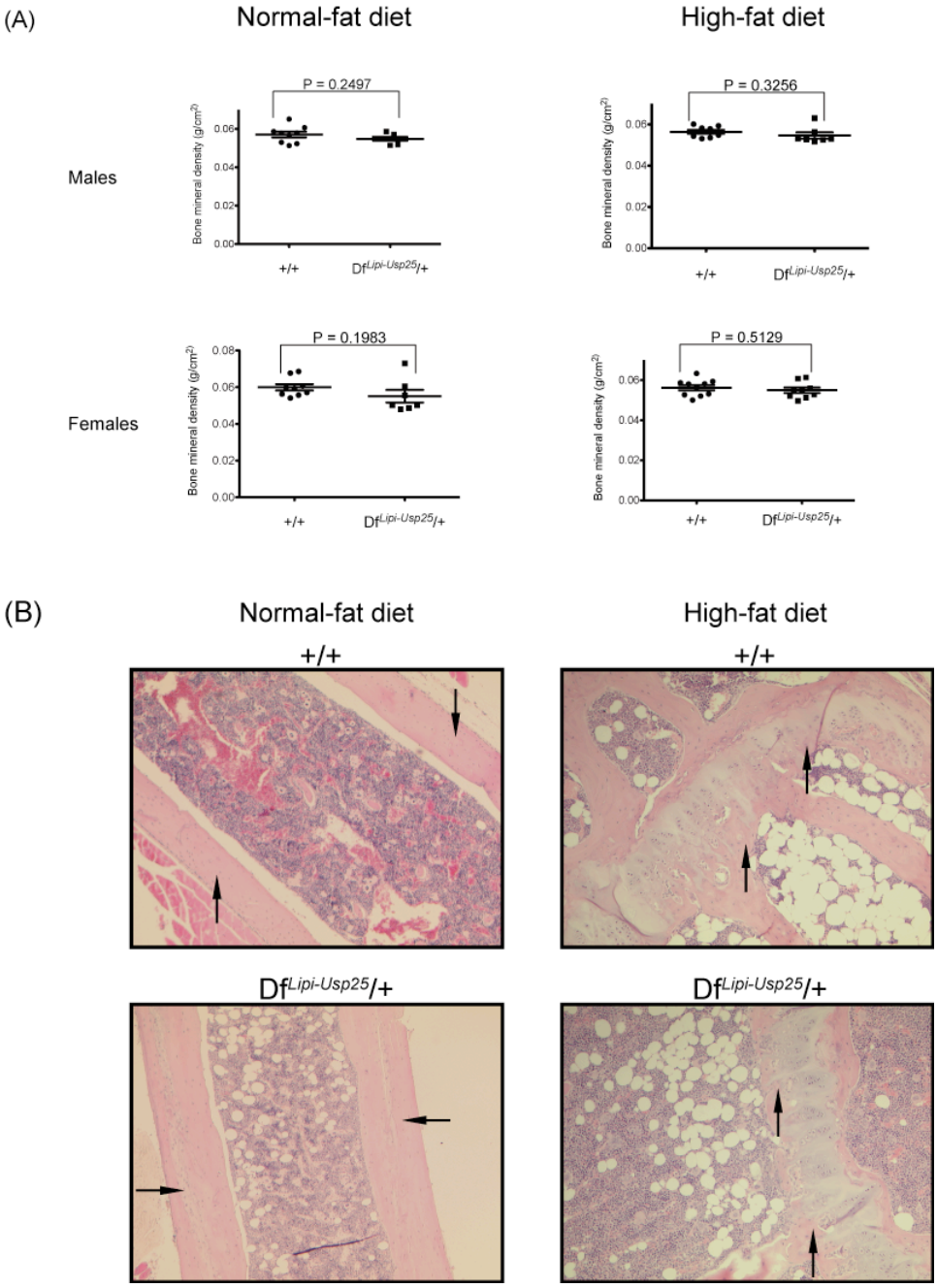

Figure 3.19. DEXA and histopathological analysis of bones collected from 25-week old control (+/+) and monosomic (*Df*$^{Lipi\text{-}Usp25}$/+) littermates fed on a normal-fat or high-fat diet. (A) DEXA results showing bone mineral density in male and female littermates fed on a normal-fat or high-fat diet. Data was statistically analysed using the two-tailed Student's *t*-test. Normal-fat diet: 7 monosomic (*Df*$^{Lipi\text{-}Usp25}$/+) males were compared with 9 controls (+/+) males and 7 monosomic (*Df*$^{Lipi\text{-}Usp25}$/+) females were compared with 9 control (+/+) females. High-fat diet: 7 monosomic (*Df*$^{Lipi\text{-}Usp25}$/+) males were compared with 8 controls (+/+) males and 9 monosomic (*Df*$^{Lipi\text{-}Usp25}$/+) females were compared with 10 control (+/+) females. **(B)** Haematoxylin and eosin-stained bone sections from control (+/+) and monosomic (*Df*$^{Lipi\text{-}Usp25}$/+) mice fed on a normal-fat or high-fat diet. No changes in the cortical bone ossification levels (left panel; visible as pink staining of the cortical bone shaft; indicated by arrows) and no changes in the endochondral ossification of the cartilage (right panel; visible as pink staining of the cartilage; indicated by arrows) and were observed between the monosomic (*Df*$^{Lipi\text{-}Usp25}$/+) and control (+/+) mice. Images are representative and taken at x50 or x100 magnification.

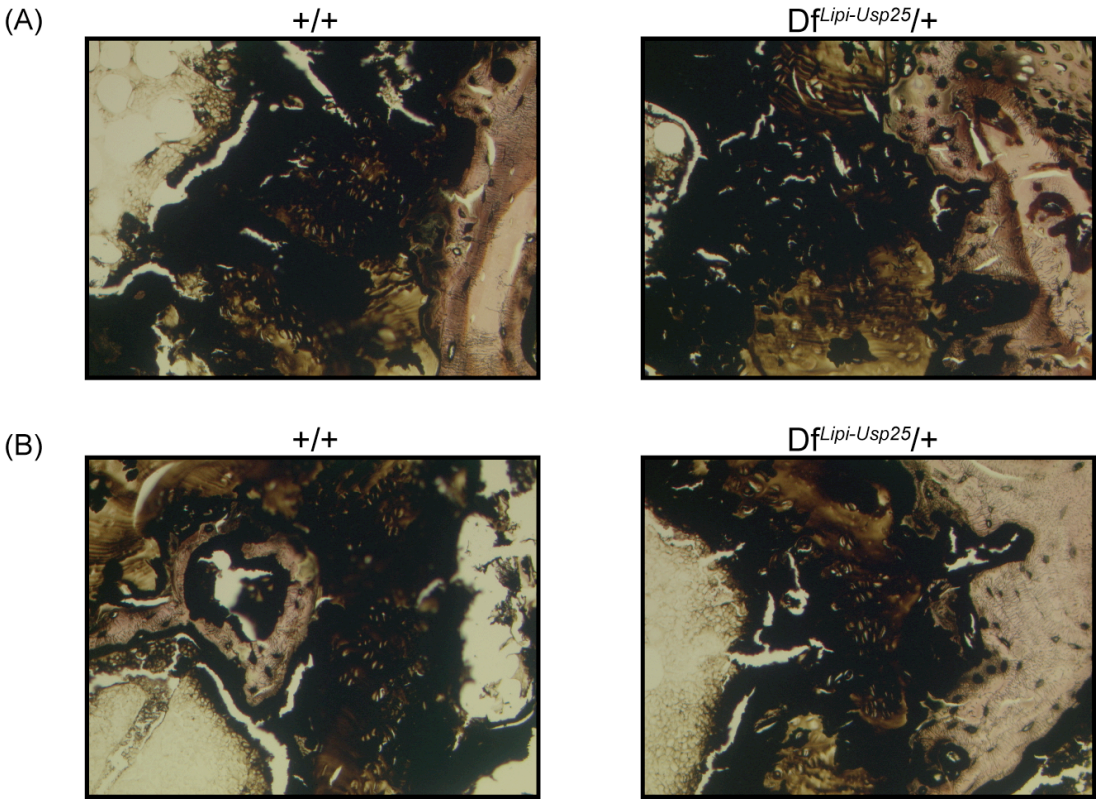

Figure 3.20. Histopathological analysis of bones collected from 25-week old control (+/+) and monosomic (*Df*$^{Lipi\text{-}Usp25}$/+) littermates fed on a normal-fat. (A) Von Kossa-stained tibia sections from control (+/+) and monosomic (*Df*$^{Lipi\text{-}Usp25}$/+) males. No changes in the calcium deposition (visible as black staining) were observed between the monosomic (*Df*$^{Lipi\text{-}Usp25}$/+) and control (+/+) males. Images are representative and taken at x200 magnification. **(B)** Von Kossa-stained tibia sections from control (+/+) and monosomic (*Df*$^{Lipi\text{-}Usp25}$/+) females. No changes in the calcium deposition (visible as black staining) were observed between the monosomic (*Df*$^{Lipi\text{-}Usp25}$/+) and control (+/+) females. Images are representative and taken at x200 magnification.

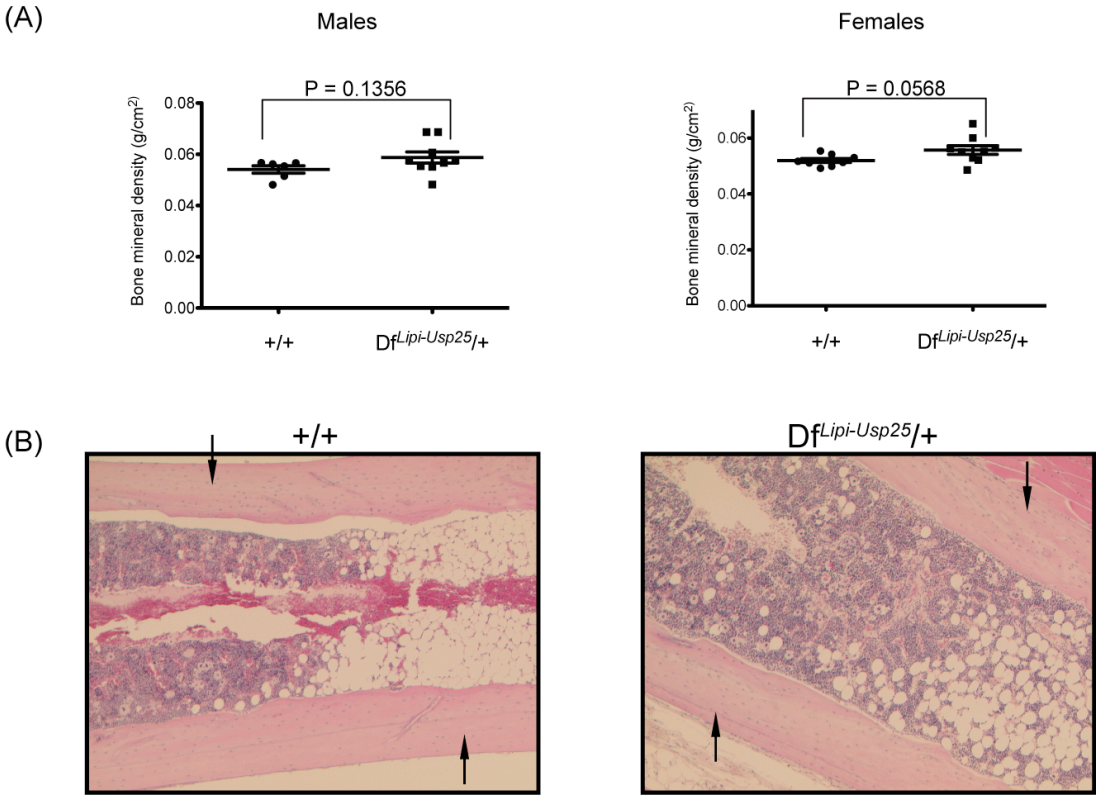

Figure 3.21. DEXA and histopathological analysis of bones collected from 1-year old control (+/+) and monosomic (*Df*$^{Lipi\text{-}Usp25}$/+) littermates fed on a normal-fat diet. **(A)** DEXA results showing bone mineral density in male and female littermates. Data was statistically analysed using the two-tailed Student's *t*-test. 9 monosomic (*Df*$^{Lipi\text{-}Usp25}$/+) males were compared with 6 control (+/+) males and 9 monosomic (*Df*$^{Lipi\text{-}Usp25}$/+) females were compared with 8 control (+/+) females. **(B)** Haematoxylin and eosin-stained bone sections from control (+/+) and monosomic (*Df*$^{Lipi\text{-}Usp25}$/+) mice. No changes in the cortical bone ossification levels (visible as pink staining of the cortical bone shaft) were observed between the monosomic (*Df*$^{Lipi\text{-}Usp25}$/+) and control (+/+) mice. Images are representative and taken at x50 magnification.

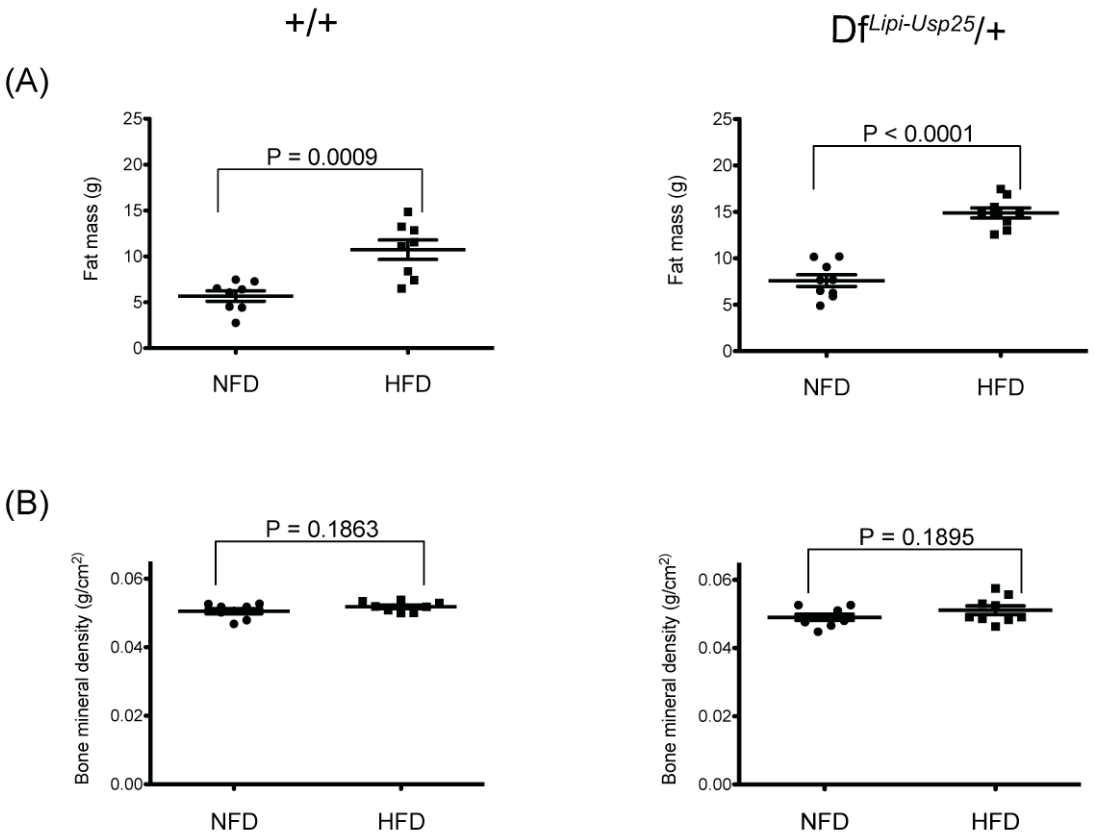

Figure 3.22. DEXA analysis of 8-week old control (+/+) and monosomic (*Df*$^{Lipi\text{-}Usp25}$/+) male littermates fed on a normal-fat or high-fat diet (group 1). (A) DEXA results showing fat mass in control (+/+) and monosomic (*Df*$^{Lipi\text{-}Usp25}$/+) male littermates fed on a normal-fat or high-fat diet. **(B)** DEXA results showing bone mineral density in control (+/+) and monosomic (*Df*$^{Lipi\text{-}Usp25}$/+) male littermates fed on a normal-fat or high-fat diet. Data was statistically analysed using the two-tailed Student's *t*-test. Normal-fat diet: 9 monosomic (*Df*$^{Lipi\text{-}Usp25}$/+) males were compared with 8 control (+/+) males. High-fat diet: 9 monosomic (*Df*$^{Lipi\text{-}Usp25}$/+) males were compared with 8 control (+/+) males. NFD - normal fat diet, HFD - high fat diet.

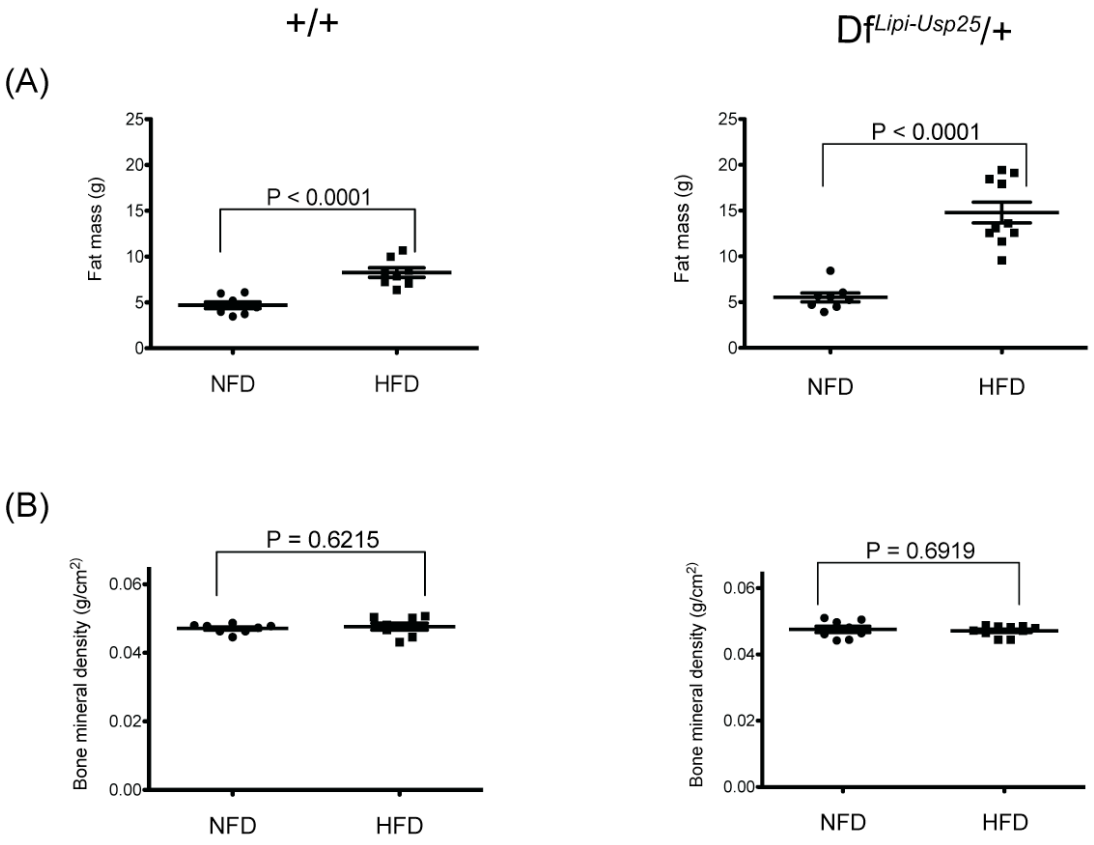

Figure 3.23. DEXA analysis of 8-week old control (+/+) and monosomic (*Df*$^{Lipi\text{-}Usp25}$/+) female littermates fed on a normal-fat or high-fat diet (group 2). (A) DEXA results showing fat mass in control (+/+) and monosomic (*Df*$^{Lipi\text{-}Usp25}$/+) female littermates fed on a normal-fat or high-fat diet. **(B)** DEXA results showing bone mineral density in control (+/+) and monosomic (*Df*$^{Lipi\text{-}Usp25}$/+) female littermates fed on a normal-fat or high-fat diet. Data was statistically analysed using the two-tailed Student's *t*-test. Normal-fat diet 8 monosomic (*Df*$^{Lipi\text{-}Usp25}$/+) females were compared with 8 control (+/+) females. High-fat diet: 10 monosomic (*Df*$^{Lipi\text{-}Usp25}$/+) females were compared with 8 control (+/+) females. NFD - normal fat diet, HFD - high fat diet.

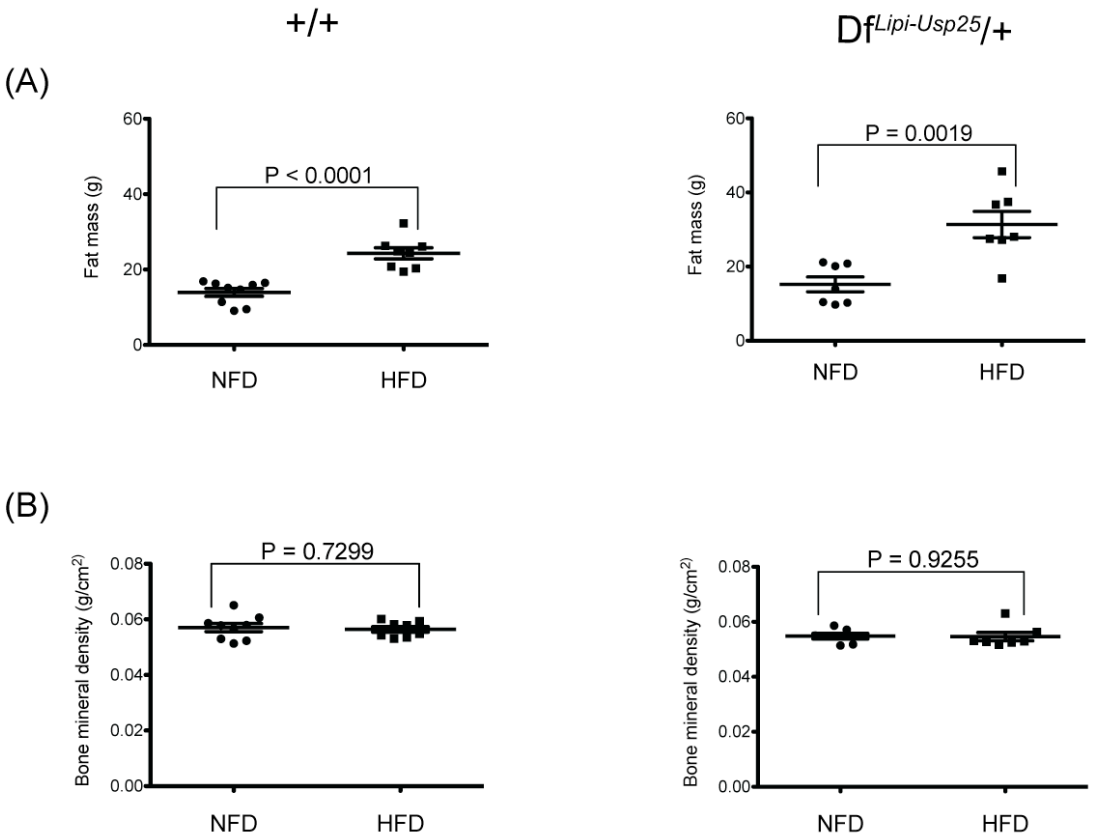

Figure 3.24. DEXA analysis of 25-week old control (+/+) and monosomic (*Df*$^{Lipi\text{-}Usp25}$/+) male littermates fed on a normal-fat or high-fat diet (group 3). (A) DEXA results showing fat mass in control (+/+) and monosomic (*Df*$^{Lipi\text{-}Usp25}$/+) male littermates fed on a normal-fat or high-fat diet. **(B)** DEXA results showing bone mineral density in control (+/+) and monosomic (*Df*$^{Lipi\text{-}Usp25}$/+) male littermates fed on a normal-fat or high-fat diet. Data was statistically analysed using the two-tailed Student's *t*-test. Normal-fat diet: 7 monosomic (*Df*$^{Lipi\text{-}Usp25}$/+) males were compared with 9 controls (+/+) males. High-fat diet: 7 monosomic (*Df*$^{Lipi\text{-}Usp25}$/+) males were compared with 8 controls (+/+) males. NFD - normal fat diet, HFD - high fat diet.

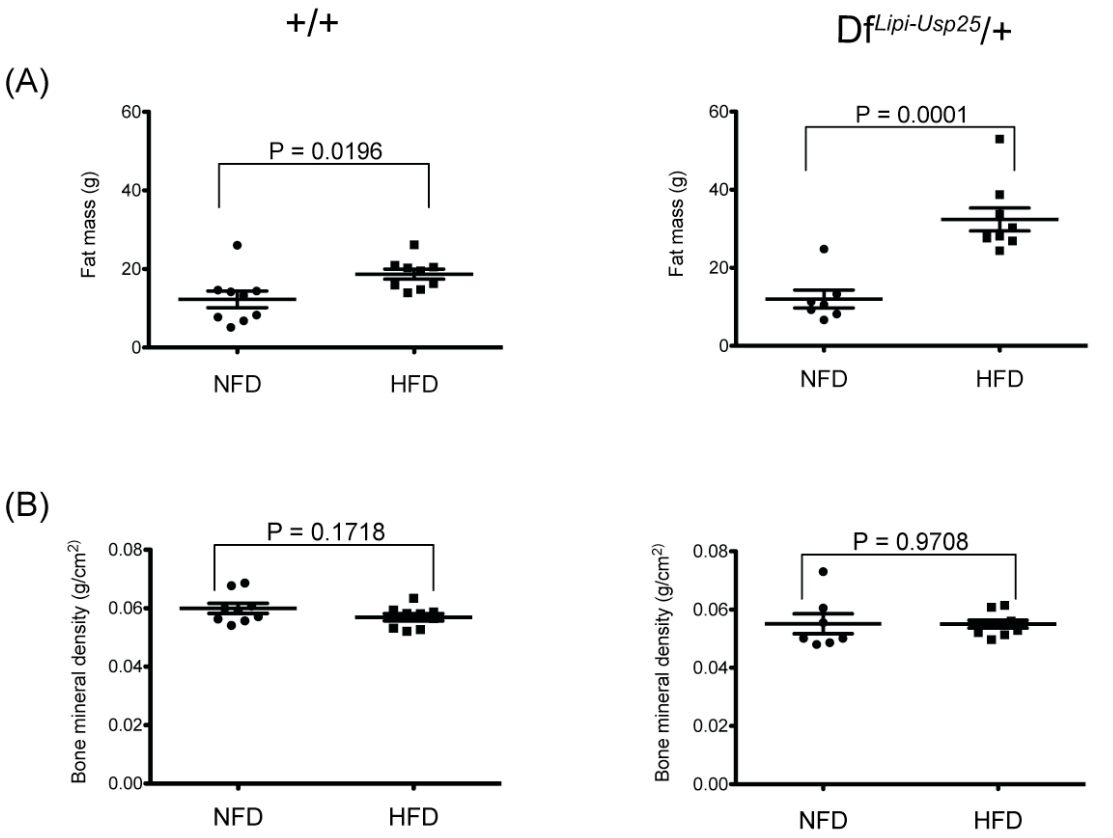

Figure 3.25. DEXA analysis of 25-week old control (+/+) and monosomic *(Df*$^{Lipi\text{-}Usp25}$*/+)* female littermates fed on a normal-fat or high-fat diet (group 4). (A) DEXA results showing fat mass in control (+/+) and monosomic (*Df*$^{Lipi\text{-}Usp25}$/+) female littermates fed on a normal-fat or high-fat diet. **(B)** DEXA results showing bone mineral density in control (+/+) and monosomic (*Df*$^{Lipi\text{-}Usp25}$/+) female littermates fed on a normal-fat or high-fat diet. Data was statistically analysed using the two-tailed Student's *t*-test. Normal-fat diet: 7 monosomic (*Df*$^{Lipi\text{-}Usp25}$/+) females were compared with 9 control (+/+) females. High-fat diet: 9 monosomic (*Df*$^{Lipi\text{-}Usp25}$/+) females were compared with 10 control (+/+) females. NFD - normal fat diet, HFD - high fat diet.

3.3.11 DIFFERENTIAL RESPONSES OF MONOSOMIC FEMALES TO INFECTION WITH *CITROBACTER RODENTIUM* LUX MIGHT HAVE BEEN CAUSED BY SUBTLE CHANGES IN THE MICROENVIRONMENT

To determine whether monosomic *Df*$^{Lipi\text{-}Usp25}$ mice show differences in the susceptibility to bacterial infections, 8 monosomic and 8 control males fed on a NFD were infected with *Salmonella* Typhimurium TET C, while 8 monosomic and 8 control females fed on a NFD were infected with *Citrobacter rodentium* lux.

No differences in the susceptibility to infection with *Salmonella* Typhimurium TET C were identified between control and monosomic mice. Specifically, no significant differences were observed in bacterial enumeration of spleens, livers and caecal contents (**Figure 3.26**), and upon histopathological analysis of spleens and livers between control and monosomic mice. Also, no significant changes were identified by enzyme-linked immunosorbent assay (ELISA) (**Figure 3.26**).

In contrast, a significant decrease in the amount of viable bacteria present in faecal samples (bacterial shedding) was observed between control and monosomic female mice infected with *Citrobacter rodentium* lux on day 13 and 17 post infection (P=0.0237 and P=0.0265 respectively) (**Figure 3.27**). No significant changes were detected in bacterial enumeration of spleens, livers, caecal patches, caecums, distal colons and ceacal contents (**Figure 3.28**), and upon histopathological analysis of spleens, livers, caecums and distal colons between control and monosomic female mice (**Figure 3.29**). The observed significant difference in the number of enumerated bacteria from faecal samples suggests the monosomic females might be resistant to the infection with *Citrobacter rodentium* lux. To confirm this finding, we infected another group of control and monosomic females (n=8 per genotype) with *Citrobacter rodentium* lux. Surprisingly, not only did we not observe any significant difference in the number of enumerated bacteria from faecal samples, but we also noticed that the amount of bacteria present in faecal samples was increased in the monosomic females compared to controls (**Figure 3.30**). After obtaining this contradicting result, we decided to carry

out the infection with *Citrobacter rodentium* lux in a third group of mice (n=8 per genotype). On this occasion, we did not observe a significant difference in the number of enumerated bacteria from faecal samples but we did notice that the amount of bacteria present in faecal samples was decreased in the monosomic females compared to the controls, concomitant with the analysis from the first group (**Figure 3.31**). Thus, in conclusion, analysis of the results from the second and third batch of monosomic females and their wildtype female littermates did not confirm the resistance of the monosomic females to the infection with *Citrobacter rodentium* lux. We can only speculate what may have been responsible for the observed differences in the responses to the infection with *Citrobacter rodentium* lux. It has been observed that even very subtle changes in the microenvironment in which mice are bred and kept, can affect the subsequent response to the bacterial infection (Simon Clare, personal communication). In our experiments, even though all three batches of mice were bred and kept in the same room prior to testing, they were bred at different time-points and kept on different racks, and thus were potentially exposed to slightly different microenvironments.

(A)

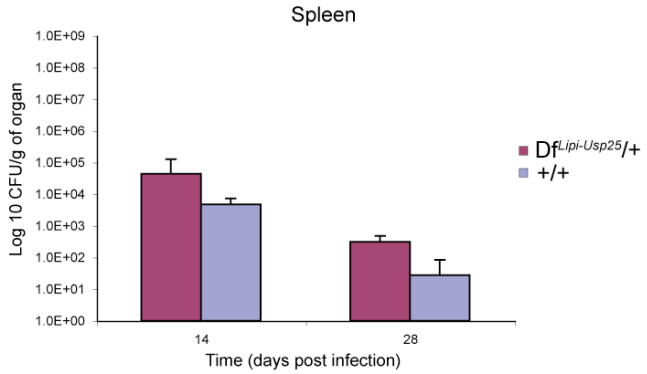

(B)

(C)

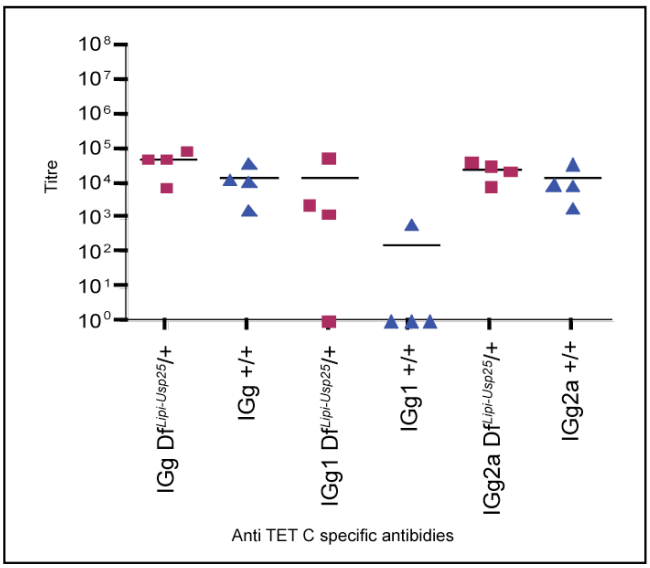

Figure 3.26. Bacterial enumeration and ELISA results for monosomic (*Df*$^{Lipi\text{-}Usp25}$/+) and control (+/+) male littermates infected with *Salmonella* Typhimurium TET C. **(A)** Bacterial counts from spleens collected from monosomic (*Df*$^{Lipi\text{-}Usp25}$/+) and control (+/+) littermates. **(B)** Bacterial counts from livers collected from monosomic (*Df*$^{Lipi\text{-}Usp25}$/+) and control (+/+) littermates. Data was statistically analysed using the two-tailed Mann-Whitney test. At each time-point 4 males per genotype were analysed. **(C)** ELISA assay results for IGg, IGg1 and IGg2a antibodies for monosomic (*Df*$^{Lipi\text{-}Usp25}$/+) and control (+/+) littermates. At each time-point 4 males per genotype were analysed.

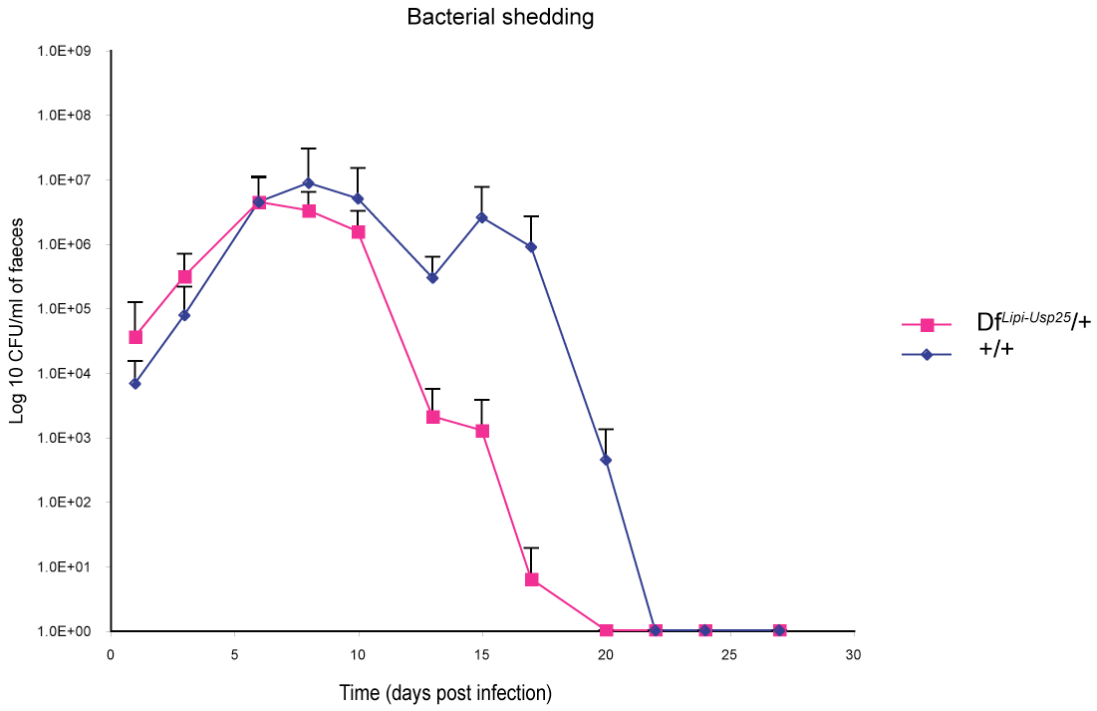

Figure 3.27. Bacterial shedding results for the first group of monosomic (*Df*$^{Lipi\text{-}Usp25}$/+) and control (+/+) female littermates infected with *Citrobacter rodentium* lux. Bacterial counts from faeces collected from monosomic (*Df*$^{Lipi\text{-}Usp25}$/+) and control (+/+) littermates. Data was statistically analysed using the two-tailed Mann-Whitney test. 8 females per genotype were analysed at collection days 0 – 13, while 4 females per genotype were analysed at collection days 14 – 28.

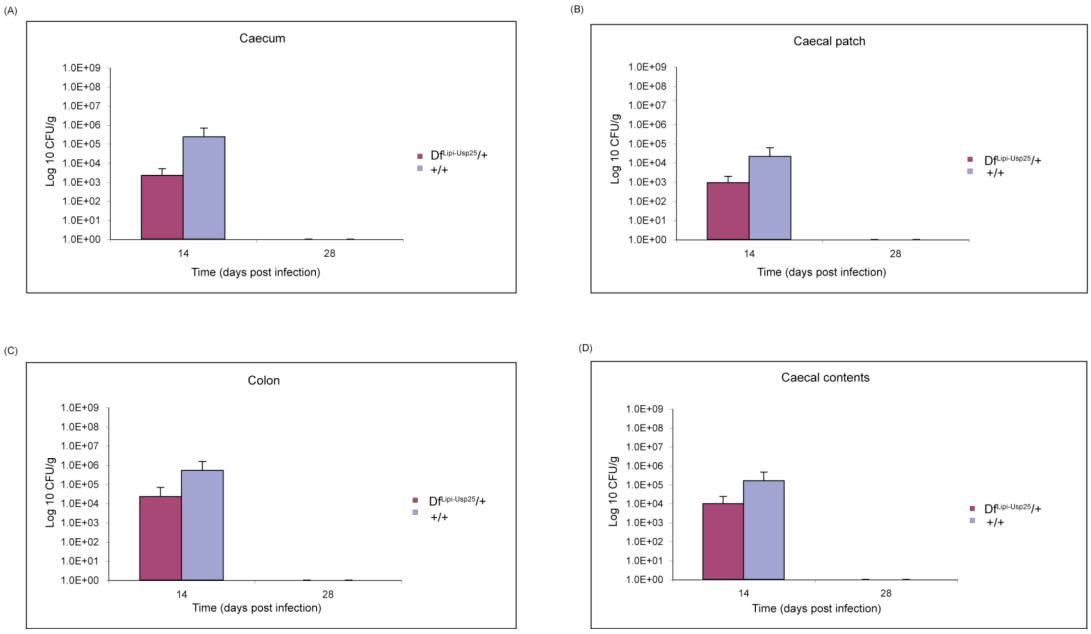

Figure 3.28. Bacterial enumeration results for monosomic (*Df*$^{Lipi\text{-}Usp25}$/+) and control (+/+) female littermates infected with *Citrobacter rodentium* lux. (A) Bacterial counts from caecums collected from monosomic (*Df*$^{Lipi\text{-}Usp25}$/+) and control (+/+) littermates. **(B)** Bacterial counts from caecal patches collected from monosomic (*Df*$^{Lipi\text{-}Usp25}$/+) and control (+/+) littermates. **(C)** Bacterial counts from colons collected from monosomic (*Df*$^{Lipi\text{-}Usp25}$/+) and control (+/+) littermates. **(D)** Bacterial counts from caecal contents collected from monosomic (*Df*$^{Lipi\text{-}Usp25}$/+) and control (+/+) littermates. Data was statistically analysed using the two-tailed Mann-Whitney test. At each time-point 4 females per genotype were analysed.

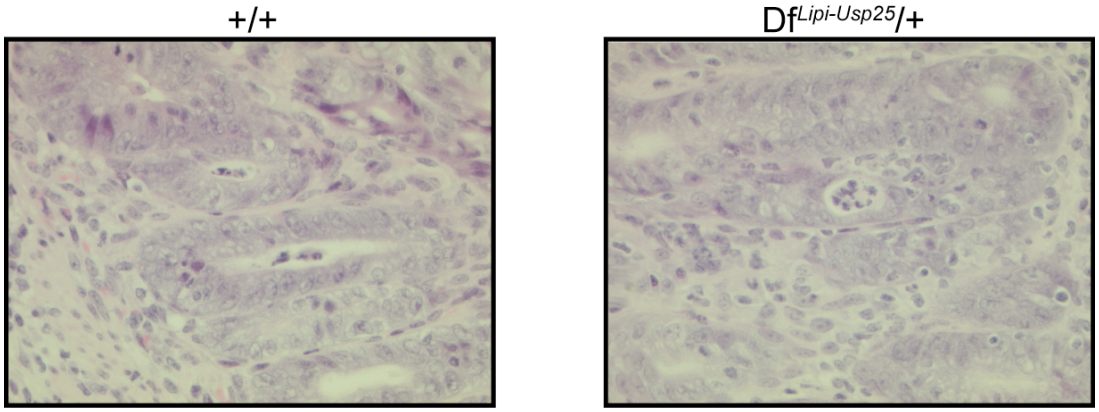

Figure 3.29. Histopathological analysis of caecums collected from control (+/+) and monosomic (*Df*$^{Lipi\text{-}Usp25}$/+) female littermates infected with *Citrobacter rodentium* lux. Haematoxylin and eosin-stained ceacum sections from control (+/+) and monosomic (*Df*$^{Lipi\text{-}Usp25}$/+) littermates. No changes were observed between ceacum sections collected from control (+/+) and monosomic (*Df*$^{Lipi\text{-}Usp25}$/+) littermates. Images are representative and taken at x400 magnification.

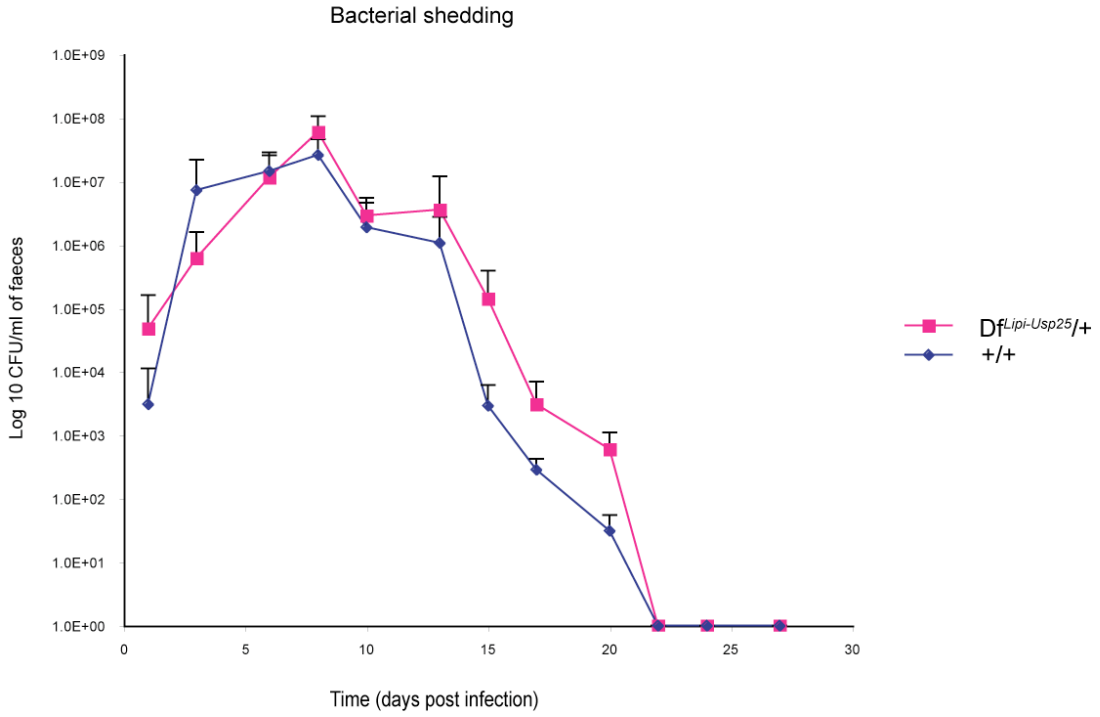

Figure 3.30. Bacterial shedding results for the second group of monosomic (*Df*$^{Lipi\text{-}Usp25}$/+) and control (+/+) female littermates infected with *Citrobacter rodentium* lux. Bacterial counts from faeces collected from monosomic (*Df*$^{Lipi\text{-}Usp25}$/+) and control (+/+) littermates. Data was statistically analysed using the two-tailed Mann-Whitney test. 8 females per genotype were analysed at collection days 0 – 13 were analysed, while 4 females per genotype were analysed at collection days 14 – 28.

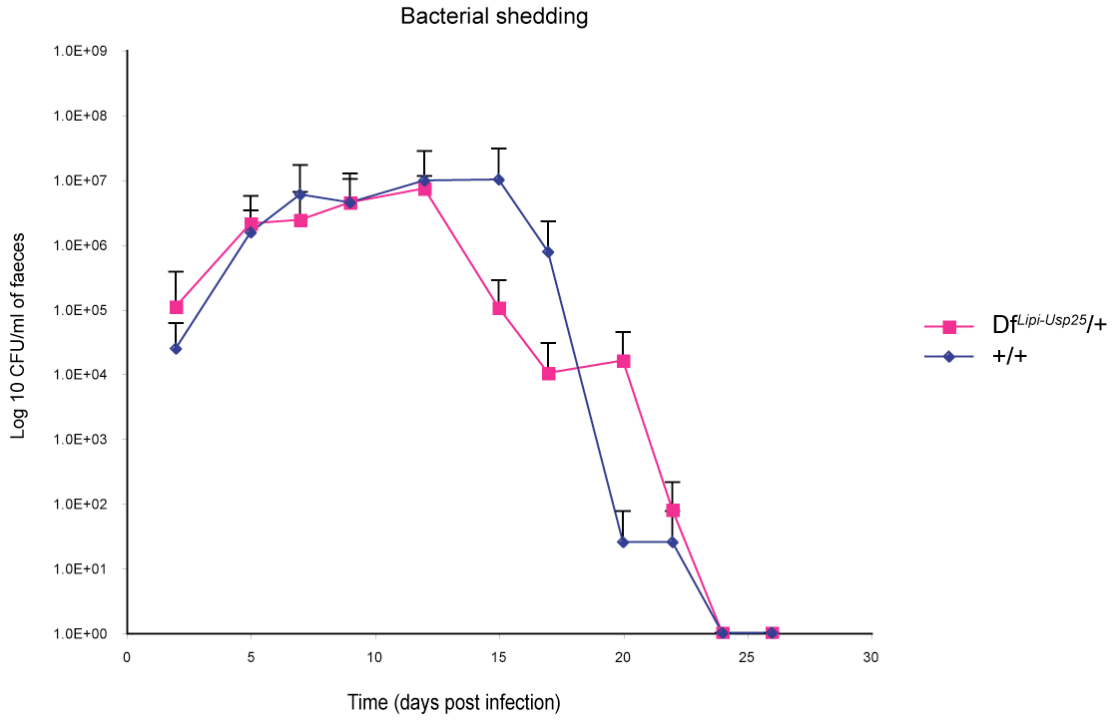

Figure 3.31. Bacterial shedding results for the third group of monosomic (*Df*$^{Lipi\text{-}Usp25}$/+) and control (+/+) female littermates infected with *Citrobacter rodentium* lux. Bacterial counts from faeces collected from monosomic (*Df*$^{Lipi\text{-}Usp25}$/+) and control (+/+) littermates. Data was statistically analysed using the two-tailed Mann-Whitney test. 8 females per genotype were analysed at collection days 0 – 13 were analysed, while 4 females per genotype were analysed at collection days 14 – 28.

3.3.12 AGEING STUDY SUGGESTS AN INCREASED PREDISPOSITION TO TUMOUR FORMATION IN MONOSOMIC MICE

In order to check whether the monosomic and/or nullisomic deletion of the *Lipi–Usp25* region in mice results in an increased predisposition to cancer, monosomic ($Df^{Lipi\text{-}Usp25}$/+) mice were crossed with Bloom's syndrome protein deficient ($Blm^{m3/m3}$) mice to generate a cohort for an ageing study. We used $Blm^{m3/m3}$ mice in our study to increase the chance of obtaining a nullisomic deletion in some cells of the monosomic mice. This is because *Blm*-deficient ES cells have a high rate of mitotic recombination (Guo 2004) and thus the generation of homozygous mutations is significantly elevated in ES cells maintained on a *Blm*-deficient background (Guo 2004). Also, *Blm*-deficient mice show increased susceptibility to cancer, as 29% of *Blm*-deficient mice develop tumours (lymphomas, carcinomas and sarcomas) by 20 months of age (Luo 2000). From all the mice obtained, we selected and further analysed only mice with the following genotypes: $Df^{Lipi\text{-}Usp25}$/+;$Blm^{m3/m3}$ (n=30), $Df^{Lipi\text{-}Usp25}$/+;$Blm^{+/+}$ (n=20), and $Df^{+/+}$;$Blm^{m3/m3}$ (n=10).

The data presented below summarizes the results obtained from this study up until the end of July 2011. At this time, 23 $Df^{Lipi\text{-}Usp25}$/+;$Blm^{m3/m3}$ (77%), 9 $Df^{Lipi\text{-}Usp25}$/+;$Blm^{+/+}$ (45%) and 10 $Blm^{m3/m3}$ (100%) mice had been culled due to illness or found dead.

The most frequent reason mice had to be culled was on humane grounds due to excessive skin ulceration. Specifically, mice from all 3 cohorts developed severe ulceration of their backs, ears, necks, penises or eyes, and were therefore culled (**Table 3.3, Figure 3.32A, 3.32B**). Histopathological analysis of the tissues from these mice showed no pathological changes except increased extramedullary haematopoiesis in the spleen (**Figure 3.32C, 3.32D**), which is a physiological reaction to bleeding from the ulcerated areas. In addition, there were also cases of mice showing severe inflammation and hyperactive bone marrow or multiple abscesses in the kidney (multiple colonies of bacteria surrounded by neutrophils). However, in some cases, when mice were culled due to signs of morbidity (pale extremities, hunched posture and piloerection) or were found dead (**Table 3.3**), histopathological

analysis either did not reveal any pathology or only showed moderate fatty changes in the liver (**Figure 3.33**), similar to that observed in the livers of healthy 1-year-old monosomic mice fed on a normal-fat diet (**Figure 3.12A**). Thus the cause of sickness/death in these mice remains unknown. Macroscopic observations and histopathological diagnosis from all these mice are detailed in **Table 3.3**.

Interestingly, in many cases histopathological analysis showed the presence of cancer (**Table 3.3**). Although mice from all 3 cohorts developed tumours, the incidence was slightly higher in $Df^{Lipi\text{-}Usp25}/+;Blm^{m3/m3}$ (11/23 mice; 48%) than in $Df^{Lipi\text{-}Usp25}/+;Blm^{+/+}$ (3/9 mice; 33%) and $Blm^{m3/m3}$ (2/10 mice; 20%) mice. Of all cancers, lymphoma was the most prevalent, being found in 7/11 $Df^{Lipi\text{-}Usp25}/+;Blm^{m3/m3}$ (63%), 1/3 $Df^{Lipi\text{-}Usp25}/+;Blm^{+/+}$ (33%) and 2/2 $Blm^{m3/m3}$ (100%) mice (**Table 3.3**). The other cancers detected in $Df^{Lipi\text{-}Usp25}/+;Blm^{m3/m3}$ and $Df^{Lipi\text{-}Usp25}/+;Blm^{+/+}$ mice included hepatocellular carcinoma (3 mice), invasive adenocarcinoma of the kidneys and pancreas (1 mouse), adenocarcinoma of the small intestine (1 mouse), undifferentiated carcinoma of the uterus (1 mouse), bone osteosarcoma (1 mouse), and squamous skin carcinoma (1 mouse) (**Table 3.3**).

In order to check for loss of the second *Lipi–Usp25* region in tumour samples collected from $Df^{Lipi\text{-}Usp25}/+;Blm^{m3/m3}$ mice, FISH analysis was performed in the tissue sections mounted on glass slides. In all analysed samples, no homozygous loss of the *Lipi–Usp25* region was detected (**Figure 3.35D, 3.35E, 3.41C, 3.42C**), which is perhaps not so surprisingly given the small sample size (n=3). Interestingly, in the $Df^{Lipi\text{-}Usp25}/+;Blm^{m3/m3}$ mouse diagnosed with invasive adenocarcinoma of the kidney and pancreas, the triplication of the chromosome carrying the deletion of the *Lipi–Usp25* region was observed in 10% of the cells located in the tumour area (kidney and pancreas) (**Figure 3.35E**). Thus, in total for this mouse, 10% of the cells located in the tumour area of the kidney and pancreas had only one wildtype chromosome and four chromosomes with the deletion of the *Lipi–Usp25* region, and so the potential influence of these cells on tumour development and/or progression cannot be ruled out.

Table 3.3. Summary of the histopathological findings observed in culled or dead mice subjected to ageing study that did not develop tumour.

Histopathological findings	Cohort
No histopathological changes	*Df*$^{Lipi\text{-}Usp25}$*/+;Blm*$^{m3/m3}$ *Df*$^{Lipi\text{-}Usp25}$*/+;Blm*$^{+/+}$ *Blm*$^{m3/m3}$
Extramedullary haematopoiesis in the spleen (**Figure 3.32C, 3.32D**)	*Df*$^{Lipi\text{-}Usp25}$*/+;Blm*$^{m3/m3}$ *Df*$^{Lipi\text{-}Usp25}$*/+;Blm*$^{+/+}$ *Blm*$^{m3/m3}$
Moderate fatty changes in the liver (**Figure 3.33**)	*Df*$^{Lipi\text{-}Usp25}$*/+;Blm*$^{m3/m3}$ *Df*$^{Lipi\text{-}Usp25}$*/+;Blm*$^{+/+}$
Inflammation, including: • severe acute inflammation of the bladder, prostate and kidneys in a pattern of a pyelonephritis • severe acute inflammation in the cornea of an eye with the squamous epithelium of the cornea being occupied by neutrophils (**Figure 3.34A**) • severe acute and chronic inflammation in the surface of the heart (**Figure 3.34B**)	*Df*$^{Lipi\text{-}Usp25}$*/+;Blm*$^{m3/m3}$
Multiple abscesses in the kidney; multiple colonies of bacteria surrounded by neutrophils in the kidney	*+/+;Blm*$^{m3/m3}$
Lymphoma, including: • low grade lymphoma in the liver (big foci) (**Figure 3.35A, 3.35B**), and in the spleen and lungs (small foci) • low grade lymphoma in the liver, spleen and lung (**Figure 3.36A, 3.36B**); lymph node with low grade lymphoma in the pancreas • low grade lymphoma in the lungs (big foci), and in the liver, pancreas and salivary glands (small foci) • low grade lymphoma in the liver • low grade lymphoma in the liver and intestine • low grade lymphoma in the kidneys (big foci) (**Figure 3.37A, 3.37B**) and in the pancreas, liver and salivary glands (small foci) • high grade lymphoma in the mesentery of the intestine (**Figure 3.38A**); lymphoma spread into the spleen • high grade lymphoma in the spleen, liver, kidney and abdominal fat • high grade lymphoma in the spleen, thymus, fat, surface of the heart and lungs (**Figure 3.39A, 3.39B**); abdominal lymph node with high grade lymphoma • high grade lymphoma in the liver and kidney (small foci); abdominal lymph node with high grade lymphoma (**Figure 3.40A, 3.40B)**	*Df*$^{Lipi\text{-}Usp25}$*/+;Blm*$^{m3/m3}$ *Df*$^{Lipi\text{-}Usp25}$*/+;Blm*$^{+/+}$ *Blm*$^{m3/m3}$

Table 3.3 continued. Summary of the histopathological findings observed in culled or dead mice subjected to ageing study that developed tumour.

Histopathological findings	Cohort
Adenocarcinoma, including: • invasive adenocarcinoma of the kidneys (**Figure 3.41A, 3.41B**) and pancreas (**Figure 3.41C**) • adenocarcinoma with a moderate level of dysplasia of the small intestine (**Figure 3.42A, 3.42B**)	*Df*$^{Lipi\text{-}Usp25}$*/+;Blm*$^{m3/m3}$
Hepatocellular carcinoma (Figure 3.38B; Figure 3.43A, 3.43B; Figure 3.44A, 3.44B)	*Df*$^{Lipi\text{-}Usp25}$*/+;Blm*$^{m3/m3}$
Invasive malignant undifferentiated carcinoma of the uterus invading into the uterus wall (Figure 3.45A) and fat (Figure 3.45B)	*Df*$^{Lipi\text{-}Usp25}$*/+;Blm*$^{m3/m3}$
Bone osteosarcoma in the tibia and femur (Figure 3.46B), metastatic osteosarcoma in the spleen, kidney, small intestine and liver (Figure 3.46C)	*Df*$^{Lipi\text{-}Usp25}$*/+;Blm*$^{+/+}$
Squamous skin carcinoma invading into the fat (Figure 3.47A, 3.47B)	*Df*$^{Lipi\text{-}Usp25}$*/+;Blm*$^{+/+}$

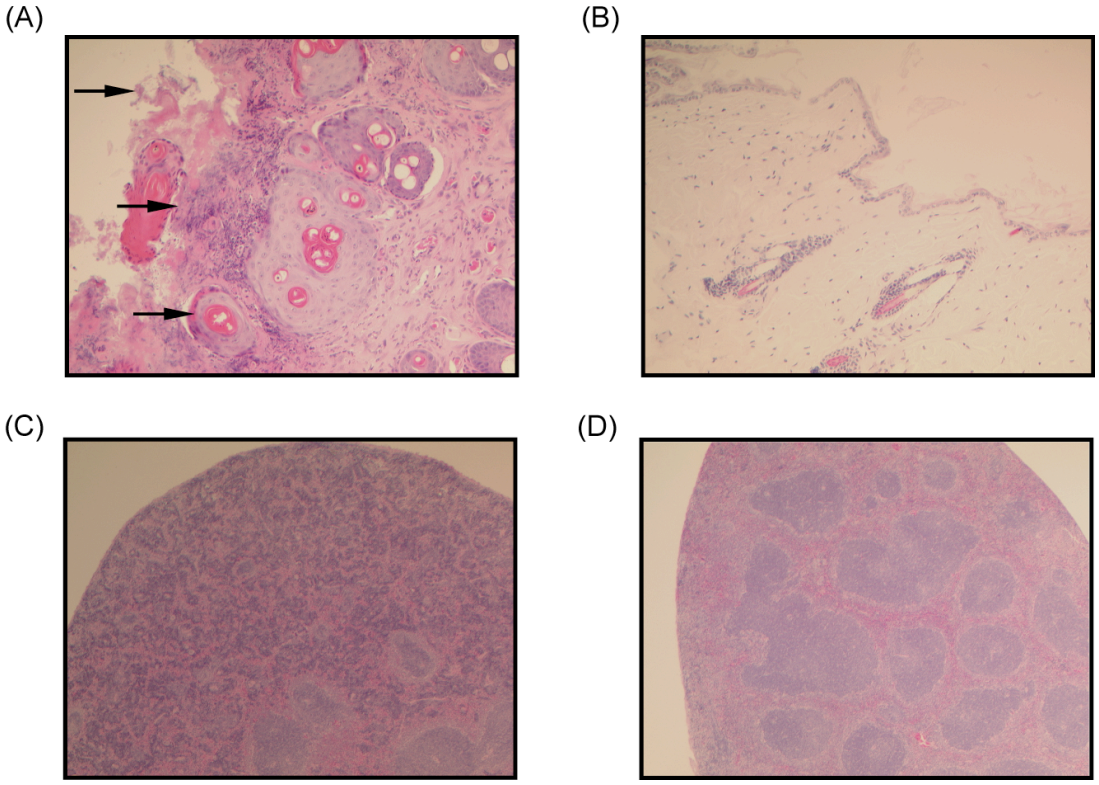

Figure 3.32. Histopathological analysis of haematoxylin and eosin-stained skin sections collected from *Df*$^{Lipi\text{-}Usp25}$/+;*Blm*$^{m3/m3}$, *Df*$^{Lipi\text{-}Usp25}$/+;*Blm*$^{+/+}$ and +/+;*Blm*$^{m3/m3}$ mice that were culled due to severe ulceration. **(A)** Skin ulcer section collected from the *Df*$^{Lipi\text{-}Usp25}$/+;*Blm*$^{m3/m3}$ mouse. The discontinuity of the skin, loss of outer skin layers and inflammation of the tissue can be observed (indicated by arrows). Image is representative and taken at x100 magnification. **(B)** Normal appearance of the skin section collected from the same *Df*$^{Lipi\text{-}Usp25}$/+;*Blm*$^{m3/m3}$ mouse. Sample was collected from a place adjacent to the ulcer. Images are representative and taken at x100 magnification. **(C)** Spleen collected from the *Df*$^{Lipi\text{-}Usp25}$/+;*Blm*$^{m3/m3}$ mouse. Increased extramedullary haematopoiesis can be observed (visible as dark puple staining). Image is representative and taken at x25 magnification. **(D)** Normal appearance of the spleen section collected from a different *Df*$^{Lipi\text{-}Usp25}$/+;*Blm*$^{m3/m3}$ mouse that did not have any skin ulceration. Image is representative and taken at x25 magnification.

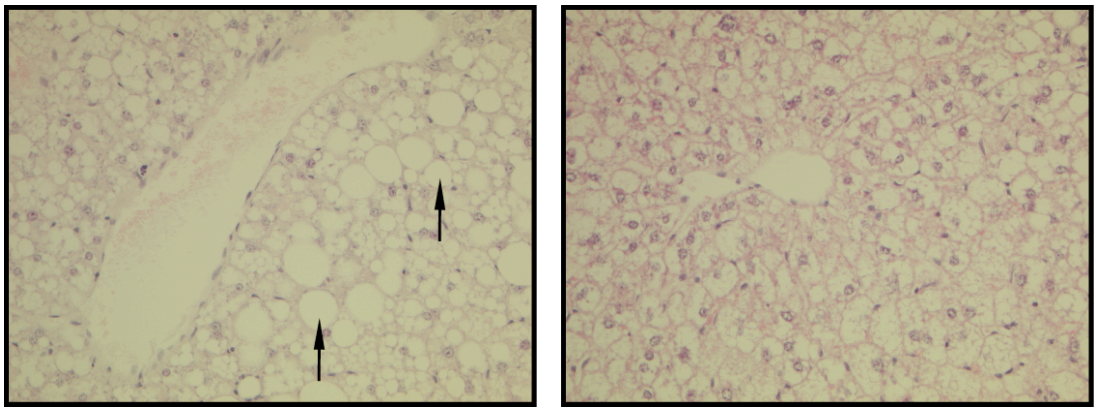

Figure 3.33. Histopathological analysis of haematoxylin and eosin-stained livers collected from *Df*$^{Lipi\text{-}Usp25}$/+;*Blm*$^{m3/m3}$ and *Df*$^{Lipi\text{-}Usp25}$/+;*Blm*$^{+/+}$ mice that were found dead or culled as they looked pale or had hunched piloerection. Livers of some *Df*$^{Lipi\text{-}Usp25}$/+;*Blm*$^{m3/m3}$ and *Df*$^{Lipi\text{-}Usp25}$/+;*Blm*$^{+/+}$ mice showed moderate fatty changes (left side; visible as white oval cells; indicated by arrows) compared to no fatty changes in livers of other *Df*$^{Lipi\text{-}Usp25}$/+;*Blm*$^{m3/m3}$ and *Df*$^{Lipi\text{-}Usp25}$/+;*Blm*$^{+/+}$ mice (right side). Images are representative and taken at x200 magnification.

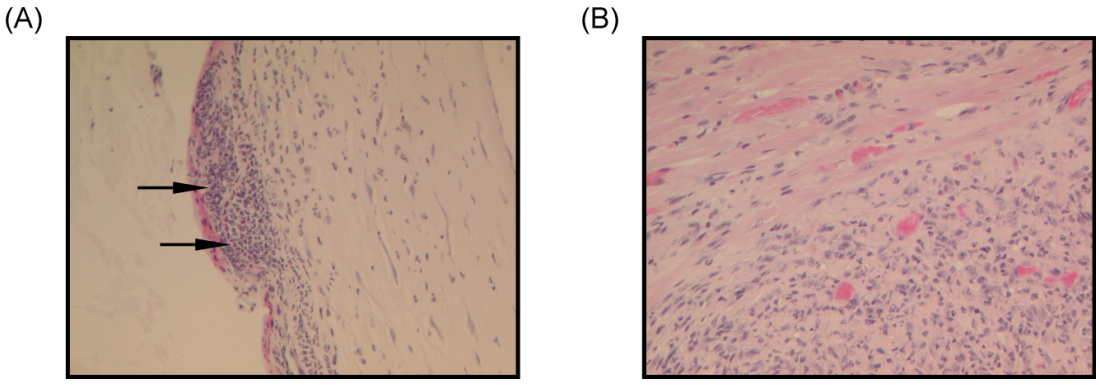

Figure 3.34. Histopathological analysis of haematoxylin and eosin-stained bladder and bone collected from *Df*$^{Lipi\text{-}Usp25}$/+;*Blm*$^{m3/m3}$ mice that were culled sick. (A) Eye section showing the signs of severe acute inflammation in the cornea (indicated by arrows). **(B)** Heart section showing the signs of severe acute and chronic inflammation on its surface. Images are representative and taken at x200 magnification.

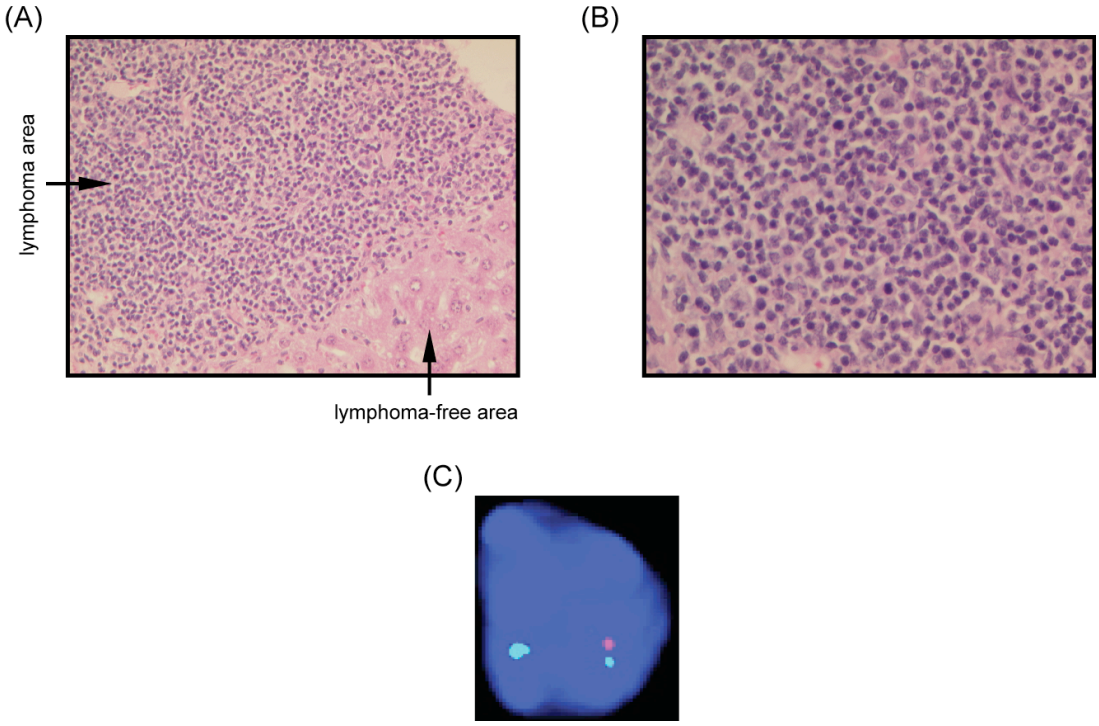

Figure 3.35. Analysis of liver collected from *Df*$^{Lipi\text{-}Usp25}$/+;*Blm*$^{m3/m3}$ mouse. **(A)** Histopathological analysis of haematoxylin and eosin stained liver section showing high grade lymphoma. Arrows show tumour and tumour-free area of liver. Image is representative and taken at x200 magnification. **(B)** Histopathological analysis of haematoxylin and eosin stained section showing lymphoma infiltration into liver. Image is representative and taken at x400 magnification. **(C)** FISH analysis with BAC probes that mapped in the region of the deletion (red) and outside (green) conducted on the tumour area of kidney section. 100% of the cells showed two green and one red signal (normal monosomic cells).

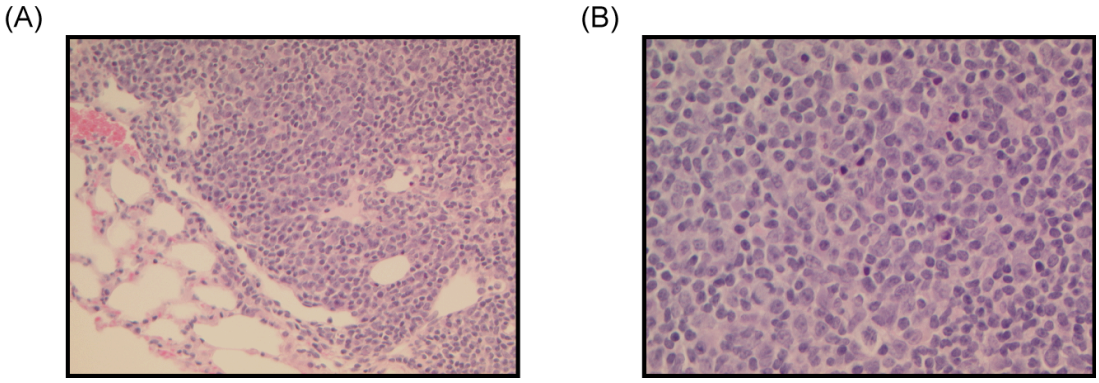

Figure 3.36. Analysis of lungs collected from *Df*$^{Lipi\text{-}Usp25}$/+;*Blm*$^{m3/m3}$ mouse. **(A)** Histopathological analysis of haematoxylin and eosin stained lung section showing low grade lymphoma. Image is representative and taken at x200 magnification. **(B)** Histopathological analysis of haematoxylin and eosin stained lung section showing low grade lymphoma. Image is representative and taken at x400 magnification.

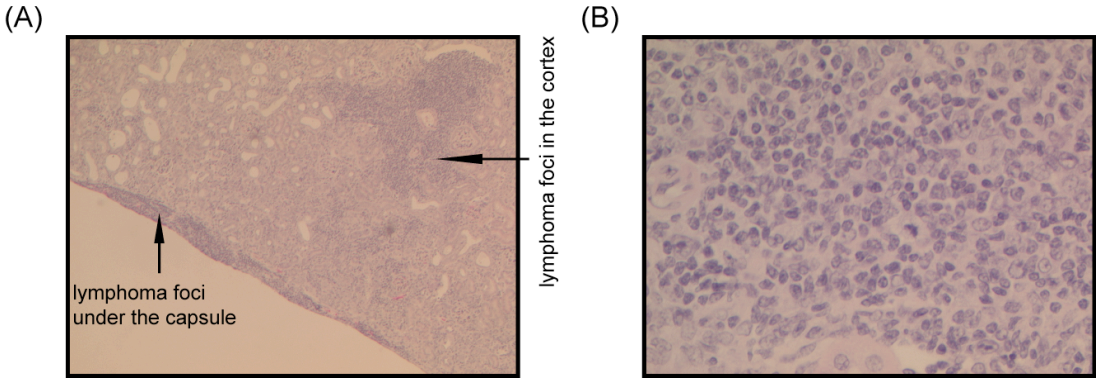

Figure 3.37. Analysis of kidney collected from *Df*$^{Lipi\text{-}Usp25}$/+;*Blm*$^{+/+}$ mouse. (A) Histopathological analysis of haematoxylin and eosin stained kidney section showing high grade lymphoma changes under the capsule and in the cortex. Image is representative and taken at x50 magnification. **(B)** Histopathological analysis of haematoxylin and eosin stained section showing high grade lymphoma in the kidney. Image is representative and taken at x400 magnification.

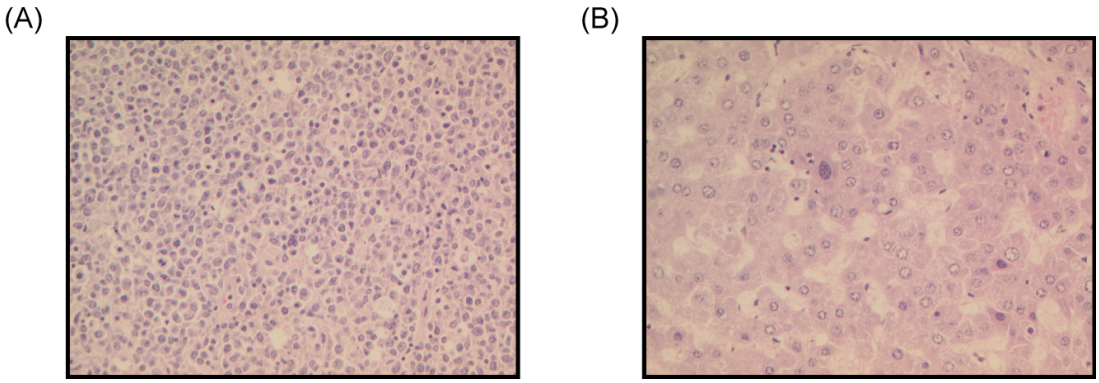

Figure 3.38. Analysis of abdominal lymph node and liver collected from *Df*$^{Lipi\text{-}Usp25}$/+;*Blm*$^{m3/m3}$ mouse. (A) Histopathological analysis of haematoxylin and eosin stained abdominal lymph node section showing high grade lymphoma. Image is representative and taken at x200 magnification. **(B)** Histopathological analysis of haematoxylin and eosin stained section showing hepatocellular carcinoma. Image is representative and taken at x200 magnification.

(A) (B)

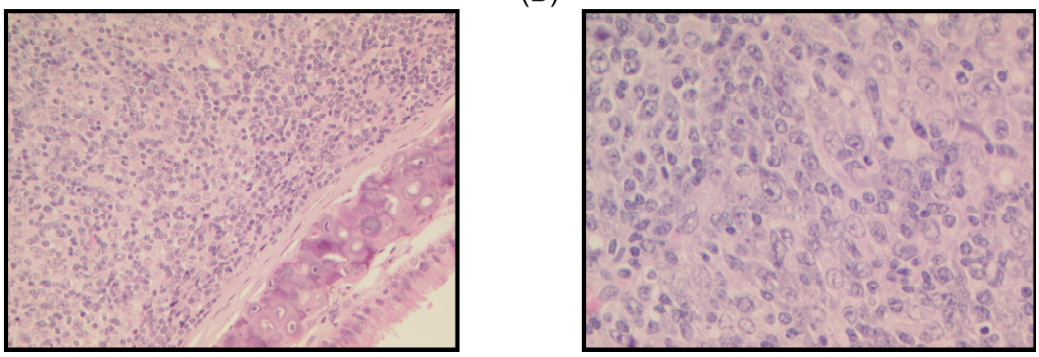

Figure 3.39. Analysis of lungs collected from +/+;*Blm*$^{m3/m3}$ mouse. (A) Histopathological analysis of haematoxylin and eosin stained lung section showing high grade lymphoma in the lung. Image is representative and taken at x200 magnification. **(B)** Histopathological analysis of haematoxylin and eosin stained lung section showing high grade lymphoma in the lung. Image is representative and taken at x400 magnification.

(A) (B)

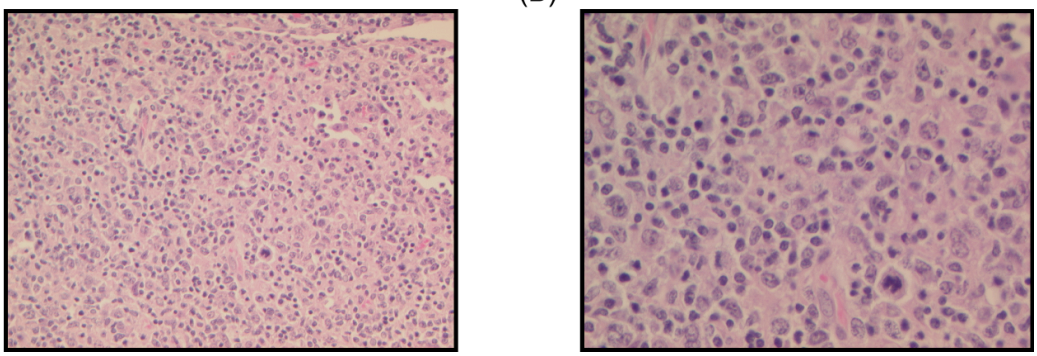

Figure 3.40. Analysis of abdominal lymph node collected from +/+;*Blm*$^{m3/m3}$ mouse. (A) Histopathological analysis of haematoxylin and eosin stained abdominal lymph node section showing high grade lymphoma. Image is representative and taken at x200 magnification. **(B)** Histopathological analysis of haematoxylin and eosin stained abdominal lymph node section showing high grade lymphoma. Image is representative and taken at x400 magnification.

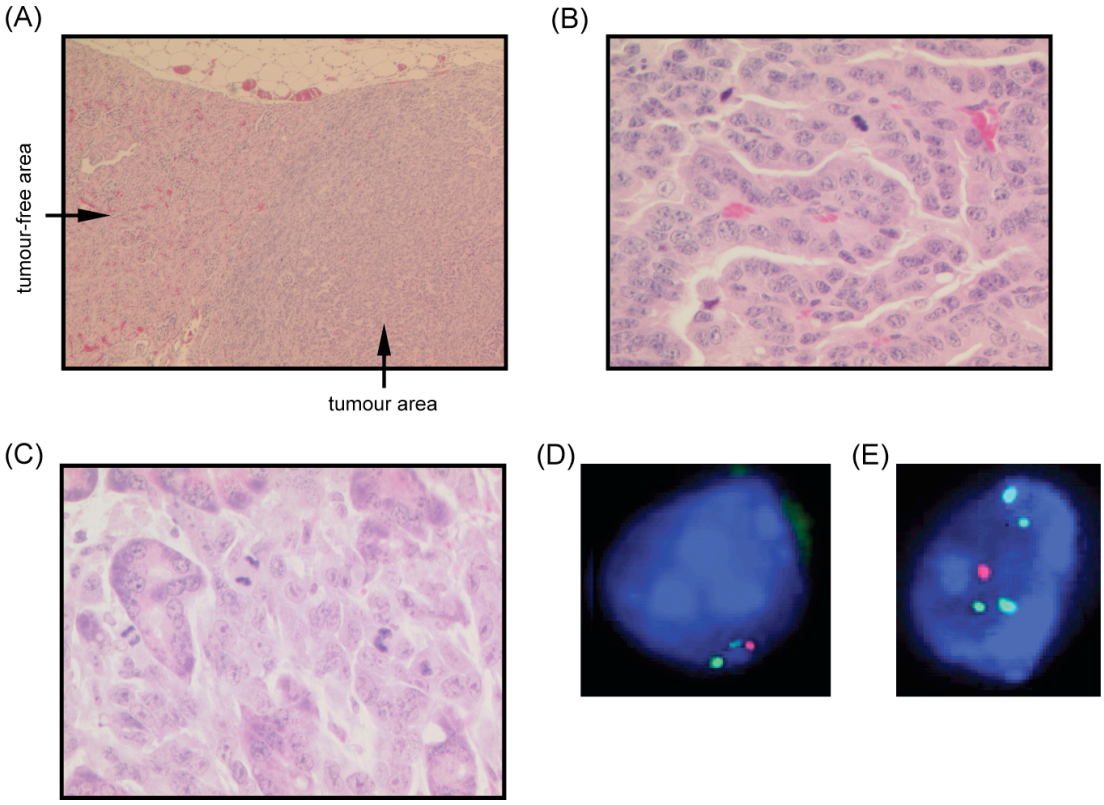

Figure 3.41. Analysis of kidneys and pancreas collected from *Df*$^{Lipi\text{-}Usp25}$/+;*Blm*$^{m3/m3}$ mouse. (A) Histopathological analysis of haematoxylin and eosin stained kidney section showing invasive adenocarcinoma. Arrows show tumour and tumour-free area of kidney. Image is representative and taken at x50 magnification. **(B)** Histopathological analysis of haematoxylin and eosin stained kidney section showing invasive adenocarcinoma changes. Image is representative and taken at x400 magnification. **(C)** Histopathological analysis of haematoxylin and eosin stained pancreas section showing invasive adenocarcinoma changes. Image is representative and taken at x400 magnification. **(D), (E)** FISH analysis with BAC probes that mapped in the region of the deletion (red) and outside (green) conducted on the tumour area of a kidney section. 90% of the cells showed two green and one red signal (normal monosomic cells) **(D)**. Interestingly, 10% of the cells showed four green and one red signal (abnormal cells) **(E)**, thus showing the existence of two additional monosomic chromosomes in the cell.

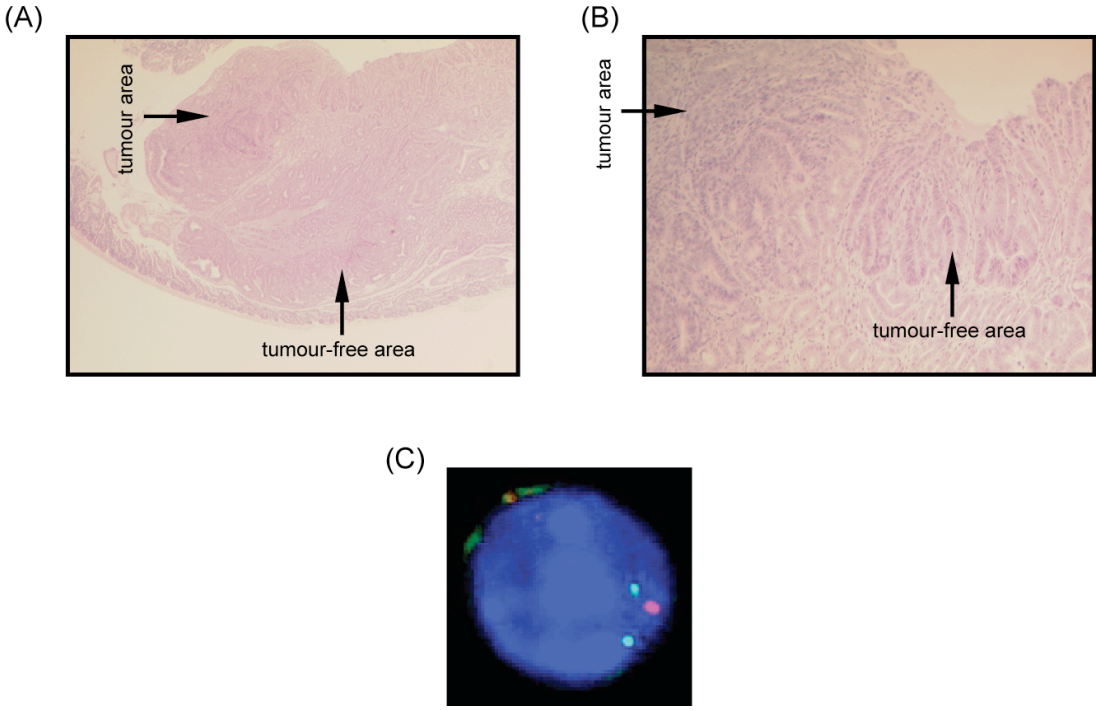

Figure 3.42. Analysis of small intestine collected from *Df*$^{Lipi\text{-}Usp25}$/+;*Blm*$^{m3/m3}$ mouse. **(A)** Histopathological analysis of haematoxylin and eosin stained small intestine section showing adenocarcinoma. Arrows show tumour and tumour-free area of small intestine. Image is representative and taken at x25 magnification. **(B)** Histopathological analysis of haematoxylin and eosin stained small intestine section showing adenocarcinoma changes. Image is representative and taken at x100 magnification. **(C)** FISH analysis with BAC probes that mapped in the region of the deletion (red) and outside (green) conducted on the tumour area of kidney section. 100% of the cells showed two green and one red signal (normal monosomic cells).

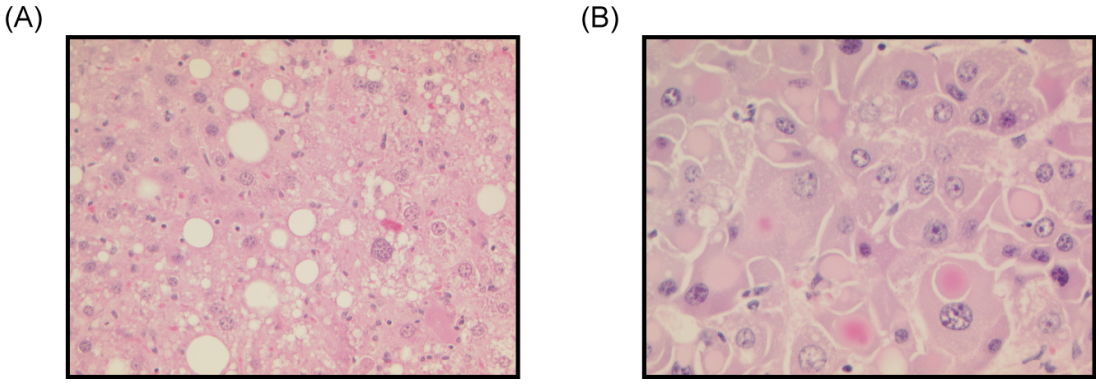

Figure 3.43. Analysis of liver collected from *Df*$^{Lipi\text{-}Usp25}$/+;*Blm*$^{m3/m3}$ mouse. **(A)** Histopathological analysis of haematoxylin and eosin stained liver section showing hepatocellular carcinoma. Image is representative and taken at x200 magnification. **(B)** Histopathological analysis of haematoxylin and eosin stained liver section showing hepatocellular carcinoma. Image is representative and taken at x400 magnification.

(A) (B)

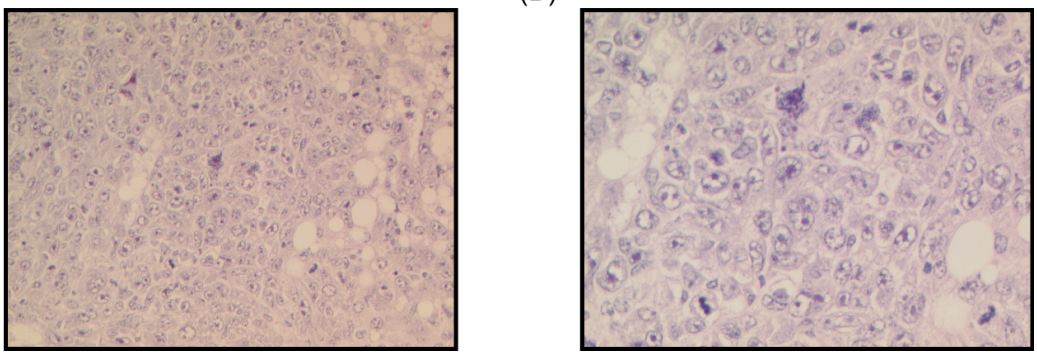

Figure 3.44. Analysis of liver collected from *Df*$^{Lipi\text{-}Usp25}$/+;*Blm*$^{m3/m3}$ mouse. **(A)** Histopathological analysis of haematoxylin and eosin stained liver section showing poorly differentiated hepatocellular carcinoma invading into the fat. Image is representative and taken at x200 magnification. **(B)** Histopathological analysis of haematoxylin and eosin stained liver section showing poorly differentiated hepatocellular carcinoma invading into the fat. Image is representative and taken at x400 magnification.

(A) (B)

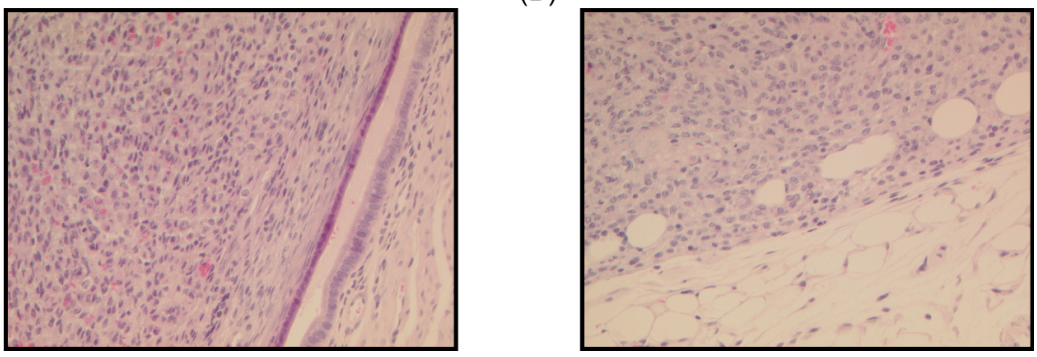

Figure 3.45. Analysis of uterus collected from *Df*$^{Lipi\text{-}Usp25}$/+;*Blm*$^{m3/m3}$ mouse. **(A)** Histopathological analysis of haematoxylin and eosin stained uterus section showing undifferentiated carcinoma invading into the uterus wall. Image is representative and taken at x200 magnification. **(B)** Histopathological analysis of haematoxylin and eosin stained uterus section showing undifferentiated carcinoma invading into the fat. Image is representative and taken at x200 magnification.

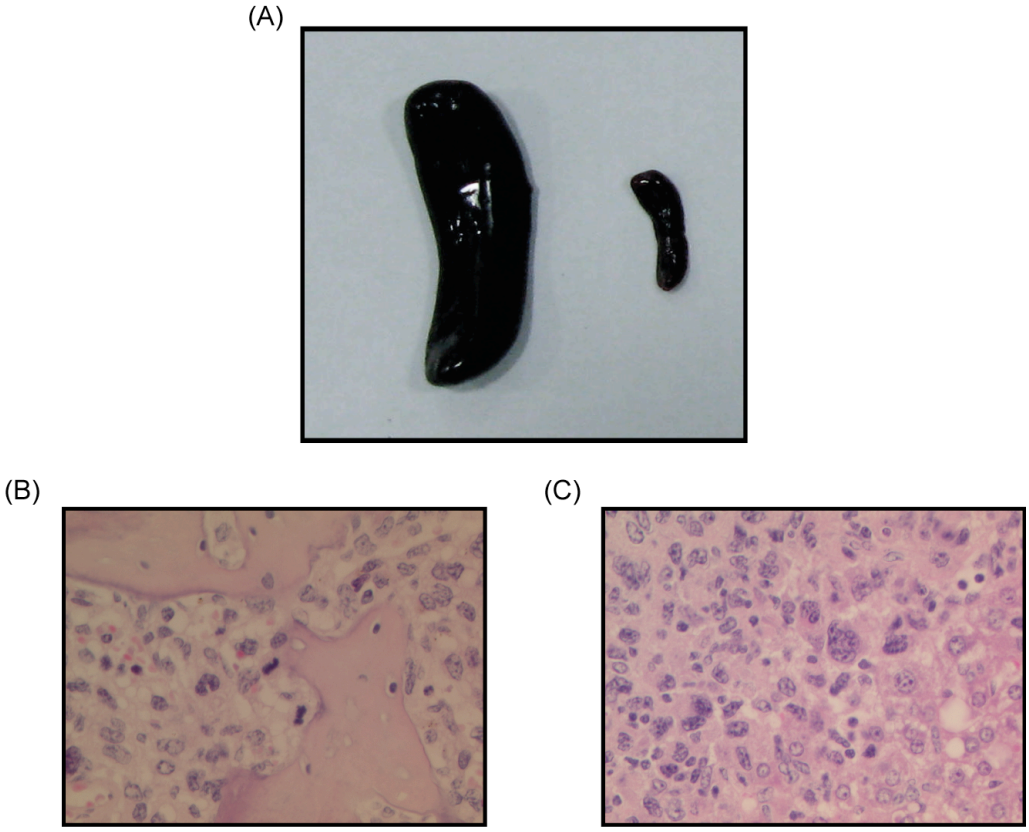

Figure 3.46. Analysis of spleen, bone and liver collected from *Df*$^{Lipi\text{-}Usp25}$/+;*Blm*$^{+/+}$mouse. **(A)** Photo showing greatly enlarged spleen collected from this mouse (left side) compared to a normal spleen (right side) collected from a healthy mouse. **(B)** Histopathological analysis of haematoxylin and eosin stained bone section showing osteosarcoma. Image is representative and taken at x400 magnification. **(C)** Histopathological analysis of haematoxylin and eosin stained liver section showing metastatic osteosarcoma. Image is representative and taken at x400 magnification.

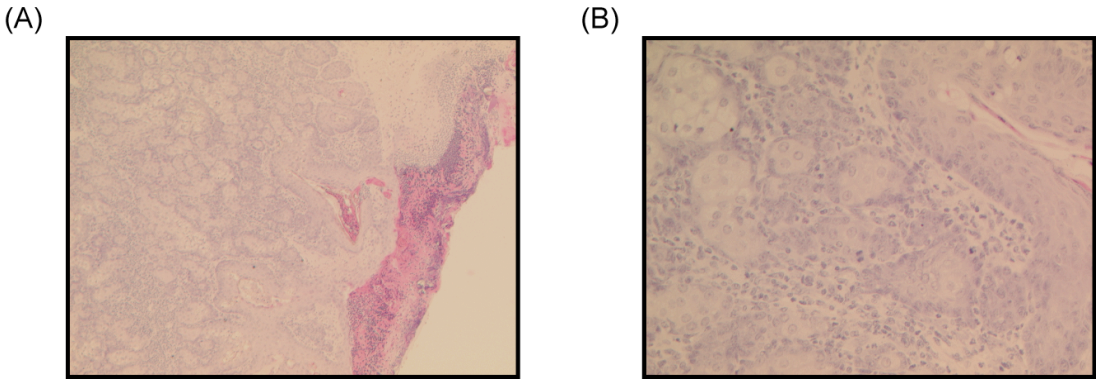

Figure 3.47. Analysis of skin section collected from *Df*$^{Lipi\text{-}Usp25}$/+;*Blm*$^{+/+}$ mouse. **(A)** Histopathological analysis of haematoxylin and eosin stained skin section showing squamous skin carcinoma invading into fat. Image is representative and taken at x50 magnification. **(B)** Histopathological analysis of haematoxylin and eosin stained skin section showing squamous skin carcinoma changes. Image is representative and taken at x400 magnification.

3.4 DISCUSSION

We generated and phenotypically characterized the *Df*$^{Lipi\text{-}Usp25}$ mouse, a monosomic model for the 1.6 Mb *Lipi–Usp25* region. The deleted region is syntenic to the centromeric part of the human chromosome 21, and contains six genes that are conserved between human and mouse.

Homozygous deletion of the region (nullisomy) resulted in mid-gestational embryonic lethality mostly due to neural tube degeneration with evidence of prominent apoptosis, suggesting that at least one of the genes in the *Lipi–Usp25* region is required for the development and maintenance of the neural tube. However, as all six genes in this region are normally expressed in the developing brain of the mouse embryo at both E9.5 and E10.5 (Reymond 2002), and have not been reported to be involved in apoptosis and/or neural tube development, it is difficult to speculate which genes might be responsible. However, two genes, namely *Samsn1* and *Nrip1*, are unlikely to be potential candidates for the observed embryonic lethality, as homozygous null *Samsn1* and *Nrip1* mice are viable (White 2000; Wang 2010).

Detailed phenotypical analysis of monosomic *Df*$^{Lipi\text{-}Usp25}$ mice found them to be viable, fertile and displaying no obvious differences from controls (wildtype littermates) in terms of morphology, motor skills, haematology and clinical chemistry. They did, however, show deficits in long-term memory retention in a socially relevant testing paradigm. Social recognition is hippocampus-dependent (Kogan 2000) and has been used for learning and memory testing (Richter 2005; Engelmann 2011) and for assessing cognitive impairment in mice (Mitsui 2009). The ability of retaining long-term memory is crucial for any learning process and any abnormalities in memory retention can affect learning capacity. Indeed, the observed deficit in long-term memory retention in monosomic *Df*$^{Lipi\text{-}Usp25}$ mice had a significant impact on their learning abilities, as monosomic mice were incapable of distinguishing a familiar stimulus animal from an unfamiliar one 24 hours after the initial training was conducted. As intellectual disability and learning difficulties are identified in all Monosomy 21 patients carrying “centromeric” deletions (Wakui

2002; Tinkel-Vernon 2003, Lyle 2008; Roberson 2010; Lindstrand 2010), it is tempting to speculate that the deficit in long-term memory retention might be at least in part responsible for a decline in learning abilities in Monosomy 21 individuals and thus that haploinsufficiency of a gene (or genes) mapped within the *Lipi–Usp25* deletion may contribute to the intellectual disability/learning impairment of humans with Monosomy 21. However, as all six genes in this region are normally expressed in the developing brain of the mouse embryo (Reymond 2002), and as four of these genes (*Hspa13*, *Samsn1*, *Nrip1* and *Usp25*) are normally expressed in the adult mouse brain, it is hard to speculate which genes might be responsible for observed impairment in learning and long-term memory retention. To date, only the mouse models for the *Samsn1* and *Nrip1* genes have been generated (White 2000; Wang 2010). However, the cognitive abilities of the homozygous and heterozygous *Samsn1* and *Nrip1* mice were not analysed and so these genes cannot be excluded from a list of potential candidates for learning and long-term memory impairment.

Although these monosomic mice did not model the other clinical phenotypes commonly seen in Monosomy 21 patients, given that all currently known Monosomy 21 patients with the “centromeric” deletions span much larger regions of HSA21 than represented in our monosomic mice, we cannot rule out the possibility that genes in the *Lipi–Usp25* region work in synergy with other genes mapped to the “centromeric” region of HSA21, and that only loss of all of these genes together would give the clinical phenotypes observed. In addition, there are 2 genes in the 21q11.2–q21.1 region of HSA21 for which there are no mouse orthologs, namely *ABCC13* and *AF165138.7*. Thus our model does not account for the possible roles that these genes may play in the phenotype.

Monosomic $Df^{Lipi\text{-}Usp25}$ mice fed on a HFD showed a significantly increased fat percentage estimate at 8-, 14-, and 25-weeks of age compared to the controls. However, significant increases in fat percentage estimates over controls were not observed when the monosomic mice were fed a NFD, except at 8-weeks of age. Considering the fact that the overall fat percentage estimate was much higher in both groups of mice on a HFD (containing

21% crude fat) compared to a NFD (containing 9% crude fat), the HFD can be regarded as an environmental factor that increases fat percentage estimates in the mice. Nevertheless, given that monosomic mice showed significantly higher percentage fat estimates than controls, it is clear there is also a genetic factor affecting this phenotypic change. Although the interaction between genetic susceptibility loci and environmental factors in the development of obesity have been shown in different analyses performed both in humans and mice (Poehlman 1986; Bouchard 1990; Heitmann 1995; Asnicar 2001; Luan 2001; Nieters 2002; Sato 2010), to our knowledge this interaction has not been shown before in patients with deletions encompassing the 21q11.2–q21.1 region.

Although four studies have reported on the presence or absence of obesity in Monosomy 21 patients with deletions encompassing the 21q11.2–q21.1 region (Roland 1990; Korenberg 1991; Ahlbom 1996; Tinkel-Vernon 2003), only a study by Roland *et al* found a positive correlation (two cases that showed mild intellectual disability, some facial abnormalities and obesity (Roland 1990)). Unfortunately, without knowledge of the type of a diet of these individuals, we can only speculate as to whether the observed obesity in these patients was caused by the interaction between the genetic component (deletion of the 21q11.2–q21.3 region) and the environmental factor (consumption of food highly-enriched in fat). Thus studies of other obese patients with deletions of/or encompassing the 21q11.2–q21.1 region are required to identify a possible interaction between deletions of this region and a high-fat diet, and to understand a possible link of both genetic and environmental factors with increased fat deposition.

There are six genes in the *Lipi–Usp25* region: *Lipi*, *Rbm11*, *Hspa13*, *Samsn1*, *Nrip1* and *Usp25*. To date, the mouse models for *Samsn1* and *Nrip1* genes have been generated and neither of them showed signs of obesity (White 2000; Wang 2010). Homozygous *Samsn1*-knockout (*Samsn1*$^{-/-}$) mice are viable, fertile and display enhanced adaptive immunity compared to their wildtype littermates (Wang 2010). However, no phenotypic data is available for *Samsn1+/-* mice (Wang 2010). Homozygous *Nrip1*-knockout (*Nrip1*$^{-/-}$) mice are viable but 15–20% smaller than their heterozygous and wildtype

littermates (White 2000). Moreover, *Nrip1*$^{-/-}$ females are infertile due to ovulatory dysfunction, while heterozygous *Nrip1*-knockout (*Nrip1*$^{+/-}$) females are partially infertile (White 2000). In addition, Nrip1 can affect the function of adipose tissue by blocking both mitochondrial respiration and energy uncoupling, as well as preventing expression of key regulatory genes in white adipose tissue (WAT), including the uncoupling protein 1 (*Ucp1*) gene. *Nrip1*$^{-/-}$ mice fed a NFD showed a 20% reduction in body weight compared with wildtype controls, and remained leaner than controls even when fed a HFD (Leonardsson 2004). On average, the body weight of *Nrip1*$^{-/-}$ mice increased by 3.8%, while the body weight of their wildtype littermates increased by 14.5%. The histopathological analysis of WAT showed that adipose cells were much smaller in *Nrip1*$^{-/-}$ mice fed on either diet compared to their wildtype littermates. Histopathological analysis of livers from *Nrip1*$^{-/-}$ mice showed they were resistant to both age-induced hepatic steosis and HFD-induced fatty changes in the liver. The resistance to HFD-induced obesity and hepatic steosis in *Nrip1*$^{-/-}$ mice might be explained by both the increased expression of genes in energy expenditure and mitochondrial uncoupling, and the decreased expression of some genes encoding lipogenic enzymes (Leonardsson 2004). However, it is not known whether the heterozygous deletion of *Nrip1* would provide resistance to HFD-induced obesity and hepatic steatosis, as only *Nrip1-/-* mice were evaluated for their resistance to HFD-induced obesity and hepatic steatosis (Leonardsson 2004). As none of the other genes in the *Lipi–Usp25* region are known to be involved in lipid and carbohydrate metabolism or maintenance of energy homeostasis, it is difficult to hypothesize which missing genes cause the development of HFD-induced increase in fat deposition and fatty changes in the livers of our monosomic mice.

To investigate potential molecular mechanisms leading to the HFD-induced increase in fat deposition in the monosomic mice, we performed microarray expression analysis and found significant differential gene expression in adipocytes between control and monosomic *Df*$^{Lipi\text{-}Usp25}$ mice. qRT-PCR analysis on a subset of these genes found six of them to show significantly altered expression in the monosomic mice relative to controls: transmembrane protein 45a (*Tmem45a*) was upregulated in the monosomic

mice whilst plexin D1 (*Plxnd1*), low density lipoprotein receptor-related protein associated protein 1 (*Lrpap1*), SAM domain, SH3 domain and nuclear localization signals, 1 (*Samsn1*) and lamin A (*Lmna*) were down-regulated.

Of these six genes, knockout mice have been generated for each of the four down-regulated genes (Willnow 1995; Sullivan 1999; Umans 1999; Gitler 2004; Yang 2005; Fong 2006; Davies 2008; Wang 2010). As stated above, *Samsn1*$^{-/-}$ mice are viable, fertile and displayed enhanced adaptive immunity compared to their wildtype littermates (Wang 2010). Homozygous *Plxnd1*-knockout (*Plxnd1*$^{-/-}$) mice all die within the first 24 hours due to abnormal atrial development, congenital heart abnormalities (including defects of cardiac outflow tract and aortic branchial arch), and reduced amount of differentiated smooth muscle cells around arch arteries (Gitler 2004). However, no phenotypic data is available for *Plxnd1*$^{+/-}$ mice (Gitler 2004). Two homozygous *Lrpap1*-knockout (*Lrpap1*$^{-/-}$) mouse models have been generated so far (Willnow 1995; Umans 1999). *Lrpap1*$^{-/-}$ mice were phenotypically identical to their wildtype littermates, expressed a normal level of low-density lipoprotein (LDL) receptor in the liver and brain but showed abnormal activity of lipoprotein receptor-related protein (LRP) expression in the liver and brain due to significant reduction of functional LRP. The reduced activity of functional LRP in the liver resulted in defected clearance of α2-macroglobulin from plasma (Willnow 1995). Umans *et al* confirmed observations made by Willnow *et al* but also reported that nearly 50% of pups died at or shortly after birth (Umans 1999). They found that the expression of both LRP and LDL receptor was significantly increased in pregnant *Lrpap1*$^{-/-}$ females compared to their wildtype littermates, and showed that both LRP and LDL receptor are required for maintenance of a normal lipid metabolism during pregnancy but did not find an explanation for the increased perinatal lethality of *Lrpap1*$^{-/-}$ mice (Umans 1999). No phenotypic data is available for *Lrpap1*$^{+/-}$ mice (Willnow 1995; Umans 1999). Several *Lmna*-knockout (*Lmna*$^{-/-}$) mouse models have been generated up to date to examine the function of lamin A and C, and their involvement in a range of human disorders (Sullivan 1999; Yang 2005; Fong 2006; Davies 2008; Davies 2010). Sullivan *et al* generated *Lmna*$^{-/-}$ mice that lacked the expression of both lamin A and C (Sullivan 1999). At birth *Lmna*$^{-/-}$ mice were identical to both their heterozygous

and wildtype littermates. However, by 4 weeks of age they showed severe growth retardation, and a significant reduction in body weight (around 50% decreased compared to their heterozygous and wildtype littermates) and fat stores. Also, *Lmna*$^{-/-}$ mice displayed an abnormal gait, and their posture showed progressive signs of scoliosis/kyphosis, and none survived past 8 weeks of age. Histopathological analysis of these mice showed absence of WAT, thymic atrophy, reduction in spleen size, and striking evidence of muscular dystrophy. *Lmna*$^{-/-}$ mice also showed changes in the nuclear envelope integrity and mislocalization of emerin in the cardiac and skeletal muscles; such a phenotype resembles Emery-Dreifuss muscular dystrophy (EDMD) (Sullivan 1999). In contrast, *Lmna*$^{+/-}$ mice did not show any phenotypic or histopathological abnormalities, and did not die prematurely (Sullivan 1999). Fong *et al* generated *Lmna*-knockout (*Lmna*^{LCO}) mice that lacked the expression of lamin A only (Fong 2006). Both *Lmna*$^{LCO/+}$ and *Lmna*$^{LCO/LCO}$ mice were phenotypically normal, showed no evidence of growth retardation or muscular dystrophy, and showed no changes in the nuclear shape and envelope integrity or localization of emerin (Fong 2006). Both Yang *et al* and Davies *et al* generated *Lmna*-knock-in mice (*Lmna*$^{HG/+}$ and *Lmna*$^{ggHG/+}$ respectively) that lacked the expression of lamin C and expressed a truncated version of lamin A, commonly known as progerin (Yang 2005; Davies 2008). These two mouse models differed only at one amino acid position, namely methionine in the CaaX motif in the *Lmna*$^{HG/+}$ allele (mice expressed progerin terminating with a farnesylcysteine) was replaced with a leucine *Lmna*$^{ggHG/+}$ allele (mice expressed progerin terminating with a geranylgeranylcysteine). Both *Lmna*$^{HG/+}$ and *Lmna*$^{ggHG/+}$ mouse models expressed progerin, a protein that is synthetized instead of normal prelamin A in humans with Hutchinson-Gilford progeria syndrome (HGPS), a very rare genetic disorder that is characterized by a variety of ageing-like phenotypes, such as osteoporosis, premature atherosclerosis alopecia, cardiovascular problems, loss of eye sight and hair (Yang 2005; Davies 2008). Both *Lmna*$^{HG/+}$ and *Lmna*$^{ggHG/+}$ mouse models displayed a variety of phenotypes. However, neither of them showed changes in body weight and fat stores. In particular, *Lmna*$^{HG/+}$ mice showed growth retardation, and developed a bone-disease phenotype (bone fragility) before 4 months of age (Yang 2005). In

contrast, *Lmna*$^{ggHG/+}$ mice developed a milder bone-disease phenotype and lived longer compared to *Lmna*$^{HG/+}$ mice (Davies 2008). Davies *et al* also generated another homozygous *Lmna*-knock-in mouse (*Lmna*$^{nPLAO/nPLAO}$) that expressed only non-farnesylated prelamin A (Davies 2010). *Lmna*$^{nPLAO/nPLAO}$ mice had normal weight and did not exhibit a bone-disease phenotype (bone fragility). They showed apparently normal development up to 20 weeks of age when premature mortality started to be evident due to a dilated cardiomyopathy. No phenotypic data was available on *Lmna*$^{nPLAO/+}$ mice (Davies 2010).

Taken altogether, out of the currently available mouse models for the *Plxnd1*, *Lrpap1*, *Samsn1* and *Lmna* genes, only *Lmna*$^{-/-}$ mice showed changes in body weight and fat stores, namely they exhibited significant reduction in body weight and fat stores (Sullivan 1999). No changes in body weight and fat stores were observed in heterozygous *Lmna*-knockout and knock-in mouse models, meaning that these mice retained some level of lamin A and/or C expression (Sullivan 1999; Yang 2005; Fong 2006; Davies 2008). As *Lmna* expression was significantly decreased but still detectable in our monosomic mice, which resembles *Lmna* expression observed in heterozygous *Lmna*-knockout and knock-in mice, we believe that decreased *Lmna* expression may have had no influence on changes in fat percentage in our monosomic *Df*$^{Lipi\text{-}Usp25}$ mice.

Interestingly, point mutations in the lamin A or C gene result in familial partial lipodystrophy of the Dunnigan type 2 (FPLD2 OMIM ID: 151660), which is an autosomal dominant disorder characterized by loss of subcutaneous adipose tissue in the limbs and buttocks from puberty, accumulation of fat in the neck and face, liver steosis, and insulin resistance (Wojtanik 2009). FPLD-transgenic mice expressed in their adipose tissue one copy of either human lamin A or C containing the most common R482Q mutation. FPLD-transgenic mice displayed many features that are observed in human patients with FPLD2, including insulin resistance, fatty livers, and lack of subcutaneous adipose tissue accumulation starting several weeks postnatally related to defects in preadipocytes differentiation into functional adipocytes (Wojtanik 2009). Thus abnormal distribution and differentiation of adipose tissue in FPLD2 patients prompts the question of a possible association

between common single nucleotide polymorphisms (SNPs) in *LMNA* and increased risk of obesity. Indeed, an association between the *LMNA* 1908T/C SNP and elevated plasma leptin concentration, and increased obesity-related indices, including body mass index (BMI), body fat percentage and ratio of waist-to-hip circumference was identified in 306 adult nondiabetic aboriginal Canadian Oji-Cree population (Hegele 2000). The association between the *LMNA* 1908T/C SNP and obesity-related indices was subsequently replicated in 186 adult nondiabetic aboriginal Canadian Inuits (Hegele 2001). However, no association between the *LMNA* 1908T/C SNP and obesity-related indices was found in 255 adult Pima Indians (Weyer 2001). Instead, an association between the *LMNA* 1908T/C SNP and smaller age-, sex- and body fat percentage-adjusted mean subcutaneous abdominal adipocyte size was identified (Weyer 2001). Thus further studies are required to confirm the association between the *LMNA* 1908T/C SNP and obesity-related indices.

Monosomy 21 is a rare human disease with variable clinical appearances due to differing gene dosage errors on chromosome 21 resulting in variable severity and expressivity of major phenotypic features, including intellectual disability, dysmorphism, and cardiac and/or renal abnormalities (Chettouh 1995; Riegel 2005; Lyle 2008; Lindstrand 2010; Roberson 2010). Attempts to generate genotype-phenotype correlations in this disease are complicated by both the small number of patients available for study (there is a lack of informative sets of partial Monosomy 21 patients (Lyle 2008)) and the fact that some patients with Monosomy 21 also carry anomalies involving other human chromosomes, such as segmental trisomies and deletions (Lyle 2008; Katzenstein 2009). We show here that haploinsufficiency of a gene (or genes) in the *Lipi–Usp25* region of MMU16, syntenic to the human 21q11.2–q21.1 region, results in a deficit in memory retention and high-fat diet-induced increase in fat deposition in monosomic mice. These partially monosomic mice have contributed new insights into genes involved in Monosomy 21-associated intellectual disability and will play a critical role in future studies of genotype-phenotype correlations in Monosomy 21 patients and unraveling of the molecular mechanisms underlying this phenotype. Moreover, some changes in gene expression in subcutaneous fat of the

monosomic mice were identified, including down-regulation of *Samsn1* (one of the deleted genes in this region) and *Lmna*, although there is complex genetic regulation of fat metabolism and deposition contributing to obesity, involving gene expression in the central nervous system, liver, central and peripheral fat amongst other places. Thus further studies will be required to understand the molecular causes of increased fat deposition.

Detailed histopathological analysis of monosomic $Df^{Lipi\text{-}Usp25}$ mice found no anatomical abnormalities of any organs. Initial results, suggesting the existence of decreased endochondral ossification in the cartilage of tibias of 10-week old monosomic mice fed on a NFD, were not replicated in further studies. Specifically, normal levels of bone mineral density (BMD) and cartilage endochondral ossification were observed in 8-, 25-week and 1-year old monosomic mice, and no differences in the level of calcium deposition were detected between a 25-week old control and monosomic mice. Thus we concluded that a deletion of the *Lipi–Usp25* region does not play a role in bone development and metabolism. We also decided to test a hypothesis linking increased fat mass with increased bone mass, thus suggesting a protective effect of fat mass on bone tissue (Zhao 2008; Holecki 2010). However, we did not observe any differences in the level of BMD at 8 or 25 weeks of age between control and monosomic mice fed on either a NFD or a HFD. Thus altogether our results do not support the hypothesis of a beneficial effect of increased fat mass on bone tissue.

Analysis of monosomic $Df^{Lipi\text{-}Usp25}$ males showed no changes in the susceptibility to infection with *Salmonella* Typhimurium TET C. Although initial results suggested a decrease in the susceptibility of the monosomic females to infection with *Citrobacter rodentium* lux, this finding was not replicated in further studies. We speculate that our inability to confirm the resistance of the monosomic females to the infection with *Citrobacter rodentium* lux in our further analysis might be related to subtle differences in the microenvironment (e.g. breeding and keeping different batches of mice on different racks), to which different batches of tested mice were exposed, as even small changes in the microenvironment has been reported to influence murine responses to the bacterial infection (Simon Clare; personal communication).

The tumour watch study consisting of 30 *Df*$^{Lipi\text{-}Usp25}$*/+;Blm*$^{m3/m3}$, 20 *Df*$^{Lipi\text{-}Usp25}$*/+;Blm*$^{+/+}$ and 10 *+/+; Blm*$^{m3/m3}$ mice was set up to validate whether monosomic and/or nullisomic deletion of the *Lipi–Usp25* region increases a risk of developing cancer, as partial loss of the proximal end of the long arm of human chromosome 21 has been found in several types of solid tumours, including cancers of the ovary, stomach, breast, oral cavity and bone (Cliby 1993; Ohgaki 1998; Yamamoto 2003; Aoki 2005; Chen 2005; dos Santos Aguiar 2007), and heterozygous deletions spanning the chromosomal region 21q11.2–q21.1 have been detected in 50 cancer cell lines (see dataset released by the Cancer Genome Project; http://www.sanger.ac.uk/cgi-bin/genetics/CGP/cghviewer/CghHome.cgi). At the point of writing this thesis (the end of July 2011), the tumour watch study is still ongoing, as 7 *Df*$^{Lipi\text{-}Usp25}$*/+;Blm*$^{m3/m3}$ (23% of the cohort) and 11 *Df*$^{Lipi\text{-}Usp25}$*/+;Blm*$^{+/+}$ (55% of the cohort) mice are still alive. Nevertheless, histopathological analysis of the mice that have been culled or found dead, revealed the presence of cancer in 11 *Df*$^{Lipi\text{-}Usp25}$*/+;Blm*$^{m3/m3}$ (48%), 3 *Df*$^{Lipi\text{-}Usp25}$*/+;Blm*$^{+/+}$ (33%) and 2 *Blm*$^{m3/m3}$ (20%) mice. The tumours found in *Df*$^{Lipi\text{-}Usp25}$*/+;Blm*$^{m3/m3}$ mice included 7 lymphomas and 6 carcinomas (including 3 hepatocellular carcinomas, 1 invasive adenocarcinoma of the kidneys and pancreas, 1 adenocarcinoma of the small intestine, and 1 undifferentiated carcinoma of the uterus). 1 lymphoma, 1 bone osteosarcoma and 1 squamous skin carcinoma were among the tumours found in *Df*$^{Lipi\text{-}Usp25}$*/+;Blm*$^{+/+}$ mice, while 2 lymphomas were detected in *Blm*$^{m3/m3}$ mice. Although these findings are preliminary, the development of tumours in *Df*$^{Lipi\text{-}Usp25}$*/+;Blm*$^{+/+}$ mice and higher incidence of tumours in *Df*$^{Lipi\text{-}Usp25}$*/+;Blm*$^{m3/m3}$ mice compared to *Blm*$^{m3/m3}$ alone suggests that a gene (or genes) mapped within the *Lipi–Usp25* region plays a role in cancer development and/or progression.

CHAPTER 4

MODELLING A DELETION OF THE HUMAN REGION 5q35.2–q35.3 IN MICE

4.1 GENERAL OVERVIEW

Haploinsufficiency of the human 5q35 region spanning the *NSD1* gene results in a rare condition known as Sotos syndrome. Patients with Sotos syndrome display a variety of clinical features, including pre- and postnatal overgrowth, advanced bone age, intellectual disability, and hypotonia, as well as facial, cardiovascular and/or urinary/renal abnormalities. To search for dosage-sensitive genes involved in this disease, we used chromosome engineering to generate a monosomic mouse model carrying a deletion of the *4732471D19Rik* to *B4galt7* interval, syntenic with 5q35.2–q35.3 in humans. Haploinsufficiency for the 36 genes in this interval resulted in no gross morphological defects. In particular, no overgrowth was observed. However, histopathological analysis showed dilation of the pelvicalyceal system in the kidneys of monosomic mice, which mimics the renal abnormality observed in patients with Sotos syndrome. Thus haploinsufficiency of a gene (or genes) within the *4732471D19Rik–B4galt7* interval successfully models the renal abnormality observed in patients with Sotos syndrome.

4.2 INTRODUCTION

4.2.1 OVERVIEW OF SOTOS SYNDROME

Sotos syndrome (SoS OMIM ID: 117550), also known as cerebral gigantism, is named after Dr Juan Sotos who in 1964, first described a group of children with overgrowth, acromegaly, and intellectual disability (Sotos 1964). Indeed, SoS is one of the most commonly diagnosed overgrowth disorders after Beckwith-Wiedeman syndrome (Baujat 2007). Patients with SoS are also diagnosed with prenatal overgrowth, facial abnormalities, macrocephaly, advanced bone age, large hands and feet, and coordination problems. Moreover, hypotonia, poor feeding, jaundice, frequent ear and chest infections, cardiac and urinary/renal defects, seizures, scoliosis, and behavioural problems have also been observed in some SoS patients. However, the variety and degree of severity of SoS symptoms decrease with age, and some clinical features, including overgrowth, hypotonia, poor feeding and infections, become much less apparent in children after the first few years of life (Cole 1994; Tatton-Brown 2007). Patients with SoS might also have an elevated level of predisposition to cancer as some SoS individuals have been diagnosed with neuroblastoma, ganglioglioma, sacrococcygeal teratoma, hepatoblastoma, acute lymphoblatic leukeamia or small cell lung carcinoma (Saugier-Veber 2007). However, the overall risk of tumourgenesis is estimated to be lower than 3% in SoS individuals (Tatton-Brown 2007).

4.2.2 THE MOLECULAR AND GENETIC BASIS OF SOTOS SYNDROME

SoS shows an autosomal dominant mode of inheritance (Baujat 2007). In 2002, the nuclear receptor SET domain containing protein 1 (*NSD1*) was identified as a causative gene for SoS after *NSD1* was found to be disrupted in a child carrying an apparently balanced *de novo* t(5;8)(q35;q24.1) translocation (Kurotaki 2002). Subsequent analysis of patients clinically diagnosed with SoS showed that haploinsufficiency of *NSD1* due to intragenic *NSD1* mutations, partial *NSD1* deletions or chromosomal microdeletions

spanning the 5q35 region encompassing the entire *NSD1* gene accounted for more than 90% of cases (Kurotaki 2002; Cecconi 2005; Douglas 2005; Tatton-Brown 2005; Saugier-Veber 2007; Tatton-Brown 2007), while deletions and uniparental disomies of the 11p15 region or deletions of the *GPC3* gene have been identified in some SoS individuals that did not show any *NSD1* anomalies (Douglas 2005; Tatton-Brown 2007).

The prevalence of intragenic *NSD1* mutations and 5q35 microdeletions encompassing the *NSD1* gene depends greatly on the ethnic origin. Namely, up to 80% of non-Japanese SoS cases but only approximately 12% of Japanese SoS cases are identified with intragenic *NSD1* mutations, while more than 50% of Japanese SoS cases but only approximately 10% of non-Japanese SoS cases are detected with 5q35 microdeletions (Tatton-Brown 2005; Baujat 2007; Saugier-Veber 2007). The increased frequency of 5q35 microdeletions in Japanese SoS cases might be attributed to an inversion polymorphism causing a predisposition to microdeletions that is commonly found in the Japanese (Visser 2005).

More than 200 different intragenic *NSD1* mutations have been described so far in patients with SoS (Kurotaki 2003; Faravelli 2005; Tatton-Brown 2005; Saugier-Veber 2007). The large number of distinct mutations and the low number of recurrent mutations might be attributed to the lack of mutational hot spots in the *NSD1* gene (Faravelli 2005; Saugier-Veber 2007). Also, the vast majority of intragenic *NSD1* mutations occur *de novo*, and only a few familial cases have been reported (Kurotaki 2003; Tatton-Brown 2005). Two types of intragenic *NSD1* mutations, namely truncating and missense mutations, have been identified both in Japanese and non-Japanese SoS individuals (Kurotaki 2003; Faravelli 2005; Tatton-Brown 2005; Saugier-Veber 2007). Interestingly, truncating mutations are detected throughout the *NSD1* gene, while missense mutations are identified only in the functional domains of the *NSD1* gene (Faravelli 2005; Tatton-Brown 2005; Tatton-Brown 2007).

Partial *NSD1* deletions are identified in approximately 5% of patients with SoS (Douglas 2005). Partial *NSD1* deletions have unique breakpoints and occur throughout the gene. However, an increased tendency towards deletions spanning exon 1 and 2 of the *NSD1* gene is observed (Douglas

2005). This is most likely due to the high density of Alu repeats flanking these exons that mediate non-allelic homologous recombination (NAHR). In contrast, partial deletions that do not have breakpoints within Alu repeats seem to be mediated by non-homologous end joining (NHEJ) (Douglas 2005).

Interestingly, the type of chromosomal rearrangement and the size of 5q35 microdeletions differ between SoS individuals of different ethnic origin. In particular, a 1.9 Mb microdeletion spanning the 5q35.2–q35.3 region (**Figure 4.1**) has been identified in the majority of Japanese SoS cases (Kurotaki 2003; Visser 2005; Saugier-Veber 2007; Tatton-Brown 2007). This deletion results from intrachromosomal rearrangements, and is mediated through NAHR between low-copy repeats (LCRs) flanking the *NSD1* gene (**Figure 4.1**) (Kurotaki 2003; Tatton-Brown 2005). In contrast, most of the 5q35 microdeletions identified in non-Japanese SoS cases have unique breakpoints, and thus differ in size, and most likely result from interchromosomal rearrangements (Tatton-Brown 2005). Notably, in both Japanese and non-Japanese SoS cases, a significant bias towards microdeletions of the paternal 5q35 region is observed. However, this might be at least partially attributed to the increased rate of recombination at the 5q telomere in males compared to females (Tatton-Brown 2005).

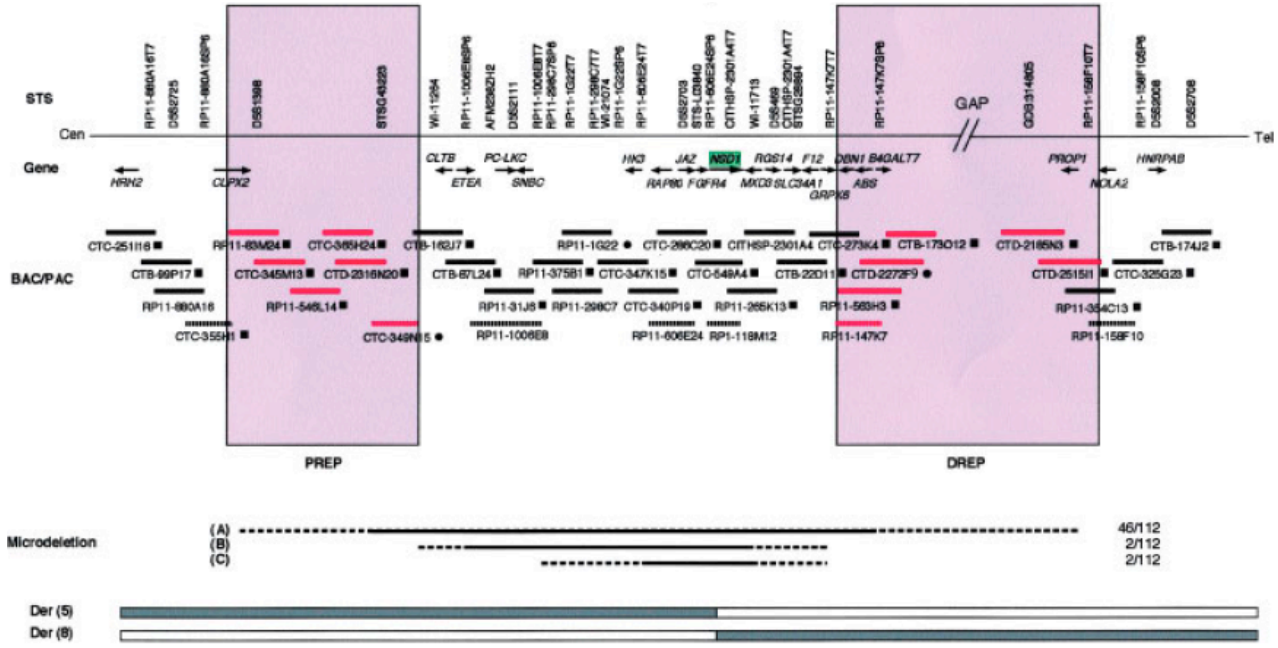

Figure 4.1. Physical map covering microdeletions and their flanking regions, and a summary of 50 microdeletions identified by FISH or microarray CGH analysis. Thirty-seven BAC/PAC clones were incorporated in this map. Small horizontal arrows show the orientation of a gene. Microdeletions A, B, and C are found in 46, 2, and 2 of 112 SoS cases respectively. Long horizontal lines indicate confirmed (solid lines) and possibly deleted (dotted lines) regions respectively. Purple boxes indicate regions of LCRs (low copy repeats), PREP (proximal-repeat) and DREP (distal-repeat). Figure taken from Kurotaki *et al*., 2003.

4.2.3 PHENOTYPIC DIFFERENCES BETWEEN SOTOS SYNDROME CASES CARRYING INTRAGENIC MUTATIONS AND 5q35 MICRODELETIONS

The major clinical symptoms of SoS, including pre- and postnatal overgrowth, facial abnormalities, hypotonia, and intellectual disability, are diagnosed both in SoS patients carrying intragenic *NSD1* mutations and in SoS individuals carrying 5q35 microdeletions (Tatton-Brown 2005). However, in contrast to SoS individuals with intragenic *NSD1*, SoS patients with the 5q35 microdeletions tend to show less pronounced overgrowth, yet more profound intellectual disability (Kurotaki 2003; Nagai 2003; Tatton-Brown 2005; Saugier-Veber 2007). Moreover, several studies have reported increased frequency of cardiovascular and urinary/renal abnormalities in SoS patients carrying 5q35 microdeletions (Kurotaki 2003; Nagai 2003; Saugier-Veber 2007). Thus it is possible that genes other than the *NSD1* gene

could be dosage-sensitive, and therefore responsible for the extended variability and degree of severity of phenotypes observed in SoS patients with the 5q35 microdeletion.

4.2.4 THE *NSD1* GENE

The *NSD1* gene maps to the 5q35 region, consists of 23 exons and is expressed in a variety of tissues, including human foetal and adult brain, skeletal muscle, kidney, spleen, thymus, and lung, as well as adult peripheral blood leukocytes and placenta (Kurotaki 2001).

NSD1 encodes a 2,696 amino acid protein that belongs to an emerging family of proteins that includes NSD2 and NSD3 (Kurotaki 2001). NSD1 contains multiple functional domains, including a Su(var)3-9, Enhancer-of-Zeste, Trithorax (SET) domain, SET-associated cysteine-rich (SAC) domain, five zinc-finger plant homeodomains (PHDs), two proline-tryptophan-tryptophan-proline (PWWP) domains, and two distinct nuclear receptor (NR) interaction domains (NID^{-L} and NID^{+L}) (**Figure 4.2**) (Kurotaki 2001; Tatton-Brown 2007). SET domains are found in proteins that regulate gene transcription, play a role in position-effect-variegation (PEV), and are involved in the establishment and maintenance of chromatin structure (Jenuwein 1998; Kurotaki 2001), while SAC domains are present in proteins that function as histone-methyltransferases (HMTases) (Huang 1998). Interestingly, both SET and SAC domains have been shown to be involved in methylation of lysine 36 of histone 3 and lysine 20 of histone 4 (Tatton-Brown 2007). Also, PHD domains are found in proteins that interact with chromatin and are involved in chromatin-mediated regulation of gene transcription and modulation of chromatin structure (Huang 1998). Thus, altogether, the presence of SAC, SET and PHD domains in the NSD1 protein suggests an involvement of the *NSD1* gene in modulation of chromatin structure and regulation of gene transcription. The function of PWWP domains has not been fully elucidated. However, they are believed to be involved in protein-protein interaction (Stec 2000). Interestingly, NID^{-L} and NID^{+L} domains possess binding properties of NR interaction domains found in NR corepressors and coactivators that suggests that the NSD1 protein functions as a bifunctional

transcriptional co-factor that can either activate or repress transcription in response to ligand binding (Huang 1998), which further supports a putative role of the *NSD1* gene in regulation of gene transcription.

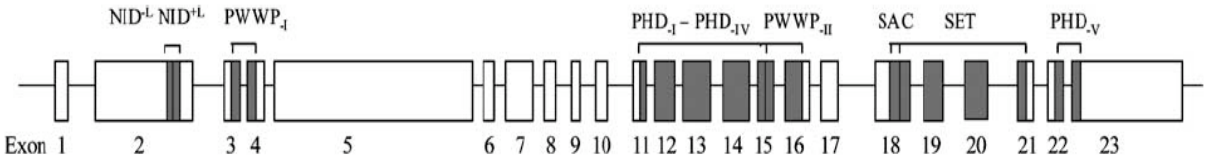

Figure 4.2. Schematic representation of the *NSD1* gene. Figure taken from Tatton-Brown *et al*., 2007. NID^{-L} and NID^{+L} - nuclear receptor (NR) interaction domains; $PWWP_{-I}$ and $PWWP_{-II}$ - proline-tryptophan-tryptophan-proline domains; PHD_{-I} - PHD_{-V} - zinc-finger plant homeodomains; SAC - SET-associated cysteine-rich domain; SET - Su(var)3-9, Enhancer-of-Zeste, Trithorax domain.

4.2.5 A MOUSE MODEL OF SOTOS SYNDROME

The mouse orthologue of the *NSD1* gene was identified in 1998 during a search for factors mediating transcriptional responses induced by binding of ligands to nuclear receptors (Huang *et al*., 1998). The murine *Nsd1* gene is highly conserved with the human *NSD1* gene, showing 86% homology at the nucleotide level and 83% homology at amino acid level (Kurotaki 2001).

In 2003 a mouse knock-out of the *Nsd1* gene was developed by gene disruption (Vani Rayasam 2003). The targeted intragenic deletion of exon 2 of the *Nsd1* gene resulted in a frameshift mutation with a premature stop codon in exon 3. The truncated NSD1 protein was devoid of NID^{-L} and NID^{+L} and all conserved domains. Heterozygous *Nsd1* mice were viable, fertile and did not display any gross phenotypic abnormalities. Most notably, heterozygous *Nsd1* mice showed a normal growth rate and did not display any signs of overgrowth, and thus did not recapitulate the major clinical feature of SoS patients. However, vani Rayasam *et al* speculated that if the overgrowth in the heterozygous *Nsd1* mice is less pronounced than in human SoS individuals, this phenotype might have been missed. Alternatively, analysis of the mice at earlier timepoints might have shown an overgrowth phenotype. No homozygous *Nsd1* mice were present among progeny from heterozygote

Nsd1 intercrosses, showing that the *Nsd1* mutation resulted in prenatal death. Collection of embryos from heterozygote *Nsd1* intercrosses at different timepoints during gestation revealed the absence of homozygous *Nsd1* embryos at or after E10.5, which indicates that the *Nsd1* gene is essential for early post-implantation development. Further analysis showed that homozygous *Nsd1* embryos displayed increased apoptosis in the embryonic ectodermal cells, were able to initiate mesodermal formation, but failed to complete gastrulation (presumably due to abnormal ectodermal development). Moreover, vani Rayasam *et al* showed that the Nsd1 protein has an intrinsic histone methylotransferase activity that was capable of methylating lysine 36 of histone 3 and lysine 20 of histone 4, which provided further evidence supporting the involvement of the *Nsd1* gene in modulation of chromatin structure and regulation of gene transcription.

Interestingly, none of the other mouse models carrying knock-out mutations of individual genes located within the most frequently detected human SoS 5q35 microdeletion have shown a dominant phenotype, suggesting that *Sncb*, *Unc5a*, *Fgfr4*, *Mxd3*, *Rgs14*, *Slc34a1*, *F12*, *Grk6*, *Dbn1* and *Dok3* are not dosage-sensitive, and therefore, at least individually, are not likely to be responsible for the extended variability and degree of severity of clinical features observed in SoS patients with the 5q35 microdeletions (Mouse Genome Informatics - http://www.informatics.jax.org).

4.2.6 GENERATION OF A NEW MOUSE MODEL OF SOTOS SYNDROME

To our knowledge only one mouse model of SoS has been generated to date (Vani Rayasam 2003). This mouse model provides phenotypic data only on the deletion of the *Nsd1* gene, and thus the contribution of other genes within the SoS deletion to the phenotype remains unclear. To this end, we used chromosome engineering to generate a new mouse model of SoS, $Df^{4732471D19Rik\text{-}B4galt7}$, carrying a deletion syntenic to the human region 5q35.2–q35.3, in order to allow investigation of the contribution of the 36 genes at the distal end of human chromosome 5 to the development of clinical features commonly diagnosed in SoS patients.

4.3 RESULTS

4.3.1 GENERATION OF MONOSOMIC MICE FOR THE 1.5 Mb *4732471D19Rik–B4galt7* REGION

The *4732471D19Rik* and *B4galt7* genes are located at the proximal and distal ends, respectively, of a 1.5 Mb region in the B1 band of mouse chromosome 13 (MMU13), which is syntenic to the human region 5q35.2–q35.3 (**Figure 4.3**). This region on human chromosome 5 (HSA5) contains 36 genes, and all of these genes have orthologous counterparts in the syntenic region of MMU13 (**Table 4.1**). The *4732471D19Rik–B4galt7* deletion was generated using chromosomal engineering (Zheng 1999) as described in Material and Methods (**Figure 4.4A**). Briefly, AB2.2 ES cells were sequentially electroporated with targeting vectors containing a portion of the *Hprt* selection cassette (5' or 3'*Hprt*), a *loxP* site and a coat colour marker (agouti or tyrosinase). The targeting vector containing the 5' *Hprt* cassette (MICER clone: MHPN55m07) (Adams 2004) was inserted proximal to *4732471D19Rik* and the targeting vector containing the 3' *Hprt* cassette (MICER clone: MHPP265c24) (Adams 2004) was inserted distal to *B4galt7* (**Figure 4.4A**). The correct insertion of both targeting vectors was confirmed by Southern blot analysis on *Bst*EII- or *Spe*I-digested genomic DNA extracted from ES clones, selected either in G418 or puromycin using a 5′ and 3′ Southern external probe respectively (**Figure 4.4A and 4.4B**). Double-targeted clones, in which both targeting vectors were inserted on the same chromosome (*cis*), were electroporated with a Cre-expression vector, and subsequently selected in medium containing HAT to isolate ES clones carrying a chromosomal deletion generated via recombination of the *loxP* sites (**Figure 4.4A**). The deletion allele was designated $Df^{4732471D19Rik\text{-}B4galt7}$ (alternatively named *Ms(4732471D19Rik-B4galt7)2Dja* and abbreviated as *Ms2Dja*). The presence of the deletion in *Hprt*-resistant ES clones was confirmed by FISH (**Figure 4.4C**). The positive ES clones were used to generate chimaeras, which transmitted $Df^{4732471D19Rik\text{-}B4galt7}$ to their progeny.

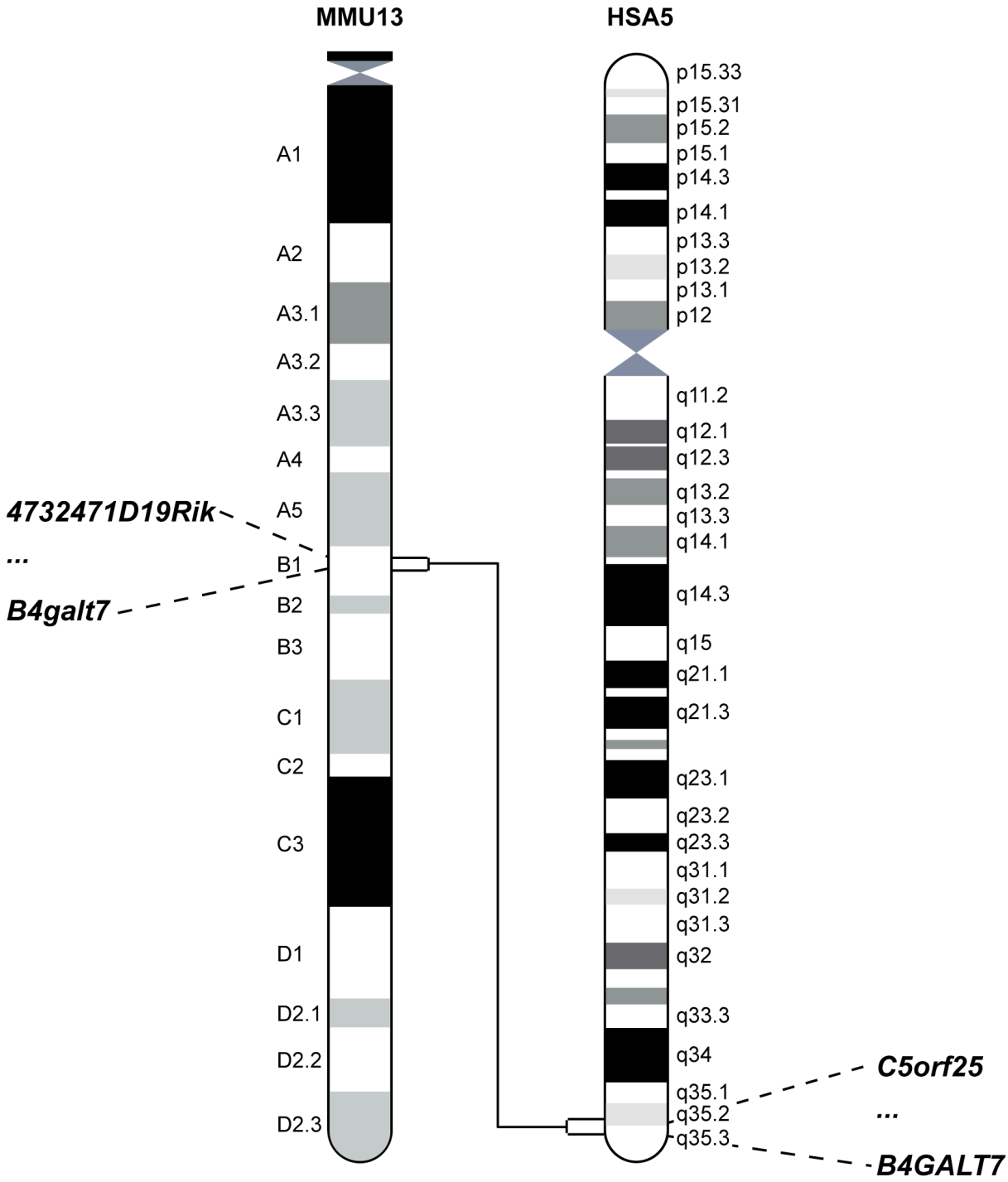

Figure 4.3. Schematic representation of the q35.2–q35.3 interval on HSA5 and the syntenic region in the B1 band on MMU13. Proximal and distal genes that map to the human 5q35.2–q35.3 region (NCBI build GRChr37) and the B1 band on MMU13 (NCBI build m37) have been listed.

Table 4.1. Summary of the genes mapped within the *4732471D19Rik–B4galt7* region (NCBI build m37). Functions/processes were gene-based on ontology classifications as listed by Mouse Genome Informatics (http://www.informatics.jax.org/).

Gene	Official name	Ensembl ID (v61)	Function/Processes (GO terms)
4732471D19Rik	RIKEN cDNA 4732471D19 gene	ENSMUSG00000043183	Unknown
4833439L19Rik	RIKEN cDNA 4833439L19 gene	ENSMUSG00000025871	Unknown
Arl10	ADP-ribosylation factor-like 10	ENSMUSG00000025870	GTP and nucleotide binding activity
Nop16	NOP16 nucleolar protein homolog (yeast)	ENSMUSG00000025869	Unknown
Higd2a	HIG1 domain family, member 2A	ENSMUSG00000025868	Unknown
Cltb	Clathrin, light polypeptide (Lcb)	ENSMUSG00000045547	Intracellular protein transport, vesicle-mediated transport, and peptide binding activity
Faf2	Fas associated factor family member 2	ENSMUSG00000025873	Response to unfolded proteins, and ubiquitin and ubiquitin protein ligase binding
Rnf44	Ring finger protein 44	ENSMUSG00000034928	Metal ion binding activity
Cdhr2	Cadherin-related family member 2	ENSMUSG00000034918	Cell adhesion, and negative regulation of cell growth
Gprin1	G protein-regulated inducer of neurite outgrowth 1	ENSMUSG00000069227	Neuron projection development, and phospoprotein binding activity
Sncb	Synuclein, beta	ENSMUSG00000034891	Dopamine metabolic processes, negative regulation of neuron apoptosis, and calcium ion binding activity
Eif4e1b	Eukaryotic translation initiation factor 4E family member 1B	ENSMUSG00000074895	Translational, and RNA binding and translation initiation factor activity
Tspan17	Tetraspanin 17	ENSMUSG00000025875	Unknown
Unc5a	Unc-5 homolog A (*C.elegans*)	ENSMUSG00000025876	Apoptosis, axon guidance, multicellular organismal development, and netrin receptor activity
Hk3	Hexokinase 3	ENSMUSG00000025877	Carbohydrate metabolic processes, phosphorylation, glycolysis, kinase and transferase activity, and ATP, kinase, hormone, enzyme and hexokinase binding activity
Uimc1	Ubiquitin interaction motif containing 1	ENSMUSG00000025878	Chromatin modifications, DNA repair, DNA-dependent, negative regulation of transcription, histone H2A K63-linked deubiquitination, and histone and K63-linked polyubiquitin binding activity
Zfp346	Zinc finger protein 346	ENSMUSG00000021481	Apoptosis, and metal ion and double-stranded RNA binding activity
Fgfr4	Fibroblast growth factor receptor 4	ENSMUSG00000005320	Alveolar secondary septum development, fibroblast growth factor receptor signalling pathway, protein phosphorylation, organ induction, lung development, and ATP, kinase and transferase binding activity
Nsd1	Nuclear receptor-binding SET-domain protein 1	ENSMUSG00000021488	Gastrulation with mouth forming second, histone H3-K36 methylation, and androgen receptor, zinc ion, transcription cofactor and chromatin binding activity

Table 4.1 continued. Summary of the genes mapped within the *4732471D19Rik–B4galt7* region (NCBI build m37).

Gene	Official name	Ensembl ID (v61)	Function/Processes (GO terms)
Rab24	RAB24, member RAS oncogene family	ENSMUSG00000034789	Autophagy, protein transport, small GTPase mediated signal transduction, and GTP and nucleotide binding activity
Mxd3	Max dimerization protein 3	ENSMUSG00000021485	Negative regulation of transcription, DNA-dependent regulation of transcription, and protein binding activity
Prelid1	PRELI domain containing 1	ENSMUSG00000021486	Unknown
Lman2	Lectin, mannose-binding 2	ENSMUSG00000021484	Protein transport, and metal ion and sugar binding
Rgs14	Regulator of G-protein signalling 14	ENSMUSG00000052087	Cell cycle and division, spindle organization, cell division, and GDP dissociation inhibitor, microtubule binding activity, and GTPase activator activity, and positive regulation of GTPase activity
Slc34a1	Solute carrier family 34 (sodium phosphate), member 1	ENSMUSG00000021490	Ion transport, bone remodelling, and sodium-dependent phosphate transmembrane transporter activity
Pfn3	Profilin 3	ENSMUSG00000044444	Actin cytoskeleton organization, and actin binding and ATP:ADP antiporter activity
F12	Coagulation factor XII (Hageman factor)	ENSMUSG00000021492	Plasma kallikrein-kinin cascade, Factor XII activation, positive regulation of plasminogen activation, protein autoprocessing, positive regulation of blood coagulation, zymogen activation, protein maturation by peptide bond cleavage, response to misfolded protein, and positive regulation of fibrinolysis
Grk6	G protein-coupled receptor kinase 6	ENSMUSG00000074886	Desensitization of G-protein coupled receptor protein signalling pathway, protein phosphorylation, and ATP binding, and transferase and protein serine/threonine kinase activity
Prr7	Proline rich 7 (synaptic)	ENSMUSG00000034686	Unknown
Dbn1	Drebrin 1	ENSMUSG00000034675	Actin filament organization, signal transduction, multicellular organismal development, nervous system development, cell differentiation, and actin and profiling binding activity
Pdlim7	PDZ and LIM domain 7	ENSMUSG00000021493	Actin cytoskeleton organization, ossification, multicellular organismal development, cell differentiation, and metal ion binding activity
Dok3	Docking protein 3	ENSMUSG00000035711	Ras protein signal transduction, and insulin receptor binding activity
Ddx41	DEAD (Asp-Glu-Ala-Asp) box polypeptide 41	ENSMUSG00000021494	mRNA processing, RNA splicing, and metal ion binding, ATP binding and helicase activity
Fam193b	Family with sequence similarity 193, member B	ENSMUSG00000021495	Unknown
Tmed9	Transmembrane emp24 protein transport domain containing 9	ENSMUSG00000058569	Transport
B4galt7	Xylosylprotein beta1,4-galactosyltransferase, polypeptide 7 (galactosyltransferase I)	ENSMUSG00000021504	Carbohydrate and proteoglycan metabolic process, glycosaminoglycan biosynthetic process, fibril organization, negative regulation of fibroblast proliferation, and metal ion binding, transferase and transferring glycosyl groups activity

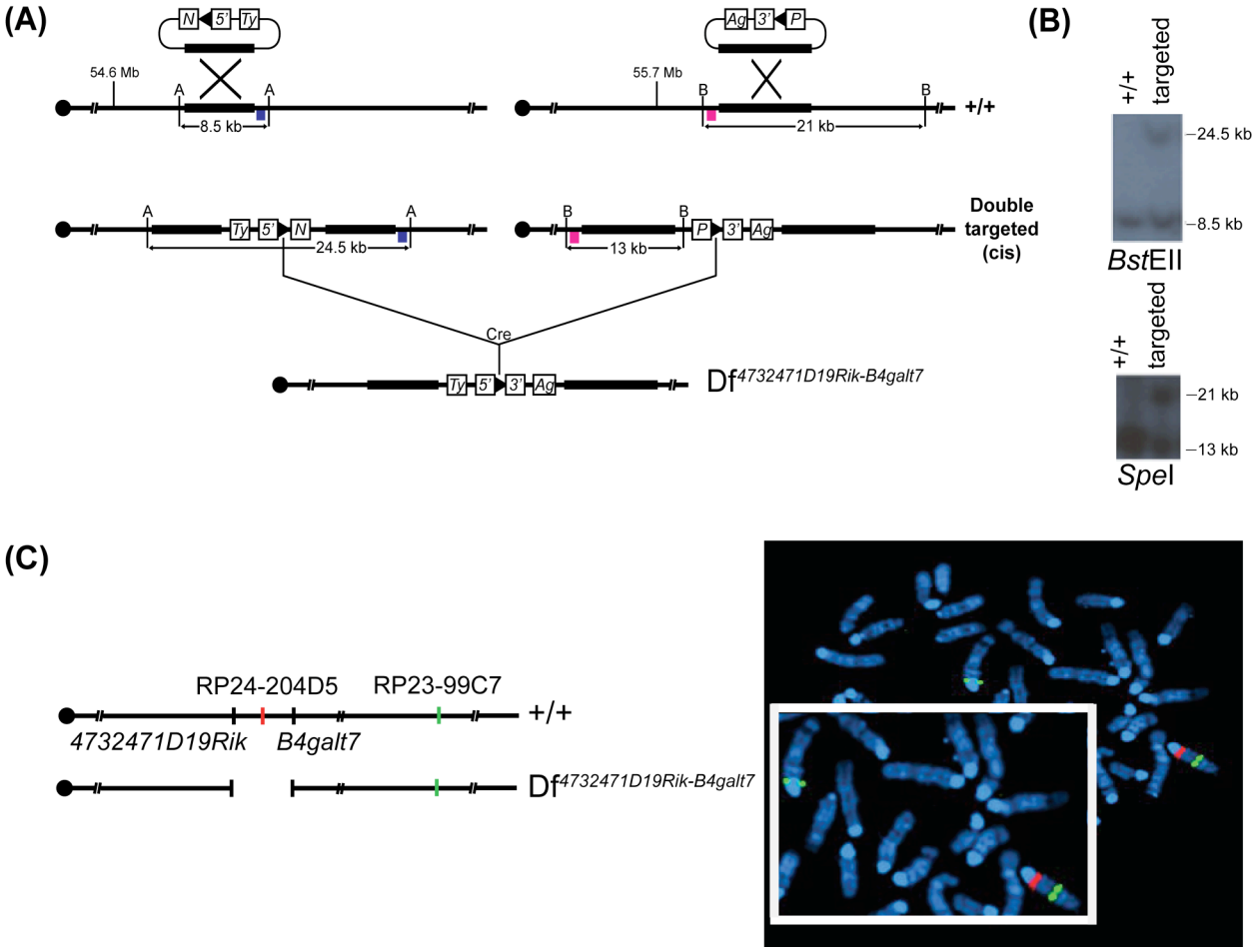

Figure 4.4. Generation of a 1.5 Mb deletion between the *4732471D91Rik* and *B4galt7* loci using Cre/*loxP*-mediated chromosomal engineering. (A) Strategy to generate the chromosomal rearrangement (using NCBI build GRChr37). The targeting vectors containing a *loxP* site (arrowhead), a selectable antibiotic resistance gene (*N* or *P*), a coat colour marker (*Ty* or *Ag*) and part of the *Hprt* gene (5′ or 3′) were integrated successively in the *Lipi* locus and the *Usp25* locus. The coloured boxes (blue and pink) indicate the location of the probes (5’ and 3’, respectively) used for Southern blotting. A, *Bst*EII; B, *Spe*I; 5’, 5’*Hprt*; 3’, 3’*Hprt*; *N*, neomycin-resistance gene; *P*, puromycin-resistance gene; *Ty*, tyrosinase minigene, *Ag*, K-14 agouti gene. **(B)** The targeting events were checked by Southern analysis showing an additional *Bst*EII fragment of 24.5 kb compared with the wildtype allele (8.5 kb) for the *4732471D19Rik* locus and an additional *Spe*I fragment of 13 kb compared with the wildtype allele (21 kb) for the *B4galt7* locus. **(C)** Interphase FISH analysis with BAC probes that map in the region of the deletion (red) and outside (green). Chromosomes from the ES cells double-targeted in *cis* ($Df^{4732471D19Rik\text{-}B4galt7}$) showed two green and only one red signal due to the deletion of the *4732471D19Rik–B4galt7* region, while chromosomes from the wildtype ES cells showed two green and two red signals.

4.3.2 PHENOTYPIC ANALYSIS OF MONOSOMIC MICE

The heterozygous (monosomic) *Df*$^{4732471D19Rik\text{-}B4galt7}$ mice were viable, fertile and did not show any gross abnormalities. In particular, no facial abnormalities or hypotonia were observed.

4.3.2.1 ANALYSIS OF BODY WEIGHT AND BODY COMPOSITION OF MONOSOMIC MICE REVEALS THAT LOSS OF ONE COPY OF THE *4732471D19Rik–B4galt7* REGION DOES NOT RESULT IN OVERGROWTH

To determine whether overgrowth in SoS patients could be observed in monosomic *Df*$^{4732471D19Rik\text{-}B4galt7}$ mice, the average weights of 8 monosomic mice and 8 wildtype littermates (controls) fed on a normal-fat diet were compared at 8 weeks of age. No statistical differences were observed between the analysed groups (**Figure 4.5**), suggesting that the overgrowth phenotype is either not recapitulated in mice (as overgrowth was also not observed in heterozygous *Nsd1* mice (Vani Rayasam 2003)) or recovered by that stage of development (as it has been shown that the overgrowth decreases with age and becomes much less apparent in SoS children after the first few years of life (Cole 1994; Tatton-Brown 2007) or perhaps overgrowth could only be observed during the gestation period, as has been shown in the *Cdkn1c* mouse model of Beckwith-Wiedemann syndrome (Tunster 2011)). In order to examine if the overgrowth is displayed in our monosomic mice during an earlier stage of pre- and/or postnatal development, I am currently in the process of analysing embryos at E15.5 and E18.5, and newborn pups at 1 day of age (P1).

8 monosomic and 8 control mice fed on a normal-fat diet were also subjected to the dual-energy X-ray absorptiometry (DEXA) analysis when they were 8 weeks of age in order to check whether any differences in body composition could be observed. However, no statistical differences in estimated total tissue mass, lean mass or fat mass were found between the two groups (**Figure 4.6A-C**). Also, no differences in bone mineral density were identified between monosomic mice and wildtype littermates (**Figure 4.7**).

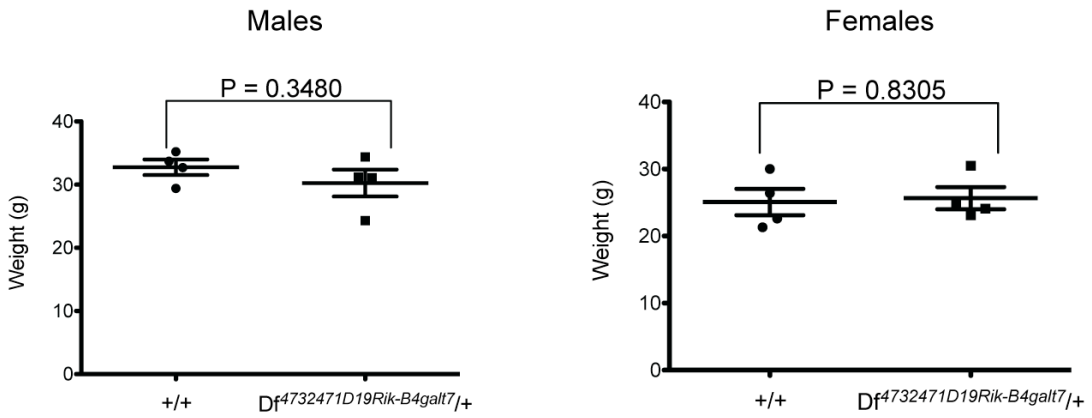

Figure 4.5. Body weight analysis of 8-week old control (+/+) and monosomic (*Df*$^{4732471D19Rik\text{-}B4galt7}$/+) littermates fed a normal-fat diet. Body weight results showing body weight in male and female littermates. Data was statistically analysed using the two-tailed Student's *t*-test. Four mice of each sex were analysed per genotype.

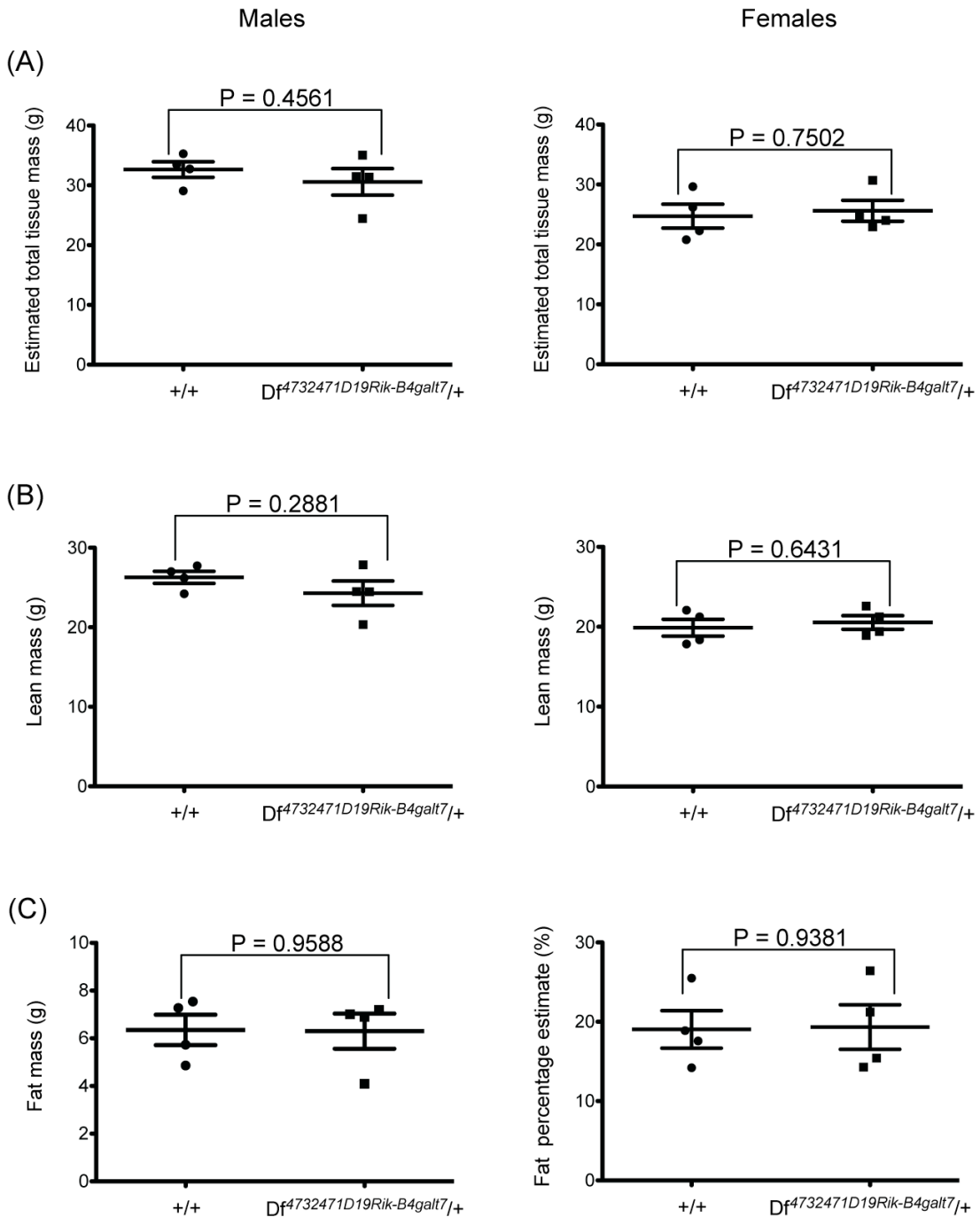

Figure 4.6. DEXA analysis of 8-week old control (+/+) and monosomic (*Df*$^{4732471D19Rik\text{-}B4galt7}$/+) littermates fed a normal-fat diet. (A) DEXA results showing estimated total tissue mass in male and female littermates. **(B)** DEXA results showing lean mass in male and female littermates. **(C)** DEXA results showing fat mass in male and female littermates. Data was statistically analysed using the two-tailed Student's *t*-test. Four mice of each sex were analysed per genotype.

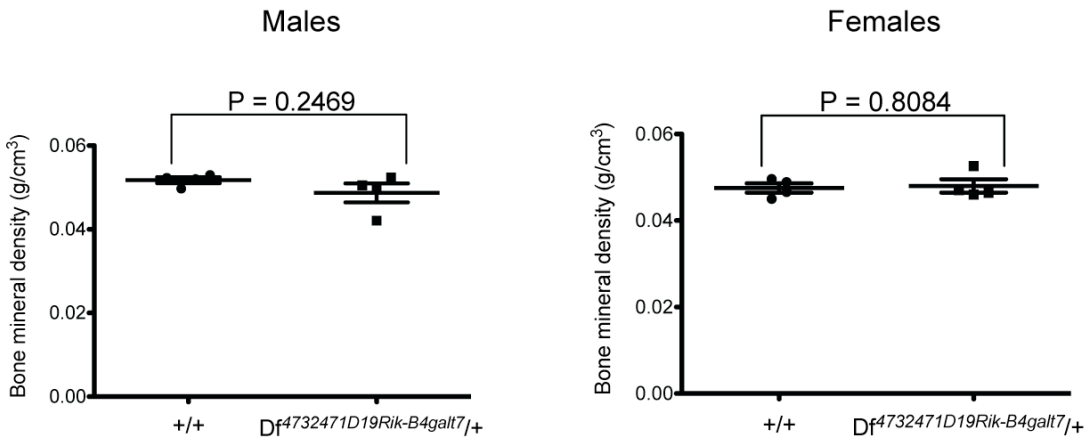

Figure 4.7. DEXA analysis of 8-week old control (+/+) and monosomic (*Df*$^{4732471D19Rik\text{-}B4galt7}$/+) littermates fed a normal-fat diet. DEXA results showing bone mineral density in male and female littermates. Data was statistically analysed using the two-tailed Student's *t*-test. Four mice of each sex were analysed per genotype.

4.3.3.2 HISTOPATHOLOGICAL ANALYSIS OF DIFFERENT TISSUES OF MONOSOMIC MICE REVEALS THAT LOSS OF ONE COPY OF THE *4732471D19Rik–B4galt7* REGION AFFECTS THE URINARY/RENAL SYSTEM

To determine whether any histopathological changes, in particular those associated with features found in SoS patients (such as advanced bone age, cardiovascular and/or urinary/renal abnormalities), could be observed in the monosomic *Df*$^{4732471D19Rik\text{-}B4galt7}$ mice, different tissues were collected from 8 monosomic mice and 8 wildtype littermates (controls) fed on a normal-fat diet when they were 8 weeks of age. The examination of a variety of tissues stained with haematoxylin and eosin (H&E) did not reveal the presence of any anatomical abnormalities of any organs, except kidneys where the dilation of the pelvicalyceal system was detected in monosomic mice (**Figure 4.8, 4.9A, 4.9B, 4.10A, 4.10B, 4.11**). Thus monosomic mice seem to recapitulate hydronephrosis, which is one of the renal abnormalities observed in patients with SoS. Interestingly, sex differences in the degree of severity of the dilation of the pelvicalyceal system were identified between monosomic males and females, as monosomic males showed mild/moderate (**Figure 4.9A and 4.9B**) to moderate/severe (**Figure 4.10A and 4.10B**) dilation of the pelvicalyceal

system while monosomic females showed only very mild dilation (**Figure 4.11**). At present, I am ageing a cohort of monosomic and control mice to investigate if observed kidney abnormalities will progress with age, and thus to determine whether dilation of the pelvicalyceal system is more pronounced in older monosomic mice. Also, we are planning to collect blood samples from those aged mice in order to analyse clinical chemistry parameters related to urinary/renal system functioning, including creatinine, urea and electrolyte.

Interestingly, histopathological analysis showed the presence of cancer (poorly differentiated sarcoma of the uterus) (**Figure 4.12**) in one of monosomic mice (1/8 mice; 12.5%). Although, the size of the analysed cohort was small, perhaps it is worth investigating whether the overall risk of tumourgenesis, currently estimated at less than 3% in individuals with Sotos syndrome (Tatton-Brown 2007), might be underestimated.

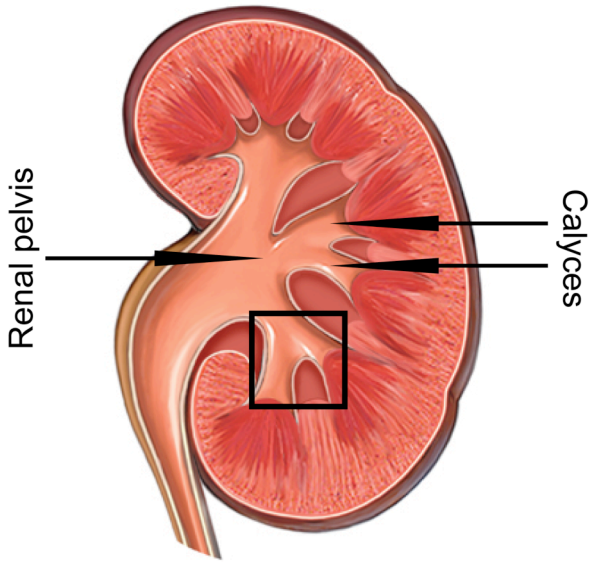

Figure 4.8. A schematic representation of a kidney. A black rectangle indicates a renal region where a dilation of the pelvicalyceal system was observed in monosomic (*Df*$^{4732471D19Rik\text{-}B4galt7}$/+) mice in all analysed kidney sections. Figure modified from www.empowher.com/files/ebsco/images/BI00031.jpg.

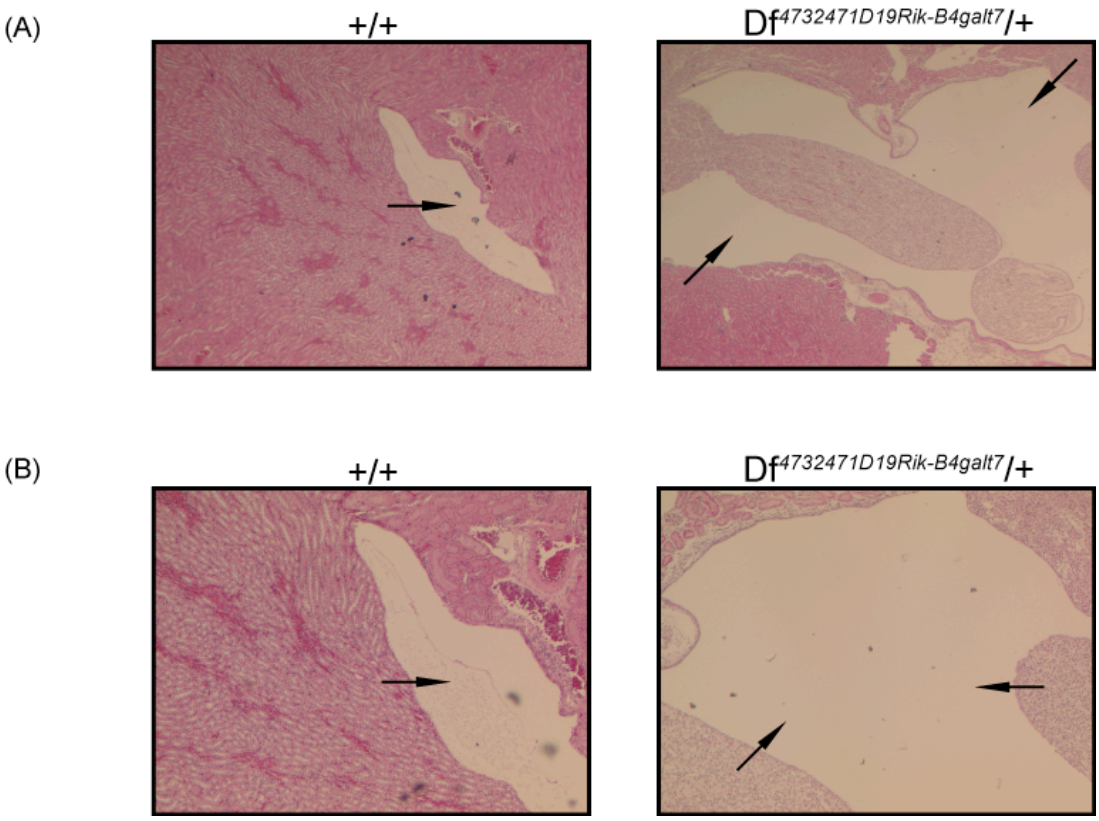

Figure 4.9. Histopathological analysis of kidneys collected from 8-week old control (+/+) and monosomic (*Df*$^{4732471D19Rik\text{-}B4galt7}$/+) male littermates fed on a normal-fat diet. (A), (B) Haematoxylin and eosin-stained kidney sections from control (+/+) and monosomic (*Df*$^{4732471D19Rik\text{-}B4galt7}$/+) males. Kidneys of monosomic (*Df*$^{4732471D19Rik\text{-}B4galt7}$/+) males showed mild/moderate dilation of the pelvicalyceal system (visible as empty spaces; indicated by arrows) compared to control (+/+) males (visible as compact structure of the pelvicalyceal system; indicated by arrows). Images are representative and taken at x25 magnification (A) and x50 magnification (B).

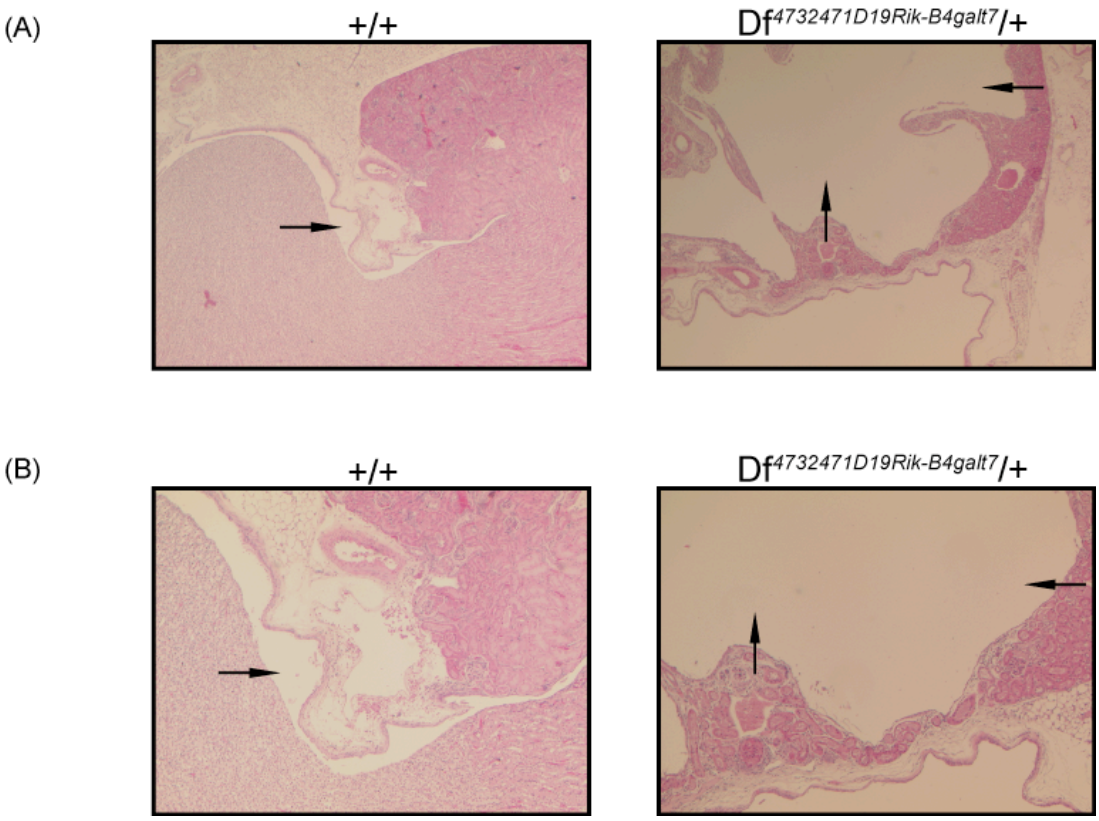

Figure 4.10. Histopathological analysis of kidneys collected from 8-week old control (+/+) and monosomic (*Df*$^{4732471D19Rik\text{-}B4galt7}$/+) male littermates fed on a normal-fat diet. (A), (B) Haematoxylin and eosin-stained kidney sections from control (+/+) and monosomic (*Df*$^{4732471D19Rik\text{-}B4galt7}$/+) males. Kidneys of monosomic (*Df*$^{4732471D19Rik\text{-}B4galt7}$/+) males showed moderate/severe dilation of the pelvicalyceal system (visible as empty spaces; indicated by arrows) compared to control (+/+) males (visible asc compact structure of the pelvicalyceal system; indicated by arrows). Images are representative and taken at x25 magnification (A) and x50 magnification (B).

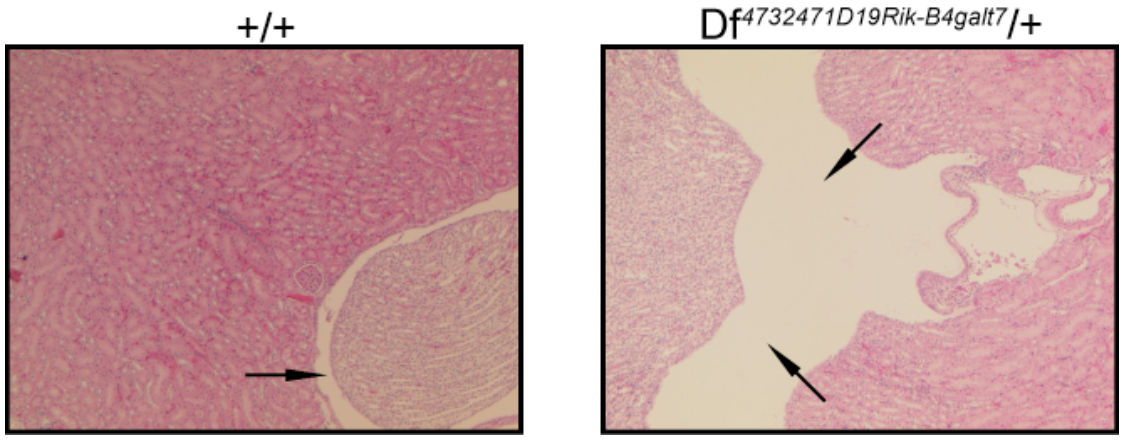

Figure 4.11. Histopathological analysis of kidneys collected from 8-week old control (+/+) and monosomic (*Df*$^{4732471D19Rik\text{-}B4galt7}$/+) female littermates fed on a normal-fat diet. Haematoxylin and eosin-stained kidney sections from control (+/+) and monosomic (*Df*$^{4732471D19Rik\text{-}B4galt7}$/+) females. Kidneys of monosomic (*Df*$^{4732471D19Rik\text{-}B4galt7}$/+) females showed very mild/mild dilation of the pelvicalyceal system (visible as empty spaces; indicated by arrows) compared to control (+/+) females (visible as compact structure of the pelvicalyceal system; indicated by arrows). Images are representative and taken at x50 magnification.

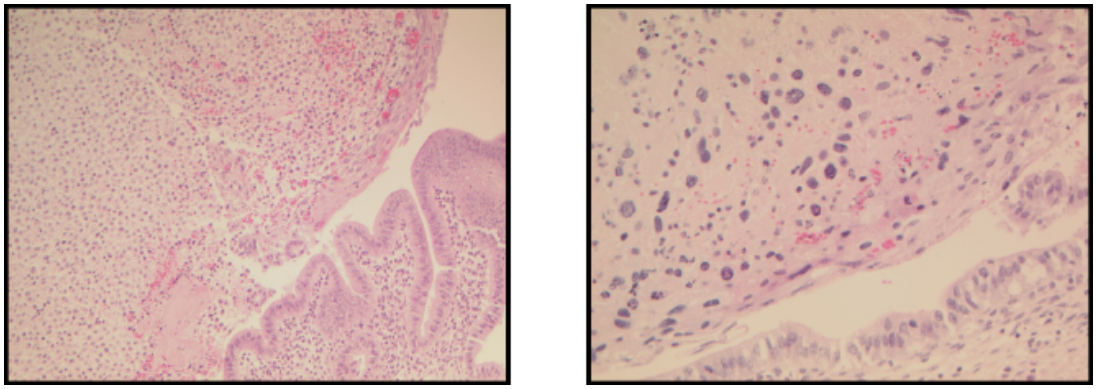

Figure 4.12. Analysis of uterus collected from a *Df*$^{4732471D19Rik\text{-}B4galt7}$/+ mouse. (A) Histopathological analysis of haematoxylin and eosin stained uterus section showing sarcoma. Images are representative and taken at x25 magnification (left) and x200 magnification (right).

4.4 DISCUSSION

We generated and phenotypically characterized the monosomic *Df*$^{4732471D19Rik\text{-}B4galt7}$ mouse, a model for the 1.5 Mb *4732471D19Rik–B4galt7* region. The deleted region is syntenic to the telomeric part of the human chromosome 5, and contains 36 genes that are conserved between human and mouse.

Gross phenotypical analysis of heterozygous (monosomic) *Df*$^{4732471D19Rik\text{-}B4galt7}$ mice found them to be viable, fertile and indistinguishable from controls (wildtype littermates). Specifically, no postnatal overgrowth was observed in 8-week old monosomic *Df*$^{4732471D19Rik\text{-}B4galt7}$ mice, and so these mice do not seem to recapitulate a cardinal feature observed in both SoS patients carrying intragenic *NSD1* mutations and 5q35 microdeletions. Interestingly, there was also no postnatal overgrowth identified in heterozygous *Nsd1* mice (Vani Rayasam 2003), suggesting that the overgrowth phenotype might not be exhibited in mice. However, it is possible that overgrowth might be present during earlier stages of postnatal development, as it has been shown that the overgrowth decreases with age and becomes much less apparent in SoS children after the first few years of life (Cole 1994; Tatton-Brown 2007). It is also possible that the overgrowth might only be displayed during prenatal development, as in a mouse model of Beckwith-Wiedemann syndrome, in which the overgrowth was only observed during embryonic development (Tunster 2011). For example, overgrowth in a mouse model of Beckwith-Wiedemann syndrome was only observed during embryonic development (Tunster 2011). So only through careful analysis of the growth dynamics of monosomic *Df*$^{4732471D19Rik\text{-}B4galt7}$ mice during gestation and early postnatal period might we see the presence of overgrowth, particularly as the overgrowth decreases with age and becomes much less apparent in SoS children after the first few years of life (Cole 1994; Tatton-Brown 2007) and SoS patients with the 5q35 microdeletions tend to show less pronounced overgrowth compared to SoS patients carrying intragenic *NSD1* mutations (Tatton-Brown 2005).

Histopathological examination of different tissues collected from

monosomic *Df*$^{4732471D19Rik\text{-}B4galt7}$ mice revealed no signs of advanced bone age or cardiovascular anomalies. However, it is worth mentioning that advanced bone age and/or cardiovascular abnormalities are observed only in a subset of SoS patients carrying 5q35 microdeletions (Nagai 2003; Tatton-Brown 2005; Saugier-Veber 2007). Histopathological examination did, however, reveal kidney abnormalities in monosomic *Df*$^{4732471D19Rik\text{-}B4galt7}$ mice compared to wildtype littermates. More specifically, both monosomic males and females showed dilation of the pelvicalyceal system at 8 weeks of age. It has been documented that some SoS patients carrying 5q35 microdeletions are identified with anomalies in the urinary/renal system, including vesicoureteric reflux, hydronephrosis, and small kidneys (Kurotaki 2003; Nagai 2003; Tatton-Brown 2005; Saugier-Veber 2007). Hydronephrosis is characterized by dilation of the renal pelvis calyces, and thus monosomic *Df*$^{4732471D19Rik\text{-}B4galt7}$ mice fully recapitulate this anomaly of the urinary/renal system. Nevertheless, further analysis of older monosomic mice is required to establish if this dilation progresses with age, to investigate whether monosomic mice show increased risk of urinary tract infections as a consequence of blocking flow of urine, and to check whether destruction of nephrons eventually leads to renal failure. To date, interestingly, none of the mouse models carrying knock-out mutations in genes mapped within the 5q35 interval have shown a dominant phenotype, thus suggesting that *Sncb*, *Unc5a*, *Nsd1*, *Fgfr4*, *Mxd3*, *Rgs14*, *Slc34a1*, *F12*, *Grk6*, *Dbn1* and *Dok3* are not dosage-sensitive, and therefore are not likely to be responsible for the renal abnormality observed in monosomic *Df*$^{4732471D19Rik\text{-}B4galt7}$ mice (Mouse Genome Informatics - http://www.informatics.jax.org).

To conclude, we show here that haploinsufficiency of a gene (or genes) in the *4732471D19Rik–B4galt7* region of MMU13, syntenic to human 5q35.2–q35.3, results in the dilation of the renal pelvicalyceal system in monosomic mice. These partially monosomic mice have contributed new insights into the existence of a dosage-sensitive gene (or genes) involved in SoS-associated anomaly of the urinary/renal system and will play a critical role in unraveling of the molecular mechanisms underlying this phenotype. On the other hand, haploinsufficiency of genes in the *4732471D19Rik–B4galt7* region

does not seem to model the other clinical phenotypes, including overgrowth, advanced bone age, hypotonia, facial and cardiovascular abnormalities, which are commonly seen in SoS patients. However, the contribution of genes mapped within the deletion to the development of intellectual disability observed in SoS individuals cannot be excluded, as such a phenotype has not yet been analysed in monosomic *Df*$^{4732471D19Rik\text{-}B4galt7}$ mice.

CHAPTER 5

GENERAL SUMMARY

5.1 OVERALL SUMMARY

Chromosomal rearrangements, such as deletions, duplications, inversions and translocations, account for a broad spectrum of human genetic disorders, including Triple-X, Klinefelter, Turner, Down, Edwards, Patau, DiGeorge, Smith-Magenis, Williams, Prader-Willi and Angelman syndrome, to name just a few examples (Iliopoulos 2006; Kesler 2007; Tucker 2007; Mégarbané 2009; Tartaglia 2010; Wikström 2011). In order to unravel dosage-sensitive genomic regions and genes, and to gain better understanding of the development and pathophysiology of these human diseases, chromosomal rearrangements need to be generated in model organisms. The mouse is an excellent organism of choice because it shares many similarities with humans, both in terms of biology and genetics, and because its genome can be easily modified using chromosome engineering techniques, allowing the generation of defined chromosomal rearrangements. To date, many mouse models carrying defined genomic rearrangements have been successfully developed (Corral 1996; Jiang 1998; Sago 1998; Yang 1998; Kimber 1999; Lindsay 1999; Tsai 1999; Zheng 1999; Puech 2000; Lindsay 2001; Merscher 2001; Walz 2003; Walz 2003; Olson 2004; Yan 2004; Bi 2005; Skryabin 2007; Li 2009), giving new insights into dosage-sensitive genes involved in these human genetic disorders, and unravelling the molecular and cellular mechanisms underlying these pathologies.

During my PhD I have used chromosome engineering techniques to develop two monosomic mouse models carrying defined chromosomal deletions syntenic with 21q11.2–q21.1 and 5q35.2–q35.3 in humans.

The first mouse model, carrying a deletion of the *Lipi–Usp25* region, was develop to model clinical features diagnosed in patients with Monosomy

21, a disorder associated with intellectual disability, craniofacial, skeletal and/or cardiac abnormalities, and respiratory complications (Chettouh 1995; Riegel 2005; Lyle 2008; Katzaki 2010; Lindstrand 2010; Roberson 2010). Monosomic mice displayed impaired long-term memory retention in a socially relevant testing paradigm. Thus these monosomic mice have broadened our understanding of genes involved in Monosomy 21-associated intellectual disability and will be of great importance in future studies of genotype-phenotype correlations in Monosomy 21 patients and in identifying the molecular causes underlying this phenotype. Moreover, monosomic mice fed on a HFD exhibited a significant increase in fat mass/fat percentage estimate, severe fatty changes in their livers, and thickened subcutaneous fat. Thus a gene (or genes) within the *Lipi–Usp25* interval is also involved in the regulation of fat deposition. The identification of the HFD-induced increase in fat deposition in our monosomic mice was somewhat surprising, as to date only one study has reported obesity in patients with Monosomy 21 syndrome (Roland 1990). Thus further studies will be required to understand the molecular mechanisms linking deletions of (or encompassing) the 21q11.2–q21.1 region and HFD-induced increased fat deposition.

The second mouse model, carrying a deletion of the *4732471D19Rik–B4galt7* region, was developed to model clinical features diagnosed in patients with Sotos syndrome, an overgrowth disorder associated with advanced bone age, intellectual disability, hypotonia, facial, cardiovascular and/or urinary/renal abnormalities (Cole 1994; Tatton-Brown 2007). Monosomic mice showed dilation of the pelvicalyceal system in the kidneys, which models the hydronephrosis observed in patients with Sotos syndrome (SoS). Thus these monosomic mice have recapitulated the abnormality of the urinary/renal system observed in patients with Sotos syndrome, contributed new insights into genes involved in SoS-associated urinary/renal abnormalities, and will play an important role in establishing genotype-phenotype correlations in patients with Sotos syndrome and identifying molecular causes of this phenotype.

5.2 CORRELATION BETWEEN THE RESULTS GATHERED FROM MONOSOMIC *Df*$^{Lipi\text{-}Usp25}$ AND *Df*$^{4732471D19Rik\text{-}B4galt7}$ MICE AND SYMPTOMS IN PATIENTS WITH MONOSOMY 21 AND SOTOS SYDNROME

The detailed phenotypic analysis of two monosomic mouse models led to the identification of a range of phenotypic abnormalities. Some of the defects, such as dilation of the pelvicalyceal system in monosomic *Df*$^{4732471D19Rik\text{-}B4galt7}$ mice, fully recapitulated clinical symptoms observed in patients with Sotos syndrome. Similarly, both monosomic *Df*$^{Lipi\text{-}Usp25}$ and *Df*$^{4732471D19Rik\text{-}B4galt7}$ mice displayed long-term memory deficit and learning impairment, and so seem to model, at least to a certain extent, the intellectual disability observed in individuals with Monosomy 21 and Sotos syndrome. However, we need to be aware of the broadness of the term “intellectual disability” since, in addition to long-term memory deficit and learning impairment, other areas, such as speech development, might also be impaired in humans. These other characteristics cannot be captured by the tests used here. Further, some of the other identified anomalies, such as increased fat deposition and liver steosis in HFD-fed monosomic *Df*$^{Lipi\text{-}Usp25}$ mice, have never been reported in Monosomy 21 indviduals. Conversely, some of the symptoms observed in humans with Sotos syndrome, including cardiac abnormalities and advanced bone age, were not identified in monosomic *Df*$^{4732471D19Rik\text{-}B4galt7}$ mice.

The inability to recapitulate some of the clinical phenotypes identified in patients with deletion syndromes clearly demonstrates the existence of significant developmental differences between mice and humans, and so places certain limitations on the use of mice as a model organism (at least in some cases). Also, we need to be aware that certain phenotypic features that are observed in humans with genomic disorders might be impossible to model or reliably identify in mice. For example, facial abnormalities, such as large/simple ears, nose or broad mouth observed in Monosomy 21 patients or high, broad forehead (the head is said to resemble an inverted pear), fronto-temporal hair sparsity, malar flushing, down-slanting palpebral fissures and a pointed chin observed in Sotos syndrome individuals, cannot be reliably

modelled in mice due to significant differences in facial appearance between mice and humans.

5.3 STRENGTHS AND WEAKNESSES OF THE APPROACH TAKEN AND THE RESULTS GENERATED

We have used chromosome engineering to generate monosomic *Df*$^{Lipi\text{-}Usp25}$ and *Df*$^{4732471D19Rik\text{-}B4galt7}$ mice to model human Monosomy 21 and Sotos syndromes, respectively. The approach taken has both strengths and weaknesses.

One of the important strengths is the similarity between mice and humans, namely they show about 99% gene identity, and have similar developmental programs and physical form. This means that human syndromes, caused by various genetic alterations, can often be accurately modelled in mice.

The other strength is the relative ease of working with mice. There are well-established methods for introducing particular mutations into the mouse genome (such as the deletions described here) which, because of the short mouse gestation period, can be achieved in reasonable time. Mice are also easy to house, as they require little space. Moreover, whilst using mice, many of the ethical considerations related to working with higher mammals can be avoided.

The approach used here offers an efficient method of determining the exact genes that are responsible for a given human phenotype. By initially deleting a chromosomal segment containing multiple genes, it is possible to construct models with successively smaller and smaller deletions, each time narrowing down the region containing the relevant gene. Ultimately, as happened for example in PWS syndrome, it is often possible to finally identify the causative gene accounting for a given syndrome.

Despite these advantages, there are certain disadvantages of working with mice and to the approach applied here. Firstly, although many features of development and anatomy are shared between mice and humans, there are also significant differences and it cannot be assumed that a given feature will be identical between these two organisms. This means that even an exact

model of a given human deletion in mice is never guaranteed to recapitulate the same syndrome. Even if certain phenotypes are shared between human patients and the mouse model, many other phenotypes may differ, and so we can never be sure that the model really represents the human syndrome. Further, certain human phenotypes can never be fully recapitulated in mice due to differences in body shape, anatomy and development. Perhaps it would be also interesting to model human deletions in another organism, perhaps one closer to humans, which might better capture the observed human phenotype.

A further problem is that some of the human genes do not have syntenic counterparts in mice, as is the case with two genes in our mouse model of Monosomy 21. Thus the deletion in mice is only an approximation to the deletion in humans. It is possible that the human genes that do not have mouse counterparts might play an important role in the human syndrome and may explain many of the observed human manifestations.

Another weakness of our approach is that we only use a few selective tests to test a particular phenotypic feature. For example, we use a social recognition test to attempt to search for such a complex condition as intellectual disability. Although it is difficult to devise better-suited tests, using such selective tests can result in misleading findings. For example, just because a group of mice performs normally in the social recognition test, does not necessarily means that they do not have other intellectual disabilities.

Finally, it is worth mentioning that, in our monosomic $Df^{4732471D19Rik\text{-}B4galt7}$ mice, a large number of genes were deleted, and so using this approach to try to determine the causative gene, by generating progressively smaller and smaller deletions, can be both difficult and time-consuming.

5.4 FURTHER STUDIES THAT COULD BE UNDERTAKEN IN BOTH MICE AND HUMANS

In order to better understand and further analyse the initial results obtained from *Lipi-Usp25* and *4732471D19Rik–B4galt7* monosomic mice, further studies in both mice and humans could be undertaken.

Both Monosomy 21 and Sotos syndrome patients are described with intellectual disability. However, this term is very broad and encompasses various intellectual impairments, such as mental retardation, learning disability and speech development. Thus, it would be interesting to re-examine Monosomy 21 and Sotos syndrome patients to clarify the type of intellectual disability. This would be a great help in designing behavioural tests that could be used to test monosomic $Df^{Lipi\text{-}Usp25}$ and $Df^{4732471D19Rik\text{-}B4galt7}$ mice more adequately in order to be able to properly correlate results obtained from mouse models with human data.

Both monosomic $Df^{Lipi\text{-}Usp25}$ and $Df^{4732471D19Rik\text{-}B4galt7}$ mice have shown hippocampal-dependent long-term memory deficit and learning abnormalities in a social recognition paradigm. Further behavioural tests could be conducted, not only to confirm these findings, but also to expand on these results by applying behavioural tests that would be able to model other aspects of human intellectual disability and would be suitable for detecting impairments in different areas of the brain. For example, to confirm the existence of a long-term memory deficit and learning abnormalities in monosomic $Df^{Lipi\text{-}Usp25}$ and $Df^{4732471D19Rik\text{-}B4galt7}$ mice in a non-social context, a novel object recognition test could be applied. For instance, Morris water maze could be used to test for anomalies in spatial learning and memory, or a cued fear conditioning test could be applied to check amygdalar activity, or a contextual fear conditioning test to investigate both amygdalar and hippocampus functioning.

Monosomic $Df^{Lipi\text{-}Usp25}$ mice have shown increased fat deposition when being fed on a high-fat diet. In our study, we were unable to determine a reason for this phenomenon. In order to understand the cause of increased fat deposition, further test could be conducted, including indirect calorimetry testing at a later stage of life of monosomic $Df^{Lipi\text{-}Usp25}$ mice. Also, it might be worth carrying out a microarray analysis on brain samples collected from HFD-fed monosomic $Df^{Lipi\text{-}Usp25}$ mice to try to find genes that might be up- or down-regulated, and so to find the genes that might be contributing to the observed phenotype. Also, it would be of interest to re-examine Monosomy 21 patients for the presence or absence of obesity. Subsequently, if any of the patients are indentified with obesity, it would be important to look into their diet

to investigate whether the observed obesity in these patients was caused by the interaction between the genetic component (deletion of the 21q11.2–q21.1 region) and an environmental factor (such as consumption of food highly-enriched in fat).

Further, in order to establish whether overgrowth, a cardinal feature diagnosed in patients with Sotos syndrome, could be observed in monosomic *Df*$^{4732471D19Rik\text{-}B4galt7}$ mice at pre- and/or postnatal stage of their development, the growth curves should be generated.

Finally, as a long term goal, mouse models carrying smaller and smaller deletions of the initial *Lipi-Usp25* and *4732471D19Rik–B4galt7* intervals could be generated to find the causative genes responsible for, on one hand, long-term memory deficit, learning abnormalities and increased fat percentage in monosomic *Df*$^{Lipi\text{-}Usp25}$ mice, and, on the other hand, for long-term memory deficit, learning abnormalities and a dilation of pelvicalyceal system in monosomic *Df*$^{4732471D19Rik\text{-}B4galt7}$ mice.

To sum up, generation and analysis of monosomic mouse models of Monosomy 21 and Sotos syndrome have broadened our understanding of these human pathologies by recapitulating Monosomy 21-associated intellectual disability and SoS-associated hydronephrosis, as well as revealing previously unreported phenotypes, such as the HFD-induced increase fat deposition in Monosomy 21 mice.

REFERENCES

Adams, D.J., Biggs, P.J., Cox, T., Davies, R., van der Weyden, L., Jonkers, J., Smith, J., Plumb, B., Taylor, R., Nishijima, I., Yu, Y., Rogers, J., Bradley, A. (2004). "Mutagenic Insertion and Chromosome Engineering Resource (MICER)." Nature Genetics **36**(8): 867-871.

Adams, D.J., Quail, M.A., Cox, T., van der Weyden, L., Gorick, B.D., Su, Q., Chan, W., Davies, R., Bonfield, J.K., Law, F., Humphray, S., Plumb, B., Liu, P., Rogers, J., Bradley, A. (2005). "A genome-wide, end-sequenced 129Sv BAC library resource for targeting vector construction." Genomics **86**(6): 753-758.

Ahlbom, B., Sidenvall, R., Anneren, G. (1996). "Deletion of chromosome 21 in a girl with congenital hypothyroidism and mild mental retardation." American Journal of Medical Genetics **64**: 501-505.

Aoki, M., Yamamoto, K., Ohyama, S., Yamamura, Y., Takenoshita, S., Sugano, K., Minamoto, T., Kitajima, M., Sugimura, H., Shimada, S. (2005). "A genetic variant in the gene encoding the stress 70 protein chaperone family member STCH is associated with gastric cancer in the Japanese population." Biochemical and Biophysical Research Communications **335**(2): 566-574.

Aoki, M., Yamamura, Y., Noshiro, H., Sakai, K., Yokota, J., Kohno, T., Tokino, T., Ishida, S., Ohyama, S., Ninomiya, I., Uesaka, K., Kitajima, M., Shimada, S., Matsuno, S., Yano, M., Hiratsuka, M., Sugimura, H., Itoh, F., Minamoto, T., Maehara, Y., Takenoshita, S., Aikou, T., Katai, H., Yoshimura, K., Takahashi, T., Akagi, K., Sairenji, M., Yamamoto, K., Sasazuki, T. (2005). "A full genome scan for gastric cancer." Journal of Medical Genetics **42**: 83-87.

Asnicar, M.A., Smith, D.P., Yang, D.D., Heiman, M.L., Fox, N., Chen, Y.F., Hsiung, H.M., Koster, A. (2001). "Absence of cocaine- and amphetamine-regulated transcript results in obesity in mice fed a high caloric diet." Endocrinology **142**(10): 4394-4400.

Baldini, A., Lindsay, E.A. (1994). "Mapping human YAC clones by fluorescence in situ hybridization using Ah-PCR from single yeast colonies." Methods in Molecular Biology **33**: 75-84.

Baujat, G., Cormier-Daire, V. (2007). "Sotos syndrome." Orphanet Journal of Rare Diseases **2**(1): 1-6.

Benjamini, Y., Yekutieli, D. (2001). "The control of the false discovery rate in multiple testing under dependency." The Annals of Statistics **29, No. 4**: 1165-1188.

Besson, V., Brault, V., Duchon, A., Togbe, D., Bizot, J. C., Quesniaux, V.F.J., Ryffel, B., Herault, Y. (2007). "Modeling the monosomy for the telomeric part of human chromosome 21 reveals haploinsufficient genes modulating the inflammatory and airway responses." Human Molecular Genetics **16(17)**: 2040-2052.

Bi, W., Ohyama, T., Nakamura, H., Yan, J., Visvanathan, J., Justice, M.J., Lupski, J.R. (2005). "Inactivation of Rai1 in mice recapitulates phenotypes observed in chromosome engineered mouse models for Smith-Magenis syndrome." Human Molecular Genetics **14**(8): 983-995.

Bosch-Comas, A., Lindsten, K., Gonzàlez-Duarte, R., Masucci, M.G., Marfany, G. (2006). "The ubiquitin-specific protease USP25 interacts with three sarcomeric proteins." Cellular and Molecular Life Sciences **63**: 723-734.

Bouchard, C., Tremblay, A., Despres, J.P., Nadeau, A., Lupien, P.J., Theriault, G., Dussault, J., Moorjani, S., Pinault, S., Fournier G. (1990). "The response to the long-term overfeeding in identical twins." New England Journal of Medicine **322**(21): 1477-1482.

Bradley A., Evans, M., Kaufman M.H., Robertson E. (1984). "Formation of germ-line chimaeras from embryo-derived teratocarcinoma cell lines." Nature **309**(5965): 255-256.

Brun, M.E., Ruault, M., Ventura, M., Roizes, G., De Sario, A. (2003). "Juxtacentromeric region of human chromosome 21: a boundary between centromeric heterochromatin and euchromatic chromosome arms." Gene **312**: 41-50.

Buiting, K. (2010). "Prader-Willi syndrome and Angelman syndrome." American Journal of Medical Genetics Part C: Seminars in Medical Genetics **154C**(3): 365-376.

Cattanach, B.M., Barr, J.A., Evans, E.P., Burtenshaw, M., Beechey, C.V., Leff, S.E., Brannan, C.I., Copeland, N.G., Jenkins, N.A., Jones, J. (1992). "A candidate mouse model for Prader-Willi syndrome which shows an absence of Snrpn expression." Nature Genetics **2**(4).

Cavailles, V., Dauvois, S., L'Horset, F., Lopez, G., Hoare, S., Kushner, P.J., Parker, M.J. (1995). "Nuclear factor RIP140 modulates transcriptional activation by the estrogen receptor." The EMBO Journal **14**(15): 3741-3751.

Cecconi, M., Forzano, F., Milani, D., Cavani, S., Baldo, C., Selicorni, A., Pantaleoni, C., Silengo, M., Ferrero, G.B., Scarano, G., Della Monica, M., Fischetto, R., Grammatico, P., Majore, S., Zampino, G., Memo, L., Cordisco, E.L., Neri, G., Pierluigi, M., Bricarelli, F.D., Grasso, M. Faravelli, F. (2005). "Mutation analysis of the NSD1 gene in a group of 59 patients with congenital overgrowth." American Journal of Medical Genetics Part A **134A**(3): 247-253.

Chen, L., Pik Wong, M., Kwong Cheung, L., Samaranayake, L.P., Baum, L., Samman, N. (2005). "Frequent allelic loss of 21q11.1~q21.1 region in advanced stage oral squamous cell carcinoma." Cancer Genetics and Cytogenetics **159**: 37-43.

Chettouh, Z., Croquette, M.F., Delobel, B., Gilgenkrants, S., Leonard,C., Maunoury, C., Prieur, M., Rethore, M.O., Sinet,' P.M., Chery, M., Delabar J.M. (1995). "Molecular mapping of 21 features associated with partial monosomy 21: involvement of the APP-SOD1 region." American Journal of Human Genetics **57(1)**: 62-71.

Claudio, J.O., Zhu, Y.X., Benn, S.J., Shukla, A.H., McGlade, C.J., Falcioni, N., Stewart, A.K. (2001). "HACS1 encodes a novel SH3-SAM adaptor protein diferentially expressed in normal and malignant hematopoietic cells." Oncogene **20**: 5373-5377.

Cliby, W., Ritland, S., Hartmann, R., Dodson, M., Hailing, K.C., Keeney, G., Podratz, K.C., Jenkins, R.B. (1993). "Human epithelial ovarian cancer allelotype." Cancer Research **53**: 2393-2398.

Cole, T.R.P., Hughes, H.E (1994). "Sotos syndrome: a study of the diagnostic criteria and natural history." Journal of Medical Genetics **31**: 20-32.

Corral, J., Lavenir, I., Impey ,H., Warren, A.J., Forster, A., Larson, T.A., Bell, S., McKenzie, A.N.J., King, G., Rabbitts, T.H. (1996). "An Mll-Af 9 fusion gene made by homologous recombination causes acute leukemia in chimeric mice: a method to create fusion oncogenes." Cell **85**: 853-861.

Davies, B.S.J., Barnes, R.H., Tu, Y., Ren, S., Andres, D.A., Spielmann, H.P., Lammerding, J., Wang, Y., Young, S.G., Fong, L.G. (2010). "An accumulation of non-farnesylated prelamin A causes cardiomyopathy but not progeria." Human Molecular Genetics **19**(13): 2682-2694.

Davies, B.S.J., Yang, S.H., Farber, E., Lee, R., Buck, S.B., Andres, D.A., Spielmann, H.P., Agnew, B.J., Tamanoi, F., Fong, L.G., Young, S.G. (2008). "Increasing the length of progerin's isoprenyl anchor does not worsen bone disease or survival in mice with Hutchinson-Gilford progeria syndrome." Journal of Lipid Research **50**(1): 126-134.

DiGeorge, A.M. (1968). "Congenital absence of the thymus and its immunologic consequences: concurrence with congenital hypoparathyroidism. White Plains, New York: March of Dimes-Birth Defects Foundation." Birth Defects **IV**(1): 116-121.

Ding, F., Prints, Y., Dhar, M.S., Johnson, D.K., Garnacho–Montero, C., Nicholls, R.D., Francke, U. (2005). "Lack of Pwcr1/MBII-85 snoRNA is critical for neonatal lethality in Prader–Willi syndrome mouse models." Mammalian Genome **16**(6): 424-431.

dos Santos Aguiar, S., de Jesus Girotto Zambaldi, L., dos Santos, A.M., Pinto Jr., W., Brandalise, S.R. (2007). "Comparative genomic hybridization analysis of abnormalities in chromosome 21 in childhood osteosarcoma." Cancer Genetics and Cytogenetics **175**: 35-40.

Douglas, J., Tatton-Brown, K., Coleman, K., Guerrero, S., Berg, J., Cole, T.R.P., FitzPatrick, D., Gillerot, Y., Hughes, H.E., Pilz, D., Raymond, F.L., Temple, I.K., Irrthum, A., Schouten, J.P., Rahman, N. (2005). "Partial NSD1 deletions cause 5% of Sotos syndrome and are readily identifiable by multiplex ligation dependent probe amplification." Journal of Medical Genetics **42**(9): 1-7.

Elsea, S.H., Girirajan, S. (2008). "Smith–Magenis syndrome." European Journal of Human Genetics **16**(4): 412-421.

Engelmann, M., Hädicke, J., Noack, J. (2011). "Testing declarative memory in laboratory rats and mice using the nonconditioned social discrimination procedure." Nature Protocols **6**(8): 1152-1162.

Evans, M.J., Kaufman, M.H. (1981). "Establishment in culture of pluripotential cells from mouse embryos." Nature **292**(5819): 154-156.

Faravelli, F. (2005). "NSD1 mutations in Sotos syndrome." American Journal of Medical Genetics Part C **137C**: 24-31.

Firth, H.V., Richards, S.M., Bevan, A.P., Clayton, S., Corpas, M., Rajan, D., van Vooren, S., Moreau, Y., Pettett, R.M., Carter N.P. (2009). "DECIPHER: Database of Chromosomal Imbalance and Phenotype in Humans Using Ensembl Resources." American Journal of Human Genetics **84**: 524-533.

Foell, J.L., Hesse, M., Volkmer, I., Schmiedel, B.J., Neumann, I., Staege, M.S. (2008). "Membrane-associated phospholipase A1 beta (LIPI) is an Ewing tumour-associated cancer/testis antigen." Pediatrian Blood Cancer **51**: 228-234.

Fong, L., Ng, J.K., Lammerding, J., Vickers, T.E., Meta, M., Coté, N., Gavino, B., Qiao, X., Chang, S.Y., Young, S.R., Yang, S.H., Stewart, C.L., Lee, R.T., Bennett, C.F., Bergo, M.O., Young, S.G. (2006). "Prelamin A and lamin A appear to be dispensable in the nuclear lamina." Journal of Clinical Investigation **116**(3): 743-752.

Frazer, K.A., Sheehan, J.B., Stokowski, R.P., Chen, X., Hosseini, R., Cheng, J.F, Fodor, S.P.A., Cox, D.R., Patil N. (2001). "Evolutionarily conserved sequences on human chromosome 21." Genome Research **11**: 1651–1659.

Gitler, A.D., Lu, M.M., Epstein, J.A. (2004). "PlexinD1 and semaphorin signaling are required in endothelial cells for cardiovascular development." Developmental Cell **7**(1): 107-116.

Groet, J., Ives, J.H., Jones, T.A., Danton, M., Flomen, R.H., Sheer, D., Hrascan, R., Pavelic, K., Nizetic, D. (2000). "Narrowing of the region of allelic loss in 21q11-21 in squamous non-small cell lung carcinoma and

cloning of a novel ubiquitin-specific protease gene from the deleted segment." Genes, Chromosomes & Cancer **27**: 153-161.

Gu, W., Zhang, F., Lupski, J.R (2008). "Mechanisms for human genomic rearrangements." Pathogenetics **1**(1):4: 1-17.

Guo, G., Wang, W., Bradley, A. (2004). "Mismatch repair genes identified using genetic screens in Blm-deficient embryonic stem cells." Nature **429**: 891-895.

Hasle, H., Haunstrup Clemmensen, I., Mikkelsen, M. (2000). "Risks of leukaemia and solid tumours in individuals with Down's syndrome." Lancet **355**: 165-169.

Hattori, M., Fujiyama, A., Taylor, T.D., Watanabe, H., Yada, T., Park, H.S., Toyoda, A., Ishii, K., Totoki, Y., Choi, D.K., Groner, Y., Soeda, E., Ohki, M., Takagi, T., Sakaki, Y., Taudien, S., Blechschmidt, K., Polley, A., Menzel, U., Delabar, J., Kumpf, K., Lehmann, R., Patterson, D., Reichwald, K., Rump, A., Schillhabel, M., Schudy, A., Zimmermann, W., Rosenthal, A., Kudoh, J., Schibuya, K., Kawasaki, K., Asakawa, S., Shintani, A., Sasaki, T., Nagamine, K., Mitsuyama, S., Antonarakis, S.E., Minoshima, S., Shimizu, N., Nordsiek, G., Hornischer, K., Brant, P., Scharfe M, Schon O, Desario A, Reichelt J, Kauer G, Blocker H, Ramser J, Beck A, Klages S, Hennig S, Riesselmann L, Dagand E, Haaf T, Wehrmeyer S, Borzym K, Gardiner, K., Nizetic, D., Francis, F., Lehrach, H., Reinhardt, R., Yaspo, M.L.; Chromosome 21 mapping and sequencing consortium (2000). "The DNA sequence of human chromosome 21." Nature **405**: 311-319.

Hegele, R.A., Cao, H., Harris, S.B., Zinman, B., Hanley, A.J., Anderson, C.M. (2000). "Genetic variation in LMNA modulates plasma leptin and indices of obesity in aboriginal Canadians." Physiological Genomics **3**: 39-44.

Hegele, R.A., Murray W.H., Young T.K. (2001). "Common genomic variation in LMNA modulates indexes of obesity in Inuit." Journal of Clinical Endocrinology & Metabolism **86**(6): 2747-2751.

Heim, K.C., White, K.A., Deng, D., Tomlinson, C.R., Moore, J.H, Freemantle, S.J., Spinella, M.J. (2007). "Selective repression of retinoic acid target

genes by RIP140 during induced tumor cell differentiation of pluripotent human embryonal carcinoma cells." Molecular Cancer **6:57**: 1-18.

Heitmann, B.L., Lissner, L., Sorensen, T.I.A, Bengtsson C. (1995). "Dietary fat intake and weight gain in women genetically predisposed for obesity." American Journal in Clinical Nutrition **61**.

Hiramatsu, T., Sonoda, H., Takanezawa, Y., Morikawa, R., Ishida, M., Kasahara, K., Sanai, Y., Taguchi, R., Aoki, J., Arai, H. (2003). "Biochemical and molecular characterization of two phosphatidic acid-selective phospholipase A1s, mPA-PLA1 and mPA-PLA1." The Journal of Biological Chemistry **278**(49): 49438-49447.

Holecki, M., Wiecek, A. (2010). "Relationship between body fat mass and bone metabolism." Polskie Archiwum Medycyny Wewnetrznej **120**(9): 361-367.

Hoogenraad, C.C., Koekkoek, B., Akhmanova, A., Krugers, H., Dortland, B., Miedema, M., van Alphen, A., Kistler, W.M., Jaegle, M., Koutsourakis, M., Van Camp, N., Verhoye, M., van der Linden, A., Kaverina, I., Grosveld, F., De Zeeuw, C.I., Galjart, N. (2002). "Targeted mutation of Cyln2 in the Williams syndrome critical region links CLIP-115 haploinsufficiency to neurodevelopmental abnormalities in mice." Nature Genetics **32**(1): 116-127.

Huang, N., vom Baur, E., Garnier, J.M., Lerouge, T., Vonesch, J.L., Lutz, Y., Chambon, P., Losson, R. (1998). "Two distinct nuclear receptor interaction domains in NSD1, a novel SET protein that exhibits characteristics of both corepressors and coactivators." European Molecular Biology Organisation Journal **17**(12): 3398–3412.

Hubbard, T.J., Aken, B.L., Beal, K., Ballester, B., Caccamo, M., Chen, Y., Clarke, L., Coates, G., Cunningham, F., Cutts, T., Down, T., Dyer, S.C., Fitzgerald, S., Fernandez-Banet, J., Graf, S., Haider, S., Hammond, M., Herrero, J., Holland, R., Howe, K., Howe, K., Johnson, N., Kahari, A., Keefe, D., Kokocinski, F., Kulesha, E., Lawson, D., Longden, I., Melsopp, C., Megy, K., Meidl, P., Ouverdin, B., Parker, A., Prlic, A., Rice, S., Rios, D., Schuster, M., Sealy, I., Severin, J., Slater, G., Smedley, D., Spudich, G., Trevanion, S., Vilella, A., Vogel, J., White, S., Wood, M., Cox, T., Curwen, V., Durbin, R., Fernandez-

Suarez, X.M., Flicek, P., Kasprzyk, A., Proctor, G., Searle, S., Smith, J., Ureta-Vidal, A,. Birney, E. (2007). "Ensembl 2007." Nucleic Acids Research **35**(D6): 10-17.

Iliopoulos, D., Sekerli, E., Vassiliou, G., Sidiropoulou, V., Topalidis, A., Dimopoulou, D., Voyiatzis, N. (2006). "Patau syndrome with a long survival (146 months): A clinical report and review of literature." American Journal of Medical Genetics Part A **140A**(1): 92-93.

Jenuwein, T., Laible, G., Dorn, R., Reuter, G. (1998). "SET domain proteins modulate chromatin domains in eu- and heterochromatin." Cellular and Molecular Life Sciences **54**: 80-93.

Jiang, Y.H., Armstrong, D., Albrecht, U., Atkins, C.M., Noebels, J.L., Eichele, G., Sweatt, D.J., Beaudet, A.L. (1998). "Mutation of the Angelman ubiquitin ligase in mice causes increased cytoplasmic p53 and deficits of contextual learning and long-term potentiation." Neuron **21**: 799-811.

Joosten, A.M.S., de Vos, S., van Opstal, D., Brandenburg H., Gaillard, J.L.J., Vermeij-Keers, C. (1996). "Full monosomy 21, prenatally diagnosed by fluorescent in situ hybrydyzation." Prenatal Diagnosis **17(3)**: 271-275.

Katzaki, E., Morin, G., Pollazzon, M., Papa, F.T., Buoni, S., Hayek, J., Andrieux, J., Lecerf, L., Popovici, C., Receveur, A., Mathieu-Dramard, M., Renieri, A., Mari, F., Philip, N. (2010). "Syndromic mental retardation with thrombocytopenia due to 21q22.11q22.12 deletion: Report of three patients." American Journal of Medical Genetics Part A **152A(7)**: 1711-1717.

Katzenstein, J.M., Oghalai, J.S., Tonini, R., Baker, D., Haymond, J., Caudle, S.E. (2009). "Neurocognitive functioning of a child with partial trisomy 6 and monosomy 21." Neurocase **15**(2): 97-100.

Kesler, S.R. (2007). "Turner Syndrome." Child and Adolescent Psychiatric Clinics of North America **16**(3): 709-722.

Kimber, W.L., Hsieh, P., Hirotsune, S., Yuva-Paylor, L., Sutherland, H.F., Chen, A., Ruiz-Lozano, P., Hoogstraten-Miller, S.L., Chien, K.R., Paylor, R., Scambler, P.J., Wynshaw-Boris, A. (1999). "Deletion of 150 kb in the minimal DiGeorge/velocardiofacial syndrome critical region in mouse." Human Molecular Genetics **8**(12): 229-2237.

Kogan, J.H., Frankland, P.W., Silva, A.J. (2000). "Long-term memory underlying hippocampus-dependent social recognition in mice." Hippocampus **10**(1): 47-56.

Kohno, T., Kawanishi, M., Matsuda, S., Ichikawa, H., Takada, M., Ohki, M., Yamamoto, T., Yokota, J. (1998). "Homozygous deletion and frequent allelic loss of the 21q11.1-q21.1 region including the ANA gene in human lung carcinoma." Genes, Chromosomes & Cancer **21**: 236-243.

Korenberg, J.R., Kalousek, D.K., Anneren, G., Pulst, S.M., Hall, J.G., Epstein, C.J., Cox, D.R. (1991). "Deletion of chromosome 21 and normal intelligence: molecular definition of the lesion." Human Genetics **87**: 112-118.

Kucera, G.T., Bortner, D.M., Rosenberg, M.P. (1996). "Overexpression of an Agouti cDNA in the skin of transgenic mice recapitulates dominant coat color phenotypes of spontaneous mutants." Developmental Biology **173**(162-173).

Kurotaki, N., Harada, N., Shimokawa, O., Miyake, N., Kawame, H., Uetake, K., Makita, Y., Kondoh, T., Ogata, T., Hasegawa, T., Nagai, T., Ozaki, T., Touyama, M., Shenhav, R., Ohashi, H., Medne, L., Shiihara, T., Ohtsu, S., Kato, Z., Okamoto, N., Nishimoto, J., Lev, D., Miyoshi, Y., Ishikiriyama, S., Sonoda, T., Sakazume, S., Fukushima, Y., Kurosawa, K., Cheng, J.F., Yoshiura, K., Ohta, T., Kishino, T., Niikawa, N., Matsumoto, N. (2003). "Fifty microdeletions among 112 cases of Sotos syndrome: Low copy repeats possibly mediate the common deletion." Human Mutation **22**(5): 378-387.

Kurotaki, N., Harada, N., Yoshiura, K., Sugano, S., Niikawa, N., Matsumoto, N. (2001). "Molecular characterization of NSD1, a human homologue of the mouse Nsd1 gene." Gene **279**: 197-204.

Kurotaki, N., Imaizumi, K., Harada, N., Masuno, M., Kondoh, T., Nagai, T., Ohashi, H., Naritomi, K., Tsukahara, M., Makita, Y., Sugimoto, T., Sonoda, T., Hasegawa, T., Chinen, Y.,Tomita, H., Kinoshita, A., Mizuguchi, T., Yoshiura, K., Ohta, T., Kishino, T., Fukushima, Y., Niikawa, N., Matsumoto, N. (2002). "Haploinsufficiency of NSD1 causes Sotos syndrome." Nature Genetics **30**(4): 365-366.

Leonardsson, G., Steel J.H., Christian M., Pocock, V., Milligan, S., Bell, J., So, P.W., Medina-Gomez, G., Vidal-Puig, A., White, R., Parker, M.G. (2004). "Nuclear receptor corepressor RIP140 regulates fat accumulation." Proceedings of the National Academy of Sciences **101**(22): 8437-8442.

Li, H.H., Roy, M., Kuscuoglu, U., Spencer, C.M., Halm, B., Harrison, K.C., Bayle, J.H., Splendore, A., Ding, F., Meltzer, L.A., Wright, E., Paylor, R., Deisseroth, K., Francke, U. (2009). "Induced chromosome deletions cause hypersociability and other features of Williams–Beuren syndrome in mice." EMBO Molecular Medicine **1**: 50-65.

Linday, E.A. (2001). "Chromosomal microdeletions: dissecting Del22q11 syndrome." Nature Reviews in Genetics **2**(11): 858-868.

Lindsay, E.A., Botta, A., Jurecic, V., Carattini-Rivera, S., Cheah, Y.C., Rosenblatt, H.M., Bradley, A., Baldini, A. (1999). "Congenital heart disease in mice deficient for the DiGeorge syndrome region." Nature **401**: 379-383.

Lindsay, E.A., Vitelli, F., Su, H., Morishima, M., Huynh, T., Pramparo, T., Jurecic, V., Ogunrinu, G., Sutherland, H.F., Scambler, P.J., Bradley, A., Baldini, A. (2001). "Tbx1 haploinsufficiency in the DiGeorge syndrome region causes aortic arch defects in mice." Nature **410**: 97-101.

Lindstrand, A., Malmgren, H., Sahlen, S., Schoumans, J., Nordgren, A., Ergander, U., Holm, E., Anderlid, B.M., Blennow, E. (2010). "Detailed molecular and clinical characterization of three patients with 21q deletions." Clinical Genetetics **77**: 145-154.

Liu, P., Zhang, H., McLellan, A., Vogel, H., Bradley, A. (1998). "Embryonic lethality and tumorigenesis caused by segmental aneuploidy on mouse chromosome 11." Genetics **150**: 1155-1168.

Livak, K.J., Schmittgen, T.D. (2001). "Analysis of relative gene expression data using real-time quantitative PCR and the 22DDCT method." Methods **25**: 402-408.

Luan, J., Browne, P.O., Harding, A.H., Halsall, D.J., O'Rahilly, S., Chatterjee, V.K.K, Wareham N.J. (2001). "Evidence for gene-nutrient interaction at the PPARg locus." Diabetes **50**: 686-689.

Luo, G., Santoro, I.M., McDaniel, L.D., Nishijima, I., Mills, M., Youssoufian, H., Vogel, H., Schultz, R.A., Bradley, A. (2000). "Cancer predisposition caused by elevated mitotic recombination in Bloom mice." Nature Genetics **26**: 424-429.

Lyle, R., Béna, F., Gagos, S., Gehrig, C., Lopez, G., Schinzel, A., Lespinasse, J., Bottani, A., Dahoun, S., Taine, L., Doco-Fenzy, M., Cornillet-Lefèbvre, P., Pelet, A., Lyonnet, S., Toutain, A., Colleaux, L., Horst, J., Kennerknecht, I., Wakamatsu, N., Descartes, M., Franklin, J.C., Florentin-Arar, L., Kitsiou, S., Yahya-Graison, E.A., Maher, C., Sinet, P.M., Delabar, J.M., Antonarakis, S.E. (2008). "Genotype–phenotype correlations in Down syndrome identified by array CGH in 30 cases of partial trisomy and partial monosomy chromosome 21." European Journal of Human Genetics **17(4)**: 454-466.

Mégarbané, A., Ravel, A., Mircher, C., Sturtz, F., Grattau, Y., Rethoré, M.O., Delabar, J.M., Mobley, W.C. (2009). "The 50th anniversary of the discovery of trisomy 21: The past, present, and future of research and treatment of Down syndrome." Genetics in Medicine **11**(9): 611-616.

Merscher, S., Funke, B., Epstein, J.A., Heyer, J., Puech, A., Lu, M.M., Xavier, R.J., Demay, M.B., Russell, R.G., Jore, B.S., Lopez, M., Pandita,R.K., Lia, M., Carrion, D., Xu, H., Schorle, H., Kobler, J.B., Scambler, P., Wynshaw-Boris, A., Skoultchi, A.I., Morrow, B.E., Kucherlapati, R. (2001). "TBX1 Is Responsible for Cardiovascular Defects in Velo-Cardio-Facial/DiGeorge Syndrome." Cell **104**: 619-629.

Mitelman, F., Mertens, F., Johansson, B. (1997). "A breakpoint map of recurrent chromosomal rearrangements in human neoplasia." Nature Genetics Special Issue: 417-474.

Mitsui, S., Osako, Y., Yokoi, F., Dang, M.T.,Yuri, K., Li, Y., Yamaguchi, N. (2009). "A mental retardation gene, motopsin/neurotrypsin/prss12, modulates hippocampal function and social interaction." European Journal of Neuroscience **30**(12): 2368-2378.

Mori, M.A., Lapunzina, P., Delicado, A., Nunez, G., Rodriguez, J.I., de Torres, M.L., Herrero, F., Valverde, E., Lopez-Pajares, I. (2004). "A prenatally diagnosed patient with full monosomy 21: Ultrasound, cytogenetic,

clinical, molecular, and necropsy findings." American Journal of Medical Genetics **127A**(1): 69-73.

Nagai, T., Matsumoto, N., Kurotaki, N., Harada, N., Niikawa, N., Ogata, T., Imaizumi, K.,Kurosawa, K., Kondoh, T., Ohashi, H., Tsukahara, M., Makita, Y., Sugimoto, T., Sonoda, T., Yokoyama, T., Uetake, K., Sakazume, S., Fukushima, Y., Naritomi, K. (2003). "Sotos syndrome and haploinsufficiency of NSD1: clinical features of intragenic mutations and submicroscopic deletions." Journal of Medical Genetics **40**: 285-289.

Nieters, A., Becker, N., Linseisen, J. (2002). "Polymorphisms in candidate obesity genes and their interaction with dietary intake of n-6 polyunsaturated fatty acids affect obesity risk in a sub-sample of the EPIC-Heidelberg cohort." European Journal of Nutrition **41**(5): 210-221.

O'Gorman, S., Dagenais, N.A., Qian, M., Marchuk, Y. (1997). "Protamine-Cre recombinase transgenes efficiently recombine target sequences in the male germ line of mice, but not in embryonic stem cells." Proceedings of the National Academy of Sciences of the United States of America **94**: 14602–14607.

Ohgaki, K., Iida, A., Kasumi, F., Sakamoto, G., Akimoto, M., Nakamura, Y., Emi, M. (1998). "Mapping of a new target region of allelic loss to a 6-cM interval at 21q21 in primary breast cancers." Genes, Chromosomes & Cancer(23): 244-247.

Olson, L.E., Richtsmeier, J.T., Leszl, J., Reeves, R.H. (2004). "A chromosome 21 critical region does not cause specific Down syndrome phenotypes." Science **306(5696)**: 687-690.

Olson, L.E., Roper, R.J., Baxter, L.L., Carlson, E.J., Epstein, C.J., Reeves, R.H. (2004). "Down syndrome mouse models Ts65Dn, Ts1Cje, and Ms1Cje/Ts65Dn exhibit variable severity of cerebellar phenotypes." Developmental Dynamics **230**(3): 581-589.

Olson, L.E., Roper, R.J., Sengstaken, C.L., Peterson, E.A., Aquino, V., Galdzicki, Z., Siarey, R., Pletnikov, M., Moran, T.H., Reeves, R.H. (2007). "Trisomy for the Down syndrome 'critical region' is necessary

but not sufficient for brain phenotypes of trisomic mice." Human Molecular Genetics **16(7)**: 774-4782.

Otterson, G.A., Flynn, G.C., Kratzkel, R.A., Coxon, A., Johnston, P.G., Kaye, F.J. (1994). "Stch encodes the 'ATPase core' of a microsomal stress70 protein." The EMBO Journal **13**(5): 1216-1225.

Overbeek, P.A., Aguilar-Cordova, E.,Hanten, G., Schaffner, D.L., Patel, P., Lebovitz, R.M., Lieberman, M.W. (1991). "Coinjection strategy for visual identification of transgenic mice." Transgenic Research **1**: 31-37.

Poehlman, E.T., Tremblay, A., Despres, J.P., Fontaine, E., Perusse, L., Theriault, G., Bouchard, C. (1986). "Genotype-controlled changes in body composition and fat morphology following overfeeding in twins." American Journal of Clinical Nutrition(43): 723-731.

Prader, A., Labhart, A., Willi, H. (1956). "Ein Syndrom von Adipositas, Kleinwuchs, Kryptorchismus und Oligophrenie nach Myatonieartigem Zustand im Neugeborenenalter." Schweizerische Medizinische Wochenschrift **86**: 1260-1261.

Puech, A., Saint-Jore, B., Merscher, S., Russell, R.G., Cherif, D., Sirotkin, H., Xu, H., Factor, S., Kucherlapati, R., Skoultchi, A.I. (2000). "Normal cardiovascular development in mice deficient for 16 genes in 550 kb of the velocardiofacialy DiGeorge syndrome region." Proceedings of the National Academy of Sciences **97**(18): 10090-10095.

Rabbitt, T.H. (1994). "Chromosomal translocations in human cancer." Nature **372**: 143-149.

Ramirez-Solis, R., Davis, A.C., Bradley, A. (1993). "Gene targeting in embryonic stem cells." Methods in Enzymology **225**: 855-878.

Ramirez-Solis, R., Liu, P., Bradley, A. (1995). "Chromosome engineering in mice." Nature **378**: 720-724.

Reymond, A., Marigo, V., Yaylaoglu, M.B., Leoni, A., Ucla, C., Scamuffa, N., Caccioppoli, C., Dermitzakis, E.T., Lyle, R., Banfi, S., Eichele, G., Antonarakis, S.E., Ballabio, A. (2002). "Human chromosome 21 gene expression atlas in the mouse." Nature **420**(6915): 582-586.

Richter, K., Wolf, G., Engelmann, M. (2005). "Social recognition memory requires two stages of protein synthesis in mice." Learning & Memory **12**(4): 407-413.

Riegel, M., Hargreaves. P., Baumer, A., Guc-Scekic, M., Ignjatovic, M., Schinzel A. (2005). "Unbalanced 18q/21q translocation in a patient previously reported as monosomy 21." European Journal of Medical Genetics **48(2)**: 167-174.

Roberson, E.D.O., Squibb Wohler, E.S., Hoover-Fong, J.E., Lisi, E., Stevens, E.L., Thomas, G.H., Leonard, J., Hamosh, A., Pevsner, J. (2010). "Genomic analysis of partial 21q monosomies with variable phenotypes." European Journal of Human Genetics **19(2)**: 235-238.

Robertson, E. (1987). "Embryo-derived stem cell lines. In Robertson, E. (ed.), Teratocarcinomas and embryonic stem cells – a practical approach." IRL Press, Oxford, UK: 77-112.

Roland, B., Cox, M., Hoar, D.I., Fowlowan, S.B., Robertson, A.S. (1990). "A familial interstitial deletion of the long arm of chromosome 21." Clinical Genetics **31**: 423-428.

Sago, H., Carlson, E.J., Smith, D.J., Kilbridge, J., Rubin, E.M.,. Mobley, W.C, Epstein C.J., Huang,T.T (1998). "Ts1Cje, a partial trisomy 16 mouse model for Down syndrome, exhibits learning and behavioral abnormalities." Protocols of National Academy of Science USA **95**: 6256-6261.

Sakata, K., Tamura, G., Nishizuka, S., Maesawa, C., Suzuki, Y., Iwaya, T., Terashima, M., Saito, K., Satodate, R. (1997). "Commonly deleted regions on the long arm of chromosome 21 in differentiated adenocarcinoma of the stomach." Genes, Chromosomes & Cancer **18**: 318-321.

Sato, M., Kawakami, T., Kondoh, M., Takiguchi, M., Kadota, Y., Himeno, S., Suzuki, S. (2010). "Development of high-fat-diet-induced obesity in female metallothionein-null mice." FASEB Journal **24**(7): 2375-2384.

Sato, S., Nakamura, Y., Tsuchiya, E. (1994). "Difference of allelotype between squamous cell carcinoma and adenocarcinoma of the lung." Cancer Research **54**: 5652-5655.

Sauer, B., Henderson, N. (1988). "Site-specific DNA recombination in mammalian cells by the Cre recombinase of bacteriophage P1." Proceedings of the National Academy of Sciences of the United States of America **85**(14): 5166-5170.

Saugier-Veber, P., Bonnet, C., Afenjar, A., Drouin-Garraud, V., Coubes, C., Fehrenbach, S., Holder-Espinasse, M., Roume, J., Malan, V., Portnoi, M.F., Jeanne, N., Baumann, C., Héron, D., David, A., Gérard, M., Bonneau, D., Lacombe, D., Cormier-Daire, V., Billette de Villemeur, T., Frébourg, T., Bürglen, L. (2007). "Heterogeneity of NSD1 alterations in 116 patients with Sotos syndrome." Human Mutation **28**(11): 1098-1107.

Shaffer, L.G., Lupski, J.R. (2009). "Molecular mechanisms for constitutional chromosomal rearrangements in humans " Annual Reviews in Genetics **34**: 297-329.

Skryabin, B.V., Gubar, L.V., Seeger, B., Pfeiffer, J., Handel, S., Robeck, T., Karpova, E., Rozhdestvensky, T.S., Brosius, J. (2007). "Deletion of the MBII-85 snoRNA gene cluster in mice results in postnatal growth retardation." PLoS Genetics **3**(12): 2529-2539.

Smith, A.C., McGavran, L., Robinson, J., Waldstein, G., Macfarlane, J., Zonona, J., Reiss, J., Lahr, M., Allen, L., Magenis, E. (1986). "Interstitial deletion of (17)(p11.2p11.2) in nine patients." American Journal of Medical Genetics **24**(3): 393-414.

Smith, A.G. (1991). "Culture and differentation of embryonic stem cells." Journal of Tissue Culture Methods **13**: 89-94.

Smyth, G.K. (2004). "Linear models and empirical bayes methods for assessing differential expression in microarray experiments." Statistical Applications in Genetics and Molecular Biology **3, No. 1, Article 3**: 1-26.

Sotos, J.F., Dodge, P.R., Muirhead, D., Crawford, J.D., Talbot, N.B. (1964). "Cerebral gigantism in childhood – a syndrome of excessively rapid growth with acromegalic features and a nonprogressive neurologic disorder." New England Journal of Medicine **271**: 109-116.

Stec, I., Nagl, S.B., van Ommen, G.J.B., den Dunnen, J.T. (2000). "The PWWP domain: a potential protein-protein interaction domain in nuclear proteins infuencing differentiation." FEBS Letters **473**: 1-5.

Stubbs, L., Carver, E.A., Cacheiro, N.L., Shelby, M., Generoso, W. (1997). "Generation and characterization of heritable reciprocal translocations in mice." Methods **13**(4): 397-408.

Sullivan, T., Escalante-Alcalde, D., Bhatt, H., Anver, M., Bhat, N., Nagashima, K., Stewart, C.L., Burke, B. (1999). "Loss of A-type lamin expression compromises nuclear envelope integrity leading to muscular dystrophy." Journal of Cell Biology **147**(5): 913-919.

Tartaglia, N.R., Howell, S., Sutherland, A., Wilson, R., Wilson, L. (2010). "A review of trisomy X (47,XXX)." Orphanet Journal of Rare Diseases **5**(1): 1-9.

Tatton-Brown, K., Douglas, J., Coleman, K., Baujat, G., Chandler, K., Clarke, A., Collins, A., Davies, S., Faravelli, F., Firth, H., Garrett, C., Hughes, H., Kerr, B., Liebelt, J., Reardon, W, Schaefer, G.B., Splitt, M., Temple, I.K., Waggoner, D., Weaver, D.D, Wilson, L., Cole, T., Cormier-Daire, V., Irrthum, A., Rahman, N. and on behalf of the Childhood Overgrowth Collaboration (2005). "Multiple mechanisms are implicated in the generation of 5q35 microdeletions in Sotos syndrome." Journal of Medical Genetics **42**(4): 307-313.

Tatton-Brown, K., Douglas, J., Coleman, K., Baujat, G., Cole, T.R.P., Das, S., Horn, D., Hughes, H.E., Temple, I.K., Faravelli, F., Waggoner, D., Tu¨rkmen, S., Cormier-Daire, V., Irrthum, A., Rahman, N. for the Childhood Overgrowth Collaboration (2005). "Genotype-phenotype associations in Sotos syndrome: an analysis of 266 individuals with NSD1 aberrations." American Journal of Human Genetics **77**: 193-204.

Tatton-Brown, K., Rahman, N. (2007). "Sotos syndrome." European Journal of Human Genetics **15**: 264-271.

Tinkel-Vernon, H., Finkemagel, S., Desposito, F., Pittore, C., Reynolds, K., Sciorra, L. (2003). "Patient with a deletion of chromosome 21q and minimal phenotype." American Journal of Medical Genetics **120A**(1): 142-143.

Tsai, T.F., Jiang, J.H., Bressler, J., Armstrong, D., Beaudet, A.L. (1999). "Paternal deletion fromSnrpn to Ube3a in the mouse causes hypotonia, growth retardation and partial lethality and provides evidence for a gene contributing to Prader–Willi syndrome." Human Molecular Genetics **8**(8): 1357-1364.

Tucker, M.E., Garringer, H.J., Weaver, D.D. (2007). "Phenotypic spectrum of mosaic trisomy 18: Two new patients, a literature review, and

counseling issues." American Journal of Medical Genetics Part A **143A**(5): 505-517.

Tunster, S.J., Van de Pette, M., John, R.M. (2011). "Fetal overgrowth in the Cdkn1c mouse model of Beckwith-Wiedemann syndrome." Disease Models & Mechanisms **July 4.**: 1-8.

Umans, L., Overbergh, L., Serneels, L., Tesseur, I., Van Leuven, F. (1999). "Analysis of expression of genes involved in apolipoprotein e-based lipoprotein metabolism in pregnant mice deficient in the receptor-associated protein, the low density lipoprotein receptor, or apolipoprotein E1." Biology of Reproduction **61**: 1216-1225.

Valero, R., Marfany, G., Gonzalez-Angulo, O., Gonzalez-Gonzalez, G., Puelles, L., Gonzalez-Duarte, R. (1999). "USP25, a novel gene encoding a deubiquitinating enzyme, is located in the gene-poor region 21q11.2." Genomics **62**: 395-405.

Van der Weyden, L., Shaw-Smith, C., Bradley, A (2009). "Chromosome engineering in ES cells." Methods in Molecular Biology **530**: 49-77.

Vani Rayasam, G., Wendling, O., Angrand, P.O., Mark, M., Niederreither, K., Song, L., Lerouge, T., Hager, G.L., Chambon, P., Losson, R. (2003). "NSD1 is essential for early post-implantation development and has a catalytically active SET domain." European Molecular Biology Organisation Journal **22**(12): 3153-3163.

Visser, R., Shimokawa, O., Harada, N., Kinoshita, A., Ohta, T., Niikawa, N., Matsumoto, N. (2005). "Identification of a 3.0-kb major recombination hotspot in patients with Sotos syndrome who carry a common 1.9-Mb microdeletion." American Journal of Human Genetics **76**: 52-67.

Wakui, K., Toyoda, A., Kubota, T., Hidaka, E., Ishikawa, M., Katsuyama, T., Sakaki, Y., Hattori, M., Fukushima Y. (2002). "Familial 14-Mb deletion at 21q11.2-q21.3 and variable phenotypic expression." Journal of Human Genetics **47(10)**: 511-516.

Walz, K., Caratini-Rivera, S., Bi, W., Fonseca, P., Mansouri, D.L., Lynch, J., Vogel, H., Noebels, J.L., Bradley, A., Lupski, J.R. (2003). "Modeling del(17)(p11.2p11.2) and dup(17)(p11.2p11.2) contiguous gene syndromes by chromosome engineering in mice: phenotypic

consequences of gene dosage imbalance." Molecular and Cellular Biology **23**(10): 3646-3655.

Walz, K., Spencer, C., Kaasik, K., Lee, C.C., Lupski, J.R., Paylor, R. (2003). "Behavioral characterization of mouse models for Smith-Magenis syndrome and dup(17)(p11.2p11.2)." Human Molecular Genetics **13**(4): 367-378.

Wang, D., Stewart, A.K, Zhuang, L., Zhu, Y., Wang, Y., Shi, C., Keating, A., Slutsky, A., Zhang, H., Wen, X.Y. (2010). "Enhanced adaptive immunity in mice lacking the immunoinhibitory adaptor Hacs1." FASEB Journal **24**(3): 947-956.

Waterston, R.H., et al. (2002). "Initial sequencing and comparative analysis of the mouse genome." Nature **402**: 520-562.

Wen, X.Y., Hegele, R.A., Wang, J., Wang, D.Y., Cheung, J., Wilson, M., Yahyapour, M., Bai, Y., Zhuang, L., Skaug, J., Young, T.K., Connelly, P.W., Koop, B.F.,Tsui, L.C., Stewart, A.K. (2003). "Identification of a novel lipase gene mutated in lpd mice with hypertriglyceridemia and associated with dyslipidemia in humans." Human Molecular Genetics **12**(10).

Weyer, C., Wolford, J.K., Hanson, R.L., Foley, J.E., Tataranni, P.A., Bogardus, C., Pratley, R.E. (2001). "Subcutaneous abdominal adipocyte size, a predictor of type 2 diabetes, is linked to chromosome 1q21– q23 and is associated with a common polymorphism in LMNA in Pima Indians." Molecular Genetics and Metabolism **72**: 231-238.

White, R., Leonardsson, G., Rosewell, I., Jacobs, M.A., Milligan, S., Parker, M. (2000). "The nuclear receptor co-repressor Nrip1 (RIP140) is essential for female fertility." Nature Medicine **6**(12): 1368-1374.

Wikström, A.M., Dunkel, L. (2011). "Klinefelter syndrome." Best Practice & Research Clinical Endocrinology & Metabolism **25**(2): 239-250.

Williams, J.C.P., Barratt-Boyes, B.G., Lowe, J.B. (1961). "Supravalvular aortic stenosis." Circulation **24**: 1311-1318.

Willnow, T.E., Armstrong, S.A., Hammer, R.E., Herz, J. (1995). "Functional expression of low density lipoprotein receptor-related protein is controlled by receptor-associated protein in vivo." Proceedings of the National Academy of Sciences **92**: 4537-4541.

Wojtanik, K.M., Edgemon, K., Viswanadha, S., Lindsey, B., Haluzik, M., Chen, W., Poy, G., Reitman, M., Londos, C. (2009). "The role of LMNA in adipose: a novel mouse model of lipodystrophy based on the Dunnigan-type familial partial lipodystrophy mutation." The Journal of Lipid Research **50**(6): 1068-1079.

Yabuuchi, H., Takayanagi, S., Yoshinaga, K., Taniguchi, N., Aburatani, H., Ishikawa, T. (2002). "ABCC13, an unusual truncated ABC transporter, is highly expressed in fetal human liver." Biochemical and Biophysical Research Communications **299**: 410-417.

Yamada, H., Yanagisawa, K., Tokumaru, S., Taguchi, A., Nimura, Y., Osada, H., Nagino, M., Takahashi, T. (2008). "Detailed characterization of a homozygously deleted region corresponding to a candidate tumor suppressor locus at 21q11-21 in human lung cancer." Genes, Chromosomes & Cancer **47**: 810-818.

Yamagata, N., Furuno, K., Sonoda, M., Sugimura, H., Yamamoto, K. (2008). "Stomach cancer-derived del223V-226L mutation of the STCH gene causes loss of sensitization to TRAIL-mediated apoptosis." Biochemical and Biophysical Research Communications **376**(3): 499-503.

Yamamoto, N., Mizoe, J., Numasawa, H., Tsujii, H., Shibahara, T., Noma, H. (2003). "Allelic loss on chromosomes 2q, 3p and 21q: possibly a poor prognostic factor in oral squamous cell carcinoma." Oral Oncology **39**(8): 796-805.

Yan, J., Keener, V.W, Bi, W., Walz, K., Bradley, A., Justice, M.J., Lupski, J.R. (2004). "Reduced penetrance of craniofacial anomalies as a function of deletion size and genetic background in a chromosome engineered partial mouse model for Smith-Magenis syndrome." Human Molecular Genetics **13**(21): 2613-2624.

Yang, S.H., Bergo, M.O., Toth, J.I., Qiao, X., Hu, Y., Sandoval, S., Meta, M., Bendale, P., Gelb, M.H., Young, S.G., Fong, L.G. (2005). "Blocking protein farnesyltransferase improves nuclear blebbing in mouse fibroblasts with a targeted Hutchinson–Gilford progeria syndrome mutation." Proceedings of the National Academy of Sciences **102** (29): 10291–10296.

Yang, T., Adamson, T.E., Resnick, J.L., Leff, S., Wevrick, R., Francke, U., Jenkins, N.A., Copeland, N.G., Brannan, C.I. (1998). "A mouse model for Prader-Willi syndrome imprinting-centre mutations." Nature Genetics **19**(1): 25-31.

Yang, Y.H., Dudoit, S., Luu, P., Lin, D.M., Peng, V., Ngai, J., Speed, T.P. (2001). "Normalization ofr cDNA microarray data: a robust composite method addressing single and multiple slide systematic variation." Nucleic Acids Research **30, No. 4, e15**: 1-10.

Yokoyama, T., Silversides, D.W., Waymire, K.G., Kwon, B.S., Takeuchi, T., Overbeek, P.A. (1990). "Conserved cysteine to serine mutation in tyrosinase is responsible for the classical albino mutation in laboratory mice." Nucleic Acids Research **18**: 7293-7298.

Young, E.J., Lipina, T., Tam, E., Mandel, A., Clapcote, S.J., Bechard, A.R., Chambers, J., Mount, H.T.J., Fletcher, P.J., Roder, J.C., Osborne, L.R. (2008). "Reduced fear and aggression and altered serotonin metabolism in Gtf2ird1-targeted mice." Genes, Brain and Behavior **7**(2): 224-234.

Yu, T., Clapcote, S.J., Li, Z., Liu, C., Pao, A., Bechard, A.R., Carattini-Rivera, S., Matsui, S.I., Roder, J.C., Baldini, A., Mobley, W.C., Bradley, A., Yu, E.Y. (2010). "Deficiencies in the region syntenic to human 21q22.3 cause cognitive deficits in mice." Mammalian Genome **21(5-6)**: 258-267.

Zhao, L.J., Jiang, H., Papasian, C.J., Maulik, D., Drees,B., Hamilton, J., Deng, H.W. (2008). "Correlation of obesity and osteoporosis: effect of fat mass on the determination of osteoporosis." Journal of bone and mineral research **23**(1): 17-29.

Zheng, B., Mills, A.A., Bradley, A. (1999). "A system for rapid generation of coat color-tagged knockouts and defined chromosomal rearrangements in mice." Nucleic Acids Research **27**(11): 2354-2360.

Zheng, B., Sage, M., Cai, W.W., Thompson, D.M., Tavsanli, B.C., Cheah, Y.C., Bradley, A. (1999). "Engineering a mouse balancer chromosome." Nature Genetics **22**: 375-378.

Zheng, B., Sage, M., Sheppeard, E.A., Jurecic, V., Bradley, A. (2000). "Engineering mouse chromosomes with Cre-loxP: range, efficiency, and somatic applications." Molecular Cell Biology **20**: 648-655.